Noah Graham
Markus Quandt
Herbert Weigel

LECTURE NOTES IN PHYSICS 777

Spectral Methods in Quantum Field Theory

Springer

Lecture Notes in Physics

The Lecture Notes in Physics

The series Lecture Notes in Physics (LNP), founded in 1969, reports new developments in physics research and teaching – quickly and informally, but with a high quality and the explicit aim to summarize and communicate current knowledge in an accessible way. Books published in this series are conceived as bridging material between advanced graduate textbooks and the forefront of research and to serve three purposes:

- to be a compact and modern up-to-date source of reference on a well-defined topic
- to serve as an accessible introduction to the field to postgraduate students and nonspecialist researchers from related areas
- to be a source of advanced teaching material for specialized seminars, courses and schools

Both monographs and multi-author volumes will be considered for publication. Edited volumes should, however, consist of a very limited number of contributions only. Proceedings will not be considered for LNP.

Volumes published in LNP are disseminated both in print and in electronic formats, the electronic archive being available at springerlink.com. The series content is indexed, abstracted and referenced by many abstracting and information services, bibliographic networks, subscription agencies, library networks, and consortia.

Proposals should be sent to a member of the Editorial Board, or directly to the managing editor at Springer:

Christian Caron
Springer Heidelberg
Physics Editorial Department I
Tiergartenstrasse 17
69121 Heidelberg / Germany
christian.caron@springer.com

N. Graham
M. Quandt
H. Weigel

Spectral Methods in Quantum Field Theory

Springer

Noah Graham
Middlebury College
Dept. Physics
515 McCardell Bicentennial Hall
Middlebury VT 05753
USA
ngraham@middlebury.edu

Markus Quandt
Universität Tübingen
Inst. Theoretische Physik
Auf der Morgenstelle 14
72076 Tübingen
Germany
quandt@tphys.physik.uni-tuebingen.de

Herbert Weigel
Universität Siegen
FB Physik
57068 Siegen
Emmy Noether Campus
Germany
weigel@physik.uni-siegen.de

Graham, N., et al., *Spectral Methods in Quantum Field Theory*, Lect. Notes Phys. 777 (Springer, Berlin Heidelberg 2009), DOI 10.1007/978-3-642-00139-0

ISBN 978-3-642-00138-3 e-ISBN 978-3-642-00139-0

DOI 10.1007/978-3-642-00139-0

Springer Dordrecht Heidelberg London New York

Lecture Notes in Physics ISSN 0075-8450 e-ISSN 1616-6361

Library of Congress Control Number: 2009920054

Cover design: Integra Software Services Pvt Ltd.

Printed on acid-free paper

Springer is part of Springer Science+Business Media (www.springer.com)

Preface

In this monograph we apply scattering theory methods to calculations in quantum field theory, with a particular focus on properties of the quantum vacuum. These methods will provide efficient and reliable solutions to a variety of problems in quantum field theory. Our approach will also elucidate in a concrete context many of the subtleties of quantum field theory, such as divergences, regularization, and renormalization, by connecting them to more familiar results in quantum mechanics.

We will use tools of scattering theory to characterize the spectrum of energy eigenstates in a potential background, hence the term *spectral methods*. This mode spectrum comprises both discrete bound states and a continuum of scattering states. We develop a powerful formalism that parameterizes the effects of the continuum by the density of states, which we compute from scattering data. Summing the zero-point energies of these modes gives the energy of the quantum vacuum, which is one of the central quantities we study. Although the most commonly studied background potentials arise from static soliton solutions to the classical equations of motion, these methods are not limited to such cases.

A novel and central feature of this approach is its ability to make direct contact between perturbative and non-perturbative treatments of quantum field theory. Although we will study field configurations corresponding to strong potentials that cannot be treated perturbatively, we will nonetheless be able to implement standard perturbative renormalization conditions specified in terms of experimental inputs. Using these conventional renormalization conditions allows us to make direct comparisons to the perturbative sector of the quantum field theory and thus compute quantum effects for non-perturbative field configurations in an accurate and unambiguous way.

The spectral method is exact to one-loop order because it sums all one-loop Feynman diagrams with any number of insertions of the background field. This property allows us to proceed where perturbation theory or the derivative expansion would not be valid. For example, in a model with no classical solitons we can demonstrate the existence of a non-topological soliton stabilized at one-loop order by quantum fluctuations.

Our methods are also efficient for practical computations: The quantities entering a numerical calculation are cutoff independent and do not involve

differences of large numbers, so the algorithms are highly convergent. In general the quantum fluctuations are described by coupled partial differential equations. For technical reasons we are restricted to systems with sufficient symmetry so that these equations of motion allow a partial wave decomposition. Fortunately, for physically interesting systems this is often the case.

The outline of the monograph is as follows: In the first chapter, we explain the basic ideas intuitively, postponing the precise and rigorous derivations to the following two chapters. In Chap. 2 we review the technical results from scattering theory that we will need. In Chap. 3 we establish the central techniques of the spectral method. On a first reading, one may want to skip the technical details in Chap. 2 and 3 and proceed to the discussion of applications in the subsequent chapters.

In Chap. 4 we employ the spectral method to compute energies of the quantum vacuum for configurations in one spatial dimension. We consider both bosonic and fermionic quantum fields and combine these results in a simple supersymmetric model. For a system with fermionic fluctuations, we show that quantum contributions to the energy can stabilize classically unstable field configurations. In Chap. 5 we show how the spectral method is able to count states as the vacuum is distorted by the background field. In particular, it allows us to compute integer and fractional charges that are induced by bosonic background fields coupled to charged fermions. Hedgehog configurations play a major role in particle physics and the spectral method is particularly well suited for their investigation. In Chap. 6 we discuss them for two renormalizable models.

The spectral method provides an elegant means to disentangle divergences that arise in quantum field theory calculations. This property is particularly valuable for the famous Casimir effect because its study requires proper identification not only of ultraviolet divergences of quantum field theory but also of divergences that originate from singular boundary conditions. We will explore these issues in Chap. 7 in our calculation of Casimir forces and stresses. In Chap. 8 we return to particle physics models similar to those already discussed in Chap. 6. However, this time we will explore string type configurations that are translationally invariant in one spatial dimension, using the formalism developed in Chap. 3 for this purpose. Finally, in Chap. 9 we consider Q-balls as an example of quantum corrections for background fields with simple time dependence.

The spectral method is an advanced technique in the theory of quantum fields. We have tried to keep the exposition as simple and self-contained as possible, given the restricted space of a lecture note. In particular, we have added a non-technical introduction to the main aspects of the method and devoted separate chapters to the more sophisticated formalism from scattering and quantum field theory. Overall, we anticipate that the volume can be mastered with a profound knowledge of quantum mechanics alone, although familiarity with the concepts of quantum field theory will be very useful. We

expect that this monograph can be used profitably as a companion to the more standard presentation of quantum field theory, since it provides explicit examples of concepts such as dimensional regularization and gauge theory anomalies in the context of ordinary quantum mechanics. It can thus serve both as a textbook for graduate students with some background in quantum field theory and as a summary report for researchers in the field. In particular, we hope that this monograph spreads the appreciation of the many advantages that spectral methods provide for the study of quantum field theories and stimulates further developments of the subject.

Many people have helped us gaining this understanding of the spectral method. In particular we gratefully acknowledge fruitful contributions by and illuminating discussions with E. Farhi, R. L. Jaffe, V. Khemani, and O. Schröder. This research has been supported by the United States Department of Energy and National Science Foundation (N. G.), Research Corporation (N. G.), and the Deutsche Forschungsgemeinschaft (M. Q. and H. W.).

Middlebury, Tübingen, Siegen, October 2008

Noah Graham
Markus Quandt
Herbert Weigel

Contents

1 Introduction

1.1 Background and Motivation

In quantum field theory, we often encounter field configurations with a strongly localized energy or charge density. In many cases, these configurations also solve the classical field equations and behave in many respects as classical particles; such configurations are known as *solitons* [1, 2]. While it is generally straightforward to compute the classical energy of such a configuration, the quantum correction to the classical energy is often essential to complete the physical picture. For reasons that will soon become obvious, this correction is commonly called the *vacuum polarization energy*. Vacuum polarization energies have been investigated for soliton configurations ranging from simple models in $1+1$ dimensions [2, 3] to chiral models for baryons[1] [5, 6] and even to cosmic strings in the standard model [7, 8]. In all these cases the quantum corrections to the classical energy may be substantial and may thus drastically alter conclusions about the stability or other properties of the field configuration.

This monograph introduces a comprehensive set of tools from scattering theory for computing one-loop, i.e., $\mathcal{O}(\hbar)$, quantum effects for a wide variety of localized field configurations. Scattering theory provides all the necessary information on the small-amplitude fluctuations about these configurations. Since we will compute the spectra of these fluctuations within scattering theory, we therefore call this approach the *spectral method*. Scattering theory also allows us to employ tools such as Levinson's theorem and the Born approximation to handle the subtleties of regularization and renormalization in quantum field theory.

In the next section we begin with a heuristic description of the spectral method for a simple case, in anticipation of the rigorous derivations in later chapters. In Chap. 2 we review aspects of scattering theory essential for our method, and we incorporate them in the usual setting of quantum field theory in Chap. 3. In subsequent chapters we introduce a number of applications, which show the practicality, efficiency, and flexibility of our method. It does have one limitation, however: We rely on a partial wave decomposition of the scattering matrix, so that the computation is technically feasible only if

[1] See Ref. [4] for a recent review on soliton models for baryons.

Graham, N., et al.: *Introduction*. Lect. Notes Phys. **777**, 1–13 (2009)
DOI 10.1007/978-3-642-00139-0_1

the problem exhibits sufficient symmetry to separate the scattering problem into block-diagonal form. As a result, the systems to be considered usually exhibit some form of rotational symmetry. Fortunately, most of the physical systems of interest do indeed have such symmetries.

The spectral method sums *all* one-loop Feynman diagrams with any number of insertions of the background field. The method is thus exact to subleading order of the $\hbar$ expansion. We will use a Born series representation to isolate the divergent terms. The Born approximation need not be a good approximation (it actually is a bad one), so we do not rely on its accuracy; rather it is useful because any specific order of this series may be identified with a limited number of Feynman diagrams. As we will show, this identification renders our computations free of any cut-off that would be needed to regularize the ultra-violet divergent loop integrals. This property drastically reduces numerical errors and facilitates a direct implementation of the standard renormalization conditions of perturbative quantum field theory, which removes ambiguities arising from finite renormalizations.

The methods that we discuss apply furthermore to the famous Casimir effect [9–11], because it can be described in terms of the quantum energy of an interacting field theory [12]. For that reason the vacuum polarization energy is frequently called the Casimir energy. The Casimir problem is usually posed as the response of a fluctuating quantum field to externally imposed boundary conditions. In reality, however, no interaction is strong enough to enforce a boundary condition on all frequencies of a fluctuating field. Rather, the fluctuating field interacts with a smooth background that implements the boundary condition in a certain, often singular limit. Hence the spectral methods are perfectly suited to investigate the Casimir problem [13].

The spectral techniques we present provide a complete, self-contained approach to the calculation of one-loop quantum corrections, which reveals the fundamental connections between quantum field theory and ordinary quantum mechanics. The foundation of this approach was first formulated by Schwinger [14], and it was applied to simple models by Dashen, Hasslacher, and Neveu [3]. As we show in Chap. 3, our calculations using the spectral method can be recast in the general form of a functional determinant arising from the path integral representation of the field theory at order $\hbar$. A number of other approaches have tackled similar problems in either an exact or approximate way:

- Green's function methods involving subtractions analogous to our Born series approach have been used in [15–18]. In particular the calculations of Refs. [17, 18] implement the full renormalization conditions and thus are directly comparable to our approach.
- The *heat kernel method*, based on the proper time representation of the determinant, can be used to provide long-wavelength approximations [19–21], which work well for sufficiently smooth background configurations. It

can also be used to form exact results [22–26], though this approach does not allow for comparison to standard renormalization conditions.
- The *world-line formalism* [27–30] represents the determinant as a stochastic ensemble of closed world lines. It is free of systematic errors and even applicable in cases where there is not enough radial symmetry for the spectral method to work. Unfortunately, the statistical errors of the Monte Carlo procedure make high-precision simulations very time consuming.
- *Generalized derivative expansions* [31–33] can often be equivalent to our approach when computed exactly. They are particularly well suited to approximate calculations for slowly varying backgrounds [34–37].
- *Functional determinant* or *partial wave cutoff methods* [1, 38–40] express path integral determinants in one space dimension in terms of the solution to a differential equation, which is then used analogously to our scattering data.
- *Direct analysis of discrete spectra* [41] provides a simple, general approach for generic problems, but suffers from computational inefficiencies because it directly subtracts cutoff-dependent quantities. Since the final result is obtained as a difference of divergent quantities, very high precision must be maintained in the calculation.
- *Semiclassical approximations* can be highly efficient in cases where these approximations are justified. An example is the *optical approach* [42–44] to the Casimir problem.

1.2 Invitation: A Sample Calculation

We begin by sketching the central elements of our approach in a toy model. The actual derivations of these results are postponed until the subsequent chapters, where we will develop the mathematical tools that will enable us to implement these intuitive ideas in a general, rigorous, and efficient way.

1.2.1 Zero-Point Energies: Summing $\frac{1}{2}\hbar\omega$

Consider a scalar quantum field φ of mass m in one space dimension, with a fixed, localized background potential $\sigma(x)$. This system is described by the Lagrangian density

$$\mathcal{L} = \frac{\hbar^2}{2}(\partial_\mu\varphi)^2 - \frac{1}{2}m^2\varphi^2 - \frac{1}{2}\sigma(x)\varphi^2\,. \tag{1.1}$$

The potential $\sigma(x)$ represents the effects of the φ field's interactions with the static background field. We would like to understand the energy associated with the quantum fluctuations of φ in its vacuum state. Upon quantization, each normal mode of oscillation $\varphi_k(x)$ of φ is associated with a simple harmonic oscillator, whose creation and annihilation operators increment and

decrement the occupation number of that mode. The energy stored in that mode is given by

$$E_k = \hbar\omega_k \left(n_k + \frac{1}{2} \right), \tag{1.2}$$

where n_k is the occupation number and $\hbar\omega_k$ is the energy of mode k. Thus even in the vacuum state, when all n_k are equal to zero, the system still has a quantum energy that we may loosely write as the mode sum

$$E = \sum_k \frac{1}{2}\hbar\omega_k \,. \tag{1.3}$$

There are two serious problems with this expression:

1. It is not actually a sum. The normal modes of our system potentially comprise both discrete bound states and a continuum of scattering states. Although one could discretize the system by putting it in a box, our approach will not take this direction, because we will rely on the powerful tools of continuum scattering theory. Regardless of the approach we take, however, it will be essential to carefully weight the sum and integral to avoid over- or undercounting of states.
2. The sum is not finite. This problem is clear because the summand itself approaches infinity. While the resolution of such divergences through regularization and renormalization is well understood in perturbative quantum field theory, it will require considerable care to precisely implement this standard procedure in a practical calculation. Our final result must take as input physical parameters, such as masses, charges, and coupling constants at fixed external momenta, and yield an unambiguous answer, with no undetermined or ambiguous finite parts. In this procedure it will be crucial to solve the previous problem of carefully enumerating the spectrum of states, because the final answer after renormalization can be of the same order of magnitude as the smallest energies in the sum.

To see how these problems interact, we consider the first step in the solution to the second problem: Since only energy differences—not absolute energies—are detectable, we will compute the change in the quantum energy between the free and interacting cases,[2]

$$\Delta E = E - E^{(0)} = \sum_k \frac{1}{2}\hbar\omega_k - \sum_k \frac{1}{2}\hbar\omega_k^{(0)} \,. \tag{1.4}$$

Here we recognize the justification for the term *vacuum polarization energy* introduced earlier: ΔE measures the energy change caused by the polarization of the vacuum modes that stems from the interaction with the background

[2] Of course, general relativity is sensitive to absolute energies. This subtraction then represents the renormalization to zero of the cosmological constant, which we will not attempt to justify.

potential. While the leading divergence cancels in the subtraction of Eq. (1.4), the difference is still divergent even in our simple model. Furthermore, this expression highlights the importance of a consistent enumeration of the spectrum of small oscillation modes: Neglecting even a single ω_k or summing a slightly different number of terms in the two sums would lead to a drastic change in the final result.

1.2.2 From Discrete to Continuous: Phase Shifts and the Density of States

Next we address the issue of counting of states. To simplify the problem, we consider a potential $\sigma(x)$ that is symmetric under $x \to -x$. We also restrict our attention to the antisymmetric small oscillation modes. The symmetric case proceeds similarly, but it requires some additional technical details that we describe in later sections. From here on, we work in units where $\hbar = 1$.

The small oscillation wavefunctions $\varphi_k(x)$ obey the relativistic Klein–Gordon equation

$$\left(-\frac{d^2}{dx^2} + \sigma(x)\right)\varphi_k(x) = k^2\varphi_k(x), \tag{1.5}$$

where $\varphi_k(0) = 0$ because we are in the antisymmetric channel and $k^2 = \omega^2 - m^2$. We begin by considering scattering states, for which $k^2 > 0$.

In the absence of any potential, the solution to this equation would simply be $\varphi_k^{(0)}(x) = \sin kx$. Far away, where the potential approaches zero, our solution should approach this free solution, but it could be phase shifted:

$$\varphi_k(x) \approx \sin(kx + \delta(k)) \qquad \text{for } x \text{ large}, \tag{1.6}$$

where the phase shift $\delta(k)$ depends on k but not x. The phase shift contains the essential information to our calculation. An attractive potential pulls the wavefunction in, giving a positive $\delta(k)$, while a repulsive potential pushes it out, giving a negative $\delta(k)$. The former case is illustrated in Fig. 1.1. Since it is a phase, $\delta(k)$ is defined only modulo π. We fix this ambiguity by requiring it to be a continuous function of k, vanishing as $k \to \infty$. (For more complex cases we will encounter later, we will have to relax the second requirement.)

To understand how phase shifts are going to help us, we imagine placing the system in a box by imposing the boundary condition $\varphi_k(x) = 0$ at $x = L$ for large L. The boundary condition yields a discrete spectrum of allowed values of k, since we must have $\sin(kL + \delta(k)) = 0$. We can imagine enumerating these possibilities as

$$\begin{aligned} &\vdots \\ k_{n+1}L + \delta(k_{n+1}) &= (n+1)\pi \\ k_nL + \delta(k_n) &= n\pi \\ &\vdots \end{aligned} \tag{1.7}$$

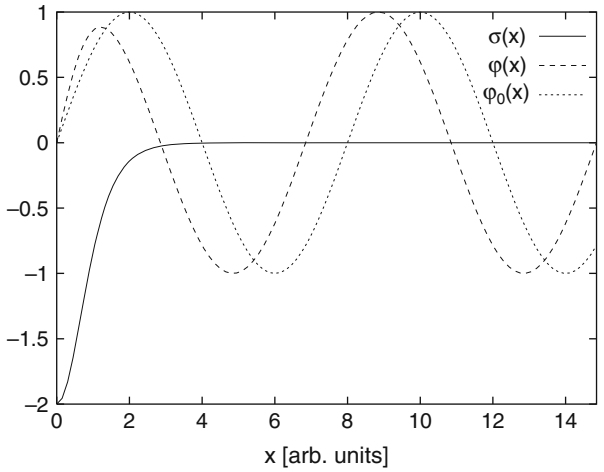

Fig. 1.1 An example of a free wavefunction $\varphi_k^{(0)}(x)$, the full wavefunction $\varphi_k(x)$, and the corresponding potential $\sigma(x)$

We then subtract the lower line from the upper to obtain

$$(k_{n+1} - k_n)L + \delta(k_{n+1}) - \delta(k_n) = \pi\,. \tag{1.8}$$

Since L is large, $(k_{n+1}-k_n)$ must be small, because the rest of the terms in the equation are small or of order one. Next we divide through by $\pi(k_{n+1} - k_n)$. Since $(k_{n+1} - k_n)$ is small, we may approximate the difference in phase shifts by a derivative,

$$\frac{1}{\pi}\left(L + \frac{d\delta(k)}{dk}\right) = \frac{1}{k_{n+1} - k_n}. \tag{1.9}$$

The right-hand side is the inverse of the spacing between adjacent levels, otherwise known as the density of states $\rho(k)$.

To return to the continuum, we would like to send $L \to \infty$. The density of states is becoming infinite in this limit, since the spacing between adjacent levels is going to zero. However, if we compare the density of states $\rho(k)$ in the presence of the potential to the free density of states $\rho^{(0)}(k)$ with no potential, the difference is finite:

$$\Delta\rho(k) = \rho(k) - \rho^{(0)}(k) = \frac{1}{\pi}\frac{d\delta(k)}{dk} \tag{1.10}$$

and it is always this quantity that will be important to our calculations. In the next chapter we will rederive this result more rigorously, i.e., without reference to artificial boundaries (see also Ref. [13]).

1.2.3 Counting States: Levinson's Theorem

When comparing the free and interacting systems, it will be extremely important to maintain a consistent counting of the modes over which we sum.

Any mismatch would lead to an error that would swamp the true result. In particular, we would like to make sure that the number of modes we consider is the same in both cases. In the continuum, this requirement is enforced by Levinson's theorem [45, 46], which tells us that

$$\delta(0) - \delta(\infty) = n\pi, \tag{1.11}$$

where n is the number of bound states (discrete solutions with $k^2 < 0$) that have appeared in the interacting case. This result implies that

$$\int_0^\infty \Delta\rho(k)\, dk + n = 0\,. \tag{1.12}$$

In other words, any net change in the total number of states in the continuum as we turn on the potential is balanced by the appearance of a corresponding number of bound states. In some very special cases, examples of which we will encounter in Chap. 4, bound states emerge at threshold with $k = 0$; such states are "half-bound" and contribute to the total number of bound states with weight 1/2.

1.2.4 Divergences: The Born Approximation

Having developed the tools for summing over the spectrum of quantum states, we now turn to the calculation of interest. We can replace the difference of sums in Eq. (1.4) by a sum over a finite number of bound states and an integral over the continuum, which is weighted by the change in the density of states between the interacting and free cases. Formally, we have

$$\Delta E = \sum_j \frac{1}{2}\,\omega_j + \int_0^\infty \frac{1}{2}\,\omega\,\left(\frac{1}{\pi}\frac{d\delta}{dk}\right) dk\,, \tag{1.13}$$

where ω_j are the bound state energies and $\omega = \sqrt{k^2 + m^2}$ gives the energy of each continuum mode. As we have anticipated, this quantity is divergent: The phase shifts for a localized potential typically go like $1/k$ at large k, yielding a logarithmically divergent integral. This result reflects the standard logarithmic divergences of a scalar field theory in one space dimension. (In higher dimensions we will consider cases in which symmetry lets us decompose the calculation into a sum over effective one-dimensional problems for each partial wave. In that case, the individual channels will have the logarithmic divergences of one dimension, but the sum over channels will introduce the additional divergences associated with the higher space dimension.) Since these divergences arise from the behavior of the integrand at large k, they are entirely due to short-distance effects. The physical effects we are interested in, however, should be associated with the length scales of the problem at hand, such as the characteristic size of the potential or the Compton wavelength of the φ particle. Thus, while the divergences dominate the calculation of the

integral, they contain little information. Still, it is essential to handle these divergences in a precise way: simply "canceling the infinities" in an arbitrary way yields only a result that is accurate up to a finite constant; in other words this result is meaningless.

The quantum field theory prescription for dealing with this situation is well understood. First, one identifies the divergences, either with an explicit cutoff or by introducing dimensional or Pauli–Villars regularization procedures. Next, one introduces local counterterms to the "bare" Lagrangian that modify existing parameters in the Lagrangian, such as mass, charge, and the values of coupling constants at specific external momenta. Since *Nature* provides only the values of these constants in the full theory, including all quantum effects, the combination of the bare parameters and the counterterms is what must be matched to experimental inputs. These quantities are then held fixed as the regulator is removed through the process of renormalization. As a result, although the bare parameters and counterterms both diverge, the theory is defined precisely in terms of experimentally accessible data. Any other quantities we choose to calculate are then precise predictions of the theory, with no room for ambiguities in "finite parts."

In the case at hand, the counterterm is simply proportional to the potential $\sigma(x)$. Thus we must introduce a local counterterm $c\sigma(x)$ in the Lagrangian. Its coefficient depends on the regulator in such a way that the counterterm contribution to the energy, $-c\int_{-\infty}^{\infty}\sigma(x)\,dx$, cancels the divergences in the quantum calculation. In the standard "no-tadpole" renormalization scheme, this counterterm exactly cancels the diagram with one external leg, that is, one insertion of the background field $\sigma(x)$. But it is simple to extract the piece of the vacuum energy that is linear in the potential; it is just given by the Born approximation

$$\Delta E^{(1)} = \frac{1}{2\pi}\int_0^\infty \omega\,\frac{d\delta^{(1)}}{dk}\,dk\,, \tag{1.14}$$

where

$$\delta^{(1)}(k) = -\frac{1}{2k}\int_{-\infty}^{\infty}\sigma(x)\sin^2 kx\,dx\,. \tag{1.15}$$

There are never any bound states in the Born approximation, so this contribution to the energy arises entirely from the continuum. As written, it is not manifestly proportional to $\int dx\,\sigma(x)$. However, when we incorporate the contribution from the symmetric channel, which is given by Eq. (1.15) with $\sin^2 kx \longrightarrow \cos^2 kx$, we will obtain a result of the expected form.[3]

We stress that the Born approximation is unlikely to be a *good* approximation to the exact phase shift in cases of interest to us, and in no way is our calculation relying on its validity as an approximation. For us, the interesting physical phenomena are likely to be encoded in the bound states and

[3] However, the divergent piece of Eq. (1.15), which may be identified from the large k behavior of $\delta^{(1)}(k)$ by approximating $\sin^2 kx \to \frac{1}{2}$, is of this local form.

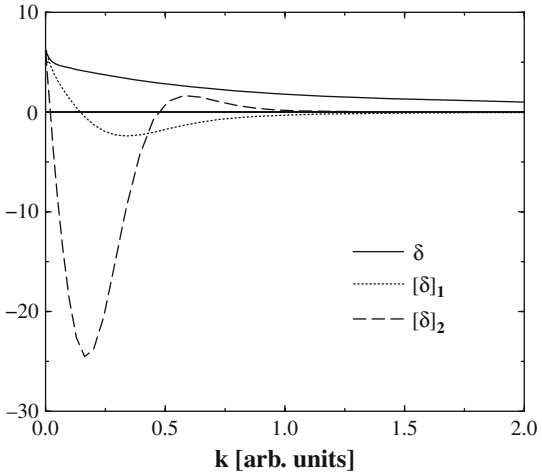

Fig. 1.2 A typical example for the role of the Born approximation. Here $[\delta]_n = \delta - \sum_{m=1}^{n} \delta^{(m)}$ refers to the phase shift with the n first terms of the Born series subtracted

low-energy scattering data, which correspond to physics at the characteristic length scale of the potential. There, the Born approximation will differ significantly from the exact result. Indeed, as we will soon observe, the final result is simply given by integrating over the error in the first Born approximation! The Born approximation is accurate, however, for high energies and weak potentials. It captures the uninteresting perturbative short-distance physics that dominates the bare calculation but is canceled by the counterterms. In Fig. 1.2 we show a typical example for the phase shift and its Born approximations. Obviously the Born approximation is very bad for small k. At large momenta, however, it becomes accurate, so that integrals over Born-subtracted phase shifts converge nicely. Figure 1.2 also shows the point made above: Any term in the Born series has $\delta^{(n)}(0) = 0$ and thus there are no bound states in the Born approximation, in accordance with Levinson's theorem.

The final result for the renormalized quantum vacuum energy is then the difference

$$\Delta E_{\rm ren} = \Delta E - \Delta E^{(1)} = \frac{1}{2}\sum_j \omega_j + \frac{1}{2\pi}\int_0^\infty \omega \frac{d}{dk}\left(\delta(k) - \delta^{(1)}(k)\right) dk\,. \quad (1.16)$$

Since the Born approximation becomes exact at large k, this subtraction improves the convergence of the integral, so that the logarithmic divergence now disappears and we have a finite result. In particular, there is no impediment to integrating by parts, which, together with Levinson's theorem, yields

$$\Delta E_{\rm ren} = \frac{1}{2}\sum_j (\omega_j - m) - \frac{1}{2\pi}\int_0^\infty \frac{k}{\omega}\left(\delta(k) - \delta^{(1)}(k)\right) dk. \quad (1.17)$$

In this form, it is clear that the final result is proportional to the binding energy of the bound states, and thus it varies smoothly if we change the number of bound states by modifying the background potential. This expression is also significantly easier to work with computationally than Eq. (1.16), since no numerical derivatives must be computed. In this form it is obviously necessary to ensure that the phase shift is defined to be continuous and to vanish as $k \to \infty$, without any mod π ambiguities.

It is important to note, however, that these manipulations are entirely formal. Combining the divergent integrals in Eqs. (1.13) and (1.14) is ill-defined. For example, we could obtain a different, but still finite, result by carrying out a change of variables or integration by parts in one integral but not the other before combining them. As demonstrated in Ref. [47], integrating the unregulated integral by parts introduces such finite ambiguities, corresponding physically to the difference between holding the number of modes fixed and holding the energy cutoff fixed when subtracting the divergent sums. Such ambiguities are intolerable in a treatment that is to make predictive statements about physical systems, such as the stability of solitons or the energy density in the vacuum. In subsequent sections we will justify this subtraction procedure by regulating both expressions consistently using dimensional regularization. We will then combine the finite, regularized expressions in an unambiguous way before taking the limit in which the regulator is removed.

As a check, we note that if we included the analogous calculation with the symmetric channel as well, the total quantity to be subtracted would be

$$\Delta E^{(1)} = \frac{1}{2\pi} \int_0^\infty \omega \left(\frac{d\delta^{(1)}}{dk} + \frac{d\delta_S^{(1)}}{dk} \right) dk, \tag{1.18}$$

where the Born approximation to the symmetric channel phase shift is

$$\delta_S^{(1)}(k) = -\frac{1}{2k} \int_{-\infty}^\infty \sigma(x) \cos^2 kx \, dx, \tag{1.19}$$

giving a total contribution to the energy of

$$\Delta E^{(1)} = -\frac{1}{4\pi} \int_0^\infty dk \, \frac{\omega}{k} \int_{-\infty}^\infty \sigma(x) \, dx, \tag{1.20}$$

which is indeed just a (divergent) constant times $\int_{-\infty}^\infty \sigma(x) \, dx$. Hence this divergent contribution to the energy can indeed be absorbed by a local counterterm in the Lagrangian. Furthermore, we can adjust this counterterm such that expansion of the vacuum polarization energy has no contribution linear in $\sigma(x)$ but starts at quadratic order. In field theory, this choice parallels the requirement that the tadpole graph, the diagram with a loop in φ and one insertion of the background field, is zero. Therefore, it is often called the *no-tadpole* renormalization scheme. If we imagine that $\sigma(x)$ is determined by dynamics not captured by our model, the no-tadpole scheme implies that to

leading order this result is unchanged by the quantum fluctuations φ. Loosely speaking, we state that the quantum fluctuations do not alter the vacuum expectation value (VEV) of $\sigma(x)$ in the no-tadpole scheme.

1.2.5 Computational Techniques

One of the strengths of this technique lies in its ability to precisely express the difference between divergent quantities in a physically tractable way. Without this simplification, sophisticated numerical algorithms are needed to carry out the intermediate computations with extremely high accuracy even in simple cases [41], because the subtraction procedure leads to a substantial loss of precision. For our approach to be practical, however, we must be able to compute phase shifts and their Born approximations efficiently.

To do so, we will employ the generalizations of the variable phase method [48]. Continuing with our special case of the antisymmetric channel in one dimension, we write the scattering solution in terms of the phase shift $\delta(k)$ and an unknown complex function $\beta_k(x)$ in the form

$$\varphi_k(x) = \frac{1}{2i}\left(e^{ikx}e^{i\delta(k)}e^{i\beta_k(x)} - e^{-ikx}e^{-i\delta(k)}e^{-i\beta_k^*(x)}\right), \tag{1.21}$$

where $\beta_k(x)$ obeys the nonlinear differential equation

$$-i\beta_k''(x) + 2k\beta_k'(x) + \left(\beta_k'(x)\right)^2 + \sigma(x) = 0\,. \tag{1.22}$$

Comparing Eq. (1.21) to Eq. (1.6), we obtain the boundary condition that $\beta_k(x)$ and $\beta_k'(x)$ vanish as $x \to \infty$. We note that if the potential is zero, then the phase shift vanishes and $\beta_k(x) = 0$ for all x. Essentially, we have "factored out" the free solution. The boundary condition $\varphi(0) = 0$ then implies that

$$\delta(k) = -\mathrm{Re}\,\beta_k(0)\,. \tag{1.23}$$

This approach automatically yields a phase shift that is continuous in k and vanishing as $k \to \infty$, so it resolves all mod π ambiguities. Furthermore, iteration of Eq. (1.22) yields an efficient way to compute Born approximations to the phase shift: We simply integrate the differential equations in powers of the potential $\sigma(x)$, to obtain

$$\begin{aligned} -i\beta_k^{(1)\prime\prime}(x) + 2k\beta_k^{(1)\prime}(x) + \sigma(x) &= 0 \\ -i\beta_k^{(2)\prime\prime}(x) + 2k\beta_k^{(2)\prime}(x) + (\beta_k^{(1)\prime}(x))^2 &= 0 \\ &\vdots \end{aligned} \tag{1.24}$$

with all the $\beta_k^{(i)}(x)$ and $\beta_k^{(i)'}(x)$ vanishing as $x \to \infty$. Then we have

$$\begin{aligned}\delta^{(1)}(k) &= -\mathrm{Re}\,\beta_k^{(1)}(0)\\ \delta^{(2)}(k) &= -\mathrm{Re}\,\beta_k^{(2)}(0)\\ &\vdots\end{aligned} \tag{1.25}$$

In the numerical integration routine, all required orders of β_k may be assembled into one vector, so that all the required orders of the Born approximation are computed simultaneously with a single pass. The result is a system of coupled linear differential equations with sources for the $\beta^{(i)}$. The potential $\sigma(x)$ acts as the source for $\beta^{(1)}$. For the higher $\beta^{(i)}$, the source is calculated from all the $\beta^{(j)}(x)$ with $j < i$.

References

1. S. Coleman, *Aspects of Symmetry*. Cambridge University Press, 1985. 1, 3
2. R. Rajaraman, *Solitons and Instantons*. North Holland, 1982. 1
3. R. F. Dashen, B. Hasslacher, and A. Neveu, *Phys. Rev.* **D10** (1974) 4114. 1, 2
4. H. Weigel, *Chiral Soliton Models for Baryons*. Springer–Lecture Notes in Physics, Vol. 743, 2008. 1
5. B. Moussallam and D. Kalafatis, *Phys. Lett.* **B272** (1991) 196. 1
6. F. Meier and H. Walliser, *Phys. Rept.* **289** (1997) 383. 1
7. A. Achucarro and T. Vachaspati, *Phys. Rept.* **327** (2000) 347. 1
8. N. Graham, M. Quandt, O. Schröder, and H. Weigel, *Nucl. Phys.* **B758** (2006) 112. 1
9. H. B. G. Casimir, *Indag. Math.* **10** (1948) 261. 2
10. V. M. Mostepanenko and N. N. Trunov, *The Casimir Effect and its Applications*. Clarendon Press, Oxford, UK, 1997. 2
11. K. A. Milton, *The Casimir Effect: Physical Manifestations of Zero-Point Energy*. World Scientific, River Edge, USA, 2001. 2
12. R. L. Jaffe, *Phys. Rev.* **D72** (2005) 021301. 2
13. N. Graham et al., *Nucl. Phys.* **B645** (2002) 49. 2, 6
14. J. Schwinger, *Phys. Rev.* **94** (Jun, 1954) 1362. 2
15. M. Li and R. J. Perry, *Phys. Rev.* **D37** (1988) 1670. 2
16. B. Moussallam, *Phys. Rev.* **D40** (1989) 3430. 2
17. J. Baacke, *Z. Phys.* **C47** (1990) 263. 2
18. J. Baacke, *Z. Phys.* **C53** (1992) 402. 2
19. D. Ebert and H. Reinhardt, *Nucl. Phys.* **B271** (1986) 188. 2
20. I. G. Avramidi, *Nucl. Phys.* **B355** (1991) 712. 2
21. I. G. Avramidi, *J. Math. Phys.* **36** (1995) 5055. 2
22. J. A. Zuk, *Phys. Rev.* **D43** (1991) 1358. 3
23. M. Bordag, *J. Phys.* **A28** (1995) 755. 3
24. M. Bordag and K. Kirsten, *Phys. Rev.* **D53** (1996) 5753. 3
25. M. Bordag and K. Kirsten, *Phys. Rev.* **D60** (1999) 105019. 3
26. M. Bordag, M. Hellmund, and K. Kirsten, *Phys. Rev.* **D61** (2000) 085008. 3
27. H. Gies and K. Langfeld, *Nucl. Phys.* **B613** (2001) 353. 3

28. H. Gies and K. Langfeld, *Int. J. Mod. Phys.* **A17** (2002) 966. 3
29. K. Langfeld, L. Moyaerts, and H. Gies, *Nucl. Phys.* **B646** (2002) 158. 3
30. H. Gies, K. Langfeld, and L. Moyaerts, *JHEP* **06** (2003) 018. 3
31. D. Cangemi, E. D'Hoker, and G. V. Dunne, *Phys. Rev.* **D51** (1995) 2513. 3
32. G. V. Dunne, *Phys. Lett.* **B467** (1999) 238. 3
33. L.-H. Chan, *Phys. Rev.* **D55** (1997) 6223. 3
34. I. J. R. Aitchison and C. M. Fraser, *Phys. Lett.* **B146** (1984) 63. 3
35. I. J. R. Aitchison and C. M. Fraser, *Phys. Rev.* **D31** (1985) 2605. 3
36. J. A. Bagger and S. G. Naculich, *Phys. Rev. Lett.* **67** (1991) 2252. 3
37. J. A. Bagger and S. G. Naculich, *Phys. Rev.* **D45** (1992) 1395. 3
38. A. Parnachev and L. G. Yaffe, *Phys. Rev.* **D62** (2000) 105034. 3
39. G. V. Dunne, J. Hur, and C. Lee, *Phys. Rev.* **D74** (2006) 085025. 3
40. G. V. Dunne, J. Hur, C. Lee, and H. Min, *Phys. Rev.* **D77** (2008) 045004. 3
41. R. J. Perry, *Nucl. Phys.* **A467** (1987) 717. 3, 11
42. R. L. Jaffe and A. Scardicchio, *Phys. Rev. Lett.* **92** (2004) 070402. 3
43. A. Scardicchio and R. L. Jaffe, *Nucl. Phys.* **B704** (2005) 552. 3
44. A. Scardicchio and R. L. Jaffe, *Nucl. Phys.* **B743** (2006) 249. 3
45. K. Chadan and P. C. Sabatier, *Inverse Problems in Quantum Scattering Theory*. Springer, New York, 1977. 7
46. R. G. Newton, *Scattering Theory of Waves and Particles*. Springer, New York, 1982. 7
47. A. Rebhan and P. van Nieuwenhuizen, *Nucl. Phys.* **B508** (1997) 449. 10
48. F. Calegero, *Variable Phase Approach to Potential Scattering*. Academic Press, New York and London, 1967. 11

2 Review of Scattering Theory

As we have seen in the introduction, the tools of scattering theory—phase shifts, bound states, and the Born approximation—are central to our calculational techniques. In this chapter, we develop these tools and derive the key results we will need. We focus particularly on the use of the analytic structure of the scattering data to efficiently compute the Green and Jost functions.

For those readers who are more interested in field theory applications, much of the technical discussion in this chapter can be skipped on a first reading. More comprehensive discussion of these subjects can be found in standard references on scattering theory, such as [1, 2].

2.1 Scattering Theory in Arbitrary Dimension

Our ultimate goal is to apply scattering theory to calculations in quantum field theory. Because we will cut off the divergences of quantum field theory using dimensional regularization, it will be important to us to be able to carry out scattering theory calculations in arbitrary dimensions with generalized spherical symmetry. Our starting point is the time-independent Schrödinger equation for the wavefunction with energy $\omega = \pm\sqrt{k^2 + m^2}$ in partial wave ℓ of a radially symmetric potential in n space dimensions,

$$-\psi'' + \frac{1}{r^2}\left(\alpha - \frac{1}{2}\right)\left(\alpha + \frac{1}{2}\right)\psi + \sigma(r)\psi - k^2\psi = 0\,, \tag{2.1}$$

where

$$\alpha = \ell - 1 + \frac{n}{2}.$$

To set up a regular scattering problem, we assume that the background potential σ is sufficiently localized, so that

$$\int_0^\infty r\sigma(r)dr < \infty\,. \tag{2.2}$$

Asymptotically, the scattered particles become free, and their behavior as $r \to \infty$ should be compared to the free outgoing spherical wave[1]

[1] Whenever a fractional power of k appears it should be considered as the limit $\mathsf{Im}\, k \searrow 0$.

Graham, N., et al.: *Review of Scattering Theory*. Lect. Notes Phys. **777**, 15–32 (2009)
DOI 10.1007/978-3-642-00139-0_2

$$w_\ell(kr) = (-1)^{\alpha+1}\sqrt{\frac{\pi}{2}kr}\,\left[J_\alpha(kr) + iY_\alpha(kr)\right]\,, \tag{2.3}$$

where J_α and Y_α are the Bessel functions of first and second kind, respectively [3]. Next we define various solutions to Eq. (2.1) that only differ in the boundary conditions that they obey:

– The *Jost solution*, $f_\ell(k,r)$. It behaves like an outgoing wave at $r \to \infty$, with

$$\lim_{r\to\infty} \frac{f_\ell(k,r)}{w_\ell(kr)} = 1\,. \tag{2.4}$$

For $k \neq 0$ the two solutions $f_\ell(\pm k, r)$ are linearly independent because their Wronskian is non-zero.

– The *regular solution*, $\phi_\ell(k,r)$. It is defined by its k-independent behavior near the origin[2]

$$\lim_{r\to 0} \frac{\Gamma(\alpha+1)}{\sqrt{\pi}} \left(\frac{r}{2}\right)^{-(\alpha+\frac{1}{2})} \phi_\ell(k,r) = 1\,, \tag{2.5}$$

which determines this solution uniquely. The k-independence implies that $\phi_\ell(k,r)$ is an even function of k (since the Schrödinger equation is) and holomorphic in k for all radii r. By completeness, ϕ_ℓ can be represented as a linear combination of the two Jost solutions,

$$\phi_\ell(k,r) = \frac{i}{2}\left[k^{-\alpha-\frac{1}{2}} F_\ell(k) f_\ell(-k,r) + (-k)^{-\alpha-\frac{1}{2}} F_\ell(-k) f_\ell(k,r)\right]\,. \tag{2.6}$$

When evaluating fractional exponents in Eq. (2.6), k and $-k$ must be connected by paths in the upper-half k-plane (see property (1) below) [2]. The coefficient function is called the *Jost function*; it can be computed from the Wronskian of ϕ_ℓ and f_ℓ. Alternatively, it can also be read off from the asymptotic behavior of the Jost solution $f_\ell(k,r)$ near the origin,

$$F_\ell(k) = \lim_{r\to 0} \frac{f_\ell(k,r)}{w_\ell(kr)}\,. \tag{2.7}$$

– The *physical scattering solution*, $\psi_\ell(k,r)$. It is also regular at the origin and thus proportional to $\phi_\ell(k,r)$, but differently normalized:

$$\psi_\ell(k,r) = \frac{k^{\alpha+\frac{1}{2}}}{F_\ell(k)} \phi_\ell(k,r)\,. \tag{2.8}$$

The reason for distinguishing two regular solutions is that ϕ_ℓ has a simple boundary condition at $r = 0$, while ψ_ℓ has a *physical* boundary condition at $r \to \infty$: For $k > 0$, the representation

[2] The symmetric channel in one spatial dimension is different and must be discussed separately.

$$\psi_\ell(k,r) = \frac{i}{2}\left[f_\ell(-k,r) + e^{-(\alpha+\frac{1}{2})\pi}\frac{F_\ell(-k)}{F_\ell(k)}f_\ell(k,r)\right] \tag{2.9}$$

combined with Eq. (2.4) implies that ψ_ℓ has an asymptotic description in terms of incoming and outgoing spherical waves. The prefactor of the outgoing wave is the *scattering matrix*

$$S_\ell(k) \equiv \frac{F_\ell(-k)}{F_\ell(k)}\,. \tag{2.10}$$

From $F_\ell(-k^*) = F_\ell^*(k)$, we conclude that $S_\ell(k)$ must be a pure phase when k becomes real, and the *phase shift* $\delta_\ell(k) = \frac{1}{2i}\ln S_\ell(k)$ is thus identified with the (negative) phase of the Jost function

$$F_\ell(k) = |F_\ell(k)|\exp\left[-i\delta_\ell(k)\right] \qquad \text{for} \qquad k \in \mathbb{R}\,. \tag{2.11}$$

We list the most important analytic properties of the scattering solutions without proof. For more details the interested reader is referred to the literature [1, 2].

The regular and Jost solutions are bound by

$$\begin{aligned} |\phi_\ell(k,r)| &< C\left(\frac{r}{1+|k|r}\right)^{\alpha+\frac{1}{2}} \mathrm{e}^{r\,|\mathsf{Im}\,k|}, \\ |f_\ell(k,r)| &< K\left(\frac{r}{1+|k|r}\right)^{-\alpha+\frac{1}{2}} \mathrm{e}^{-r\mathsf{Im}k}\,. \end{aligned} \tag{2.12}$$

The positive constants C and K are independent of k and r. In particular, the regular solution is an *entire* function of k for all r, and the Jost solution is *holomorphic* in the upper complex k-plane, where $\mathsf{Im}\,k > 0$. For our approach, the most important quantity is the Jost function $F_\ell(k)$, which has the following properties [1, 2]:

1. the Jost function is holomorphic in the upper complex k-plane, where $\mathsf{Im}\,k > 0$;
2. the Jost function is symmetric under complex conjugation, $F_\ell(-k^*) = F_\ell^*(k)$;
3. the Jost function approaches unity as $|k| \to \infty$ everywhere in the upper complex k-plane. In particular, this implies $\lim\limits_{k\to\infty}\delta_\ell(k) = 0$ when $\mathsf{Im}\,k \searrow 0$;
4. the roots of the Jost function in the upper complex k-plane are simple and located on the imaginary axis, $k_j = i\kappa_i$ with $\kappa_j \in \mathbb{R}$. They correspond to the bound state energies $\omega_j = \sqrt{m^2 - \kappa_j^2}$ in the Schrödinger Eq. (2.1).

2.2 Green's Functions from Scattering Data

We now apply the technical machinery sketched in the last section to find efficient computation methods for the scattering data that enter the phase shift approach to quantum field theory. We begin with the *Green's function*, which is most commonly written in terms of the physical solution as

$$G_\ell(r,r';k) = -\frac{2}{\pi}\int_0^\infty dq\,\frac{\psi_\ell^*(q,r)\psi_\ell(q,r')}{(k+i\epsilon)^2-q^2} - \sum_j \frac{\psi_{\ell,j}(r)\psi_{\ell,j}(r')}{k^2+\kappa_j^2}\,. \tag{2.13}$$

The $i\epsilon$ prescription has been chosen such that the Green's function is meromorphic in the upper complex k-plane with simple poles at the bound state momenta $k = i\kappa_j$. However, the Green's function can also be rewritten as

$$G_\ell(r,r',k) = \frac{\phi_\ell(k,r_<)f_\ell(k,r_>)}{F_\ell(k)}(-k)^{\alpha-\frac{1}{2}}\,, \tag{2.14}$$

where $r_<$ ($r_>$) is the smaller (larger) of the arguments r and r', respectively. This expression has its (simple) poles precisely at the zeros of the Jost function, which are the imaginary bound state momenta. Thus both representations, Eqs. (2.13) and (2.14), have the same analytic structure in the upper complex k-plane, the same asymptotics as $|k| \to \infty$, and they both solve the same inhomogeneous differential equation, so they must be identical.

The form (2.14) is not yet suited for an efficient numerical evaluation. Although G_ℓ is analytic in the upper half-plane, f_ℓ and ϕ_ℓ contain pieces that oscillate for real k and exponentially decrease and increase, respectively, in the upper complex k-plane. We will eventually be interested in the case $r = r'$, whence the exponential factors in the product $f_\ell \cdot \phi_\ell$ cancel. Numerically, however, such a cancellation of large numbers is unstable and involves a substantial loss of precision. A better strategy is to factor out the dangerous exponential components with the following *ansatz*,[3]

$$\begin{aligned} f_\ell(k,r) &\equiv w_\ell(kr)g_\ell(k,r) \\ \phi_\ell(k,r) &\equiv \frac{(-k)^{-\alpha+\frac{1}{2}}}{2\alpha}\frac{h_\ell(k,r)}{w_\ell(kr)}\,, \end{aligned} \tag{2.15}$$

where $w_\ell(kr)$ is the free Jost solution introduced above. Notice that $g_\ell(k,r)$ is the ratio of the interacting and free Jost solution. In view of (2.7), we have the smooth limit

$$\lim_{r\to 0} g_\ell(k,r) = F_\ell(k)\,. \tag{2.16}$$

[3] For $n = 1$ and $n = 2$, the s-wave channel $\ell = 0$ is somewhat different and requires special treatment.

With these definitions,

$$G_\ell(r,r,k) = \frac{h_\ell(k,r)\, g_\ell(k,r)}{2\alpha\, g_\ell(k,0)}\,. \tag{2.17}$$

The two functions g_ℓ and h_ℓ are holomorphic in the upper complex k-plane and, most importantly, they are bounded according to

$$\begin{aligned} |g_\ell(k,r)| &\le \text{const.}\,, \\ |h_\ell(k,r)| &\le \text{const.}\,\frac{2\alpha r}{1+|k|r}\,, \end{aligned} \tag{2.18}$$

so that neither g_ℓ nor h_ℓ grow exponentially during the numerical integration. Thus the representation of the partial wave Green's function in terms of g_ℓ and h_ℓ is numerically tractable on the positive imaginary axis. After analytically continuing to $k = it$, the function $g_\ell(it,r)$ obeys

$$g_\ell''(it,r) = 2t\,\xi_\ell(tr)\, g_\ell'(it,r) + \sigma(r) g_\ell(it,r)\,, \tag{2.19}$$

with the boundary conditions

$$\lim_{r\to\infty} g_\ell(it,r) = 1 \qquad \text{and} \qquad \lim_{r\to\infty} g_\ell'(it,r) = 0\,. \tag{2.20}$$

Here the prime indicates a derivative with respect to the radial coordinate r. Using these boundary conditions, the differential equation is integrated numerically for $g_\ell(it,r)$, starting at $r=\infty$ and proceeding to $r=0$. For real τ, the function

$$\xi_\ell(\tau) \equiv -\frac{d}{d\tau}\ln\left[w_\ell(i\tau)\right] \tag{2.21}$$

entering the differential equation is real with $\lim_{\tau\to\infty}\xi_\ell(\tau) = 1$, so that $g_\ell(it,r)$ (and also $h_\ell(it,r)$ that will appear below) are manifestly real. The key ingredient for the computation of quantum corrections is the function

$$\nu_\ell(t) \equiv \lim_{r\to 0} g_\ell(it,r)\,. \tag{2.22}$$

The second function $h_\ell(it,r)$ obeys a similar equation

$$h_\ell''(it,r) = -2t\,\xi_\ell(tr)\, h_\ell'(it,r) + \left[\sigma(r) - 2t^2\,\frac{d\xi_\ell(\tau)}{d\tau}\bigg|_{\tau=tr}\right] h_\ell(it,r)\,, \tag{2.23}$$

with the boundary conditions

$$h_\ell(it,0) = 0 \qquad \text{and} \qquad h_\ell'(it,0) = 1\,. \tag{2.24}$$

This system of equations for $h_\ell(it,r)$ has to be integrated numerically from $r=0$ to $r=\infty$.

Our field theory applications will require us to compute these quantities both exactly and approximately as a Born expansion in powers of the

potential. Fortunately, the computation of the Born approximations is also straightforward in this formalism. We expand the solutions to the differential Eqs.(2.19) and (2.23) about the free solutions,

$$g_\ell(it,r) = 1 + g_\ell^{(1)}(it,r) + g_\ell^{(2)}(it,r) + \cdots , \tag{2.25}$$

$$h_\ell(it,r) = 2\alpha r I_\alpha(tr) K_\alpha(tr) + h_\ell^{(1)}(it,r) + h_\ell^{(2)}(it,r) + \cdots , \tag{2.26}$$

where the superscript labels the order of the background potential $\sigma(r)$ and $I_\alpha(z)$ and $K_\alpha(z)$ are modified Bessel functions. Higher order approximations obey inhomogeneous linear differential equations with the boundary conditions

$$\lim_{r\to\infty} g_\ell^{(j)}(it,r) = 0 \quad \text{and} \quad \lim_{r\to\infty} g_\ell^{(j)\prime}(it,r) = 0, \tag{2.27}$$

$$h_\ell^{(j)}(it,0) = 0 \quad \text{and} \quad h_\ell^{(j)\prime}(it,0) = 0\,. \tag{2.28}$$

In these equations σ is the source term for $g^{(1)}$, $\sigma g^{(1)}$ is the source term for $g^{(2)}$, and so on. We thus obtain a coupled system of linear differential equations, which can be solved in a single numerical integration pass.

The differential equation system (2.19), (2.23), and its Born iterations are the central calculations needed to obtain the Green's function Eq. (2.13), which enters the energy density, and the Jost function Eq. (2.22), which enters the total energy. For computations on the real k-axis, these formulae can be rotated back to yield the variable phase approach discussed in the introduction.

2.3 Phase Shifts and Density of States

A central quantity that we will use in our investigations is the *density of states*. For a system with a discrete spectrum, the density of states in partial wave ℓ would be

$$\rho_\ell(k) = \sum_n \delta(k - k_{\ell,n})\,, \tag{2.29}$$

where $k_{\ell,n}$ are the wave numbers of the discrete solutions and the right-hand side is a sum of Dirac delta functions. To convert this result to an expression suitable for analysis in the continuum, we rewrite it as

$$\rho_\ell(k) = \lim_{\epsilon\to 0} \sum_n \frac{1}{\pi} \mathsf{Im} \frac{1}{k - k_n - i\epsilon}\,. \tag{2.30}$$

Using Eq. (2.13), we have the density of scattering states

$$\rho_\ell(k) = \frac{2k}{\pi} \mathsf{Im} \int_0^\infty dr\, G_\ell(r,r,k)\,, \tag{2.31}$$

which is valid only as a formal expression, since it contains singularities as the arguments of the Green's function coincide. As expected from Eq. (1.9), ρ_ℓ is proportional to the volume, which is infinite in the continuum limit. However, the difference between the density of states in the interacting and the free theories,

$$\rho_\ell(k) - \rho_\ell^{(0)}(k) = \frac{2k}{\pi}\,\mathsf{Im}\int_0^\infty dr\,(G_\ell(r,r,k) - G_\ell^{(0)}(r,r,k))\,, \tag{2.32}$$

remains finite in the continuum limit. Here $G^{(0)}$ represents the free Green's function. To make the integral on the right-hand side well defined, we require a particular prescription, which we will now explain. In doing so, we moreover relate the density of states to scattering results we have derived above. In particular, we demonstrate a key relation between the integral over space of the Green's function and the Jost function,

$$\frac{2k}{i}\int_0^\infty dr\,\left[G_\ell(r,r,k) - G_\ell^{(0)}(r,r,k)\right] = i\frac{d}{dk}\ln F_\ell(k)\,, \tag{2.33}$$

which is valid everywhere in the upper half-plane $\mathsf{Im}\,k > 0$, where the spatial integral is indeed well defined.

We start by differentiating the Wronskian of the Jost solution, $f_\ell(k,r)$, and the regular solution, $\phi_\ell(k',r)$ [4],

$$\frac{d}{dr}W\left[f_\ell(k,r),\phi_\ell(k',r)\right] = \left(k^2 - k'^2\right) f_\ell(k,r)\phi_\ell(k',r), \tag{2.34}$$

where all quantities in this relation are analytic for $\mathsf{Im}\,k > 0$. We integrate both sides from $r = 0$ to $r = R$. Since the regular solution $\phi_\ell(k,r)$ becomes k-independent at small r, we can compute the boundary term at $r = 0$ by replacing k' with k and using the standard Wronskian,

$$W[f_\ell(k,r),\phi_\ell(k,r)] = (-k)^{\frac{1}{2}-\alpha}\,F_\ell(k)\,, \tag{2.35}$$

giving

$$W\left[f_\ell(k,R),\phi_\ell(k',R)\right] = (-k)^{\frac{1}{2}-\alpha}\,F_\ell(k) + \left(k^2 - k'^2\right)\int_0^R dr\,f_\ell(k,r)\phi_\ell(k',r)\,. \tag{2.36}$$

Next we differentiate with respect to k, set $k' = k$, and use the representation (2.14) for the Green's function to obtain

$$\frac{(-k)^{\alpha-\frac{1}{2}}}{F_\ell(k)}W\left[\dot f_\ell(k,R),\phi_\ell(k,R)\right] = \frac{\alpha-\frac{1}{2}}{k} + \frac{\dot F_\ell(k)}{F_\ell(k)} + 2k\int_0^R dr\,G_\ell(r,r,k)\,, \tag{2.37}$$

where $\dot f_\ell(k,R) \equiv \frac{d}{dk}f_\ell(k,R)$ and $\dot F_\ell(k) \equiv \frac{d}{dk}F_\ell(k)$. To eliminate the first term on the right-hand side, we subtract the same equation for the non-interacting case, giving

$$\frac{(-k)^{\alpha-\frac{1}{2}}}{F_\ell(k)} W\left[\dot{f}_\ell(k,R),\phi_\ell(k,R)\right] - (-k)^{\alpha-\frac{1}{2}}\, W\left[\dot{f}_\ell^{(0)}(k,R),\phi_\ell^{(0)}(k,R)\right] = \frac{\dot{F}_\ell(k)}{F_\ell(k)} + 2k\int_0^R dr\, \left[G_\ell(r,r,k) - G_\ell^{(0)}(r,r,k)\right] . \quad (2.38)$$

To complete the proof of Eq. (2.33), we have to show that the left-hand side of Eq. (2.38) vanishes as $R \to \infty$. To see this, we write the boundary condition (2.4) for the Jost solution in the form

$$f_\ell(k,R) = w_\ell(kR)\, \left[1 + \mathscr{O}(R^{-1})\right] , \qquad R \to \infty, \quad (2.39)$$

which can also be inferred from the integral equation obeyed by $f_\ell(k,r)$. Differentiating with respect to k and using the asymptotics of the free Jost solution $w_\ell(kR)$,

$$\dot{w}_\ell(kR) = \frac{d}{dk}\, w_\ell(kR) = iR\, w_\ell(kR)\, \left[1 + \mathscr{O}(R^{-2})\right] ,$$

it is easy to show the asymptotic behavior

$$\dot{f}_\ell(k,R) = iR\, f_\ell(k,R)\, \left[1 + \mathscr{O}(R^{-2})\right] . \quad (2.40)$$

The first term on the left-hand side of Eq. (2.38) can thus be estimated by

$$\begin{aligned} &\frac{(-k)^{\alpha-\frac{1}{2}}}{F_\ell(k)}\, W[\dot{f}_\ell(k,R),\phi_\ell(k,R)] = \\ &i\frac{(-k)^{\alpha-\frac{1}{2}}}{F_\ell(k)}\, \{R\, W[f_\ell(k,R),\phi_\ell(k,R)] - \, f_\ell(k,R)\phi_\ell(k,R)\}\, \left[1 + \mathscr{O}(R^{-2})\right] \\ &= -i\, [R + G_\ell(R,R,k)]\, \left[1 + \mathscr{O}(R^{-2})\right] , \end{aligned} \quad (2.41)$$

where we have used the Wronskian of f_ℓ and ϕ_ℓ and the definition of the Green's function, Eq. (2.14). Subtracting the analogous equation in the free case, the term proportional to R drops out and we are left with

$$\frac{(-k)^{\alpha-\frac{1}{2}}}{F_\ell(k)} W\left[\dot{f}_\ell(k,R),\phi_\ell(k,R)\right] - (-k)^{\alpha-\frac{1}{2}}\, W\left[\dot{f}_\ell^{(0)}(k,R),\phi_\ell^{(0)}(k,R)\right] = -i\left[G_\ell(R,R,k) - G_\ell^{(0)}(R,R,k)\right]\, \left[1 + \mathscr{O}(R^{-1})\right] . \quad (2.42)$$

We estimate the large-R behavior of the difference $\Delta_\ell(k,R) \equiv G_\ell(R,R,k) - G_\ell^{(0)}(R,R,k)$ from Eqs. (2.42) and (2.38),

$$-\, i\, \Delta_\ell(k,R)\, [1 + \mathscr{O}(R^{-1})] = \frac{\dot{F}_\ell(k)}{F_\ell(k)} + 2k\int_0^R dr\, \Delta_\ell(k,r)\, . \quad (2.43)$$

From the bounds Eq. (2.12) we infer that the left-hand side of Eq. (2.43) is finite for any R. Thus the integral on the right-hand side must be finite,

which in particular enforces $\Delta_\ell(k,R) \to 0$ in the limit $R \to \infty$ with $\mathrm{Im}k > 0$. This completes the proof of Eq. (2.33).

We can extract further information from the above integral equation. At large R, the leading order solution is $\Delta_\ell(k,R) \propto \exp(2ikR)$. This suggests the product *ansatz* $\Delta_\ell(k,R) = \widetilde{\Delta}_\ell(k,R)\exp(2ikR)$. The integral equation and the bounds, Eq. (2.12), enforce $\widetilde{\Delta}_\ell(k,R)$ to be a rational function; it cannot be an exponential. In particular on the real axis $\widetilde{\Delta}_\ell(k,R)$ must be bounded, so that $\lim_{R\to\infty}\widetilde{\Delta}_\ell(k,R) = C_\ell(k)$, where $C_\ell(k)$ is an R-independent integration constant. Therefore, we find for $k \in \mathbb{R}$,

$$\frac{\dot{F}_\ell(k)}{F_\ell(k)} + 2k\int_0^R dr\,\left[G_\ell(r,r,k) - G_\ell^{(0)}(r,r,k)\right] = C_\ell(k)\exp(2ikR)\left[1+\mathscr{O}(R^{-1})\right], \tag{2.44}$$

which oscillates as $R \to \infty$. As is typical for continuum problems, we must specify that the limit where k becomes real is taken *after* computing the spatial integral to eliminate the contribution from these oscillations at the upper limit of integration. Finally we relate the Jost function to the phase shift by Eq. (2.11). Taking the imaginary part of Eq. (2.33) and using Eq. (2.30) yields the relationship between the density of states and the phase shift,

$$\frac{1}{\pi}\frac{d\delta_\ell}{dk} = \frac{2k}{\pi}\mathsf{Im}\int_0^\infty \left(G_\ell(r,r,k+i\epsilon) - G_\ell^{(0)}(r,r,k+i\epsilon)\right)dr = \rho_\ell(k) - \rho_\ell^{(0)}(k)\,. \tag{2.45}$$

We can also rewrite Eq. (2.45) as

$$\frac{2}{\pi}\int_0^\infty dr\,\left(\psi_\ell^*(k,r)\psi_\ell(k,r) - \psi_\ell^{(0)*}(k,r)\psi_\ell^{(0)}(k,r)\right) = \frac{1}{\pi}\frac{d\delta_\ell}{dk}\,. \tag{2.46}$$

As argued above, the momentum on the left-hand side is understood to be defined with the $i\epsilon$ prescription necessary to keep the spatial integral well defined.

2.4 Levinson's Theorem and Finite Energy Sum Rules

The renormalization program we will carry out in the next chapter will require a set of *sum rules* relating bound state and scattering data, which include and generalize Levinson's theorem, Eq. (1.11). In their basic form, they were first derived by Puff [5] and they were later re-analyzed and extended in Ref. [6]. Here, we present a derivation of these formulae, including the special case of the symmetric channel in $n = 1$ space dimensions.

The sum rules are statements about the spectrum of the Schrödinger operator in potential scattering theory. They relate information from the continuous part of the spectrum—the phase shifts—to the bound state energies:

$$\int_0^\infty \frac{dk}{\pi}k^{2p}\frac{d}{dk}\left[\delta_\ell(k)\right]_q + \sum_j(-\kappa_{\ell,j}^2)^p = 0\,. \tag{2.47}$$

Here, ℓ is the angular momentum channel and $p, q \in \mathbb{N}$ are non-negative integers with $q \geq p$. The brackets denote the q-times Born subtracted phase shift,

$$[\delta_\ell(k)]_q = \delta_\ell(k) - \sum_{i=1}^{q} \delta_\ell^{(i)}(k)\,. \tag{2.48}$$

The roots of the Jost function $F_\ell(k)$ are located on the imaginary axis at $k = i\kappa_{\ell,j}$ $(j = 1, 2, \ldots)$; they correspond to *bound states* with energies $\omega_{\ell,j} = (m^2 - \kappa_{\ell,j}^2)^{\frac{1}{2}}$.

The sum rules in Eq. (2.47) hold in *any* number of space dimensions n, as long as the scattering wavefunction vanishes at $r = 0$. The only exception is the symmetric channel in $n = 1$, where instead the *derivative* of the wavefunction vanishes at the origin. This change has a profound impact on the analytic structure of scattering data, which underlies the sum rules. We will discuss the subtleties of the symmetric channel in Sect. 2.4.3 below.

2.4.1 Overview and Simplified Derivation

To understand the origin of the sum rules, consider first the case $p = q = 0$, which is Levinson's theorem. Our starting point is the integral

$$I_\ell = \int_{-\infty}^{\infty} dk\, \frac{\dot{F}_\ell(k)}{F_\ell(k)}\,, \tag{2.49}$$

where $F_\ell(k)$ is the Jost function introduced in Eq. (2.7) via the Jost solution $f_\ell(k, r)$. From the Schrödinger equation obeyed by $f_\ell(k, r)$ and its complex conjugate, it is easily seen that $F_\ell(-k) = F_\ell^*(k)$ for real k. If we write

$$F_\ell(k) = |F_\ell(k)|\, e^{-i\delta_\ell(k)}\,,$$

it immediately follows that the modulus $|F_\ell|$ is an even function of real k, while the phase shift $\delta_\ell(k)$ is odd. The integral in Eq. (2.49) thus becomes

$$I_\ell = (-2i) \int_0^{\infty} dk\, \frac{d\delta_\ell(k)}{dk}\,.$$

On the other hand, we can also evaluate I_ℓ by contour integration in the upper complex k-plane. The integration range on the real axis is closed by a large circle in the upper complex k-plane, as shown in Fig. 2.1. Since F_ℓ has simple roots at the bound state momenta $k = i\kappa_{\ell,j}$ on the imaginary axis, the function $\dot{F}_\ell(k)/F_\ell(k)$ has simple poles with unit residue at the bound states, with no other singularities in the upper complex k-plane. In addition, $F_\ell(k)$ goes to unity at large $|k|$, so $\dot{F}_\ell(k)/F_\ell(k)$ falls off as $|k|^{-2}$ in the upper complex plane, and the semi-circle at infinity in Fig. 2.1 does not contribute. By Cauchy's theorem,

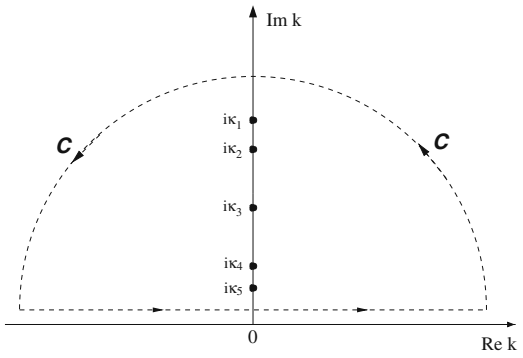

Fig. 2.1 The integration contour for Levinson's theorem and its generalizations

$$I_\ell = 2\pi i \ \mathrm{Res}\left\{\dot{F}_\ell(k)/F_\ell(k)\,;\ \mathsf{Im}\,k > 0\right\} = 2\pi i \sum_{j(\ell)} 1\,,$$

where $j(\ell)$ runs over the bound states in the ℓth partial wave. Combining the two expressions for I_ℓ gives Levinson's theorem

$$\int_0^\infty \frac{dk}{\pi}\,\frac{d\delta_\ell(k)}{dk} + \sum_{j(\ell)} 1 = 0\,, \tag{2.50}$$

or equivalently, $\delta(\infty) - \delta(0) = \pi n_\ell$, where n_ℓ is the number of bound states in channel ℓ.

It is clear that this derivation can be generalized: We could consider a starting integral with the function $\dot{F}_\ell/F_\ell$ replaced by $u(k)\,\dot{F}_\ell(k)/F_\ell(k)$, where $u(k)$ is *any* even function of k that is holomorphic in the upper complex plane. The only tricky point is to ensure that the semi-circle at infinity does not contribute; if this is the case, the general sum rule follows immediately,

$$\int_0^\infty \frac{dk}{\pi}\,u(k)\,\frac{d}{dk}\,[\delta_\ell(k)] + \sum_{j(\ell)} u(i\kappa_{\ell,j}) = 0\,. \tag{2.51}$$

The key point in the derivation of Eq. (2.47) is thus to compensate for the rise of $u(k) = k^{2p}$ by subtracting enough Born approximations from the Jost function or phase shifts, which improves the convergence at large $|k|$. In general, $q \geq p$ subtractions are required. The proof must also ensure that the Born subtractions do not interfere with the analytic structure of $\dot{F}_\ell(k)/F_\ell(k)$.

2.4.2 Proof of the Regular Sum Rules

To simplify the notation, we shall present the complete proof of the sum rules Eq. (2.47) for the *antisymmetric* channel in $n = 1$ and drop the channel index ℓ. In higher space dimensions n, the method of proof is unchanged;

some of the exponentials in the integral equations below must be replaced by Bessel functions and the corresponding bounds on the solution are slightly more complicated. Other than that, the generalization to all regular channels is straightforward.

We begin by parameterizing the Jost solution to the Schrödinger Eq. (2.1) in $n = 1$,

$$f(k,r) = \exp\left(ikr + i\beta(k,r)\right) . \tag{2.52}$$

The free Jost solutions are just plane waves e^{ikr} and the *Jost function* is $F(k) = f(k,0)$. Up to a factor of $-i$, the complex exponent $\beta(k,r)$ thus agrees with the logarithm of the Jost function. We already argued that $F(-k) = F^*(k)$ for real k. As a consequence, the (negative) phase of the Jost function—otherwise known as the *phase shift*—can be written as

$$\delta(k) = \frac{1}{2i}\left[\ln F(-k) - \ln F(k)\right] = -\mathsf{Re}\,\beta(k,0)\,. \tag{2.53}$$

To compute $\beta(k,0)$, we insert our parameterization into the Schrödinger Eq. (2.1). The result is an ordinary nonlinear differential equation

$$-i\beta''(k,r) + 2k\beta'(k,r) + \beta'^2(k,r) + \sigma(r) = 0\,, \tag{2.54}$$

where primes denote differentiation with respect to the radial coordinate, r. The scattered particle becomes free at large distances, $f(k,r) \to 1$ at $r \to \infty$. This result implies the boundary conditions

$$\beta(k,\infty) = 0 \qquad \text{and} \qquad \beta'(k,r)|_{r=\infty} = 0\,. \tag{2.55}$$

For the following, it is convenient to recast Eqs. (2.54) and (2.55) into a nonlinear integro-differential equation,

$$\beta(k,r) = \frac{1}{2k}\int_r^\infty ds\,\left(1 - e^{2ik(s-r)}\right)\Gamma(k,s), \tag{2.56}$$

where[4]

$$\Gamma(k,r) \equiv \beta'^2(k,r) + \sigma(r). \tag{2.57}$$

By differentiation, we find a similar equation for $\beta'(k,r)$,

$$\beta'(k,r) = i\int_r^\infty ds\, e^{2ik(s-r)}\Gamma(k,s). \tag{2.58}$$

Since $\beta(k,r)$ appears on both sides of these equations, we can start with $\Gamma(k,r) = \sigma(r)$ and $\beta^{(0)}(k,r) \equiv 0$ and solve for $\beta(k,r)$ by iteration. The result is a formal expansion in powers of the scattering potential $\sigma(r)$,

[4] For $n > 1$ space dimensions we merely need to modify the kernel $\Gamma(k,s)$ by a suitable combination of Bessel functions. Though similar in notation, this kernel should not be confused with (in)complete Gamma functions.

$$\beta(k,r) = \sum_{\nu=0}^{\infty} \beta^{(\nu)}(k,r)\,.$$

In view of Eq. (2.53), this expansion coincides with the usual *Born series*. The νth order Born term $\beta^{(\nu)}(k,r)$ obeys, from the iterated Eq. (2.56),

$$\beta^{(\nu)}(k,r) = \frac{1}{2k}\int_r^\infty ds\left(1-e^{2ik(s-r)}\right)\Gamma^{(\nu)}(k,s)\,. \tag{2.59}$$

Here, $\Gamma^{(\nu)}$ denotes the term in the expansion of Γ which is of νth order in the potential $\sigma(r)$. Notice that $\sigma(r)$ only appears explicitly at level $\nu = 1$, while higher orders $\Gamma^{(\nu)}$ involve only $\beta'^{(\mu)}$ with $\mu < \nu$.

The first few Born terms from this iteration are

$$\begin{aligned}
\beta^{(1)}(k) &= \frac{1}{2k}\int_0^\infty ds\,\left(1-e^{2iks}\right)\sigma(s)\,,\\
\beta^{(2)}(k) &= \frac{1}{2k}\int_0^\infty ds\,\left(1-e^{2iks}\right)[\beta'^{(1)}(k,s)]^2\,,\\
\beta^{(3)}(k) &= \frac{1}{2k}\int_0^\infty ds\,\left(1-e^{2iks}\right)2\beta'^{(1)}(k,s)\beta'^{(2)}(k,s)\,.
\end{aligned} \tag{2.60}$$

Similar relations can also be found for the derivatives, which appear as sources in Eqs. (2.60),

$$\begin{aligned}
\beta'^{(1)}(k,r) &= i\int_r^\infty ds\, e^{2ik(s-r)}\sigma(s)\,,\\
\beta'^{(2)}(k,r) &= i\int_r^\infty ds\, e^{2ik(s-r)}[\beta'^{(1)}(k,s)]^2\,,\\
\beta'^{(3)}(k,r) &= i\int_r^\infty ds\, e^{2ik(s-r)}2\beta'^{(1)}(k,s)\beta'^{(2)}(k,s)\,.
\end{aligned} \tag{2.61}$$

The exponential factors in Eq. (2.59) guarantee that $\beta^{(\nu)}(k,r)$ is analytic in the upper complex k-plane provided that $\Gamma^{(\nu)}$ is, and the same holds for $\beta'^{(\nu)}(k,r)$. Starting with $\Gamma^{(1)} = \sigma(r)$, we can now derive the analytical properties of $\beta^{(\nu)}$ and $\beta'^{(\nu)}$ by induction. For instance, the large $|k|$-behavior of $\beta^{(\nu)}$ follows from the respective integral equations by a simple integration by parts, which allows to estimate the remainder using the Riemann–Lebesgue lemma. For the value at the origin, $\beta^{(\nu)}(k) \equiv \beta^{(\nu)}(k,0)$, we find:

1. If the potential $\sigma(r)$ is regular and sufficiently short-ranged [1, 2], the function $\beta^{(\nu)}(k)$ is holomorphic in the upper half-plane including $k = 0$.
2. At large momenta $|k| \to \infty$ (again in the upper complex k-plane), $\beta^{(\nu)}(k)$ decays as $|k|^{-2\nu+1}$. Similarly $\beta'^{(\nu)}(k) = \frac{d\beta^{(\nu)}(k,r)}{dr}\Big|_{r=0}$ decays as $|k|^{-2\nu+2}$.

Finally, we define the approximate Jost function

$$F_q(k) \equiv \exp\left[i \sum_{\nu=1}^{q} \beta^{(\nu)}(k) \right] . \tag{2.62}$$

Notice that the Born series expands the *logarithm* of the Jost function, rather than the function itself. Thus, Eq. (2.62) gives the qth order Born approximation to $F(k)$, and its (negative) phase is consequently the phase shift in qth order Born approximation. Since $\beta^{(\nu)}(-k) = -\beta^{(\nu)*}(k)$ for real k (cf. Eq. (2.54)), we can again follow our previous steps and relate the phase shift to the exponents $\beta^{(\nu)}(k)$,

$$\delta_q(k) = -\mathsf{Re} \sum_{\nu=1}^{q} \beta^{(\nu)}(k) . \tag{2.63}$$

The analytical properties of $F_q(k)$ follow directly from those of $\beta^{(\nu)}(k)$ and the convergence of the Born series $\beta(k) = \sum_{\nu=1}^{\infty} \beta^{(\nu)}(k)$ at large $|k|$ in the upper half-plane [1, 2]:

(a) the Born approximation $F_q(k)$ is analytic and has no zeros in the upper complex k-plane including $k = 0$;

(b) the difference $|\ln F(k) - \ln F_q(k)|$ falls like $|k|^{-2q-1}$ as $|k| \to \infty$ in the upper complex k-plane.

With these analytic properties of scattering data at hand, it is now easy to prove the basic sum rule Eq. (2.47) as outlined in the last section. We start with the integral

$$\begin{aligned} I_{p,q} &\equiv \int_{-\infty}^{\infty} dk\, k^{2p} \frac{d}{dk} [\ln F(k) - \ln F_q(k)] \qquad (2.64) \\ &= \int_0^{\infty} dk\, k^{2p} \frac{d}{dk} [\ln F(k) - \ln F(-k) - \ln F_q(k) + \ln F_q(-k)] \\ &= -2i \int_0^{\infty} dk\, k^{2p} \frac{d}{dk} [\delta(k) - \delta_q(k)] = -2i \int_0^{\infty} dk\, k^{2p} \frac{d[\delta(k)]_q}{dk} . \end{aligned}$$

This integral can also be computed by contour integration as indicated in Fig. 2.1. The analytic property (b) above ensures that the integral along the semi-circle at $|k| \to \infty$ vanishes for $q \geq p$. Moreover, $d \ln F/dk$ has simple poles of unit residue at each bound state, and $d \ln F_q/dk$ is holomorphic in the upper k-plane (property (a) above). Therefore, Cauchy's theorem gives

$$I_{p,q} = 2\pi i \ \mathrm{Res} \left\{ k^{2p} \dot{F}(k)/F(k) \,;\, \mathsf{Im}\, k > 0 \right\} = 2\pi i \sum_j (i\kappa_j)^{2p} ,$$

as long as $q \geq p$. Together with Eq. (2.64), this result proves the basic sum rules Eq. (2.47).

2.4.3 The Symmetric Channel in One Dimension

The symmetric channel in one space dimension is special since the *derivative* of the scattering wavefunction vanishes at the origin rather than the wavefunction itself. As we will see, this change leads to subtleties that can introduce anomalous contributions to the sum rules when too many subtractions are attempted:

$$\int_0^\infty \frac{dk}{\pi}\, k^{2p} \frac{d}{dk} \left[\delta(k)\right]_q = -\sum_j (-\kappa_j^2)^p + I_{p,q}^{\text{anom}} \,. \tag{2.65}$$

As before, we need $q \geq p$ subtractions for the integral to converge. The anomalous term only arises when $q \geq 2p$. As a result, the "minimally subtracted" sum rules are non-anomalous, *except* for the case $p = q = 0$, which is Levinson's theorem. For that special case we will compute $I_{0,0}^{\text{anom}} = \frac{1}{2}$ and recover the modified theorem in the symmetric channel [7],

$$\int_0^\infty \frac{dk}{\pi} \frac{d}{dk} \delta(k) = \frac{1}{\pi}(\delta(\infty) - \delta(0)) = \frac{1}{2} - \sum_j 1 = \frac{1}{2} - n \,. \tag{2.66}$$

This formula seems to be incorrect for the trivial case of vanishing potential. In that case, however, there exists a "half-bound" state at $k = 0$ whose wavefunction approaches a constant (rather than a generic linear function) at large distances. In the contour integration that proves the sum rules, we must then avoid the bound state pole at $k = 0$ using a small semi-circle around the origin. Thus the integral picks up *half* the usual contribution from a bound state. Such states can occur in any channel, when a state is on the threshold of binding. Since the symmetric channel in one dimension has a bound state for an arbitrarily weak attractive potential (and no bound state for an arbitrarily weak repulsive potential), the free background is an example of this otherwise exceptional situation.

Next we turn to the proof of the anomalous sum rule Eq. (2.65). The regular solution to the Schrödinger equation obeys the boundary conditions $\phi'(k, 0) = 0$ and $\phi(k, 0) = 1$. Since the scattering wavefunction $\psi(k, r)$ is proportional to it, we can represent $\psi(k, r)$ in terms of the Jost solution

$$\psi(k, r) = \frac{1}{2ki} \left[G(k) f(-k, r) - G(-k) f(k, r)\right] \,, \tag{2.67}$$

where $G(k) \equiv \frac{df(k,r)}{dr}\Big|_{r=0}$ replaces the definition in Eq. (2.7). From the defining asymptotic behavior

$$\psi(k, r) \to e^{-ikr} + e^{2i\delta(k)} e^{ikr} \quad \text{for} \quad r \to \infty, \tag{2.68}$$

we now read off the phase shift,

$$\delta(k) = \frac{1}{2i} \left[\ln(-G(-k)) - \ln G(k) \right] . \tag{2.69}$$

So far, these relations look very similar to the antisymmetric channel, with the Jost function $F(k)$ replaced by $G(k)$. Using our previous parameterization (2.52) of the Jost solution, we find

$$G(k) = i(k + \beta'(k,0))\, e^{i\beta(k,0)} . \tag{2.70}$$

We will proceed as before and compute the integral in the sum rule (2.65) by contour integration. To eliminate the large circle in the upper k-plane (cf. Fig. 2.1), the Born approximation $\ln G_q(k)$ must again be subtracted. In view of Eq. (2.70), the correct Born approximation to $G(k)$ is therefore

$$\begin{aligned} \ln G_q(k) &= \lfloor \ln(k + \beta'(k)) \rfloor_q + \ln F_q(k) + \frac{\pi}{2} \\ &= \ln(k) + \lfloor \ln(1 + \frac{\beta'(k)}{k}) \rfloor_q + \ln F_q(k) + \frac{\pi}{2} , \end{aligned} \tag{2.71}$$

where the bracket notation "$\lfloor \ldots \rfloor_q$" indicates that all terms up to order q in the background potential should be *kept*, the complement of Eq. (2.48). As we will observe, the anomaly arises because $G_q(k)$ fails to be analytic at $k = 0$; instead, the threshold pole at $k = 0$ contributes with half its residuum, which is the anomaly. This situation can arise even for $q = 0$ because of the half-bound state in the non-interacting case. Using the analytic properties of $F_q(k)$, $\beta(k,r)$, and $\beta'(k,r)$ derived in the last section, it is now easy to verify that

(a) the Born approximation $G_q(k)$ is analytic and has no zeros in the upper complex k-plane except for $k = 0$;

(b) the difference $|\ln G(k) - \ln G_q(k)|$ decays like $|k|^{-2q-1}$ at large momenta $|k|$ in the upper complex k-plane;

(c) the function $k^{2p} d \ln G_q(k)/dk$ has a simple pole with residue $2I^{\rm anom}_{p,q}$ at $k = 0$. In the (symmetrized) contour integral this pole contributes with *half* its residue, i.e., $I^{\rm anom}_{p,q}$;

(d) The anomaly vanishes for $2p > q$.

To complete the analysis, we compute the residue from the singularity of $G_q(k)$ at $k = 0$. Only the first term in Eq. (2.71) is potentially singular, since we already established that $\ln F_q(k)$ is analytic at $k = 0$. Thus the only part of the integrand in Eq. (2.64) (now with the replacements $F(k) \to G(k)$ and $F_q(k) \to G_q(k)$) that may be singular at $k = 0$ arises from

$$k^{2p}\frac{d}{dk}\lfloor \ln(k+\beta'(k))\rfloor_q = k^{2p}\left\lfloor \frac{1+\frac{d\beta'(k)}{dk}}{k+\beta'(k)}\right\rfloor_q$$
$$= k^{2p-1}\left\lfloor \left(1+\frac{d\beta'(k)}{dk}\right)\sum_{t=0}^{\infty}\left(\frac{-\beta'(k)}{k}\right)^t\right\rfloor_q \quad (2.72)$$

Since the functions $\beta'^{(\nu)}(k)$ are all analytic near $k=0$, an anomalous contribution to the sum rule will only result if the prefactor k^{2p-1} is overcome by the $1/k$ terms in the sum on the right-hand side of Eq. (2.72). Note that the "$\lfloor\ldots\rfloor_q$" prescription terminates the sum over t. Though the particular upper limit depends on the order at which $\beta'(k)$ is considered, we have at least $t \le q$. The most singular term from that sum is $(-\beta'^{(1)}(k)/k)^q \sim k^{-q}$, which outweighs the prefactor k^{2p-1} if $q \ge 2p$. If $q = 2p$ the singularity is a simple pole at $k=0$; for $q > 2p$ there are poles of higher order as well. It is now straightforward (though increasingly tedious) to pull out the residue of the simple pole from Eq. (2.72), which is twice the anomalous contribution to the sum rule:

$$I^{\rm anom}_{p,q} = \frac{1}{2}\,\mathrm{Res}\left\{k^{2p-1}\left\lfloor\left(1+\frac{d\beta'(k)}{dk}\right)\sum_{t=0}^{\infty}\left(\frac{-\beta'(k)}{k}\right)^t\right\rfloor_q ; k=0\right\}. \quad (2.73)$$

Let us finally illustrate this result by looking at some important special cases:

$p = q = 0$: *Levinson's Theorem*
Since the zeroth order Born approximation vanishes, $\beta^{(0)}(k,r) \equiv 0$, the residue solely arises from the prefactor, which is just $1/k$ and we have $I^{\rm anom}_{0,0} = 1/2$. As mentioned above, this result is the modification of Levinson's theorem in the symmetric channel, Eq. (2.66) [7].

$p = q > 0$: *Minimal Subtraction*
This is the minimal number of subtractions which will render the integral in the sum rules finite. The most singular term in the sum on the right-hand side of Eq. (2.72) (through qth order in the potential) is proportional to $(-\beta'_1(0))^q/k^{q+1}$. Combined with the prefactor the integrand in the contour integral behaves as $k^{2p-1-q} = k^{p-1}$ near $k=0$. For $p = q > 0$, there is thus no threshold pole and $I^{\rm anom}_{p,p} = 0$: the minimally subtracted form of the sum rules is non-anomalous.

$2p > q$: *Oversubtraction Without Anomaly*
By the same argument as above, the most singular term in the integrand now behaves as k^{2p-1-q} near $k=0$, so that no anomaly arises even for oversubtractions, as long as $q < 2p$.

$q = 2p$: *Computation of the Anomaly*
In this case we have $I^{\rm anom}_{p,2p} = \frac{1}{2}\left[-\beta'^{(1)}(0)\right]^{2p}$. From the integral Eqs. (2.61), we have

$$\beta'^{(1)}(0) = i\int_0^\infty dr\,\sigma(r),$$

so that the anomaly takes the explicit form

$$I^{\rm anom}_{p,2p} = \frac{(-1)^p}{2}\left[\int_0^\infty dr\,\sigma(r)\right]^{2p} . \tag{2.74}$$

The first non-trivial application of this result is the $p = 1$ sum rule with two Born subtractions (i.e., one oversubtraction):

$$\int_0^\infty \frac{dk}{\pi}\,k^2\frac{d}{dk}\left[\delta(k) - \delta^{(1)}(k) - \delta^{(2)}(k)\right] = \sum_j \kappa_j^2 - \frac{1}{2}\left[\int_0^\infty dr\,\sigma(r)\right]^2 . \tag{2.75}$$

This relation was first discovered in Ref. [8] by direct evaluation of the Feynman graph corresponding to the second Born approximation. Here we see that it follows from a careful analysis of the analytic properties of the Born approximation near $k = 0$.

References

1. K. Chadan and P. C. Sabatier, *Inverse Problems in Quantum Scattering Theory*. Springer, New York, 1977. 15, 17, 27, 28
2. R. G. Newton, *Scattering Theory of Waves and Particles*. Springer, New York, 1982. 15, 16, 17, 27, 28
3. M. Abramowitz and I. A. Stegun, *Handbook of Mathematical Functions*. National Bureau of Standards, 1964. 16
4. R. G. Newton, Chapter 12.1. In *Scattering Theory of Waves and Particles*. Springer, New York, 1982. 21
5. R. D. Puff, *Phys. Rev.* **A11** (1975) 154. 23
6. N. Graham, R. L. Jaffe, M. Quandt, and H. Weigel, *Annals Phys.* **293** (2001) 240. 23
7. G. Barton, *J. Phys.* **A18** (1985) 479. 29, 31
8. N. Graham, R. L. Jaffe, M. Quandt, and H. Weigel, *Phys. Rev. Lett.* **87** (2001) 131601. 32

3 Quantum Field Theory and the Spectral Method

The techniques of quantum field theory are by now a standard topic in theoretical physics, but their realization in the spectral method is rather subtle. In this chapter, we begin with a review of standard results of quantum field theory and then show how spectral techniques apply in this context. We develop a general set of tools applicable both to calculations of the Casimir energy and to more general observables, such as the energy *density*, relevant for general relativity, or the *interface tension* of a brane-like background configuration. These subjects will be picked up in the applications.

3.1 Small-Amplitude Quantum Corrections

We begin by considering a single real boson φ in $d = (n + 1)$ spacetime dimensions, as discussed in the introduction. However, our methods can be applied to fermions as well; sign changes and some minor differences in the dimensional regularization and renormalization procedures are addressed in Sect. 3.6. Gauge couplings require some extra care; a detailed investigation can be found in the applications, cf.Sect. 8.2.

We consider the bare Lagrangian density

$$\mathscr{L} = \frac{1}{2}\partial_\mu\varphi\,\partial^\mu\varphi - \frac{m^2}{2}\,\varphi^2 - V(\varphi)\,, \tag{3.1}$$

with an interaction potential $V(\varphi)$. We are interested in the quantum contributions to the energy of a localized and time-independent background configuration $\varphi_0(\boldsymbol{x})$, which is either a solution to the classical equation of motion or held in place by an external source. In both cases, φ_0 is a stationary point of the classical action, with the (finite) classical energy $E_{\rm cl}$. The quantum fluctuations ϕ about the background φ_0 are described by the Lagrangian density

$$\mathscr{L} = \frac{1}{2}\partial_\mu\phi\,\partial^\mu\phi - \frac{m^2}{2}\,\phi^2 - \frac{1}{2}\,V''(\varphi_0(\boldsymbol{x}))\,\phi^2 + \cdots\,. \tag{3.2}$$

The leading quantum corrections to $E_{\rm cl}$ arise from the small-amplitude oscillations about φ_0; it is therefore permissible to truncate the Lagrangian, Eq. (3.2) at quadratic order. In this *harmonic* approximation, the background φ_0 acts as an external potential

Graham, N., et al.: *Quantum Field Theory and the Spectral Method*. Lect. Notes Phys. **777**, 33–61 (2009)
DOI 10.1007/978-3-642-00139-0_3

$$\sigma(\boldsymbol{x}) \equiv V''(\varphi_0(\boldsymbol{x})) \tag{3.3}$$

for the fluctuations ϕ. The soliton $\varphi_0(\boldsymbol{x})$ is assumed to be localized, and so the potential $\sigma(\boldsymbol{x})$ is localized as well and we may apply the approach developed in the previous chapter. The Lagrangian for the small-amplitude oscillations thus becomes

$$\mathscr{L} = \frac{1}{2}\partial_\mu\phi\,\partial^\mu\phi - \frac{1}{2}\left(m^2 + \sigma(\boldsymbol{x})\right)\phi^2 . \tag{3.4}$$

3.2 The Canonical Formalism

In the introduction we defined the vacuum energy as the formal expression Eq. (1.3), with the background potential entering through its distortion of the spectrum of small oscillations in the harmonic approximation. We also noted that this definition, if taken too literally, leads to subtle ambiguities that eventually render practical calculations all but meaningless. From a field theory point of view, a much better starting point is the energy *density* of the vacuum, defined unambiguously from the *VEV* (vacuum expectation value) of the energy-momentum tensor, $T_{\mu\nu}$.

The direct application of Noether's theorem gives the *canonical* form[1]

$$T_{\mu\nu} = \frac{\partial\mathscr{L}}{\partial(\partial^\mu\phi)}\,\partial_\nu\phi - g_{\mu\nu}\mathscr{L} . \tag{3.5}$$

For the simple boson model of Eq. (3.4), we obtain

$$T_{\mu\nu} = \partial_\mu\phi\,\partial_\nu\phi + \frac{1}{2}g_{\mu\nu}\left[-\partial_\alpha\phi\,\partial^\alpha\phi + \left(m^2 + \sigma(\boldsymbol{x})\right)\phi^2\right] . \tag{3.6}$$

Upon quantization, the *energy density* associated with small-amplitude vacuum fluctuations ϕ is thus given by the vacuum expectation value

$$\epsilon(\boldsymbol{x}, t) = \left\langle \Omega \left| \hat{T}_{00}(\boldsymbol{x}, t) \right| \Omega \right\rangle . \tag{3.7}$$

Here we denote the *true* vacuum (the lowest energy state) in the presence of a non-trivial background σ by $|\Omega\rangle$, while $|0\rangle$ is reserved for the *trivial* vacuum when $\sigma = 0$. The field ϕ in this formula is the canonically quantized

[1] If ϕ is generalized to be a gauge field, the analog of Eq. (3.5) is neither symmetric nor gauge invariant. Both deficiencies may be cured by adding a total derivative in such a way that both the integrated charges (energy and momentum) and their conservation is maintained. The resulting energy–momentum tensor can also be obtained directly either by varying the action with respect to the spacetime metric, as one does in general relativity (the only situation in which such total derivative terms are important) or by replacing the ordinary derivatives in the Noether definition by covariant ones.

field operator. As it stands, Eq. (3.7) is not yet well defined, since the short-distance divergences in the matrix element need to be renormalized by adding suitable counterterms to $\hat{T}_{00}$. We will discuss renormalization in greater detail in Sect. 3.6.

The vacuum *energy* is now simply the spatial integral over the density,

$$E_{\rm vac}(t) = \int d^n x\, \epsilon(\boldsymbol{x}, t)\,. \tag{3.8}$$

If the background potential σ is time dependent, the energy density ϵ will be as well. Furthermore, the classical conservation law for $T_{\mu\nu}$ translates into a *Ward identity* for the expectation value Eq. (3.7), which ensures that the vacuum energy is conserved, $\partial E_{\rm vac}/\partial t = 0$.

If the potential σ is derived from a soliton background, the energy $E_{\rm vac}$ represents the leading quantum correction to its mass or energy. In other applications, $E_{\rm vac}$ is the energy of the vacuum under the influence of external conditions that can be parameterized by σ, such as the Casimir force between two grounded plates in quantum electrodynamics. As will be shown in Chap. 7, the formalism of quantum field theory can be combined with the spectral method to gain new insight into Casimir problems as well.

As we have defined it, $E_{\rm vac}$ is $\mathscr{O}(\hbar)$. In quantum field theory language this is the *one-loop* contribution to the quantum energy.

Other methods to compute the vacuum energy $E_{\rm vac}$, such as the world-line formalism [1–4] or the derivative expansion [5–9], are often based on the effective *action* in Euclidean space, cf.Sect. 3.3. Formally, the result is an expression very similar to Eq. (3.8), in which $E_{\rm vac}$ is given as the space integral of some space-dependent density. In general, however, this action density will differ from the true energy density of the vacuum, Eq. (3.7), by a total derivative. This distinction can be important when comparing our method to other approaches.

3.2.1 The Vacuum Energy Density

Before starting with our derivation, we must emphasize one practical restriction of the spectral method: The general framework requires enough *symmetry* to separate the scattering problem into partial waves, so that we can apply the scattering theory techniques of the previous chapter. Though other methods are more general in this respect, for applications in particle physics, at least, most extended field configurations of interest tend to be highly symmetric. Moreover, the separation into partial waves may occur in larger spaces involving a combination of position space and isospin or other gauge quantum numbers. The restriction may even be relaxed to include coordinates in which the background field is translationally invariant, so that brane- or string-like configurations can be treated as well, cf. Sect. 8.2. If the spectral method

applies, it is of unrivaled efficiency and, unlike most other approaches, involves no approximations or systematic errors (beyond the basic one-loop truncation in Eq. (3.4)).

For the simple boson model at hand, we will assume that the interaction $\sigma(\boldsymbol{x})$ only depends on the radial coordinate $r = |\boldsymbol{x}|$. It is then clear that the energy density $\epsilon(\boldsymbol{x})$ will also be rotationally symmetric. We define $\epsilon(r)$ as the energy density in a spherical shell of radius r,

$$\epsilon(r) = \frac{2\pi^{n/2}}{\Gamma(\frac{n}{2})} r^{n-1} \langle \Omega | \hat{T}_{00}(x) | \Omega \rangle_{\text{ren}} \,. \tag{3.9}$$

The subscript "ren" indicates that the matrix element must be properly renormalized to find a finite and unambiguous answer. This procedure will be carried out in Sect. 3.6 by adding suitable counterterms. For the moment, we suppress their explicit appearance.

The canonical quantization of our model (3.4) proceeds along the standard lines: We define the canonical momentum by $\pi \equiv \partial \mathscr{L} / \partial \dot{\phi}$ and elevate the Hamiltonian to the operator quantity

$$\hat{H} = \frac{1}{2} \int d^3x \left[\hat{\pi}^2(t, \boldsymbol{x}) + (\nabla \hat{\phi}(t, \boldsymbol{x}))^2 + (m^2 + \sigma)\, \hat{\phi}^2(t, \boldsymbol{x}) \right] . \tag{3.10}$$

Next, the canonical *equal time commutation rules* must be imposed on the field operator and its conjugate momentum. The Heisenberg equations of motion become

$$\begin{aligned} i\, \partial_0 \hat{\phi}(t, \boldsymbol{x}) &= \left[\hat{\phi}(t, \boldsymbol{x}), \hat{H} \right] = i\, \hat{\pi}(\boldsymbol{x}, t) \\ i\, \partial_0 \hat{\pi}(t, \boldsymbol{x}) &= \left[\hat{\pi}(t, \boldsymbol{x}), \hat{H} \right] = i\, (\Delta - m^2 - \sigma(\boldsymbol{x}))\, \hat{\phi}(t, \boldsymbol{x}) \,. \end{aligned} \tag{3.11}$$

Finally, $\hat{\pi}(t, \boldsymbol{x})$ can be eliminated to find the expected equation of motion for the field operator,

$$\partial_0^2 \hat{\phi}(t, \boldsymbol{x}) = (\Delta - m^2 - \sigma(\boldsymbol{x}))\, \hat{\phi}(t, \boldsymbol{x}) \,. \tag{3.12}$$

Now we use the spherical symmetry of the background potential to carry out a partial wave decomposition,

$$\hat{\phi}(t, \boldsymbol{x}) = \sum_{\{\ell\}} \hat{\phi}_\ell(t, r)\, \mathscr{Y}_{\{\ell\}}(\hat{x}) \,, \tag{3.13}$$

where $\mathscr{Y}_{\{\ell\}}(\hat{x})$ are the n-dimensional spherical harmonics and $\{\ell\}$ refers to the set of all angular quantum numbers in n space dimensions. Upon inserting Eq. (3.13) in the field equation, the partial wave channels decouple and we obtain an infinite set of equations for the radial field operators $\hat{\phi}_\ell(t, r)$. We make a *Fock decomposition* and introduce creation and annihilation operators, $a_\ell^\dagger(k)$ and $a_\ell(k)$, via

$$\hat{\phi}_\ell(t,r) = r^{\frac{1-n}{2}} \int_0^\infty \frac{dk}{\sqrt{\pi\omega}} \left[\psi_\ell(k,r)\, e^{-i\omega t} a_\ell(k) + \psi_\ell^*(k,r)\, e^{i\omega t} a_\ell^\dagger(k)\right] + r^{\frac{1-n}{2}} \sum_j \frac{1}{\sqrt{2\omega_j}} \left[\psi_{\ell j}(r)\, e^{-i\omega_j t} a_{\ell j} + \psi_{\ell j}(r)\, e^{i\omega_j t} a_{\ell j}^\dagger\right], \quad (3.14)$$

where $\omega \equiv \sqrt{m^2+k^2}$ and $\omega_j = \sqrt{m^2-\kappa_j^2}$ are the scattering and bound state energies, respectively. The c-number wavefunctions $\psi_\ell(k,r)$ obey the time-independent Schrödinger equation (2.1) and form a complete set in each angular momentum channel ℓ,

$$\frac{2}{\pi}\int_0^\infty dk\, \psi_\ell^*(k,r)\psi_\ell(k,r') + \sum_j \psi_{\ell j}(r)\psi_{\ell j}(r') = \delta(r-r')\,, \quad (3.15)$$

where we have normalized the wavefunctions ψ_ℓ such that the creation and annihilation operators obey the standard commutation relations,

$$[a_\ell(k), a_{\ell'}^\dagger(k')] = \delta(k-k')\delta_{\ell\ell'}\,. \quad (3.16)$$

These relations ensure the usual particle interpretation: $a_\ell^\dagger(k)$ occupies a ψ_ℓ-mode of momentum k when acting on $|\Omega\rangle$.

Inserting the Fock decomposition into the energy density, Eq. (3.9), the result is most clearly expressed in terms of the *local spectral density*, $\rho_\ell(k,r)$, that is defined via the Green's function (2.13)

$$\rho_\ell(k,r) \equiv -2ik\, G_\ell(r,r;k)\,, \qquad \mathsf{Im}\, k \geq 0 \quad (3.17)$$

in the upper complex k-plane. The local density of scattering states is then obtained from $\rho_\ell(k,r)$ when k approaches the real axis from above,

$$\mathsf{Re}\,\rho_\ell(k,r) = \mathsf{Im}\,\{2k\, G_\ell(r,r;k)\} = 2\psi_\ell^*(k,r)\psi_\ell(k,r)\,, \quad \mathsf{Im}(k) \searrow 0\,. \quad (3.18)$$

Using that $\mathsf{Re}\,(G_\ell(r,r;k))$ and $\mathsf{Im}\,(G_\ell(r,r;k))$ are, respectively, even and odd functions of the (real) momentum parameter k in the differential equation (2.1), we obtain [10]

$$\epsilon(r) = \sum_\ell D(\ell) \int_{-\infty}^\infty \frac{dk}{2\pi i}\omega \left[1 + \frac{1}{4\omega^2} D_r\right] k G_\ell(r,r,k) + \sum_\ell D(\ell) \sum_j \omega_j \left[1 + \frac{1}{4\omega_j^2} D_r\right] \psi_{\ell j}(r)^2 + \epsilon_{\rm ct}(r)\,. \quad (3.19)$$

Here, $D_r = \partial_r(\partial_r - (n-1)/r)$ is a radial derivative operator and $\epsilon_{\rm ct}(r)$ denotes the contribution from the counterterms in the energy density operator $\hat{T}_{00}$, cf. Eqs. (3.7) and (3.9). Finally, the degeneracy factor $D(\ell)$ in each channel ℓ is the dimension of the corresponding irreducible tensor representation of

the rotation group $SO(n)$. It is the dimension of the space of symmetric tensors with ℓ indices, each running from 1 to n with all traces (contractions) removed. Working out the combinatorics gives

$$D(\ell) = \frac{\Gamma(n+\ell-2)}{\Gamma(n-1)\,\Gamma(\ell+1)}\,(n+2\ell-2)\,, \tag{3.20}$$

which reduces to the familiar degeneracy factor $2\ell+1$ for $n = 3$. In Eq. (3.19), the quantum energy density is expressed as an integral of the single-particle energies $\omega(k)$ over all real k, weighted by the local density of states in each channel ℓ, plus a similar contribution from the bound states ω_j. For practical purposes, however, it is much more convenient to rotate the integration contour to the upper complex k-plane (see Fig. 3.1). We get three contributions:

1. the residues from the bound state poles $k = i\kappa_j$ on the positive imaginary axis exactly cancel the explicit bound state contribution in G_ℓ (i.e.,the last term in Eq. (2.13)) [11];
2. the discontinuity of the square root cut in the single-particle scattering energies $\omega = \sqrt{m^2 + k^2}$ yields an integral along the imaginary axis, $k = it$ with $t \in [m, \infty]$;
3. the large semi-circle at infinity gives no contribution if the integrand falls off fast enough as $|k| \to \infty$.

The last point is usually *not* true, however, since the contribution from $|k| \to \infty$ in fact *diverges* in space dimensions $n \geq 1$. This problem is, of course, related to the usual ultraviolet divergences that plague any matrix element in quantum field theory. To solve it, the decay of the Green's function at large $|k|$ has to be improved in Eq. (3.19) *before* rotating the integration contour. We will be able to accomplish this by subtracting a few low order

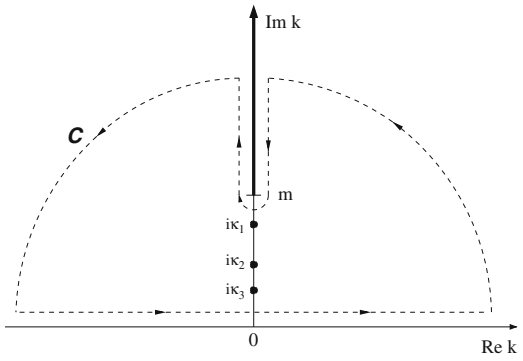

Fig. 3.1 Deformation of the momentum integration contour in Eq. (3.19)

Born approximations to the Green's function, because the Born approximate becomes accurate at large $|k|$. The required number N of subtractions depends on the model and the dimension of spacetime. By Eq. (3.17), the subtraction carries over to the local spectral density, which is the primary quantity of interest. We will use the notation of Eq. (2.48),

$$[\rho_\ell(k,r)]_N \equiv \rho_\ell(k,r) - \rho_\ell^{(0)}(k,r) - \cdots - \rho_\ell^{(N)}(k,r) \tag{3.21}$$

for the N times Born subtracted density, and likewise for the Green's function, phase shifts, etc.

Formally, the Born series is an expansion of the Green's function G_ℓ in powers of the interaction $\sigma(r)$ such that $\rho_\ell^{(N)} = \mathscr{O}\left(\sigma^N\right)$. When used in Eq. (3.19), the Born terms thus correspond to an expansion of the vacuum energy density in powers of σ. Perturbative quantum field theory describes the very same expansion quite differently in terms of *Feynman diagrams*. Thus we use a simple strategy:

> Subtract a sufficient number N of terms of the Born series from the spectral density to remove the large $|k|$ divergence, and add back in exactly what was subtracted in the form of Feynman diagrams. The diagrams can then be combined with the counterterms in the usual fashion of perturbative quantum field theory to provide a finite and unambiguous answer.

This simple prescription shifts the renormalization procedure entirely to the perturbative sector (which is well understood), while the non-perturbative spectral contribution is manifestly finite. However, some care is necessary in carrying out this substitution. The low-order Feynman diagrams and likewise the low-order Born approximations in Eq. (3.19) are typically divergent, which is why we subtracted them in the first place. As mentioned in the introduction, the formal manipulation of such divergent quantities may lead to unexpected ambiguities. To avoid these problems, we use a *common* regularization procedure for both the Feynman and Born series simultaneously. *Dimensional regularization* is typically the most convenient choice. In Sect. 3.5, we present a detailed treatment of the case $N = 1$, in which we show rigorously that the lowest order Born and Feynman terms are equal as functions of dimension.

After the Born subtraction, the final expression for the energy density in a spherical shell of radius r becomes[2]

[2] Notice that the Feynman sum starts at $i = 1$, i.e.,the vacuum bubble diagram is *not* inserted back. Thus Eq. (3.22) really represents the *change* in the vacuum energy density due to the interaction. In other words, we have adopted the renormalization condition that the energy density of the trivial vacuum is zero.

$$\epsilon(r) = -\sum_{\ell} D(\ell) \int_m^\infty \frac{dt}{2\pi} \sqrt{t^2 - m^2} \left[1 - \frac{1}{4(t^2 - m^2)} D_r\right] [\rho_\ell(it, r)]_N + \sum_{i=1}^{N} \epsilon_{\rm FD}^{(i)}(r) + \epsilon_{\rm CT}(r)\,. \tag{3.22}$$

Both lines in this expression are now separately finite. The renormalization of $\epsilon_{\rm FD}$ in the second line is standard; we will briefly review it in Sect. 3.6. Formally, the first line in Eq. (3.22) represents the infinite sum of all Feynman diagrams of order $(N+1)$ and higher. Renormalization group arguments prove that the final result is cutoff- and scheme-independent.

One final remark is in order: The transfer of the ultraviolet divergences into Feynman diagrams only determines the *minimal* number N of Born subtractions. There is, of course, nothing to prevent *oversubtraction* of more Born terms, as long as the corresponding Feynman diagrams are added back in.[3] Such an oversubtracted formula is sometimes useful to improve the numerical stability of calculations of the spectral part of the density formula (3.22), in particular the sum over angular momentum channels. On the other hand, the calculation of higher order Feynman diagrams quickly becomes difficult, so we usually subtract only the minimal number of Born approximations.

3.2.2 The Vacuum Energy

Next we turn to the *vacuum energy* $E_{\rm vac}[\sigma]$, which is obtained by integrating the energy density given by Eq. (3.22). Since both the t-integral and the sum over channels in Eq. (3.22) are absolutely convergent, the order of integration can be interchanged, with the result

$$E_{\rm vac}[\sigma] = -\sum_{\ell} D(\ell) \int_m^\infty \frac{dt}{2\pi} \sqrt{t^2 - m^2} \int_0^\infty dr\ [\rho_\ell(it, r)]_N + \sum_{i=1}^{N} E_{\rm FD}^{(i)} + E_{\rm CT}\,. \tag{3.23}$$

Of course, $E_{\rm FD}^{(i)}$ and $E_{\rm ct}$ are the radial integrals of the corresponding densities. In practice, the Feynman diagrams for the total energy are most conveniently computed from the functional determinant representation in Euclidean space, cf.Sect. 3.5.

The first term in Eq. (3.23) can be rewritten using Eq. (2.33) on the imaginary axis $k = it$, which yields

$$\int_0^\infty dr\ [\rho(it, r)]_0 = \frac{d}{dt} \ln F_\ell(it) \equiv \frac{d\nu_\ell(t)}{dt}, \tag{3.24}$$

[3] The oversubtracted diagrams and Born approximations give *finite* contributions to the energy density, so their equality can be established without using a regulator.

where the logarithm of the Jost function on the imaginary axis,

$$\nu_\ell(t) \equiv \ln\, F_\ell(it), \tag{3.25}$$

is a *real* function. In Eqs. (2.19) we have derived an efficient method for computing $\nu_\ell(t)$. The final result for the vacuum energy is then

$$E_{\rm vac}[\sigma] = \sum_\ell D(\ell) \int_m^\infty \frac{dt}{2\pi} \frac{t}{\sqrt{t^2-m^2}} \left[\nu_\ell(t)\right]_N + \sum_{i=1}^N E_{\rm FD}^{(i)} + E_{\rm CT}\,. \tag{3.26}$$

Using the tools developed in the previous chapter the formulations (3.19) and (3.26) are well suited for numerical evaluation. Even so, it is instructive to return to the real axis, $t \to -ik$. For this purpose, one reverses the deformation of the momentum integration contour that led to Eq. (3.26), thereby picking up the discrete contributions from the bound state poles. The real part, $\mathsf{Re}(\nu_\ell)$, is odd in k and does not contribute to the integral, whence only $\mathsf{Im}(\nu_\ell)$ survives, which is the phase shift. After an integration by parts using Levinson's theorem, we obtain

$$\begin{aligned} E_{\rm vac}[\sigma] = \sum_\ell D(\ell) \left[\int_0^\infty \frac{dk}{2\pi} \sqrt{k^2+m^2}\, \frac{d}{dk} [\delta_\ell(k)]_N + \frac{1}{2} \sum_j \omega_j \right] \\ + \sum_{i=1}^N E_{\rm FD}^{(i)} + E_{\rm CT}\,. \end{aligned} \tag{3.27}$$

As discussed in the introduction, this formula represents the sum over modes of $\frac{1}{2}\hbar\omega$, weighted by the density of states.

The equations (3.19), (3.26), and (3.27) are the basis of the spectral method. In the next sections, we will discuss the perturbative part of our approach and show how to evaluate and renormalize the relevant Feynman diagrams. Traditionally, such graphs are computed using a set of Feynman rules for vertices, propagators, and symmetry factors. A direct and concise approach to this calculation starts from the more modern *path integral* representation of the vacuum energy.

3.3 The Path Integral Approach

In this section we briefly review the relation between the vacuum energy and the vacuum to vacuum transition amplitude as computed in the path integral formalism.

The starting point is a static background field $\sigma(\boldsymbol{x})$ coupled to our quantum field φ. To be specific we again consider the Lagrangian density

$$\begin{aligned}\mathscr{L} &= \tfrac{1}{2}\left((\partial_\mu\varphi)(\partial^\mu\varphi) - (m^2+\sigma(\boldsymbol{x})-i\epsilon)\varphi^2\right)\\ &= \tfrac{1}{2}\varphi\left[-\Box - m^2 - \sigma(\boldsymbol{x}) + i\epsilon\right]\varphi,\end{aligned} \tag{3.28}$$

up to total derivate terms that do not involve the background σ. The role of the additional $i\epsilon$ term will shortly become clear.

For a static system the Hamiltonian of the stationary Schrödinger problem is well defined and we may assume that the background $\sigma(\boldsymbol{x})$ is adiabatically switched on at a large early time $-T/2$ and off at a very late time $T/2$. That is, the time scale on which $\sigma(\boldsymbol{x})$ varies is large but nevertheless smaller than T. During that transition the vacuum state picks up a phase proportional to its energy when the background is present [12]

$$E_{\mathrm{vac}}[\sigma] = \frac{i}{T}\ln\left(\frac{\langle \mathrm{vac}^+|\mathrm{vac}^-\rangle_\sigma}{\langle \mathrm{vac}^+|\mathrm{vac}^-\rangle_0}\right). \tag{3.29}$$

The path integral in quantum field theory is the superposition of vacuum to vacuum transition amplitudes. When evaluated in Euclidian spacetime, large time intervals project the ground state contribution from that superposition. Hence

$$\langle \mathrm{vac}^+|\mathrm{vac}^-\rangle_\sigma \propto \int [d\varphi]\ \mathrm{e}^{\,i\int d^D x\mathscr{L}}, \tag{3.30}$$

as $T \to i\infty$. Formally, the path integral may be written as a product of infinitely many ordinary integrals. Since the integration variable φ appears only quadratically in our model Lagrangian these are Gaußian integrals, each of which contributes a factor proportional to the inverse square root of the operator between the two factors of φ. Thus we obtain the vacuum transition amplitude as

$$\begin{aligned}\langle \mathrm{vac}^+|\mathrm{vac}^-\rangle_\sigma &\propto \left(\mathrm{Det}\left[\Box + m^2 + \sigma(\boldsymbol{x}) - i\epsilon\right]\right)^{-\frac{1}{2}}\\ &\propto \left(\mathrm{Det}\left[-\Box_{\mathrm{E}} + m^2 + \sigma(\boldsymbol{x})\right]\right)^{-\frac{1}{2}},\end{aligned} \tag{3.31}$$

where the continuation to Euclidean space, $x_0 \to -ix_4$, is indicated in the second line. We now recognize that the $i\epsilon$ prescription in Eq. (3.28) ensures the convergence of the path integral, Eq. (3.30). Furthermore, it avoids the poles in the functional determinant by continuing to real x_4, which defines the Wick rotation.[4] Substituting this expression into Eq. (3.29) yields the vacuum polarization energy

$$E_{\mathrm{vac}}[\sigma] = \frac{-i}{2T}\,\mathrm{Tr}\ln\frac{\Box + m^2 + \sigma(\boldsymbol{x}) - i\epsilon}{\Box + m^2 - i\epsilon}. \tag{3.32}$$

Formally this is the result we seek, but of course it must be properly regularized and renormalized.

[4] More precisely, correlation functions are analytic functions of the complex time variable $z = x_4 + ix_0$ in the half-plane $x_4 > 0$ [13].

In the above discussion the potential emerged as an external background field. In some instances, however, we consider non-trivial (usually static) configurations in self-interacting theories. We call such a configuration $\varphi_{\rm cl}$ to indicate it is a classical background, and assume it to be a soliton-like configuration with non-zero classical energy. The quantum correction to this energy results from small-amplitude fluctuations, η, with the $\mathscr{O}(\hbar)$ contribution arising from the η^2 terms. (Here we employ natural units $\hbar = c = 1$, but use $\hbar$ as a counting device for quantum corrections.) In general the expansion around $\varphi_{\rm cl}$ also generates a term linear in η, which is canceled by introducing an additional source field $J(x)$ that also couples linearly to field variable. The source is chosen to make $\varphi_{\rm cl}$ a stationary point of the action, so that the terms linear in η vanish. We then compute the vacuum transition amplitude as a functional of the source,

$$\begin{aligned}\langle \mathrm{vac}^+|\mathrm{vac}^-\rangle_J &= \mathrm{e}^{iW[J]} = \mathrm{e}^{i\int d^Dx[\mathscr{L}(\varphi_{\rm cl})+J\varphi_{\rm cl}]} \\ &\times \int [d\eta]\, \exp\left\{\tfrac{-i}{2}\int d^Dx\,\eta\left[\Box + m^2 + V''(\varphi_{\rm cl}) - i\epsilon\right]\eta\right\}, \quad (3.33)\end{aligned}$$

where the expansion about $\varphi_{\rm cl}$ is indicated by the Taylor expansion of the self-interaction potential. The Legendre transformation

$$\Gamma[\varphi] = W[J] - \int d^dx\, J(x)\varphi(x) \quad \text{with} \quad \varphi(x) = \frac{\delta}{\delta J(x)}W(J)\,, \qquad (3.34)$$

defines the effective action. Using $\varphi - \varphi_{\rm cl} = \mathscr{O}(\hbar)$ and the fact that $\varphi_{\rm cl}$ is a stationary point of $\int d^Dx\,[\mathscr{L}(\varphi_{\rm cl}) + J\varphi_{\rm cl}]$, we have [14]

$$\Gamma[\varphi_{\rm cl}] = \int d^dx \mathscr{L}(\varphi_{\rm cl}) + \frac{i}{2}\mathrm{Tr}\ln\frac{\Box + m^2 + V''(\varphi_{\rm cl}) - i\epsilon}{\Box + m^2 - i\epsilon} + \mathscr{O}\left(\hbar^2\right). \quad (3.35)$$

When transformed to Euclidean space, $-\Gamma/T$ is to be interpreted as the vacuum energy when a (static) source is present during the large time interval T [12]. Since the source fixes φ, this is thus the vacuum energy of a prescribed field configuration,

$$TE_{\rm vac}[\varphi_{\rm cl}] = -\int d^dx \mathscr{L}(\varphi_{\rm cl}) - \frac{i}{2}\mathrm{Tr}\ln\frac{\Box + m^2 + V''(\varphi_{\rm cl}) - i\epsilon}{\Box + m^2 - i\epsilon} + \mathscr{O}\left(\hbar^2\right). \qquad (3.36)$$

Hence we find formally the same expression for the $\mathscr{O}(\hbar)$ quantum correction to the vacuum energy, regardless of whether we consider an external background or a soliton-type configuration in a self-interacting theory.

3.4 Connecting the Functional and Canonical Formalisms

We now show how to formally connect the functional determinant representation for the energy in Eq. (3.32) to the spectral sum in Eq. (3.27). We follow the treatment of Ref. [15]. For a time-independent background potential, the differential operator in Eq. (3.32) is separable into eigenfunctions of $-\partial_t^2$ and

the single-particle Hamiltonian $-\nabla^2 + m^2 + \sigma(\boldsymbol{x})$. The eigenvalues of the former are given by Ω_n^2, where $\Omega_n = 2\pi n/T$ are the Matsubara frequencies with $n = 0, 1, 2, 3 \ldots$, while the eigenvalues of the latter are ω_j^2, where the ω_j are the eigenenergies that appear in the spectral sum, Eq. (1.3). To evaluate the determinant, we take the product over all such modes. We note that throughout this calculation, we can absorb all coefficients that do not depend on the dynamics into rescalings of the functional measures, which will be labeled by $\mathcal{C}_i$. Also, we formulate the problem in Minkowski space but for simplicity omit the $i\epsilon$ prescription. We have

$$\begin{aligned}\left(\det\left[-\Box - m^2 - \sigma(\boldsymbol{x})\right]\right)^{-\frac{1}{2}} &= \prod_{n=0}^{\infty}\prod_{\omega_j}\left[\left(\frac{2\pi n}{T}\right)^2 - \omega_j^2\right]^{-1/2} \\ &= \mathcal{C}_1 \prod_{\omega_j \geq 0}\prod_{n=1}^{\infty}\left[1 - \left(\frac{\omega_j T}{2\pi n}\right)^2\right]^{-1} = \mathcal{C}_2 \prod_{\omega_j \geq 0}\left[\sin\frac{\omega_j T}{2}\right]^{-1} \\ &= \mathcal{C}_3 \exp\left[-\frac{i}{2}\sum_{\omega_j \geq 0}\omega_j T\right]\prod_{\omega_j \geq 0}\left[1 - e^{-i\omega_j T}\right]^{-1}. \end{aligned} \tag{3.37}$$

We have taken the opposite sign in the argument of the functional determinant, but this choice is arbitrary; it drops out when compared to the non-interacting case with $\sigma = 0$, as in Eq. (3.32). We now expand each factor in the second product as a geometric series,

$$\left[1 - e^{-i\omega_j T}\right]^{-1} = \sum_{n_j=0}^{\infty} e^{-in_j\omega_j T}, \tag{3.38}$$

where $n_j = 0, 1, 2, \ldots$ can be interpreted as the occupation number for mode j. Thus we can rewrite the second factor as a sum over all occupations numbers of every mode,

$$\det\left[-\Box - m^2 - \sigma(\boldsymbol{x})\right]^{-1/2} = \mathcal{C}' \exp\left[-\frac{i}{2}T\sum_j \omega_j\right]\sum_{\{n_j\}}\exp\left[-iT\sum_j n_j\omega_j\right]. \tag{3.39}$$

We evaluate the functional integral for T large, with infinitesimal negative imaginary part, so this expression is dominated by the contribution when all occupation numbers n_j vanish, i.e., $n_j = 0$, which is the vacuum configuration. Thus we have found that the effective action becomes $\mathcal{C}' \exp[-iE_{\text{vac}}T]$, where the vacuum polarization energy is given by the formal sum of zero-point energies $E_{\text{vac}} = \sum_j \frac{\omega_j}{2}$.

3.5 Feynman Diagrams and the Born Series

Next we discuss the energy density and its Feynman series and show that the integral of this series equals the expansion of Eq. (3.31) order by order.

We find the energy density as the quantum mechanical expectation value $\epsilon(x) = \langle T_{00}(x)\rangle$, cf.Eq. (3.7). For the model with the background field σ coupled to the quantum field φ we consider[5]

$$\epsilon(x) = \frac{1}{2}\frac{\int [d\varphi]\, \varphi(x)\hat{T}_x\varphi(x)\, \mathrm{e}^{i\int d^dy\, \frac{1}{2}\left[\dot\varphi^2-(\boldsymbol{\partial}\varphi)^2-\left(m^2+\sigma\right)\varphi^2\right]}}{\int [d\varphi]\, \mathrm{e}^{i\int d^dy\, \frac{1}{2}\left[\dot\varphi^2-(\boldsymbol{\partial}\varphi)^2-(m^2+\sigma)\varphi^2\right]}}, \tag{3.40}$$

with the position space operator

$$\hat{T}_x = \overleftarrow{\partial}_t \overrightarrow{\partial}_t + \overleftarrow{\boldsymbol{\partial}} \cdot \overrightarrow{\boldsymbol{\partial}} + m^2 + \sigma(\boldsymbol{x})\,. \tag{3.41}$$

Total derivative terms that arise when turning derivative operators that act to the left into ones that act to the right will not contribute to the integrated density. To compute the expectation value of an object that is quadratic in the field, we add an interaction that couples that object linearly to a source, compute a logarithmic derivative with respect to the source, and then set the source to zero. The functional integral is proportional to the inverse square root of the determinant of the quadratic operator, giving

$$\begin{aligned}\epsilon(x) &= \frac{i}{2}\mathrm{Tr}\left\{\left[-\Box - (m^2+\sigma)\right]^{-1}\delta^d(\hat{x}-x)\left[-\partial_t^2 - \boldsymbol{\partial}^2 + (m^2+\sigma)\right]\right\} \\ &= -i\,\mathrm{Tr}\left\{\left[-\Box - (m^2+\sigma)\right]^{-1}\delta^d(\hat{x}-x)\,\partial_t^2\right\} + \cdots\,,\end{aligned} \tag{3.42}$$

where the ellipsis in the last line refers to non-dynamical contributions that do not involve σ. To set up the Feynman series we note that the free propagator is $S_0 = \left[-\Box - m^2\right]^{-1}$ so that $\left[-\Box - (m^2+\sigma)\right]^{-1} = \left[1 - S_0\sigma\right]^{-1} S_0$. Since the background field σ is static, it is useful to introduce frequency states $|\omega\rangle$ with $\langle\omega|\sigma|\omega'\rangle = \sigma\delta(\omega-\omega')$. Then the νth order term in the Feynman series of the energy density is

$$\epsilon^{(\nu)}_{\mathrm{FD}}(x) = i\int\frac{d\omega}{2\pi}\,\mathrm{Tr}'\left\{\omega^2\left(S_0(\omega)\sigma\right)^\nu S_0(\omega)\delta^{d-1}(\boldsymbol{x}-\hat{\boldsymbol{x}})\right\}\,, \tag{3.43}$$

where $S_0(\omega) = (\omega^2 + \boldsymbol{\partial}^2 - m)^{-1}$ and Tr' is the trace over all remaining degrees of freedom, spatial and discrete. Since the above expression gives the $\mathscr{O}(\sigma^\nu)$ contribution to the energy density, it is indeed the Feynman diagram contribution to Eq. (3.22) with ν external σ-legs, up to total derivatives. The spatial integration trivially yields the νth order contribution to the quantum energy that we actually require in Eq. (3.27),

$$\begin{aligned}E^{(\nu)}_{\mathrm{FD}} &= \int d^{d-1}x\,\epsilon^{(\nu)}_{\mathrm{FD}}(x) = i\int\frac{d\omega}{2\pi}\,\mathrm{Tr}'\left\{\omega^2 S_0(\omega)\left(S_0(\omega)\sigma\right)^\nu\right\} \\ &= -\frac{i}{2}\int\frac{d\omega}{2\pi}\,\mathrm{Tr}'\left\{\omega\left(\frac{\partial}{\partial\omega}S_0(\omega)\right)\left[\sigma S_0(\omega)\sigma S_0(\omega)\sigma\ldots\right]\right\}\,,\end{aligned} \tag{3.44}$$

[5] The $i\epsilon$ prescriptions in Minkowski space as in Eq. (3.28) are understood.

with ν factors of σ but only $\nu-1$ factors of S_0 in the square bracket. We integrate by parts and pick up derivatives from these $\nu-1$ propagators. Due to the cyclic property of the trace, each of these terms gives an equal contribution,

$$\begin{aligned} E_{\rm FD}^{(\nu)} &= \frac{i}{2}\int\frac{d\omega}{2\pi}\,{\rm Tr}'\Big\{\,(S_0(\omega)\sigma)^\nu \\ &\qquad\qquad +(\nu-1)\omega\left(\frac{\partial}{\partial\omega}S_0(\omega)\right)[\sigma S_0(\omega)\sigma S_0(\omega)\sigma\ldots]\,\Big\} \\ &= \frac{i}{2\nu}\int\frac{d\omega}{2\pi}\,{\rm Tr}'\,(S_0(\omega)\sigma)^\nu\ , \end{aligned} \tag{3.45}$$

which results from identifying the derivative terms in Eqs. (3.44) and (3.45). The series can be straightforwardly summed,

$$\begin{aligned} E_{\rm vac} &= \sum_\nu E_{\rm FD}^{(\nu)} = -\frac{i}{2}\int\frac{d\omega}{2\pi}\,{\rm Tr}'\ln\left(1-S_0(\omega)\sigma\right) \\ &= -\frac{i}{2}\int\frac{d\omega}{2\pi}\,{\rm Tr}'\ln\left(S_0^{-1}(\omega)-\sigma\right)+\cdots = -\frac{i}{2T}{\rm Tr}\ln\left(-\Box-m^2-\sigma\right)\ , \end{aligned} \tag{3.46}$$

just as in Eq. (3.32), up to a non-dynamical and thus irrelevant constant. Appendix B of Ref. [16] contains the analogous derivation for a fermion coupled to a background gauge field.

We briefly sketch the techniques to compute the diagrams that are formally written in Eqs. (3.43) and (3.45), since they are evaluated using conventional Feynman rules.

If we want to carefully keep track of all total derivatives and integrations by parts, we need to consider the coordinate space operator $\hat{T}_x=\hat{T}_x^{(0)}+\hat{T}_x^{(1)}$ that appears in Eq. (3.41), augmented by the δ-functions as in Eq. (3.42). As indicated by the superscripts, it contains pieces of zeroth and first order in the background potential $\sigma(\boldsymbol{x})$. We compute them in momentum space

$$\begin{aligned} \langle k'|\hat{T}_x^{(0)}\delta^d(x-\hat{x})|k\rangle &= e^{i(k'-k)x}\,\left[k'^0k^0+\boldsymbol{k}'\cdot\boldsymbol{k}+m^2\right], \\ \langle k'|\hat{T}_x^{(1)}\delta^d(x-\hat{x})|k\rangle &= \sigma(\boldsymbol{x})e^{i(k'-k)x}\,. \end{aligned} \tag{3.47}$$

The Feynman series consists of all graphs with a single ϕ-loop and arbitrary insertions of $\hat{T}_x^{(0)}$, $\hat{T}_x^{(1)}$, and $\sigma(\boldsymbol{x})$. To order σ^1, for instance, we have the two diagrams shown in Fig. 3.2. The graph in the right panel is a total derivative and there is no counterterm for it. This diagram therefore should be finite in all dimensions $d\le 4$, which is confirmed by explicit calculation [10].

The tadpole graph in the left panel is divergent in two or more spacetime dimensions. To define it, we employ dimensional regularization to $d=n+1$ spacetime dimensions,

$$\frac{1}{2i}{\rm Tr}'\,\left[\hat{T}_x^{(1)}\delta^{d-1}(x-\hat{x})(-\partial^2-m^2)^{-1}\right]=\frac{i}{2}\sigma(\boldsymbol{x})\int\frac{d^dk}{(2\pi)^d}\,\frac{1}{k^2-m^2}\,. \tag{3.48}$$

Fig. 3.2 First-order Feynman diagrams contribution to the energy density $\langle T_{00} \rangle$. The solid circle represents the ϕ-loop and the insertions $\hat{T}_x^{(0,1)}$ from the energy density operator are explained in the main text. In the right panel a single background field from the expansion of the propagator in Eq. (3.42) is inserted

This diagram is renormalized by a counterterm proportional to $\sigma(\boldsymbol{x})$ in the action or, equivalently, in T_{00}. For space dimensions $n \leq 2$, the tadpole counterterm $c_1\,\sigma(\boldsymbol{x})$ in T_{00} (or $\mathscr{L}$) and one Born subtraction ($N = 1$) is sufficient to remove all divergences. The precise definition of c_1, including all finite contributions, must be fixed by physical input. We imagine that there is a Lagrangian whose stationary condition exactly yields the prescribed background field σ and demand the so-called *no-tadpole condition*, i.e., the quantum corrections do not alter this stationary point, meaning that the counterterm exactly cancels the diagram, Eq. (3.48). This condition is possible because the diagram is local and directly proportional to $\sigma(\boldsymbol{x})$. As in a self-interacting theory, the no-tadpole condition ensures that the VEV of the background field is fixed.

In $n = 3$, an additional *mass counterterm* $c_2\sigma^2(\boldsymbol{x})$ is required because of the diagram obtained from the right panel of Fig. 3.2 by substituting $T_x^{(1)}$ in place of $T_x^{(0)}$. As a result, we have to perform $N = 2$ Born subtractions. The coefficient c_2 may be fixed by a specific choice of the renormalization condition, and any result we obtain is only meaningful if accompanied by this choice. The results from different renormalization conditions can be converted into another by means of a renormalization group transformation.

The same analysis can be repeated for the vacuum energy E_{vac}. When we expand the determinant in σ, the νth order term can be represented as the one-loop diagram with ν insertions of $\sigma(\boldsymbol{x})$:

$$\operatorname{Tr}\ln\left[\frac{\Box + m^2 + \sigma(r)}{\Box + m^2}\right] =$$

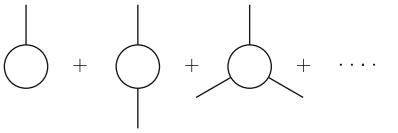

(3.49)

To first order in σ, the relevant Feynman diagram can be obtained either from expanding the functional determinant in Eq. (3.49) or by integrating the density Eq. (3.48) over all space,[6]

[6] As mentioned earlier, the diagram in the right panel of Fig. 3.2 is a total derivative and does not contribute to the vacuum energy.

$$E^{(1)}_{\rm FD} = \frac{i}{2}\int d^n x\,\sigma(\boldsymbol{x})\cdot\int\frac{d^dk}{(2\pi)^d}\,\frac{1}{k^2-m^2} = \frac{\langle\sigma\rangle}{2\,(4\pi)^{\frac{n+1}{2}}}\,\Gamma\Big(\frac{1-n}{2}\Big)\,m^{n-1}. \tag{3.50}$$

As expected, it depends only on the spatial average of the potential,

$$\langle\sigma\rangle = \int d^n x\,\sigma(\boldsymbol{x}) = \frac{2\pi^{\frac{n}{2}}}{\Gamma(\frac{n}{2})}\int_0^\infty \sigma(r)\,r^{n-1}dr. \tag{3.51}$$

The no-tadpole scheme will again fix the VEV of the background σ, with the counterterm $c_1\sigma(x)$ in the starting Lagrangian adjusted to cancel Eq. (3.50) exactly. In spacetime dimensions $d \geq 4$, the second-order diagram becomes ultraviolet divergent as well, and a mass counterterm $c_2\sigma^2(x)$ must be added to the Lagrangian in order to obtain a finite result. We will discuss this renormalization from a slightly more general perspective in the next section.

We can use the explicit expressions to demonstrate that the low-order Born approximations are equivalent to corresponding Feynman diagrams, without any ambiguous finite parts, when identical regularization prescriptions are employed. For simplicity, let us concentrate on the lowest order (tadpole) diagram. The formula for the Feynman graph was already determined in dimensional regularization, cf.Eq. (3.50) above. It must now be compared to the contribution of the first Born approximation to the vacuum energy, computed in dimensional regularization as well. Since there are never any bound states in the Born series, Eq. (3.27) implies

$$E^{(1)}_{\rm BA} = \sum_{\ell=0}^\infty D(\ell)\int_0^\infty\frac{dk}{2\pi}(\omega-m)\frac{d\delta^{(1)}_\ell(k)}{dk}\,. \tag{3.52}$$

The subtraction of the rest mass m from the scattering energy avoids possible infrared divergences; it is justified by Levinson's theorem, Eq. (2.50). The degeneracy factor $D(\ell)$ is given in Eq. (3.20) above. The first Born approximation to the phase shift can be worked out explicitly in n spatial dimensions,

$$\delta^{(1)}_\ell(k) = -\frac{\pi}{2}\int_0^\infty J_{\frac{n}{2}+\ell-1}(kr)^2\,\sigma(r)r\,dr\,. \tag{3.53}$$

We insert this formula in Eq. (3.52) and use the Bessel function identity

$$\sum_{\ell=0}^\infty\frac{(2q+2\ell)\Gamma(2q+\ell)}{\Gamma(\ell+1)}J_{q+\ell}(z)^2 = \frac{\Gamma(2q+1)}{\Gamma(q+1)^2}\left(\frac{z}{2}\right)^{2q} \tag{3.54}$$

for $q = \frac{n}{2}-1$. The sum over channels in Eq. (3.52) can then be taken in closed form,

$$E^{(1)}_{\rm BA} = -\frac{\langle\sigma\rangle}{2(4\pi)^{\frac{n}{2}}\Gamma\left(\frac{n}{2}\right)}(n-2)\int_0^\infty(\omega-m)k^{n-3}\,dk\,. \tag{3.55}$$

Finally, the k-integral can be calculated in the convergence domain $0 < n < 1$ and then analytically continued in n,

$$\int_0^\infty (\omega - m) k^{n-3}\, dk = -\frac{m^{n-1}}{4\sqrt{\pi}} \Gamma\left(\frac{1-n}{2}\right) \Gamma\left(\frac{n-2}{2}\right) . \tag{3.56}$$

Combining Eqs. (3.55) and (3.56) then coincides *exactly* with Eq. (3.50).[7]

Similar results can also be proved for fermions [17–20]. Our starting point is the free Dirac equation in n spatial dimensions,

$$(-i\boldsymbol{\alpha} \cdot \boldsymbol{\partial} + \beta m)\, \Psi = H\Psi = \omega \Psi . \tag{3.57}$$

The spinor Ψ has $2N_d$ components and accordingly the Dirac matrices α_j and β have $2N_d \times 2N_d$ elements, where $N_d = 2^{(n-1)/2}$ for n odd and $N_d = 2^{n/2}$ for n even. We will generalize the case of n odd, though our results will not depend on this choice. We choose the basis

$$\beta = \begin{pmatrix} \mathbb{1}_{N_d \times N_d} & 0 \\ 0 & -\mathbb{1}_{N_d \times N_d} \end{pmatrix} \qquad \text{and} \qquad \alpha_j = \begin{pmatrix} 0 & \Lambda_j \\ \Lambda_j & 0 \end{pmatrix} \qquad j = 1, \ldots, n . \tag{3.58}$$

The Clifford algebra is obtained by demanding the anti-commutator $\{\Lambda_i, \Lambda_j\} = 2\delta_{ij}$ for the $N_d \times N_d$ matrices Λ_j. In analogy to the spin generators in $n = 3$ we define the commutator

$$[\Lambda_i, \Lambda_j] = 2i\Sigma_{ij}, \tag{3.59}$$

which obeys the $SO(n)$ commutation relation

$$[\Sigma_{ij}, \Sigma_{kl}] = i\left(\delta_{ik}\Sigma_{jl} + \delta_{jl}\Sigma_{ik} - \delta_{il}\Sigma_{jk} - \delta_{jk}\Sigma_{il}\right) . \tag{3.60}$$

Furthermore, we define the orbital angular momentum operator

$$L_{ij} = -i\left(x_i \partial_j - x_j \partial_i\right), \tag{3.61}$$

which also satisfies the $SO(n)$ algebra

$$[L_{ij}, L_{kl}] = i\left(\delta_{ik}L_{jl} + \delta_{jl}L_{ik} - \delta_{il}L_{jk} - \delta_{jk}L_{il}\right) . \tag{3.62}$$

We can then put these together to form the total spin operator

$$J_{ij} = L_{ij} + \frac{1}{2}\Sigma_{ij}, \tag{3.63}$$

which commutes with the Hamiltonian: $[H, J_{ij}] = 0$. Having obtained the algebra, we next need to find the Casimir eigenvalues of

$$L^2 = \frac{1}{2}\sum_{i,j} L_{ij}^2 , \quad \Sigma^2 = \frac{1}{2}\sum_{i,j} \Sigma_{ij}^2, \quad \text{and} \quad J^2 = \frac{1}{2}\sum_{i,j} J_{ij}^2 . \tag{3.64}$$

[7] A factor $\frac{1}{2}$ was omitted in Eqs. (A.17) and (A.19) of Ref. [17].

The eigenvalues of L^2 are those of $SO(n)$, $\ell(\ell+n-2)$. To find Σ^2, we consider its trace, which is just the number of independent matrices Σ_{ij}, $\frac{1}{2}n(n-1)$. Then to obtain the Casimir eigenvalue of J^2, all we need to find is $\langle L\cdot\Sigma\rangle = \langle\frac{1}{2}\sum_{i,j}L_{ij}\Sigma_{ij}\rangle$. We use the second-order equations obtained from Eq. (3.57), which are generalized Bessel equations. We first remark that $\hat{\boldsymbol{r}}\cdot\boldsymbol{\Lambda}$ has zero total spin ($[\hat{\boldsymbol{r}}\cdot\boldsymbol{\Lambda}, J_{ij}]=0$) and eigenvalue $\ell=1$ with respect to L^2. Therefore, the appropriate spinor with definite parity can be parameterized as

$$\Psi = \begin{pmatrix} if(r)Y_{l,s,j} \\ g(r)\,(\hat{\boldsymbol{r}}\cdot\boldsymbol{\Lambda})\,Y_{l,s,j}\end{pmatrix}, \tag{3.65}$$

where $Y_{l,s,j}$ denote generalized spinor spherical harmonics. The radial functions obey the coupled first-order equations

$$\begin{aligned}\left[\partial_r + \frac{n-1+R}{2r}\right] g(r) &= (m-\omega)f(r),\\ \left[\partial_r + \frac{n-1-R}{2r}\right] f(r) &= (m+\omega)g(r),\end{aligned} \tag{3.66}$$

where $R=\langle L\cdot\Sigma\rangle+n-1$ contains the desired eigenvalue. We can decouple these equations to obtain second-order equations for $f(r)$ and $g(r)$. By demanding that $f(r)$ and $g(r)$ obey generalized Bessel equations with orbital angular momentum ℓ and ℓ', respectively, we find

$$R = 1\pm(n-2-2\ell) \qquad \text{and} \qquad R=-1\pm(n-2+2\ell')\,. \tag{3.67}$$

In view of the properties of $\hat{\boldsymbol{r}}\cdot\boldsymbol{\Lambda}$ mentioned above we have $\ell'=\ell\pm1$. Hence the two relations in Eq. (3.67) are consistent if

$$R=n+2\ell-1 \quad \text{for} \quad \ell'=\ell+1 \qquad \text{and} \qquad R=3-n-2\ell \quad \text{for} \quad \ell'=\ell-1\,. \tag{3.68}$$

Putting these results together we find the Casimir eigenvalue

$$J^2 = \ell(\ell+n-2)+\frac{n(n-1)}{8}+\begin{cases}\ell, & \ell'=\ell+1\\ 2-n-\ell, & \ell'=\ell-1\end{cases}. \tag{3.69}$$

Defining $j=\frac{1}{2}(\ell+\ell')$ yields

$$J^2 = \left(j-\frac{1}{2}\right)\left(j+n-\frac{3}{2}\right)+\frac{n(n-1)}{8} \tag{3.70}$$

for both cases. The above definition of j also ensures that (as for $n=3$) there are two independent solutions for a given j: (i) $\ell=j+\frac{1}{2},\ell'=j-\frac{1}{2}$ and (ii) $\ell=j-\frac{1}{2},\ell'=j+\frac{1}{2}$. These solutions have opposite parity.

Finally, we have to find the degeneracy factor, $D_F(j)$, for spinor fields. We use two trace relations that are simple in the basis appropriate for Σ_{ij} and L_{ij}. Written in the basis for J_{ij} they connect different representations and provide information about the degeneracy factor. We have

$$\sum_{j=\ell-\frac{1}{2}}^{j=\ell+\frac{1}{2}} D_F(j)(R(j)-n+1)=0 \tag{3.71}$$

and

$$\sum_{j=\ell-\frac{1}{2}}^{j=\ell+\frac{1}{2}} D_F(j)=N_d D(\ell), \tag{3.72}$$

where we have defined $D_F(-\frac{1}{2})=0$, independent of n. The first condition is nothing but the tracelessness of $\langle L\cdot\Sigma\rangle$ while the second gives the number of states for a given orbital angular momentum ℓ, with $D(\ell)$ taken from Eq. (3.20). Equation (3.71) can be re-expressed as

$$D_F\left(\ell+\frac{1}{2}\right)=\frac{n+\ell-2}{\ell}\,D_F\left(\ell-\frac{1}{2}\right), \tag{3.73}$$

which after substitution into Eq. (3.72) yields the final result

$$D_F(j)=N_d\left(j+\frac{1}{2}\right)\frac{\Gamma(n+j-\frac{3}{2})}{\Gamma(n-1)\Gamma(j+\frac{3}{2})}\,. \tag{3.74}$$

Equation (3.73) represents a recursion relation between $D_F(j)$ and $D_F(j+1)$ that can straightforwardly be shown to be satisfied by the degeneracy factor of Eq. (3.74). We note that as $n\to 1$, Eq. (3.74) gives zero in all channels except $j=\frac{1}{2}$, where it is one. As in the bosonic case, this limit gives the reduction to the positive and negative parity channels in one dimension.

For n spatial dimensions, the fermion generalization of Eq. (3.53) requires us to sum over parity channels. We find

$$\delta^{(1)}_{n,j}(k)=-\frac{\pi}{2}\int_0^\infty dr\sigma(r)r\left(J_{\frac{n}{2}+j-\frac{3}{2}}(kr)^2+J_{\frac{n}{2}+j-\frac{1}{2}}(kr)^2\right) \tag{3.75}$$

for $k=\sqrt{\omega^2-m^2}$. The leading Born approximation to the Casimir energy is then given by

$$\Delta E^{(1)}_n[\phi\,]=-\frac{1}{\pi}\int_0^\infty dk(\sqrt{k^2+m^2}-m)\sum_j D_F(j)\frac{D_F\delta^{(1)}_{n,j}}{dk}\,. \tag{3.76}$$

Summing over all channels we find the full first order Born approximation to the phase shift

$$\begin{aligned}\delta^{(1)}_n(k)&=\sum_{j=\frac{1}{2},\frac{3}{2}\cdots} D_F(j)\delta^{(1)}_{n,j}(k)\\&=-\frac{\pi}{2}\int_0^\infty dr\sigma(r)r\sum_{j=\frac{1}{2},\frac{3}{2}\cdots} D_F(j)\left(J_{\frac{n}{2}+j-\frac{3}{2}}(kr)^2+J_{\frac{n}{2}+j-\frac{1}{2}}(kr)^2\right)\end{aligned}$$

$$= -\frac{\pi}{2}\int_0^\infty dr\sigma(r)rD_F \sum_{\ell=0,1,2\ldots} \left((\ell+\tfrac{1}{2})J_{\frac{n}{2}+\ell-1}(kr)^2 + D_F(\ell-\tfrac{1}{2})J_{\frac{n}{2}+\ell-1}(kr)^2\right)$$

$$= -\frac{\pi}{2}\int_0^\infty dr\sigma(r)r \sum_{\ell=0,1,2\ldots} N_d D(\ell) J_{\frac{n}{2}+\ell-1}(kr)^2 . \tag{3.77}$$

Using Eq. (3.54) again with $q = \frac{n}{2} - 1$, we sum over ℓ and obtain for the tadpole part of the Casimir energy

$$\Delta E^{(1)}[\phi] = 2N_d \frac{\langle\sigma\rangle}{(4\pi)^{\frac{n}{2}}\Gamma\left(\frac{n}{2}\right)}(n-2)\int_0^\infty (\omega - m)k^{n-3}\,dk, \tag{3.78}$$

where $\langle\sigma\rangle$ is the same as in the bosonic case, Eq. (3.51). The k-integral can be calculated in the vicinity of $n = \frac{1}{2}$ and then analytically continued. The result is given in Eq. (3.56). Hence we find

$$\Delta E^{(1)}[\phi] = -2N_d \frac{\langle\sigma\rangle}{(4\pi)^{\frac{n+1}{2}}}\Gamma\left(\frac{1-n}{2}\right)m^{n-1}, \tag{3.79}$$

which is exactly what we obtain using standard dimensional regularization for the tadpole diagram in $n+1$ spacetime dimensions.

To summarize, we have shown—for the first non-trivial order at least—that the low-order Feynman diagrams and the corresponding Born approximations give manifestly identical results. If we tacitly assume that the theory is dimensionally regulated, the subtraction of the Born terms is thus *exactly* compensated by adding in the corresponding low-order diagrams. This is the essential content of Eqs. (3.22) and (3.27).

3.6 Some Remarks on Renormalization

In the first chapter and also in the last section, we have seen examples of how renormalization works in the spectral approach. The method of Born subtraction shifts the ultraviolet divergences completely into Feynman diagrams, which can be renormalized by counterterms in the traditional way. The literature on renormalization in perturbation theory is quite extensive and we do not intend to give a detailed treatment here. Instead, we want to emphasize some general issues that will help to clarify the nature of the divergences appearing in quantum field theory calculations. The interested reader may consult Ref. [21] for a comprehensive account of renormalization theory.

The basic idea of renormalization is to extract the short-distance divergences in matrix elements (Green's functions) of quantum fields and absorb them in the physical input parameters (couplings, masses, and fields) of the starting theory. In this way, the separation of scales which is at the heart of

all physical theories can be maintained even in a quantum world: Without renormalization, the contribution from hard virtual particles in loop diagrams would completely dominate the physical quantities of interest. But this ultraviolet contribution is more or less universal and thus contains little or no information on the specific model at hand. After renormalization, the physical quantities of interest (bound state energies, phase shifts, masses, etc.) at a low energy are determined by input parameters defined at the same low scale.

For example, for the boson model in Eq. (3.1), the renormalization of the tadpole diagram, Eq. (3.50), is sufficient to render the vacuum energy ultraviolet finite as long as we work in fewer than four spacetime dimensions. In the no-tadpole scheme, we choose the counterterm to cancel the tadpole graph completely, requiring that the VEV $\langle\sigma\rangle$ not be modified by the quantum corrections from φ. By holding the physical input quantity $\langle\sigma\rangle$ fixed, we can calculate the vacuum energy as a function of the renormalized parameters, without pollution from the high-energy physics at the cutoff scale.

There is, of course, an apparent arbitrariness in the finite parts of the counterterms, and one may think naïvely that the predictive power of the model is lost. This is not so: A change in the renormalization prescription will change the physical quantities, but it will also affect the input parameters of the theory. The observables as a function of the input parameters should remain unaffected—this is the content of the renormalization group. Technically, the counterterms combine with the renormalized parameters in the starting Lagrangian to compose the *bare* parameters defined at the cutoff scale. These bare quantities are then independent of the separation into renormalized quantities and counterterms that are determined from the renormalization prescription.

The same arguments can be made even clearer in four dimensions, where the second-order diagram diverges. Expanding the functional determinant to quadratic order in the background gives the second diagram on the right-hand side of Eq. (3.49). We find it to be

$$E^{(2)}_{\mathrm{FD}} = \frac{1}{2}\int \frac{d^n p}{(2\pi)^n}\,\tilde{\sigma}(\boldsymbol{p})\,\Pi(\boldsymbol{p}^2)\,\tilde{\sigma}(-\boldsymbol{p})\,, \tag{3.80}$$

where $\tilde{\sigma}(\boldsymbol{p})$ is the Fourier transform of the background potential. The vacuum polarization is ultraviolet divergent as $d \to 4$,

$$\Pi(\boldsymbol{p}^2) = -\frac{1}{2}\int \frac{d^d k}{(2\pi)^d}\;\frac{1}{k^2-m^2}\;\frac{1}{(k+p)^2-m^2}\bigg|_{p_0=0}\,. \tag{3.81}$$

Frequently the so-called *on-shell* renormalization prescription is used,

$$\Pi(\boldsymbol{p}^2) \longrightarrow \Pi(\boldsymbol{p}^2) - \Pi(M^2)\,. \tag{3.82}$$

With this substitution, the vacuum polarization remains finite when $d \to 4$. When σ is a dynamical field, Π is proportional to its inverse propagator.

Hence the renormalization, Eq. (3.82), suggests that M^2 be taken as the physical mass of the σ particle. Indeed, the subtraction Eq. (3.82) is equivalent to adding the mass counterterm

$$\frac{1}{2}\int \frac{d^n\boldsymbol{p}}{(2\pi)^n}\,\tilde{\sigma}(\boldsymbol{p})\,\Pi(M^2)\,\tilde{\sigma}(-\boldsymbol{p}) = c_2\int d^n x\,\sigma(\boldsymbol{x})^2 \tag{3.83}$$

to Eq. (3.1). Like the VEV $\langle\sigma\rangle$, the σ-mass M^2 is a physical input parameter to the theory, and after renormalization the finite vacuum energy can be expressed as a function of these low-energy input quantities alone. Renormalization group arguments demonstrate the scheme independence of the finite result: changing the scale M^2 will also change the other parameters explicitly and $E_{\rm vac}$ implicitly. This change occurs in such a way that the relation between $E_{\rm vac}$ and its input parameters is unaffected.

From a technical point of view, it seems very surprising that the short distance divergences universally reduce to simple monomials in the fields and their derivatives (with unknown divergent prefactors), particularly because the evaluation of individual diagrams seems to indicate the opposite: Loop diagrams of higher order in $\hbar$ have overlapping subdivergences that typically depend non-analytically on the external momentum $\boldsymbol{p}$. The corresponding counterterms are thus complicated functions containing an infinite number of derivatives. The resolution is that the counterterms must be viewed as a genuine part of the Lagrangian, i.e.,lower order counterterms must be inserted in higher order diagrams as well. The BPHZ formalism [22, 23] and Zimmermann's *forest formula* [24] prove that such counterterm insertions exactly cancel the subdivergences in higher order Feynman diagrams [24]. The result is only an overall divergence where all loop momenta become large simultaneously. For this situation, Weinberg has shown [25] that this remaining overall divergence amounts to simple polynomials in the external momenta, with the order of the polynomial determined by power counting.

Thus, the counterterms in any quantum field theory are local monomials in the fields and their derivatives, and as such correspond exactly to the terms that are typically present in the starting Lagrangian. The only difference between a renormalizable and a non-renormalizable model rests in the fact that the order of the counterterm polynomials is bounded in the former case, while it can become arbitrarily large in the latter. In renormalizable models, we can absorb the divergences in a few physical input parameters, while non-renormalizable theories require more and more independent parameters, so that the predictive power is indeed lost unless an additional criterion is established to truncate the counterterm series.[8]

To summarize, the technique of Born subtraction in the spectral method allows for a completely conventional renormalization in terms of Feynman

[8] For example, the prescribed power of the external momenta curbs the number of possible counterterms in chiral perturbation theory [30–32].

diagrams. The counterterms are fixed by physical requirements on the input parameters (masses, VEV, coupling constants, etc.) in the background field sector. In a renormalizable model, the finite ambiguities in these parameters do not reduce its predictive power, since the relation between physical quantities and the parameters is an unambiguous prediction of the theory. No such assertion can be made for ad hoc counterterms, such as those that some approaches have introduced to remove divergences that are not related to universal short-distance physics. Ad hoc surface counterterms in Casimir type of problems, for instance, are only introduced for special, mostly singular forms of the background σ; for regular σ, they must be discarded to give smooth backgrounds a finite energy. No equivalent to the renormalization group exists to ensure the scheme independence and predictive power of such approaches. We will discuss the role of renormalization and quantum field theory in Casimir type of problems in more detail in Chap. 7.

3.7 Quantum Energy of Interfaces

So far, we have focused on the quantum energy of soliton-like background configurations $\sigma(r)$ with rotational symmetry. There is, however, another important class of extended objects to which the spectral method applies: configurations that are symmetric in a n-dimensional subspace, but otherwise independent of the $m = d-1-n$ remaining spatial coordinates, so that the field configuration is translationally invariant in these m coordinates.[9] Examples include domain walls in lattice field theories [26, 27], branes in string theory and extradimensional gravity [28], large plates in Casimir problems, and flux tubes (vortices) in gauge theories and statistical mechanics. Generically, we refer to such objects as *interfaces*.

The spectral method we have developed for soliton configurations corresponds to $m = 0$. The extension to interfaces ($m > 0$) does not increase the complexity of the problem [29]: The quantum energy is still determined by the scattering data in the n non-trivial directions, and the cumulative effect of the m extra dimensions is only a simple modification of the energy factor $\omega = \sqrt{k^2 + M^2}$ in the phase shift formula, Eq. (3.27). Of course, an interface in $m+n$ dimensions cannot exactly be treated as a soliton in the n non-trivial directions, since the extra space dimensions generally induce additional ultraviolet divergences. We will address this issue in detail below. For different approaches to this problem (in the case $n = 1$), cf.Refs. [11, 33].

In the course of the analysis, it will become evident that the consistency of the underlying field theory requires certain conditions on the n-dimensional scattering data. These are actually the *finite energy sum rules* generalizing Levinson's theorem, discussed in Sect. 2.4, cf.Eq. (2.47). We will see that integrating out the m translationally invariant coordinates induces apparent

[9] As before, d is the overall number of spacetime dimensions.

singularities, each of which is proportional to a combination of a sum over bound states and an integral over phase shifts. The sum rules show that this combination vanishes, removing the singularity. In analogy to the spectral method for $m = 0$, the remaining ultraviolet divergences are renormalized by local counterterms.

For a static soliton in n dimensions described by a classical background $\sigma(\boldsymbol{x})$, the quantity of interest is the quantum energy, $E_n[\sigma]$, which is the effective action per unit time. In the case of interfaces, the relevant quantity is $\mathscr{E}_{m,n}[\sigma] = E_{m,n}[\sigma]/V_m$, the energy per unit volume of the extra dimensions. Physically, $\mathscr{E}_{m,n}$ looks like an *interface tension* when viewed from the outside and like an induced *cosmological constant* intrinsically.

3.7.1 The Interface Formula

To be specific, the model for the small-amplitude fluctuations is taken of the type (3.4), for either a real or complex boson or a Fermi field ψ with a Yukawa coupling $\lambda\bar{\psi}\sigma\psi$. To avoid confusion, the mass of the fluctuating field will be denoted by M. The n non-trivial coordinates on which the background depends will be called $\boldsymbol{x}$, and the remaining extra directions are called $\boldsymbol{y}$. The (static) field equation is now easily seen to separate, so that the solutions reflect the translational invariance with respect to $\boldsymbol{y}$,

$$\varphi(\boldsymbol{x}, \boldsymbol{y}) = \mathrm{e}^{i\boldsymbol{p}\cdot\boldsymbol{y}}\, \tilde{\varphi}(\boldsymbol{x})\,, \tag{3.84}$$

where $\boldsymbol{p} \in \mathbb{R}^m$ is the momentum conjugate to the extra dimensions $\boldsymbol{y}$. The reduced wavefunction $\tilde{\varphi}(\boldsymbol{x})$ is subject to a Schrödinger-type equation in m spatial dimensions with the potential generated by the background $\sigma(\boldsymbol{x})$. The spectral method requires rotational symmetry in the n-dimensional subspace of non-trivial coordinates $\boldsymbol{x}$, so that the non-trivial part $\tilde{\varphi}(\boldsymbol{x})$ of the wavefunction is characterized by the radial momentum k and angular momentum ℓ corresponding to the $SO(n)$ symmetry. In the n-dimensional subspace we have scattering and bound state solutions with energies $\sqrt{M^2 + k^2}$ and $\sqrt{M^2 - \kappa_{\ell,j}^2}$, respectively. These correspond to the energies of the full quantum state

$$\omega(k, p) = \sqrt{M^2 + k^2 + p^2} \qquad \text{and} \qquad \omega_{\ell,j}(p) = \sqrt{M^2 + p^2 - \kappa_{\ell,j}^2}\,,$$

where $p = |\boldsymbol{p}|$. The asymptotic behavior of $\tilde{\varphi}(\boldsymbol{x})$ is characterized by a phase shift $\delta_\ell(k)$ for a continuum state or a damping factor $\exp(-\kappa_{\ell,j}^2|\boldsymbol{x}|)$ for a bound state, which in both cases is solely determined from the field equation in the non-trivial subspace. For each such state there is an infinite set of states in the full interface problem indexed by $\boldsymbol{p}$. We want to find the associated density of states. Since there are no interactions in these directions, we have the free density of states for the interval $[\boldsymbol{p}, \boldsymbol{p} + d\boldsymbol{p}]$, which can be read off

from Eq. (1.9)[10] as $V_m/(2\pi)^m$ where $V_m = \int d^m y$. Thus the total density of states in the full interface problem factorizes

$$\rho_\ell(\boldsymbol{p}, k) = \frac{1}{\pi}\frac{d\delta_\ell(k)}{dk}\frac{V_m}{(2\pi)^m} \qquad \text{and} \qquad \rho_{\ell,j}(\boldsymbol{p}) = \frac{V_m}{(2\pi)^m}\,, \tag{3.85}$$

for scattering and bound states of $\tilde{\varphi}(\boldsymbol{x})$, respectively.

The phase shift formula (3.27) can now be applied directly to the interface by integrating over $\boldsymbol{p}$. We consider the energy per unit transverse volume, which becomes

$$\mathscr{E}_{m,n} = \frac{E_{\text{vac}}}{V_m} = \pm \int \frac{d^m p}{(2\pi)^m} \sum_\ell D_n(\ell) \Bigg[\int_0^\infty \frac{dk}{2\pi} \left(\omega(k,p) - \mu(p)\right) \frac{d\delta_\ell(k)}{dk} + \frac{1}{2}\sum_j \left(|\omega_{\ell,j}(p)| - \mu(p)\right)\Bigg] + \frac{E_{\text{ct}}}{V_m}\,. \tag{3.86}$$

The two signs refer to bosons and fermions, respectively. Note that the degeneracy factor $D_n(\ell)$ arises from the partial wave decomposition in the nontrivial subspace, Eq. (3.20). Furthermore, a p-dependent mass term

$$\mu(p) = \sqrt{M^2 + p^2} \tag{3.87}$$

has been subtracted to avoid spurious infrared divergences when Born subtractions are required. Levinson's theorem ensures that this subtraction is an identity, which merely makes the infrared finiteness of the energy manifest.

So far, the counterterms necessary for renormalization have been indicated, but neither the Born terms have been subtracted nor the corresponding Feynman diagrams have been added back in. To begin this procedure, we first subtract the Born approximation $\delta_\ell^{(1)}(k)$ from the phase shift $\delta_\ell(k)$, and add back in the contribution of the tadpole graph, $\mathscr{E}_{\text{FD}}^{(1)}$. Combined with the counterterm, $\mathscr{E}_{\text{ct}}$, this procedure yields the renormalized Feynman diagram[11] $\overline{\mathscr{E}_{\text{FD}}^{(1)}}$. The energy per unit volume then takes the form

$$\mathscr{E}_{m,n} = \pm \int \frac{d^m p}{(2\pi)^m} \sum_\ell D_n(\ell) \left[\int_0^\infty \frac{dk}{2\pi} (\omega(k,p) - \mu(p)) \frac{d}{dk}\left[\delta_\ell(k) - \delta_\ell^{(1)}(k)\right] + \frac{1}{2}\sum_j (|\omega_{\ell,j}(p)| - \mu(p))\right] + \overline{\mathscr{E}_{\text{FD}}^{(1)}} + \mathscr{E}'_{\text{ct}}\,. \tag{3.88}$$

Here $\mathscr{E}'_{\text{ct}}$ refers to any additional counterterms that might be required to renormalize higher order diagrams. In theories with only tadpole divergences we have $\mathscr{E}'_{\text{ct}} = 0$.

[10] The volume of the one-dimensional problem in that case is $2L$.

[11] With the usual no-tadpole renormalization scheme, the counterterm would cancel the diagram completely, $\overline{\mathscr{E}_{\text{FD}}^{(1)}} = 0$.

For the simple boson or Yukawa models in less than three (total) space dimensions, $d-1 = m+n < 3$, the tadpole counterterm is sufficient to renormalize the energy. Hence in Eq. (3.88) the $\boldsymbol{p}$-integral and $\overline{\mathscr{E}^{(1)}_{\rm FD}}$ must separately be finite. After the integration over the trivial momentum $\boldsymbol{p}$, we find

$$\mathscr{E}_{m,n} = \mp \frac{\Gamma(-\frac{1+m}{2})}{2(4\pi)^{\frac{m+1}{2}}} \sum_\ell D_n(\ell) \left[\int_0^\infty \frac{dk}{\pi} (\omega^{m+1}(k,0) - M^{m+1}) \, \frac{d}{dk} \left[\delta_\ell(k)\right]_1 \right.$$
$$\left. + \sum_j (|\omega_{\ell,j}(0)|^{m+1} - M^{m+1}) \right] + \overline{\mathscr{E}^{(1)}_{\rm FD}} \,. \tag{3.89}$$

This result presents a puzzle: if we take $m \to 1$, say with $n = 1$, $\mathscr{E}_{1,1}$ appears to diverge because of the pole in the gamma function. The divergence must be spurious since there is no counterterm for it. Hence the quantity in brackets must vanish for $m = 1$. Furthermore, since each partial wave is independent, each term in the sum must vanish separately. Thus consistency of renormalization theory implies a scattering sum rule which can be cast into the form

$$\int_0^\infty \frac{dk}{\pi} \, k^2 \, \frac{d}{dk} \left[\delta_\ell(k) - \delta^{(1)}_\ell(k) \right] - \sum_j (\kappa_{\ell,j})^2 = 0 \,. \tag{3.90}$$

This is the first generalization of Levinson's theorem, the case $p = q = 1$ in Eq. (2.47). Here it appears as a consistency condition in quantum field theory. Using this sum rule, the limit $m \to 1$ is harmless and we obtain the first instance of an interface formula [29]

$$\mathscr{E}_{1,n} = \pm \frac{1}{4\pi} \sum_\ell D_n(\ell) \left[\int_0^\infty \frac{dk}{\pi} \, k \log \frac{\omega(k)^2}{\mu^2} \, \left[\delta_\ell(k) - \delta^{(1)}_\ell(k) \right] \right.$$
$$\left. - \frac{1}{2} \sum_j \omega^2_{\ell,j} \log \frac{\omega^2_{\ell,j}}{\mu^2} + (\kappa_{\ell,j})^2 \right] + \overline{\mathscr{E}^{(1)}_{\rm FD}} \,, \tag{3.91}$$

where $\omega(k) \equiv \omega(k,0) = \sqrt{M^2 + k^2}$ and $\omega_{\ell,j} = \sqrt{M^2 - \kappa^2_{\ell,j}}$. The arbitrary scale μ in the logarithms cancels because of the sum rule, Eq. (3.90), and Levinson's theorem. As advertised earlier, the final expression for the interface tension depends only on the scattering data from the n non-trivial dimensions. It is therefore not fundamentally more complex than the usual phase shift approach for the vacuum polarization energy.

To extend to higher dimensions, we need to make a second Born subtraction and add back the Feynman two-point function, which will suffice for bosonic models in $m + n < 5$ dimensions. This procedure can be continued indefinitely—subtracting higher Born approximations and adding back the appropriate Feynman diagrams, which are renormalized by local counterterms.

To avoid infrared problems[12] for $n = 1$, we first subtract Eq. (3.90) divided by $2\mu(p)$ from Eq. (3.88). The net effect is to replace $[\,\omega(k,p) - \mu(p)\,]$ by $[\,\omega(k,p) - \mu(p) - k^2/2\mu(p)\,]$ under the k-integral. Next, we subtract the second Born approximation as usual and add back in the two-point Feynman diagram. Again, the integration over the trivial momentum $\boldsymbol{p}$ can be performed with the result

$$\mathscr{E}_{m,n} = \mp\frac{\Gamma(-\frac{1+m}{2})}{2(4\pi)^{\frac{m+1}{2}}}\sum_\ell D_n(\ell)\Bigg\{\sum_j\Big(|\omega_{\ell,j}|^{m+1} - M^{m+1} + \frac{m+1}{2}\kappa_{\ell,j}^2 M^{m-1}\Big) + \int_0^\infty\frac{dk}{\pi}\left[\omega(k)^{m+1} - M^{m+1} - \frac{m+1}{2}k^2M^{m-1}\right] \times\frac{d}{dk}\left[\delta_\ell(k) - \delta_\ell^{(1)}(k) - \delta_\ell^{(2)}(k)\right]\Bigg\} + \overline{\mathscr{E}_{\rm FD}^{(2)}}. \quad (3.92)$$

By construction the coefficient of the gamma function vanishes as $m \to 1$. The limit $m \to 1$ gives

$$\mathscr{E}_{1,n} = \pm\frac{1}{4\pi}\sum_\ell D_n(\ell)\left[\int_0^\infty\frac{dk}{\pi}\,k\log\frac{\omega(k)^2}{\mu^2}\,\left[\delta_\ell(k) - \delta_\ell^{(1)}(k)\delta_\ell^{(2)}(k)\right] - \frac{1}{2}\sum_j\omega_{\ell,j}^2\log\frac{\omega_{\ell,j}^2}{\mu^2} + (\kappa_{\ell,j})^2\right] + \overline{\mathscr{E}_{\rm FD}^{(2)}}\,. \quad (3.93)$$

Equations (3.91) and (3.93) are identical for values of n where only one Born subtraction is necessary. The contribution of the second Born approximation has been replaced by the second-order Feynman diagram. However, Eq. (3.93) can be continued to values of n where two subtractions are necessary.

As before, the finiteness of Eq. (3.93) as $m \to 3$ implies another sum rule,

$$\int_0^\infty\frac{dk}{\pi}\,k^4\,\frac{d}{dk}\left[\delta_\ell(k) - \delta_\ell^{(1)}(k) - \delta_\ell^{(2)}(k)\right] - \sum_j(\kappa_{\ell,j})^4 = 0\,, \quad (3.94)$$

which corresponds to Eq. (2.47) for $p = q = 2$. In the limit $m \to 3$ we then obtain,

$$\mathscr{E}_{3,n} = \pm\frac{1}{32\pi^2}\sum_\ell D_n(\ell)\left[-\int_0^\infty\frac{dk}{2\pi}4k\,\omega(k)^2\log\frac{\omega(k)^2}{\mu^2}\,[\delta_\ell(k)]_2 + \frac{1}{2}\sum_j\left((\omega_{\ell,j})^4\log\frac{(\omega_{\ell,j})^2}{\mu^2} + \mu^2(\kappa_{\ell,j})^2 - \frac{1}{2}(\kappa_{\ell,j})^4\right)\right] + \overline{\mathscr{E}_{\rm FD}^{(2)}}\,. \quad (3.95)$$

[12] See Ref. [34] for a thorough discussion of the infrared anomalies that occur for $n = 1$.

The generalization of these methods to higher dimensional interfaces $m > 3$ is straightforward [34]. Since the scattering data that enter the interface formula are the same as in the non-interface case, Eq. (3.27), the integration contour can again be rotated to the imaginary axis, as in Fig. 3.1. This formulation does not require explicit bound state contributions and is the most concise and compact version of the interface formula. For instance, a string-like interface in $3+1$ spacetime dimensions corresponds to $n = 2$ and $m = 1$. For the simple boson model, the energy per unit length of the string becomes

$$\mathscr{E}_{1,2} = \sum_{\ell=0}^{\infty} D_2(\ell) \int_M^{\infty} \frac{dt}{4\pi}\, t\, [\nu_\ell(t)]_2 + \sum_{i=1}^{2} \mathscr{E}_{\mathrm{FD}}^{(i)} + \mathscr{E}_{\mathrm{CT}}\,. \tag{3.96}$$

This result should be compared to the expression (3.26), which is valid in the absence of extra dimensions ($m = 0$). The net effect of the extra dimension is simply to change the kinematical factor under the integral—reflecting the additional divergences that arise in higher dimensions—while the key dynamical ingredient $\nu_\ell(t)$ and thus the complexity of the problem is unaffected. We will study applications with plane-like interfaces ($m = 2$) that arise in the context of the Casimir effect in Chap. 7.

References

1. H. Gies and K. Langfeld, *Nucl. Phys.* **B613** (2001) 353. 35
2. H. Gies and K. Langfeld, *Int. J. Mod. Phys.* **A17** (2002) 966. 35
3. K. Langfeld, L. Moyaerts, and H. Gies, *Nucl. Phys.* **B646** (2002) 158. 35
4. H. Gies, K. Langfeld, and L. Moyaerts, *JHEP* **06** (2003) 018. 35
5. D. Ebert and H. Reinhardt, *Nucl. Phys.* **B271** (1986) 188. 35
6. I. G. Avramidi, *Nucl. Phys.* **B355** (1991) 712. 35
7. I. G. Avramidi, *J. Math. Phys.* **36** (1995) 5055. 35
8. I. J. R. Aitchison and C. M. Fraser, *Phys. Lett.* **B146** (1984) 63. 35
9. I. J. R. Aitchison and C. M. Fraser, *Phys. Rev.* **D31** (1985) 2605. 35
10. N. Graham et al., *Nucl. Phys.* **B645** (2002) 49. 37, 46
11. M. Bordag, *J. Phys.* **A28** (1995) 755. 38, 55
12. S. Weinberg, *The Quantum Theory of Fields II*, Ch. 16. Cambridge University Press, 1995. 42, 43
13. J. Glimm and A. Jaffe, *Quantum Physics: A Functional Integral Point of View.* Springer, New York, 1987. 42
14. C. Itzykson and J. B. Zuber, *Quantum Field Theory*, Ch. 9. McGraw–Hill International Editions, 1980. 43
15. R. Alkofer, H. Reinhardt, and H. Weigel, *Phys. Rept.* **265** (1996) 139. 43
16. N. Graham, V. Khemani, M. Quandt, O. Schröder, and H. Weigel, *Nucl. Phys.* **B707** (2005) 233. 46
17. E. Farhi, N. Graham, R. L. Jaffe, and H. Weigel, *Nucl. Phys.* **B585** (2000) 443. 49
18. E. Farhi, N. Graham, R. L. Jaffe, and H. Weigel, *Nucl. Phys.* **B595** (2001) 536. 49
19. N. Graham, R. L. Jaffe, and H. Weigel, *Int. J. Mod. Phys.* **A17** (2002) 846. 49

20. E. Farhi, N. Graham, R. L. Jaffe, and H. Weigel, *Nucl. Phys.* **B630** (2002) 241. 49
21. J. C. Collins, *Renormalization. An Introduction to Renormalization, the Renormalization Group, and the Operator Product Expansion.* Cambridge University Press, UK 1984. 52
22. N. N. Bogoliubov and O. S. Parasiuk, *Acta Math.* **97** (1957) 227. 54
23. K. Hepp, *Commun. Math. Phys.* **2** (1966) 301. 54
24. W. Zimmermann, *Commun. Math. Phys.* **15** (1969) 208. 54
25. S. Weinberg, *Phys. Rev.* **118** (1960) 838. 54
26. D. B. Kaplan, *Phys. Lett.* **B288** (1992) 342. 55
27. Y. Shamir, *Nucl. Phys.* **B406** (1993) 90. 55
28. V. A. Rubakov, *Phys. Usp.* **44** (2001) 871. 55
29. N. Graham, R. L. Jaffe, M. Quandt, and H. Weigel, *Phys. Rev. Lett.* **87** (2001) 131601. 55, 58
30. S. Weinberg, *Physica* **A96** (1979) 327. 54
31. J. Gasser and H. Leutwyler, *Ann. Phys.* **158** (1984) 142. 54
32. V. Bernard and U. G. Meißner, hep-ph/0611231. 54
33. A. Parnachev and L. G. Yaffe, *Phys. Rev.* **D62** (2000) 105034. 55
34. N. Graham, R. L. Jaffe, M. Quandt, and H. Weigel, *Annals Phys.* **293** (2001) 240. 59, 60

4 Applications in One Space Dimension

In this chapter we will apply the techniques we have developed to compute vacuum polarization energies for various systems.

We start by considering models in $d = 1 + 1$ dimensions. Systems with one space dimension provide a particularly simple testing ground for our approach. We will also see that they contain subtleties that our approach is well-suited to address. In later chapters we will thoroughly investigate models in three spatial dimensions.

4.1 Vacuum Polarization Energy in Exactly Solvable Models

The two most commonly studied models in one space dimension happen to correspond to exactly solvable scattering problems. We will start with these special systems because they enable us to present the full calculation in explicit detail. First we consider the ϕ^4 kink, with Lagrangian density

$$\mathcal{L} = \frac{1}{2}\left(\partial_\mu \phi\right)\left(\partial^\mu \phi\right) - \frac{\lambda}{4}\left(\phi^2 - \frac{M^2}{2\lambda}\right)^2 , \tag{4.1}$$

which has degenerate minima at $\phi_0 = \pm M/\sqrt{2\lambda}$. In the perturbative sector the fluctuations about either minimum describe bosons of mass M. The kink is a non-perturbative static solution to the field equations,

$$\phi_K(x) = \frac{M}{\sqrt{2\lambda}} \tanh\left(\frac{Mx}{2}\right), \tag{4.2}$$

interpolating between these two vacua at $x = \pm\infty$. Sending $x \to -x$ yields the anti-kink solution. We consider small-amplitude fluctuations, η, about the kink configuration by parameterizing the field variable as $\phi = \phi_K + \eta$ and expanding the Lagrangian to quadratic order in η, which yields the small oscillation equation

$$-\frac{\partial^2 \eta}{\partial t^2} = \left[-\frac{\partial^2}{\partial x^2} + M^2 - \frac{3M^2}{2}\,\mathrm{sech}^2\left(\frac{Mx}{2}\right)\right]\eta\,. \tag{4.3}$$

Graham, N., et al.: *Applications in One Space Dimension*. Lect. Notes Phys. **777**, 63–89 (2009)
DOI 10.1007/978-3-642-00139-0_4

The potential

$$V_2(x) = -\frac{3M^2}{2}\,\mathrm{sech}^2\left(\frac{Mx}{2}\right) \tag{4.4}$$

is the $n = 2$ member of the Pöschl–Teller family [1] of exactly solvable potentials,

$$V_n(x) = -\left(\frac{n+1}{n}\right) M^2\,\mathrm{sech}^2\left(\frac{Mx}{n}\right), \tag{4.5}$$

where $n = 0, 1, 2, \ldots$ and $n \to 0$ yields the free theory $V_0(x) \equiv 0$. These potentials are symmetric and reflectionless and the corresponding bound and scattering state wavefunctions are known explicitly. While symmetry of the potential guarantees that the 2×2 S-matrix for the symmetric and antisymmetric channels is diagonal, reflectionlessness requires that it be proportional to the identity matrix. Thus the symmetric and antisymmetric phase shifts must be equal. They are given by

$$\delta_S(k) = \delta_A(k) = \sum_{j=1}^{n} \arctan\left(\frac{jM}{kn}\right), \tag{4.6}$$

and corresponding bound states at

$$k^2 = -\frac{j^2M^2}{n^2}, \tag{4.7}$$

with $j = 0, 1, 2, \ldots, n$. We note that in order to reconcile the equality of the phase shifts with the different forms of Levinson's theorem in the two channels, cf. Eqs. (2.66) and (2.50),

$$\begin{aligned} \delta_{\mathrm{S}}(0) - \delta_{\mathrm{S}}(\infty) &= \pi\left(n_{\mathrm{S}} - \frac{1}{2}\right) \\ \delta_{\mathrm{A}}(0) - \delta_{\mathrm{A}}(\infty) &= \pi n_{\mathrm{A}}\,, \end{aligned} \tag{4.8}$$

all reflectionless potentials (including the free particle) must have a "half-bound" threshold state, given here by the case $j = 0$.

By taking

$$\eta(x,t) = \mathrm{e}^{-i\omega t}\eta_\omega(x)\,, \tag{4.9}$$

with $\omega = \sqrt{k^2 + M^2}$, we can use these results to analyze the solutions to Eq. (4.3). There is a zero mode with $\omega_0 = 0$ (for $j = 2$) and an additional bound state with $\omega_1^2 = \frac{3M^2}{4}$ (for $j = 1$). The corresponding wavefunctions are

$$\begin{aligned} \eta_0 &= \sqrt{\frac{3M}{8}}\,\mathrm{sech}^2\left(\frac{M}{2}x\right) \\ \eta_1 &= \sqrt{\frac{3M}{4}}\tanh\left(\frac{M}{2}x\right)\mathrm{sech}\left(\frac{M}{2}x\right), \end{aligned} \tag{4.10}$$

where we have adopted the normalization conventions that arise in the standard construction of solutions for Pöschl–Teller potentials [1]. The zero mode arises because of translational invariance of the kink solution, $\eta_0 \propto \frac{\partial \phi_K}{\partial x}$.

The two linearly independent continuum solutions with wave vector k are [2]

$$\eta_{\rm r}(x) = \eta_{\rm l}(x)^* = \frac{{\rm e}^{ikx} M^2}{\omega\sqrt{4k^2+M^2}} \times \left[\frac{3}{2}\tanh^2\left(\frac{M}{2}x\right) - \frac{1}{2} - \frac{2k^2}{M^2} - i\frac{3k}{M}\tanh\left(\frac{M}{2}x\right)\right], \tag{4.11}$$

corresponding to right- and left-moving waves, respectively. They scatter without reflection. We can then form symmetric and antisymmetric solutions

$$\eta_{\rm S}(x) = \frac{1}{2}\left(\eta_{\rm r}(x) + \eta_{\rm l}(x)\right); \qquad \eta_{\rm A}(x) = \frac{1}{2i}\left(\eta_{\rm r}(x) - \eta_{\rm l}(x)\right). \tag{4.12}$$

From these results, we obtain the phase shifts

$$\delta_{\rm S}^{\rm kink}(k) = \delta_{\rm A}^{\rm kink}(k) = \arctan\left(\frac{M}{k}\right) + \arctan\left(\frac{M}{2k}\right) = \arctan\left(\frac{3Mk}{2k^2-M^2}\right). \tag{4.13}$$

In Sect. 2.4.3 we have observed that Eq. (2.66) implies $n_{\rm S} = \frac{1}{2}$ in the case of no interaction because there is a "half-bound" state at threshold. This state must be included in the expression for the vacuum polarization energy in the absence of the kink, so that the full bound state contribution to the kink vacuum polarization energy should actually be expressed as the difference $\frac{1}{2}\sum_i \omega_i - \frac{M}{4}$. To circumvent this technical complication, it is useful to employ Levinson's theorem and rewrite the (unrenormalized) vacuum polarization energy in terms of the binding energies,

$$\Delta E = \frac{1}{2}\sum_i (\omega_i - M) + \int \frac{dk}{2\pi}(\omega - M)\frac{d}{dk}\left(\delta_{\rm S}(k) + \delta_{\rm A}(k)\right). \tag{4.14}$$

The half-bound states at threshold then do not appear explicitly in this formulation.

To renormalize this expression we have to subtract (at least) the leading term in the Born series from the phase shifts, using the results of Chap. 2. We use Eq. (3.53) with $n = 1$ and then choose $\ell = 0$ and $\ell = 1$ to obtain results for the symmetric and antisymmetric channels, respectively,

$$\begin{aligned} \delta_{\rm S}^{(1)}(k) &= -\frac{1}{k}\int_0^\infty V(x)\cos^2 kx\, dx \\ \delta_{\rm A}^{(1)}(k) &= -\frac{1}{k}\int_0^\infty V(x)\sin^2 kx\, dx\,. \end{aligned} \tag{4.15}$$

The sum of these two results is just proportional to the integral over space of the potential from the differential equation (4.3), $\langle V\rangle = \frac{1}{2}\int_{-\infty}^{\infty} dx\, V(x) = -3M^2$, which we have normalized by analogy with the radially symmetric

case. Because the first-order Feynman diagram is completely local, it exactly cancels the counterterm in the no-tadpole renormalization scheme, and the renormalized vacuum polarization energy becomes

$$\Delta E = \frac{1}{2}\sum_j (\omega_j - M) - \int_0^\infty \frac{dk}{2\pi}\frac{k}{\omega(k)}\left(\delta_{\rm A}(k) + \delta_{\rm S}(k) + \frac{\langle V\rangle}{k}\right) . \qquad (4.16)$$

Note that the Levinson subtraction in Eq. (4.14) also eliminated a potential infrared divergence associated with the Born subtraction. The resulting integral can be straightforwardly computed from the phase shifts, Eq. (4.13), and the vacuum polarization energy of the kink in the no-tadpole scheme becomes

$$\Delta E = M\left(\frac{1}{4\sqrt{3}} - \frac{3}{2\pi}\right) , \qquad (4.17)$$

which is the standard result given in Ref. [3].

We can repeat this analysis for the sine-Gordon model, for which the Lagrangian is

$$\mathcal{L}_{SG} = \frac{1}{2}(\partial_\mu\phi)^2 + \frac{M^4}{\lambda}\left[\cos\left(\frac{\sqrt{\lambda}\phi}{M}\right) - 1\right] . \qquad (4.18)$$

The corresponding soliton solution reads [2]

$$\phi_{SG} = \frac{4M}{\sqrt{\lambda}}\arctan\left(\mathrm{e}^{-Mx}\right) , \qquad (4.19)$$

and the antisoliton solution is given by sending $x \to -x$. In both cases the small oscillation potential is again of the form in Eq. (4.5), but now with $n = 1$. We have scattering wavefunctions

$$\eta_{\rm r}(x) = \eta_{\rm l}(x)^* = \frac{1}{\omega}\,\mathrm{e}^{ikx}\,(k + iM\tanh Mx) , \qquad (4.20)$$

and a single zero mode bound state with $k^2 = -M^2$,

$$\eta_0 = \sqrt{\frac{M}{2}}\,\mathrm{sech}\,Mx\,. \qquad (4.21)$$

Its existence is again guaranteed by translation invariance of the underlying theory. The phase shifts

$$\delta_{\rm S}^{\rm SG}(k) = \delta_{\rm A}^{\rm SG}(k) = \arctan\left(\frac{M}{k}\right) \qquad (4.22)$$

are again equal in the two channels, requiring the existence of a half-bound threshold state in the antisymmetric channel. We summarize the bound states in these two models in Table 4.1.

Table 4.1 Bound states (b.s.) and half-bound states in various $d = 1{+}1$ dimensional models

	Sym. ch.		Anti-sym. ch.	
	true b.s.	half b.s.	true b.s.	half b.s.
$V \equiv 0$	0	1	0	0
SG	1	0	0	1
kink	1	1	1	0

Having gathered all this information, we can compute the vacuum polarization energy of the sine-Gordon soliton as we did for the kink in Eq. (4.16). We find $\Delta E_{SG} = -M/\pi$ in the no-tadpole renormalization scheme, again in agreement with standard results [2].

4.2 Fermions in One Spatial Dimension

Fermions do not have classical analogs and thus there is no fermionic soliton whose vacuum polarization we could compute. However, fermions can couple to boson field configurations that vary in space. Such boson fields then induce a fermion vacuum polarization energy. In this section we will compute such energies using techniques we have developed. To do so, we will transform the coupled first-order differential equations for fermions into second-order differential equations for the individual components of the fermion spinors. In preparation for this calculation, we first explain the computation of the fermion scattering data in one spatial dimension.

4.2.1 Parity-Invariant Background Fields

We begin by considering fermions coupled to a doublet of static background fields $\boldsymbol{\phi}(x) = \begin{pmatrix} \phi_1(x) \\ \phi_2(x) \end{pmatrix}$ in a way that preserves parity invariance. The fermion Lagrangian density is

$$\mathcal{L}_F = \frac{1}{2}\left(i\left[\bar{\Psi}, \partial\!\!\!/ \Psi\right] - G\left(\left[\bar{\Psi}, \Psi\right]\phi_1 + i\left[\bar{\Psi}, \gamma_5 \Psi\right]\phi_2\right)\right) . \tag{4.23}$$

Here G is the Yukawa coupling constant and we have used commutators to ensure that discrete symmetries are properly maintained, as we discuss further in Sect. 5.2. We choose the representation $\gamma^0 = \sigma_2$, $\gamma^1 = i\sigma_3$, and $\gamma_5 = \sigma_1$ for the Dirac matrices (where σ_i are the Pauli matrices), so that the Dirac Hamiltonian becomes

$$H[\boldsymbol{\phi}] = i\sigma_1 \frac{d}{dx} + G\sigma_2\phi_1(x) + G\sigma_3\phi_2(x) . \tag{4.24}$$

When $\boldsymbol{\phi}$ has a non-zero vacuum expectation value, the mass of the fermion is $M = G\sqrt{\langle\phi_1\rangle^2 + \langle\phi_2\rangle^2}$. We assume that the boson sector dynamics gives the usual vacuum choice $\langle\phi_1\rangle = v$ and $\langle\phi_2\rangle = 0$. Although the underlying fermion theory is charge conjugation invariant, the Dirac Hamiltonian in the presence of a fixed $\boldsymbol{\phi}(x)$ is not, unless $\phi_2 \equiv 0$. It is therefore necessary to consider both positive and negative-energy eigenvalues ω of the time-independent Dirac equation

$$H\psi = \omega\psi\,. \tag{4.25}$$

The associated second-order equations for the Dirac spinor, $\psi \equiv \binom{f}{g}$, are

$$\begin{aligned} -f'' - G\phi_1' f + G\phi_2'(\omega + G\phi_2)^{-1}(f' + G\phi_1 f) &= (\omega^2 - G^2\phi_1^2 - G^2\phi_2^2)f \\ -g'' + G\phi_1' g - G\phi_2'(\omega - G\phi_2)^{-1}(g' - G\phi_1 g) &= (\omega^2 - G^2\phi_1^2 - G^2\phi_2^2)g\,. \end{aligned} \tag{4.26}$$

In one spatial dimension, there are two channels for each energy. The S-matrix is 2×2 dimensional and, in general, not diagonal. We simplify this situation using parity invariance. By demanding that ϕ_1 and ϕ_2 are, respectively, even and odd under coordinate reflection we ensure that the Dirac Hamiltonian, Eq. (4.24), is invariant under parity,

$$[P, H] = 0, \quad \text{where} \quad P = \gamma_0 \Pi = \sigma_2 \Pi \tag{4.27}$$

and Π is the coordinate reflection operator that transforms x to $-x$. Thus we can choose a basis of parity eigenstates,

$$P\psi_\pm(x) \equiv \sigma_2\psi_\pm(-x) = \pm\psi_\pm(x)\,, \tag{4.28}$$

and replace the scattering problem on the line $x \in [-\infty, \infty]$ by two scattering problems on the half-line $x \in [0, \infty]$ corresponding to even and odd parity. Equation (4.28) gives boundary conditions at $x = 0$ on the parity eigenstates:

$$\psi_+(0) \propto \begin{pmatrix} 1 \\ i \end{pmatrix} \qquad \text{and} \qquad \psi_-(0) \propto \begin{pmatrix} 1 \\ -i \end{pmatrix}. \tag{4.29}$$

The solution to the Dirac equation on the half-line with either boundary condition is unique up to an overall normalization. For $x \to \infty$, this unique solution can be written as a superposition of incoming ($\propto e^{-ikx}$) and outgoing ($\propto e^{ikx}$) waves. The coefficient of the outgoing wave relative to the incoming wave defines the phase shift.

To implement this program, we introduce eigenstates of the free Dirac Hamiltonian with energy ω,

$$\begin{aligned} \varphi^0_{+k}(x) &= \frac{1}{\omega}\begin{pmatrix} \omega \\ -k + iM \end{pmatrix} \mathrm{e}^{ikx} \\ \varphi^0_{-k}(x) &= \frac{1}{\omega}\begin{pmatrix} \omega \\ k + iM \end{pmatrix} \mathrm{e}^{-ikx}\,, \end{aligned} \tag{4.30}$$

where $k = +\sqrt{\omega^2 - M^2}$. Next, we construct the eigenstates of the full interacting Dirac Hamiltonian with energy ω that are asymptotic to $\varphi^0_{\pm k}$ as $x \to \infty$,

$$\varphi_{+k}(x) = \begin{pmatrix} f(x) \\ \dfrac{i}{\omega + G\phi_2(x)}(f'(x) + G\phi_1(x)f(x)) \end{pmatrix} \tag{4.31}$$

and

$$\varphi_{-k}(x) = \begin{pmatrix} f^*(x) \\ \dfrac{i}{\omega + G\phi_2(x)}(f^{*\prime}(x) + G\phi_1(x)f^*(x)) \end{pmatrix} . \tag{4.32}$$

Here $f(x)$ is the solution to the real second-order equation for the upper component, Eq. (4.26), subject to the boundary condition that $f(x) \to e^{ikx}$ as $x \to \infty$. It is easy to verify that in the same limit $\varphi_{\pm k}(x) \to \varphi^0_{\pm k}(x)$ since the boson fields approach their vacuum values.

Since the even and odd parity channels decouple, the S-matrix is diagonal in this basis. Its diagonal elements $S_\pm = e^{2i\delta_\pm(\omega)}$ can be defined through the even and odd parity eigenstates of H,

$$\begin{aligned} \psi_+(x) &= \varphi_{-k}(x) + \frac{M - ik}{\omega} S_+(\omega)\varphi_{+k}(x) \\ \psi_-(x) &= \varphi_{-k}(x) - \frac{M - ik}{\omega} S_-(\omega)\varphi_{+k}(x) . \end{aligned} \tag{4.33}$$

If we set the interaction to zero, $\boldsymbol{\phi}$ assumes its vacuum value $\phi_1 = v, \phi_2 = 0$ and ψ_+ (ψ_-) reduces to the even (odd) parity solution to the free Dirac equation with $S_\pm = 1$, which explains the extra factor of $\frac{M-ik}{\omega}$ in Eq. (4.33).

To determine $S_\pm$ we use the fact that the eigenstates of Eq. (4.33) obey Eq. (4.29). For the positive parity channel this condition yields

$$S_+(\omega) = -\frac{(M + ik)\left[(\omega - G\phi_1(0))f^*(0) - f'^*(0)\right]}{\omega\left[(\omega - G\phi_1(0))f(0) - f'(0)\right]}, \tag{4.34}$$

and similarly for the negative parity channel

$$S_-(\omega) = \frac{(M + ik)\left[(\omega + G\phi_1(0))f^*(0) + f'^*(0)\right]}{\omega\left[(\omega + G\phi_1(0))f(0) + f'(0)\right]} . \tag{4.35}$$

To compute the phase shifts efficiently and avoid 2π ambiguities, it is convenient to factor the free solution out of $f(x)$ by writing $f(x) = e^{ikx}e^{i\beta(x,\omega)}$, cf. Eq. (2.52). Then the phase shifts are given by[1]

$$\delta_\pm(\omega) = -\operatorname{Re}\beta(0,\omega) - \arg\Big[1 + \frac{i\beta'(0,\omega) + G(\phi_1(0) - v)}{\mp\omega + Gv + ik}\Big] , \tag{4.36}$$

where the complex function $\beta(x,\omega)$ solves the differential equation

[1] Since $\omega = \sqrt{k^2 + M^2} = |ik + M|$ we have $\arg(ik + M) = 2\arg(ik + M + \omega)$. Furthermore we recall that $M = Gv$.

$$-i\beta''(x,\omega)+2k\beta'(x,\omega)+\beta'^2(x,\omega)-M^2+G^2\phi_1^2(x)+G^2\phi_2^2(x)-G\phi_1'(x)\\ +\frac{G\phi_2'(x)}{\omega+G\phi_2(x)}\big[G\phi_1(x)+i(k+\beta'(x,\omega))\big]=0, \tag{4.37}$$

subject to the boundary conditions $\beta(\infty,\omega)=\beta'(\infty,\omega)=0$. It is this equation that we solve numerically for a given background $\boldsymbol{\phi}(x)$ to determine the phase shifts, from which we then compute the vacuum polarization energy. We will use these techniques to study soliton stabilization by fermion vacuum polarization energies in Sect. 4.4. First, however, we will carry out some preparatory work needed to investigate supersymmetric models in $d=1+1$ dimensions.

4.2.2 Fermions in the sine-Gordon Background

For fermion systems in one spatial dimension we often encounter background configurations that give opposite signs in the mass term of the Dirac equation at $x\to\pm\infty$. Even though the two signs describe the same fermion, the extraction of the scattering matrix in this case is non-trivial. We elaborate on that issue in this section.

For example, in the notation of Eq. (4.23), the sine-Gordon (SG)-soliton background reads

$$G\phi_1(x)=M\tanh(Mx)\qquad\text{and}\qquad\phi_2=0\,, \tag{4.38}$$

where M is the fermion mass. It is straightforward to verify that

$$\psi=\begin{pmatrix}\frac{i}{\omega}\left[ik-M\tanh(Mx)\right]\\ 1\end{pmatrix}\mathrm{e}^{ikx} \tag{4.39}$$

solves the corresponding Dirac equation. However, this information is not sufficient to determine the phase shifts $\delta_\pm(\omega)$ from Eqs. (4.34) and (4.35), because the SG background field is not invariant under parity reflection, a fundamental ingredient for the results of the previous section. Even though the mass term in the Dirac Hamiltonian, Eq. (4.24), changes sign when passing from $x=-\infty$ to $x=+\infty$, it still describes a free fermion of mass M in both asymptotic regimes. However, we cannot directly compare the wavefunctions and extract phase shifts since the two vacua at $x=\pm\infty$ are only identified after a non-trivial chiral rotation.

To solve this problem, we generalize the configuration of Eq. (4.38) to

$$G\phi_1(x)=M\left[1+\tanh M(x-R)-\tanh M(x+R)\right]\quad\text{and}\quad\phi_2=0\,, \tag{4.40}$$

which is the superposition of an SG-soliton centered at $x=R$ and an SG anti-soliton at $x=-R$. This configuration is obviously invariant under parity and we may employ Eq. (4.36) directly to determine the phase shifts. If R becomes very large, interference effects between the solition and the anti-solition can

be ignored and by charge conjugation symmetry we must assign half of the resulting vacuum polarization energy to the soliton and the other half to the antisoliton. As a result we can compute the sum of the fermion eigenphase shifts in the SG model as exactly half of that for the configuration Eq. (4.40) in the limit $R \to \infty$. To apply the techniques of the previous section we only require the spinor in the regime $x \geq 0$, in which case the effect of the anti-SG at $x = -R$ may be ignored. The solution

$$\psi = \begin{pmatrix} \frac{1}{ik-M}\left(ik - M\tanh\left[M(x-R)\right]\right) \\ \frac{-i\omega}{ik-M} \end{pmatrix} \mathrm{e}^{ikx} \tag{4.41}$$

has the asymptotic behavior described in Eq. (4.31) and is thus suitable to identify $f(x)$. We find

$$f(0) = -\frac{M+ik}{M-ik} \qquad \text{and} \qquad f'(0) = -ik\frac{M+ik}{M-ik} = ikf(0)\,, \tag{4.42}$$

for sufficiently large R, and read off

$$\beta(0) = 2\arctan\left(\frac{k}{M}\right) - \pi \qquad \text{and} \qquad \beta'(0) = 0\,. \tag{4.43}$$

It is now straightforward to find the phase shifts from Eq. (4.36),

$$\delta_{\pm}(k) = \pi - 2\arctan\left(\frac{k}{M}\right) - \arg\left[1 - \frac{-2M}{\mp\omega + M + ik}\right] = \arctan\left(\frac{M}{k}\right)\,. \tag{4.44}$$

Here we used that $G\phi_1(0) = -M$ in the limit $R \to \infty$ and $v = M/G$. Also, we have used the momentum as the argument (instead of the energy ω) because the configuration Eq. (4.40) induces a charge conjugation invariant fermion spectrum. The phase shifts, Eq. (4.44), imply that the sum of the eigenphase shifts for fermions in the single SG soliton background is

$$\sum_{i=1}^{2} \delta_i^{(\mathrm{SG})}(k) = \arctan\left(\frac{M}{k}\right)\,. \tag{4.45}$$

Using this result we can easily compute phase shifts of any other configuration with opposite signs in the mass term by comparing it to the SG model. This *relative* phase shift parameterizes the unitary transformation that maps the state vector of such configurations onto that of the SG soliton. The subsequent unitary transformation that yields the state vector associated with free fermions is parameterized by the phase shift in Eq. (4.45). Thus we merely have to add these two phase shifts to determine the eigenphase shifts relative to free fermions. Furthermore, from Eq. (4.39) we observe that in the SG model the lower component is just a plane wave. Hence for any other problem with such an *odd* vacuum we may read off the phase shift relative to the SG model directly from the corresponding lower component.

4.2.3 Fermions in the Kink Background

The analysis of fermions in the kink background

$$G\phi_1(x) = M \tanh\left(\frac{Mx}{2}\right) \qquad G\phi_2(x) = 0\,, \tag{4.46}$$

suffers from the same subtleties as the previously discussed SG model, i.e., the mass terms at $x = \pm\infty$ have opposite signs and parity is not a good quantum number. We will demonstrate two different techniques for analyzing this case.

First, we can proceed in analogy to the SG model and consider a widely separated kink–anti-kink pair,

$$G\phi_1(x, x_0) = M\left(1 + \tanh\frac{M(x-R)}{2} - \tanh\frac{M(x+R)}{2}\right), \tag{4.47}$$

where R is large. We will take advantage of the reflectionless property of the bosonic kink potential to simplify the derivation, though our results are general.

In the neighborhood of the kink, the Dirac spinor obeys the second-order equation

$$\begin{pmatrix} -\frac{d^2}{dx^2} + V_2(x-R) & 0 \\ 0 & -\frac{d^2}{dx^2} + \tilde{V}_2(x-R) \end{pmatrix} \psi_k(x) = k^2 \psi_k(x)\,, \tag{4.48}$$

where $V_n(x)$ denotes a bosonic Pöschl–Teller potentials given by Eq. (4.5) and $\tilde{V}_n(x) \equiv \left(\frac{n-1}{n}\right)^2 V_{n-1}\left(\frac{n-1}{n}x\right)$. For the anti-kink, we obtain the same equation with the upper and lower components reversed and $R \to -R$.

An incident wave far to the left is given by

$$\psi_k(x) = e^{ikx}\begin{pmatrix} 1 \\ ie^{i\theta} \end{pmatrix}, \tag{4.49}$$

with $\theta = \arctan\frac{k}{M}$. It scatters without reflection through the antisoliton, becoming

$$\psi_k(x) = e^{ikx}\begin{pmatrix} e^{i\tilde{\delta}_2} \\ ie^{i(\delta_2+\theta)} \end{pmatrix}, \tag{4.50}$$

where

$$\delta_n(k) = 2\sum_{j=1}^{n} \arctan\left(\tfrac{jM}{kn}\right) \quad \text{and} \quad \tilde{\delta}_n(k) = \delta_{n-1}\left(\tfrac{nk}{n-1}\right) = 2\sum_{j=1}^{n-1} \arctan\left(\tfrac{jM}{kn}\right)$$

are the total phase shifts for the bosonic potentials $V_n(x)$ and $\tilde{V}_n(x)$, respectively. Note that $\tilde{\delta}_n(k)$ does not have a pole at $k = iM$, which indicates the absence of a zero mode. All the other bound states (if any) of $V_n(x)$ and $\tilde{V}_n(x)$

coincide. We further observe that the spinor Eq. (4.50) solves the free Dirac equation for $G\phi_1 = -M$ because $\delta_2(k) - \tilde{\delta}_2(k) = 2\arctan\frac{M}{k}$. The solution then scatters without reflection through the soliton, giving

$$\psi_k(x) = e^{ikx}\begin{pmatrix} e^{i(\delta_2+\tilde{\delta}_2)} \\ ie^{i(\delta_2+\tilde{\delta}_2+\theta)} \end{pmatrix}, \tag{4.51}$$

so that the total phase shift for the kink/anti-kink pair, obtained by comparison to the free solution Eq. (4.49), is $\delta_2(k) + \delta_1(2k)$. Dividing this result by 2 to obtain the phase shift for a single kink, we see that the resulting phase shift is the average of the phase shifts of the bosonic potentials for the upper and lower components. Thus we obtain the fermionic phase shifts

$$\delta_{\text{tot}}^{\text{kink}}(k) = \arctan\left(\frac{M}{k}\right) + 2\arctan\left(\frac{M}{2k}\right). \tag{4.52}$$

The total fermionic phase shift for the kink is smaller than the corresponding total bosonic phase shift (δ_2) by $\arctan\left(\frac{M}{k}\right)$. This result is general and reflects a difference in the zero modes in the two cases, which we have already indicated above but will investigate more closely below.

As a second approach we may obtain the same result by explicitly considering a single kink and comparing it to the SG model above. To this end we examine the generalized coupling between a fermion Ψ and a background potential $V_F(x)$,

$$\mathcal{L}_F = \left(i\bar{\Psi}\partial\!\!\!/\Psi - V_F(x)\bar{\Psi}\Psi\right), \tag{4.53}$$

where the background $V_F(x)$ is a real antisymmetric function of x interpolating between $\pm M$ at $x = \pm\infty$, respectively. We find the bosonic potentials

$$\begin{aligned} V(x) &= V_F(x)^2 + \frac{dV_F(x)}{dx} - M^2 \\ \widetilde{V}(x) &= V_F(x)^2 - \frac{dV_F(x)}{dx} - M^2, \end{aligned} \tag{4.54}$$

associated with the upper and lower components, respectively. We note that these bosonic potentials are invariant under spatial reflection.

The Klein–Gordon equation for the upper components has solutions $\eta_k^S(x)$ and $\eta_k^A(x)$. For $x \to \pm\infty$, these solutions are given in terms of phase shifts as

$$\eta_k^S(x) \to \cos(kx \pm \delta^S(k)) \qquad \eta_k^A(x) \to \sin(kx \pm \delta^A(k)). \tag{4.55}$$

Similarly, the Klein–Gordon equation for the lower components has solutions $\tilde{\eta}_k^S(x)$ and $\tilde{\eta}_k^A(x)$. For $x \to \pm\infty$, these solutions are given in terms of phase shifts as

$$\tilde{\eta}_k^S(x) \to i\cos(kx \pm \tilde{\delta}_S(k)) \qquad \tilde{\eta}_k^A(x) \to -i\sin(kx \pm \tilde{\delta}_A(k)), \tag{4.56}$$

where the arbitrary factors of $\pm i$ are inserted for later convenience. The first-order Dirac equation relates the upper and lower components via

$$\tilde{\eta}_k^S(x) = \frac{i}{\omega}\left[\frac{d}{dx} + V_F(x)\right]\eta_k^A(x)\,,\quad \eta_k^A(x) = \frac{i}{\omega_k}\left[\frac{d}{dx} - V_F(x)\right]\tilde{\eta}_k^S(x)\,,$$

$$\tilde{\eta}_k^A(x) = \frac{i}{\omega}\left[\frac{d}{dx} + V_F(x)\right]\eta_k^S(x)\,,\quad \eta_k^S(x) = \frac{i}{\omega}\left[\frac{d}{dx} - V_F(x)\right]\tilde{\eta}_k^A(x)\,. \quad (4.57)$$

From the above relations we infer that the bosonic phase shifts in the symmetric and antisymmetric channels are related by

$$\delta_{(S,A)}(k) = \tilde{\delta}_{(A,S)}(k) + \arctan\left(\frac{M}{k}\right)\,. \quad (4.58)$$

The Dirac spinors are given by

$$\psi_k^+(x) = \begin{pmatrix}\eta_k^S\\ \tilde{\eta}_k^A\end{pmatrix} \quad \text{and} \quad \psi_k^-(x) = \begin{pmatrix}\eta_k^A\\ \tilde{\eta}_k^S\end{pmatrix}\,. \quad (4.59)$$

The spinors in these two channels are orthogonal, since they have opposite eigenvalues with regard to the symmetry operation of spatial reflection times multiplication with σ_3. This operation generalizes parity when $V(x)$ is an odd function in space. For fermions in such a configuration we find the phase shift relative to SG model from the lower component. To get the total phase shift relative to a free fermion we then add $\arctan\left(\frac{M}{k}\right)$. Hence we find

$$\begin{aligned}\delta_{\rm tot}(k) &= \widetilde{\delta}_S(k) + \widetilde{\delta}_A(k) + \arctan\left(\frac{M}{k}\right) = \delta_S(k) + \delta_A(k) - \arctan\left(\frac{M}{k}\right)\\ &= \frac{1}{2}\sum_{i=S,A}\left(\delta_i(k) + \widetilde{\delta}_i(k)\right) = \arctan\left(\frac{M}{k}\right) + 2\arctan\left(\frac{M}{2k}\right)\,, \quad (4.60)\end{aligned}$$

which agrees with Eq. (4.52).

The fermionic bound states are thus almost identical to those of the corresponding bosonic potentials, with an important caveat: Since there is a discrepancy between the total fermionic and bosonic phase shifts, we have $\delta_A(0) + \delta_S(0) = \delta_{\rm tot}^{\rm kink}(0) + \frac{\pi}{2}$, and Levinson's theorem requires a corresponding difference between the number of fermionic and bosonic bound states. This difference is crucial to the analysis of the supersymmetric model, which we will consider below.

The origin of this discrepancy lies in the zero modes,[2] $\omega_0 = 0$. We have already noted that δ_n and $\tilde{\delta}_n$ have common poles at $k = iMn/j$ with $j = 1, \ldots, n-1$; however, at $k = iM$ only V_n has a bound state while $\tilde{V}_n$ does not. For a Dirac fermion in the background of a real scalar field, the bound states with $\omega \neq 0$ occur in charge-conjugated pairs,

[2] The zero modes should not be confused with the threshold states, for which $\omega = M$.

$$\psi_{\pm\omega}(x) = \frac{1}{\sqrt{2}} \begin{pmatrix} \eta_\omega(x) \\ \pm\tilde{\eta}_\omega(x) \end{pmatrix}, \tag{4.61}$$

where $\eta_\omega(x)$ and $\tilde{\eta}_\omega(x)$ are the bound state wavefunctions for the bosonic potentials $V(x)$ and $\widetilde{V}(x)$. Their bound state energies are guaranteed to coincide because they are related by the first-order Dirac Eq. (4.57). For $\omega = 0$ we cannot decouple the Dirac equation into second-order differential equations (since doing so involves dividing by ω), but have to consider the first-order form. Assuming $V_F(x) \geq 0$ for $x \geq 0$ (as for the kink) we find that the Dirac fermion has only a single zero energy bound state,

$$\psi_0(x) = \begin{pmatrix} e^{-\int_0^x V_F(y)dy} \\ 0 \end{pmatrix}. \tag{4.62}$$

The corresponding solution with only a lower component is not normalizable; for an antisoliton, we would find the same situation with upper and lower components reversed. Thus this solution should be considered as belonging half to the positive-energy spectrum and half to the negative-energy spectrum. In contrast, if we were to map the fermion system onto a boson model e.g., via the second-order differential equation of the upper component, every mode, including the zero mode, would be doubled in the negative-energy spectrum, yielding two bosonic zero modes.

Conversely, if we consider only positive-energy fluctuations, corresponding to a real scalar or a Majorana fermion (as will be appropriate in the following section on supersymmetric models), we must count the zero mode with a weight of one-half. The fermionic states at threshold also continue to count as $\frac{1}{2}$, the same as in the boson case. We can see this result analytically by observing that the residue of the pole at $k = iM$ in the fermion transmission coefficient $\mathcal{T}_F$ is half the residue of the pole at $k = iM$ in the bosonic transmission coefficient $\mathcal{T}_B$ because of Eq. (4.60).

Putting everything together, the fermion contribution to the vacuum polarization energy for a Majorana fermion is

$$\begin{aligned} \mathcal{E}_F[\phi_0] &= -\frac{1}{2}{\sum_j}'(\omega_j - M) - \int_0^\infty \frac{dk}{2\pi}\,(\omega - M)\frac{d}{dk}\left[\delta_{\rm tot}(k) + \frac{V_{\rm avg}}{k}\right] \\ &= -\frac{1}{2}{\sum_j}'(\omega_j - M) + \int_0^\infty \frac{dk}{4\pi}\,\frac{k}{\omega}\left[\sum_{i=S,A}\Big(\delta_i(k) + \widetilde{\delta}_i(k)\Big) + \frac{2V_{\rm avg}}{k}\right], \end{aligned} \tag{4.63}$$

where $V_{\rm avg} = (\langle V\rangle + \langle\widetilde{V}\rangle)/2$, as deduced from the second part of Eq. (4.60). The primed summation prescription is defined to contain an additional factor $\frac{1}{2}$ for the zero mode $\omega_0 = 0$. A Dirac fermion would include the contribution from negative energies as well, which for a real scalar background would simply double this result.

For the kink solution, with $V_F(x) = M \tanh\left(\frac{Mx}{2}\right)$, the bosonic potentials for the upper and lower components are $V(x) = V_2(x) = -\frac{3}{2}M^2 \operatorname{sech}^2 \frac{Mx}{2}$ and $\tilde{V}(x) = \tilde{V}_2(x) = -\frac{1}{2}M^2 \operatorname{sech}^2 \frac{Mx}{2}$, respectively. Then the fermionic vacuum polarization energies becomes

$$\mathcal{E}_F[\phi_0] = M\left(\frac{1}{\pi} - \frac{1}{4\sqrt{3}}\right) \tag{4.64}$$

for a Majorana fermion. Besides the zero mode, an ordinary bound state with $\omega_1 = \sqrt{\frac{3}{4}}M$ has contributed.

For the SG-model, $V_F(x) = M \operatorname{sech}(x)$ and the bosonic potentials are $V(x) = V_1(x) = -2M^2 \operatorname{sech}^2 Mx$ and $\tilde{V}(x) = \tilde{V}_1(x) = 0$, so that the correction to the energy from a Majorana fermion is $M/(2\pi)$.

4.3 Bosons, Fermions, Supersymmetry, Central Charge, and the BPS Bound

Here we will consider a special system in $d = 1 + 1$ dimensions in which the fermion and boson fields appear supersymmetrically. In addition to computing the combined one-loop vacuum polarization energy, we also compute one-loop vacuum expectation values of the central charge operator, by extending the techniques developed in Chap. 3. These results enable us to investigate the one-loop quantum Bogomol'nyi–Prasad–Sommerfield (BPS) [4, 5] inequality relating these two quantities.

4.3.1 Fermions

In the supersymmetric framework the fermions couple to the soliton background via

$$\mathcal{L}_F = i\bar{\Psi}\partial\!\!\!/\Psi - U'(\phi)\bar{\Psi}\Psi\,, \tag{4.65}$$

where Ψ is a Majorana fermion and the prime denotes a derivative with respect to the argument. Supersymmetry of the combined boson–fermion system is established by relating the potentials for these fields in a prescribed way:

$$\mathcal{L}_B = \frac{1}{2}\left(\partial_\mu\phi\right)^2 - \frac{1}{2}U^2(\phi)\,. \tag{4.66}$$

For the kink and sine-Gordon models discussed in the previous section we have $U(\phi) = \sqrt{\lambda/2}\left(\phi^2 - \frac{M^2}{2\lambda}\right)$ and $U(\phi) = (2M^2/\sqrt{\lambda})\sin\left(\sqrt{\lambda}\phi/2M\right)$, respectively. These couplings guarantee that the fermion and boson masses are identical, as required by supersymmetry.

In the classical regime, the solution to

$$\frac{d}{dx}\phi_0(x) = \mp U(\phi_0(x)) \tag{4.67}$$

represents the bosonic soliton (antisoliton) background. The boson fluctuations about this background experience the potential

$$V_B(x) = U'^2(\phi_0(x)) + U(\phi_0(x))U''(\phi_0(x)) - M^2\,. \tag{4.68}$$

In the fermion sector the small oscillation modes are two-component spinors obeying the Dirac equation

$$\gamma^0\left(-i\gamma^1\frac{d}{dx} + U'(\phi_0(x))\right)\psi_k(x) = \omega\psi_k(x)\,. \tag{4.69}$$

Note that the supersymmetry relation between the boson and fermion potentials together with the stationary condition, Eq. (4.67), ensure that V_B is the potential in the second-order equation for the upper component of the fermion fields, cf. Eq. (4.54).

To begin the renormalization process we have to collect the ultraviolet divergences of the full theory. They arise from boson loops with one insertion of the potential V_B and fermion loops with one and two insertions of $U' - M$. Since the Majorana condition cuts the number of fluctuating fermion modes in half, the divergence is

$$\begin{aligned}\langle \tfrac{1}{2}V_B - M(U'-M) - \tfrac{1}{2}(U'-M)^2\rangle \int \frac{d^dk}{(2\pi)^2}\frac{1}{k^2-M^2}\\ = \left\langle \frac{1}{2}UU''\right\rangle \int \frac{d^dk}{(2\pi)^2}\frac{1}{k^2-M^2}\end{aligned} \tag{4.70}$$

using dimensional regularization. Since we are only computing quantum corrections up to linear order in $\hbar$, we may compensate for these divergences by a shift in the supersymmetric potential,

$$U \to U + CU''\,, \tag{4.71}$$

where C is a (divergent) constant of order $\hbar$. Renormalization only enters as redefinition of the superpotential, thereby maintaining supersymmetry. A convenient renormalization condition to fix the finite part of C is to require that leading tadpole graphs are canceled exactly, just as we did in the previous section.

4.3.2 Supersymmetry and Central Charge

Having considered bosons and fermions separately, we now combine them to explore the consequences for supersymmetry. The total energy is simply obtained from adding the boson, Eq. (4.16), and fermion, Eq. (4.63), contributions to

$$\mathcal{E}[\phi_0] = -\frac{M}{4} + \int_0^\infty \frac{dk}{2\pi}(\omega(k) - M)\frac{d}{dk}\left[\arctan\frac{M}{k} - \frac{M}{k}\right] = -\frac{M}{2\pi}\,. \quad (4.72)$$

The first term represents the contribution from the mismatch in zero modes discussed earlier. Furthermore, we have used the relation $\delta_A(k) + \delta_S(k) = \delta_{\rm tot}(k) + \arctan\frac{m}{k}$, cf. Eq. (4.60), and $\langle V\rangle - \langle\tilde{V}\rangle = U'(\phi_0)\big|_{x\to-\infty}^{x\to+\infty} = 2M$. The result, Eq. (4.72), for the vacuum polarization energy of the supersymmetric model agrees with Refs. [6, 7], as well as the result obtained from the Yang–Baxter equation assuming the factorization of the S-matrix [8–10]. It has also been obtained using the generalized derivative expansion in Ref. [11], using the techniques of Ref. [12], and with heat kernel [13] and mode regularization [14] approaches. A similar analysis in two dimensions was carried out in [15]. A number of subtleties of this result led many earlier workers [16–28] to incorrect results. We note several consequences of our finding:

- First, the correction is non-zero, defying the naïve expectation that boson and fermion quantum corrections cancel. In fact, the unregularized result is divergent, as can be seen from a naïve analysis of the tadpole graphs.
- The non-zero result originates in the mismatch of zero modes; the system can be thought of as having a Witten index of $\frac{1}{2}$ because the positive-energy spectrum contains one bosonic zero mode but only one-half of a fermionic zero mode. These zero modes arise because ordinary (bosonic) translation is completely broken by the kink background, but only one of the two supersymmetry operators (which correspond to "fermionic" translations) is broken. However, Levinson's theorem implies that the mismatch in zero modes must also extend to the continuum density of states.
- The correction to the energy is universal, independent of the details of the potential.
- As noted in Ref. [16], the negative result seems to imply a violation of the BPS bound $\langle H\rangle \geq |\langle Z\rangle|$, where H is the Hamiltonian and Z is the central charge [29]. These expectation values are equal classically, and we have found a negative correction to $\langle H\rangle$ at one-loop order. While there is no "multiplet shortening" argument in this model requiring that the bound remains an equality, the inequality must be obeyed. As we will see, however, there is a corresponding correction to the central charge ensuring that the BPS bound both continues to be obeyed and remains an equality.

To analyze the BPS bound, we begin from the supersymmetry algebra. We define supersymmetry charge operators via

$$Q_\pm = \frac{1}{2}\left(1 \mp i\gamma^1\right)\int(\not\partial\phi + iU)\gamma^0\Psi\,dx = \int(\Pi\Psi_\pm + (\phi' \pm U)\Psi_\mp)\,dx, \quad (4.73)$$

where $\Psi_\pm = \frac{1}{2}\left(1 \mp i\gamma^1\right)\Psi$. The field operators satisfy canonical equal time (anti)commutation relations,

$$\begin{aligned} \{i\Psi_\pm(x), \Psi_\pm(y)\} &= i\delta(x-y) \\ [\phi(x), \Pi(y)] &= i\delta(x-y)\,, \end{aligned} \tag{4.74}$$

where $\Pi = \dot{\phi}$ is the momentum conjugate to ϕ; all other (anti)commutators vanish. These commutation relations imply the supersymmetry algebra

$$\{Q_\pm,\ Q_\pm\} = 2H \pm 2Z \qquad \{Q_+, Q_-\} = 2P\,, \tag{4.75}$$

where the Hamiltonian H, momentum P, and central charge Z are given by

$$\begin{aligned} H &= \int \left(\frac{1}{2}\Pi^2 + \frac{1}{2}(\phi')^2 + \frac{1}{2}U^2 + \frac{i}{2}(\Psi_-\Psi'_+ + \Psi_+\Psi'_-) + iU'\Psi_-\Psi_+ \right) dx\,, \\ P &= \int \left(\Pi\phi' + \frac{i}{2}(\Psi_+\Psi'_+ + \Psi_-\Psi'_-) \right) dx\,, \\ Z &= \int \phi' U\, dx\,. \end{aligned} \tag{4.76}$$

It is easy to check that H is the same Hamiltonian as would be determined canonically from the combined bosonic and fermionic Lagrangians. The hermiticity of $Q_\pm$ gives the BPS bound on the expectation values of H and Z in any quantum state:

$$\langle H \rangle \geq |\langle Z \rangle|\,, \tag{4.77}$$

which directly follows from taking matrix elements of the supersymmetry algebra, Eq. (4.75).

The classical energy is obtained from Eq. (4.67), with the fermion fields set to zero,

$$H_{\rm cl} = \frac{1}{2}\int \left(\phi_0'(x)^2 + U(\phi_0)^2\right) dx = \int U(\phi_0(x))\phi_0'(x) dx = \mp Z_{\rm cl}, \tag{4.78}$$

for the soliton and antisoliton, respectively, so that the BPS bound, Eq. (4.77), is saturated at the classical level. We have found a negative correction to H at one loop, so if there is no correction to Z, Eq. (4.77) will be violated.

To unambiguously compute the corrections to the central charge for a soliton, it is easier to consider corrections to $Q_+^2 = H + Z$, which is zero classically. One reason to consider Q_+^2 rather than H and Z separately is that this quantity is finite and independent of the renormalization scheme. Using Eq. (4.71) we see explicitly that the contribution from the counterterm cancels,

$$\Delta H_{\rm ct} = C\int U''(\phi_0)U(\phi_0)\, dx = -C\int U''(\phi_0)\phi_0'\, dx = -\Delta Z_{\rm ct}\,. \tag{4.79}$$

We recall that the counterterm coefficient C is already a one-loop quantity and thus only the classical fields must be substituted in Eq. (4.79).

Next we expand $\phi(x) = \phi_0(x) + \eta(x)$, where the soliton solution ϕ_0 is an ordinary real function of x. Neglecting terms of order η^3 and higher (which give higher-loop corrections), we obtain

$$\langle H+Z\rangle_\phi = \frac{1}{2}\int \left\langle \Pi^2 + \left[\left(\frac{d}{dx}+U'(\phi_0)\right)\eta\right]^2 + i\Psi_+\left(\frac{d}{dx}-U'(\phi_0)\right)\Psi_- + i\Psi_-\left(\frac{d}{dx}+U'(\phi_0)\right)\Psi_+\right\rangle_\phi dx, \tag{4.80}$$

where $\langle\ldots\rangle_\phi$ denotes the expectation value in the classical soliton background.

To evaluate this expression, we decompose the fields η and Ψ using creation and annihilation operators for the small oscillations around ϕ_0. The small oscillation modes will be given in terms of the eigenmodes of the bosonic potentials $V(x)$ and $\tilde{V}(x)$. In Chap. 3 we have already described the Fock decomposition for bosonic fluctuations, cf. Eq. (3.14), which implies the normalization as in Eq. (3.15) for $\eta_k(x)$ and $\tilde{\eta}_k(x)$, which are in turn related via Eq. (4.57). For the Majorana fields we take analogously[3]

$$\Psi(x) = \int \frac{dk}{\sqrt{\pi}}\left[\begin{pmatrix}\eta_k(x)\\ \tilde{\eta}_k(x)\end{pmatrix} b_k \mathrm{e}^{-i\omega_k t} + \begin{pmatrix}\eta_k(x)\\ \tilde{\eta}_k(x)\end{pmatrix} b_k^\dagger \mathrm{e}^{i\omega_k t}\right] + \psi_0(x) b_{\omega=0}\,, \tag{4.81}$$

where we made explicit the contribution from the zero mode, Eq. (4.62). The fermion creation and annihilation operators obey anti-commutation relations, $\{b_k,\ b_{k'}^\dagger\} = \delta(k-k')$, etc. Elementary algebra yields

$$\begin{aligned}
i\left(\frac{d}{dx}+U'(\phi_0)\right)\eta &= \int \frac{dk}{\sqrt{\pi}}\sqrt{\omega_k}\left(a_k\tilde{\eta}_k(x)\mathrm{e}^{-i\omega_k t} - a_k^\dagger\tilde{\eta}_k(x)^*\mathrm{e}^{i\omega_k t}\right),\\
i\Pi(x) &= \int \frac{dk}{\sqrt{\pi}}\sqrt{\omega_k}\left(a_k\eta_k(x)\mathrm{e}^{-i\omega_k t} - a_k^\dagger\eta_k(x)^*\mathrm{e}^{i\omega_k t}\right),\\
\Psi_+ &= \eta_{\omega=0}(x)b_{\omega=0} + \int \frac{dk}{\sqrt{\pi}}\left(b_k\eta_k(x)\mathrm{e}^{-i\omega_k t} + b_k^\dagger\eta_k(x)^*\mathrm{e}^{i\omega_k t}\right),\\
\Psi_- &= \int \frac{dk}{\sqrt{\pi}}\left(b_k\tilde{\eta}_k(x)\mathrm{e}^{-i\omega_k t} + b_k^\dagger\tilde{\eta}_k(x)^*\mathrm{e}^{i\omega_k t}\right),\\
i\left(\frac{d}{dx}+U'(\phi_0)\right)\Psi_+ &= \int \frac{dk}{\sqrt{\pi}}\,\omega_k\left(b_k\tilde{\eta}_k(x)\mathrm{e}^{-i\omega_k t} - b_k^\dagger\tilde{\eta}_k(x)^*\mathrm{e}^{i\omega_k t}\right),\\
i\left(\frac{d}{dx}-U'(\phi_0)\right)\Psi_- &= \int \frac{dk}{\sqrt{\pi}}\,\omega_k\left(b_k\eta_k(x)\mathrm{e}^{-i\omega_k t} - b_k^\dagger\eta_k(x)^*\mathrm{e}^{i\omega_k t}\right).
\end{aligned} \tag{4.82}$$

Assembling these results we find for the vacuum expectation value

$$\langle H+Z\rangle_\phi = \int dx\int\frac{dk}{2\pi}\,\omega_k\,|\eta_k(x)|^2 + \int dx\int\frac{dk}{2\pi}\,\omega_k\,|\tilde{\eta}_k(x)|^2 - \int dx\int\frac{dk}{2\pi}\,\omega_k\,|\tilde{\eta}_k(x)|^2 - \int dx\int\frac{dk}{2\pi}\,\omega_k\,|\eta_k(x)|^2 = 0\,, \tag{4.83}$$

[3] Since the equation of motion for the spinors is only linear in the time derivative a factor $\sqrt{\omega}$ arises in the mode decomposition relative to the bosons. This factor is usually included in the spinor part of the fermion field.

and the BPS bound remains saturated. If we instead considered an antisoliton, we would find the same result for $\langle Q_-^2 \rangle_{\bar{\phi}} = \langle H - Z \rangle_{\bar{\phi}}$, with the roles of Ψ_+ and Ψ_- reversed. We note that this result did not depend on any specific properties of U, so it holds for any supersymmetric soliton satisfying Eq. (4.67). Some caution is required in the manipulations yielding Eq. (4.83), because we have exchanged the order of integration in coordinate and momentum spaces. We have already discussed that this manipulation is only allowed when the momentum k has at least an infinitesimal positive imaginary part, cf. Eq. (2.46). This prescription has been imposed implicitly in all of the integrals that appear in Eq. (4.83).

In the context of Eq. (2.46) we have observed that spatial integrals over quantities that are bilinear in the fluctuating wavefunctions are related to the (derivative of) the phase shifts. We will use that relation here to perform a final consistency check on our calculation for the BPS bound by calculating the correction to Z directly. We start from the classical expression for Z in Eq. (4.76) and expand about the classical solution $\phi = \phi_0$, giving

$$\begin{aligned} \Delta Z &= \langle Z \rangle_\phi - Z_{\rm cl} \\ &= \Delta Z_{\rm ct} + \frac{m^2}{\lambda} \int \left\langle U' \eta \eta' - \frac{1}{2} U U'' \eta^2 \right\rangle_\phi dx \qquad (4.84) \\ &= \Delta Z_{\rm ct} + \frac{m^2}{2\lambda} \int \left\langle \left(\left(\frac{d}{dx} + U' \right) \eta \right)^2 - (\eta')^2 - \eta^2 (U')^2 - U U'' \eta^2 \right\rangle_\phi dx \,. \end{aligned}$$

After substituting the expansions of Eq. (4.82) we obtain

$$\begin{aligned} \Delta Z &= \Delta Z_{\rm ct} + \int dx \int \frac{dk}{2\pi} \, \omega_k \, |\tilde{\eta}_k(x)|^2 - \int dx \int \frac{dk}{2\pi} \, \omega_k \, |\eta_k(x)|^2 \\ &= \frac{M}{4} - \int \frac{dk}{2\pi} \, (\omega - M) \frac{d}{dk} \left(\tan^{-1} \frac{M}{k} - \frac{M}{k} \right) = \frac{M}{2\pi} = -\Delta H \,, \qquad (4.85) \end{aligned}$$

where we have used the relation (4.58) between the phase shifts of η and $\tilde{\eta}$ and also that it suffices to employ the classical fields in the counterterms, which allows us to identify $\Delta Z_{\rm ct}$ with $\Delta H_{\rm ct}$ as in Eq. (4.79). This term cancels the ultraviolet divergence in the integral in Eq. (4.85), leaving an unambiguous finite result.

4.3.3 SVV Anomaly

The universal result that we have found for the equal one-loop corrections to the energy and central charge suggests a broader principle at work. Niemi and Semenoff [30] derived a generalization of Levinson's theorem appropriate for the paired supersymmetric potentials such as $V(x)$ and $\tilde{V}(x)$ and showed its connection to anomalies. The existence of an anomaly was also suggested in Ref. [16]. Shifman, Vainshtein, and Voloshin (SVV)[31] (see also

Ref. [32]) made this connection explicit by demonstrating the existence of an anomaly in the central charge. Quantum corrections induce a modification in the topological current

$$\xi^{\mu} = \epsilon^{\mu\nu}\partial_{\nu}\left(W(\phi)\right) \rightarrow \epsilon^{\mu\nu}\partial_{\nu}\left(W(\phi) + \frac{1}{4\pi}W''(\phi)\right), \tag{4.86}$$

where $W(\phi)$ is the superpotential with $W'(\phi) = U(\phi)$. The central charge is then obtained by integrating ξ^0 over space, yielding

$$Z = \left(W(\phi) + \frac{1}{4\pi}W''(\phi)\right)_{x=\infty} - \left(W(\phi) + \frac{1}{4\pi}W''(\phi)\right)_{x=-\infty}. \tag{4.87}$$

The difference in $W(\phi)$ yields the classical central charge, while the difference in $W''(\phi)/(4\pi)$ is an anomalous correction. This analysis shows that the result we have derived as a one-loop matrix element actually represents an exact operator correction, as is common for quantum field theory anomalies. The generalized Levinson's theorem corresponding to this anomaly [30] reduces to the usual Levinson's theorem in this case, which, as we have seen above, is the origin of the non-vanishing quantum correction.

4.4 Soliton Stabilization by Fermions in $d = 1{+}1$

In the remainder of this chapter we use the techniques introduced in Sect. 4.2.1 to demonstrate that vacuum polarization effects can enable bosonic backgrounds to carry non-zero-fermion number N_F, and that such backgrounds can have total energy less than N_F free fermions, making them energetically stable if fermion number is conserved.

Scalar field theories can contain spatially varying (but time-independent) configurations that are local minima of the classical energy. Such solitons are often found as solutions to the nonlinear classical equations of motion. When quantum effects are taken into account, the classical description must be re-examined. Now the spatially varying soliton configuration should minimize the "effective energy," which takes into account classical and quantum effects.[4] We are now in a position to compute this quantity efficiently.

To give an example of a quantum soliton that is not present in the classical theory alone, we examine a renormalizable model in 1+1 dimensions in which a scalar field is Yukawa coupled to a fermion as in Eq. (4.23). The classical energy is minimized when the scalar field has a constant value v and there are no classical solitons. The fermion gets a mass $M = Gv$ through its Yukawa coupling. First, we calculate exactly the fermion's properly renormalized one-loop contribution to the scalar field effective energy. (By "exactly" we mean

[4] By effective energy we mean the effective action per unit time; the term "effective potential" is reserved for spatially constant configurations.

to all orders in the derivative expansion, which is crucial since we consider configurations varying on the scale $1/M$.) Then we show that for certain choices of model parameters—in particular with G large—we can exhibit a field configuration that carries fermion number and has energy below M. Since fermion number is conserved, the only decay channel is through the emission of a free fermion, which is energetically forbidden.

We search for the lowest energy configuration carrying fermion number using a few parameter variational *ansatz*. The soliton, which is the actual lowest energy configuration with fermion number one, is presumably not far from our variational minimum and has strictly lower energy. Thus, if we find a stable minimum within our ansatz space, the soliton has energy less than M and is absolutely stable.

The idea that a heavy fermion can create a soliton is not new and has been explored previously [33–45]. What we add here is the ability to exactly calculate the renormalized fermionic one-loop effective energy for any spatially varying meson background, which is essential to demonstrate stability at the quantum level. The model we consider has a two-component meson field $\boldsymbol{\phi} = (\phi_1, \phi_2)$ coupled equally to N_F fermions. We suppress the fermion flavor label but will keep track of the factor N_F as necessary. The Lagrangian is $\mathcal{L} = \mathcal{L}_B + \mathcal{L}_F$ with

$$\mathcal{L}_B = \frac{1}{2}\,\partial_\mu \boldsymbol{\phi} \cdot \partial^\mu \boldsymbol{\phi} - V(\boldsymbol{\phi})\,, \tag{4.88}$$

where

$$V(\boldsymbol{\phi}) = \frac{\lambda}{8}\left[\boldsymbol{\phi}\cdot\boldsymbol{\phi} - v^2 + \frac{2\alpha v^2}{\lambda}\right]^2 - \frac{\lambda}{2}\left(\frac{\alpha v^2}{\lambda}\right)^2 - \alpha v^3\,(\phi_1 - v) \tag{4.89}$$

and $\mathcal{L}_F$ is given in Eq. (4.23). Note that with α set to zero, the theory has a global $U(1)$ invariance

$$\phi_1 + i\phi_2 \to e^{i\varphi}\,(\phi_1 + i\phi_2) \quad \text{and} \quad \Psi \to e^{-i\varphi\gamma_5/2}\Psi\,. \tag{4.90}$$

Naïvely, one would imagine that spontaneous symmetry breaking occurs with $\alpha = 0$ so that we could pick a classical vacuum, say $\boldsymbol{\phi}_{\rm cl} = (v, 0)$, and expand the theory about this point. In $1+1$ dimensions, however, the massless mode that corresponds to motion along the chiral circle, $\boldsymbol{\phi}\cdot\boldsymbol{\phi} = v^2$, gives rise to infrared singularities and there is no spontaneous symmetry breaking [46]. By introducing $\alpha \neq 0$, we have tilted the potential to eliminate the massless mode. For α large enough it is then legitimate to expand about $\boldsymbol{\phi}_{\rm cl}$. There are two massive bosons, which we call σ and π, with masses $m_\sigma^2 = (\lambda + \alpha)\,v^2$ and $m_\pi^2 = \alpha v^2$.

The fermions get mass through their Yukawa coupling to $\boldsymbol{\phi}$. In the perturbative vacuum (i.e., when expanding about $\boldsymbol{\phi}_{\rm cl}$), the fermion has mass $M = Gv$. One could imagine that various distortions of $\boldsymbol{\phi}$ would affect the fermion spectrum. For example, one could keep $\phi_2 = 0$ and let $\phi_1 \to \phi_1(x)$

with $\lim_{x\to\pm\infty}\phi_1(x) = v$, but $\phi_1(x) < v$ over some region in x of order w. Alternatively, one could keep $\boldsymbol{\phi}\cdot\boldsymbol{\phi} = v^2$, but let $\boldsymbol{\phi} = v(\cos\theta(x), \sin\theta(x))$, where $\theta(x) \to 0$ as $x \to -\infty$ and $\theta(x) \to 2\pi$ as $x \to +\infty$. Again the deviation of $\boldsymbol{\phi}$ from $\boldsymbol{\phi}_{\rm cl}$ occurs in a region of order w. In both cases, if w is of order $1/M$, then there are bound state solutions of the single-particle Dirac equation, Eq. (4.24), with binding energies of order M, so that a fermion bound to the $\boldsymbol{\phi}$ field has an energy below M. (Because of its topological properties, the latter configuration is especially efficient at binding a fermion [47].) However, there is an energy cost for deviating from the vacuum $\boldsymbol{\phi}_{\rm cl}$, which is given by the gradient and potential terms in Eq. (4.88). Still, considering just the single bound fermion and the classical scalar energy, we might expect a total energy below M for G large enough.

Of course, Ψ describes a quantum field and any distortion of the background $\boldsymbol{\phi}(x)$ away from $\boldsymbol{\phi}_{\rm cl}$ will cause shifts in the zero-point energies of the fermion fluctuations. To form a self-consistent approximation, we must compute the effect of these shifts as well, since they are of the same order in $\hbar$ as the bound state contribution. Because we are comparing to fermions in the trivial vacuum, it is essential that we carry out this calculation using conventional renormalization conditions defined in the perturbative sector of the theory, as is made possible by our method.

We have written Eq. (4.23) as a commutator to ensure that the (complete) Lagrangian is invariant under the charge conjugation operation $\Psi \to \mathcal{C}\Psi^*$ and $(\phi_1, \phi_2) \to (\phi_1, -\phi_2)$. This symmetry implies that positive-energy modes of the fluctuating fermion are related to negative-energy modes of a *different* background. For an externally prescribed background, the fermion vacuum energy thus gets contributions from both the positive and negative-energy eigenvalues of the single-particle Dirac Hamiltonian, Eq. (4.24). Using the techniques of Sect. 4.2.1 we compute

$$\delta_F(k) = \delta_+(\omega(k)) + \delta_+(-\omega(k)) + \delta_-(\omega(k)) + \delta_-(-\omega(k))\,. \tag{4.91}$$

Here $\omega(k) = \sqrt{k^2 + M^2}$ and $\delta_\pm$ is the scattering phase shift for the positive (negative) parity channel, cf. Eqs. (4.34) and (4.35). Similarly, the spectrum of the discrete bound state energy levels $\{\omega_l\}$ need not be invariant under sign change either. Hence we have to consider the positive and negative-energy bound states individually as well. To this end we write the fermion loop contribution to the vacuum polarization energy as

$$\Delta E^F = -\frac{1}{2}\sum_l \left(|\omega_l| - M\right) - \int_0^\infty \frac{dk}{2\pi}\left(\omega(k) - M\right)\frac{d}{dk}\delta_F(k) + E_{\rm ct}\,. \tag{4.92}$$

Of course, the momentum integral in Eq. (4.92) is formally infinite. For large k, the phase shifts go to zero like $1/k$, so the integral is logarithmically divergent. We identify the leading large k behavior of $\delta_F(k)$ with the contribution of the first Born approximation plus the piece of the second Born approximation related to it by chiral symmetry, which we call $\hat{\delta}(k)$. As a

consequence of the global symmetry of Eq. (4.90), we can identify this leading piece unambiguously with the coefficient of the Lagrangian counterterm, $v^2 - \boldsymbol{\phi}\cdot\boldsymbol{\phi}$. The renormalization conditions that fix the counterterm in perturbation theory, i.e., the absence of any tadpole graph, here translate into the statement that in evaluating Eq. (4.92) we should subtract $\hat{\delta}(k)$ from $\delta_F(k)$:

$$\Delta E^F = -\frac{1}{2}\sum_l (|\omega_l| - M) - \int_0^\infty \frac{dk}{2\pi}\,(\omega(k) - M)\,\frac{d}{dk}\left(\delta_F(k) - \hat{\delta}(k)\right)\,, \tag{4.93}$$

where

$$\hat{\delta}(k) = \frac{2}{k}\int_0^\infty dx\,\left(v^2 - \boldsymbol{\phi}(x)^2\right)\,. \tag{4.94}$$

4.4.1 The One-Loop Effective Energy

We are interested in calculating the total one-loop effective energy of a static configuration $\boldsymbol{\phi}(x)$. We take $\boldsymbol{\phi}(x)$ to be specified by a few parameters $\{\zeta_i\}$ and measure energy in units of the fermion mass $M = Gv$ using the dimensionless distance $\xi = Mx$. In $1+1$ dimensions $\boldsymbol{\phi}(x)$ and v are dimensionless. For the numerical analysis, it is convenient to rescale $\boldsymbol{\phi}(x)$ by v so that $\boldsymbol{\phi}(x) \to (1,0)$ as $|\xi| \to \infty$, and to define dimensionless couplings

$$\tilde{\alpha} = \frac{\alpha}{G^2} \qquad \text{and} \qquad \tilde{\lambda} = \frac{\lambda}{G^2}\,. \tag{4.95}$$

With this rescaling and Eqs. (4.88) and (4.89), we have

$$\begin{aligned}\frac{E_{\rm cl}[\boldsymbol{\phi}\,]}{M} &= v^2\int_{-\infty}^{\infty} d\xi\left(\frac{1}{2}\boldsymbol{\phi}'\cdot\boldsymbol{\phi}' + \frac{\tilde{\lambda}}{8}\left[\boldsymbol{\phi}\cdot\boldsymbol{\phi} - 1 + \frac{2\tilde{\alpha}}{\tilde{\lambda}}\right]^2\right.\\ &\qquad\left. -\frac{\tilde{\lambda}}{2}\left(\frac{\tilde{\alpha}}{\tilde{\lambda}}\right)^2 - \tilde{\alpha}(\phi_1 - 1)\right)\\ &= v^2\mathcal{E}_{\rm cl}(\tilde{\alpha},\tilde{\lambda},\{\zeta_i\})\,,\end{aligned} \tag{4.96}$$

where a prime denotes differentiation with respect to ξ.

We see that a single fermion makes a contribution that is proportional to M and also depends on the variational parameters $\{\zeta_i\}$. Hence we can express Eq. (4.93) as $M\mathcal{E}^F(\{\zeta_i\})$. For N_F flavors the one-fermion loop contribution is therefore $N_F M\mathcal{E}^F(\{\zeta_i\})$.

The boson one-loop contribution comes from summing the square roots of the eigenvalues of the operator $-\frac{\partial^2}{\partial x^2} + \frac{\partial^2 V}{\partial\phi_i\partial\phi_j}$. Rescaling as before we find that the boson one-loop energy can be written as $M\mathcal{E}^B(\{\zeta_i\})$.

Putting together the classical energy and the one-loop energies we get

$$\frac{E_{\rm tot}[\boldsymbol{\phi}\,]}{N_F\,M} = \frac{v^2}{N_F}\mathcal{E}_{\rm cl}(\tilde{\alpha},\tilde{\lambda},\{\zeta_i\}) + \mathcal{E}^F(\{\zeta_i\}) + \frac{1}{N_F}\mathcal{E}^B(\tilde{\alpha},\tilde{\lambda},\{\zeta_i\})$$

$$+ \text{ higher loops}. \tag{4.97}$$

For N_F large we can neglect the boson one-loop contribution relative to the fermion one-loop contribution. Furthermore it can be shown that $1/v^2$ counts boson loops. Taking both N_F and v^2 large with the ratio fixed, we can thus neglect the higher loops as well. In this parameter regime we need only consider the contributions from $\mathcal{E}_{\rm cl}$ and $\mathcal{E}^F$, and the one-fermion loop approximation becomes reliable.

4.4.2 The Fermion Number

A non-trivial background $\boldsymbol{\phi}(x)$ distorts the energy levels of the Dirac Hamiltonian, Eq. (4.24), possibly introducing single-particle bound states (with positive and negative energies). We identify the lowest energy state of the system, the one with all the negative-energy levels filled, as the vacuum. If a level crosses zero as we interpolate between $\boldsymbol{\phi}_{\rm cl}(x)$ and $\boldsymbol{\phi}(x)$, this state will have non-zero-fermion number. In particular, if $\boldsymbol{\phi}(x)$ circles $\boldsymbol{\phi} = (0,0)$ as $\boldsymbol{\phi}$ goes from $(1,0)$ at $x = -\infty$ to $(1,0)$ at $x = \infty$, then the vacuum state will carry non-zero-fermion number, provided that the scale over which $\boldsymbol{\phi}$ varies, w, is much larger than the fermion Compton wavelength, $1/M$ [44, 45, 48]. In Chap. 5 show that the fermion number of the vacuum, $\mathcal{Q}_{\rm vac}$, is given in terms of the positive-energy phase shifts at $k = 0$ and the number of positive-energy bound states by

$$\mathcal{Q}_{\rm vac} = N_F \left(\frac{1}{\pi} \left[\delta_+(M) + \delta_-(M) \right] - \frac{1}{2} - n_{\omega>0} \right), \tag{4.98}$$

where $n_{\omega>0}$ is the number of bound states with positive energy. We study configurations that loop once around $\boldsymbol{\phi} = 0$, so $\mathcal{Q}_{\rm vac}$ is either 0 or N_F. We are interested in states with fermion number N_F. If $\mathcal{Q}_{\rm vac} = N_F$, then the state we want is simply the vacuum. If $\mathcal{Q}_{\rm vac} = 0$, however, we have to build the lowest energy state with fermion number N_F by filling the lowest positive energy level of Eq. (4.24) explicitly with N_F fermions. Therefore, if $\mathcal{Q}_{\rm vac} = 0$, $\mathcal{E}^F$ appearing in Eq. (4.97) must be augmented by ω_1, where $M\omega_1$ is the smallest positive eigenvalue of Eq. (4.24).

4.4.3 Results

We want to look for background configurations $\boldsymbol{\phi}$ that can produce states with fermion number N_F and whose total energy is below $N_F M$. From Eq. (4.97) with $\mathcal{E}^B$ neglected, we define

$$\mathcal{B} = \frac{v^2}{N_F} \mathcal{E}_{\rm cl} + \mathcal{E}^F - 1, \tag{4.99}$$

which is the binding energy of a configuration with fermion number N_F in units of $N_F M$. For our numerical computations, we take the *ansatz*

$$\phi_1 + i\phi_2 = 1 - R + R\, e^{i\Theta} \quad \text{where} \quad \Theta = \pi(1 + \tanh(\xi/w))\,. \tag{4.100}$$

The two variational parameters are R and w. As ξ goes from $-\infty$ to ∞, $\boldsymbol{\phi}$ moves in a circle of radius R in the $(\phi_1,\ \phi_2)$ plane, starting and ending at $(1, 0)$. The scale over which $\boldsymbol{\phi}$ varies is w.

For fixed $\tilde{\alpha}$ and $\tilde{\lambda}$ we vary R and w until we produce the configuration with the smallest $\mathcal{B}$. The results are shown in Fig. 4.1. We see that it is possible to find a configuration whose total energy is below $N_F M$. Since we are minimizing $\mathcal{B}$ subject to the constraint that ϕ is of the form Eq. (4.100), we know that the true minimum of $\mathcal{B}$ in the fermion number N_F sector also has an energy below $N_F M$. This is the stable soliton.

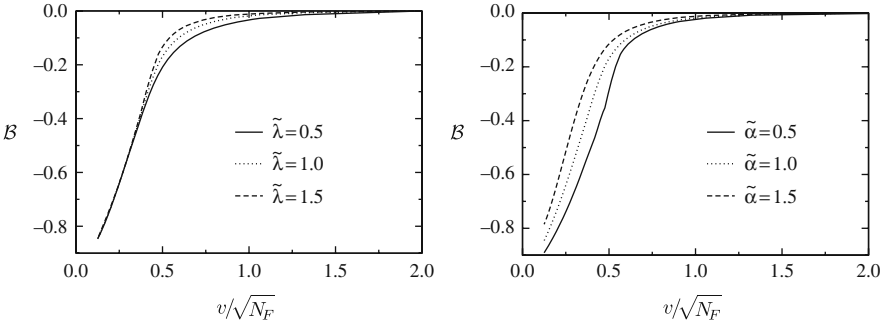

Fig. 4.1 $\mathcal{B}$ as a function of $v/\sqrt{N_F}$ for various values $\tilde{\lambda}$ with $\tilde{\alpha} = 0.25$ (*left panel*) and for various values $\tilde{\alpha}$ with $\tilde{\lambda} = 1.0$ (*right panel*). $\mathcal{B}$ negative corresponds to binding

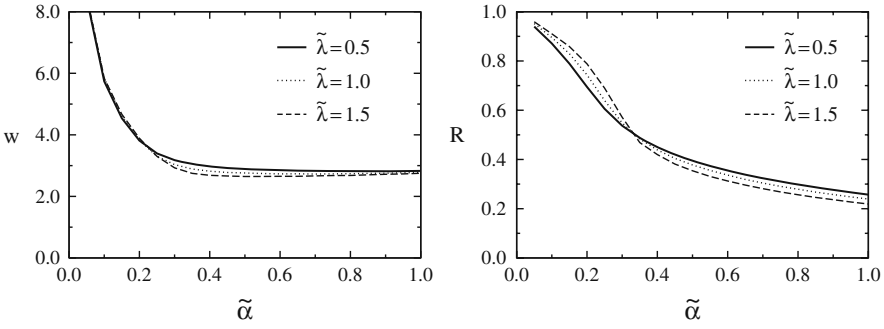

Fig. 4.2 The width $w_{\rm sol}$ (*left panel*) and the radius $R_{\rm sol}$ (*right panel*) of the configurations (4.100) that minimize the total energy as functions of the explicit symmetry breaking $\tilde{\alpha}$. Several values of the Higgs coupling constant $\tilde{\lambda}$ are considered and $v/\sqrt{N_F} = 0.375$

In Fig. 4.2 we show the width, $w_{\rm sol}$, and the radius, $R_{\rm sol}$, for the minimum energy configuration as a function of $\tilde{\alpha}$ for various values of $\tilde{\lambda}$. Note that the size of the soliton grows like $1/\sqrt{\tilde{\alpha}}$ as $\tilde{\alpha}$ goes to zero. In that region, $R_{\rm sol}$ approaches 1, so the $\boldsymbol{\phi}$ configuration approaches the chiral circle. In fact, the energy of the fermion number N_F soliton goes to zero as $\tilde{\alpha}$ goes to zero. However, for $\tilde{\alpha}$ very small the bosonic quantum fluctuations restore the classically broken symmetry. Thus we cannot trust our results for $\tilde{\alpha}$ very small and we do not believe that this large and light soliton is a reliable consequence of this model. For moderate values of $\tilde{\alpha}$, where the width of the soliton is not controlled by $1/\sqrt{\tilde{\alpha}}$, we do trust our results. For the value of $v/\sqrt{N_F}$ shown in Fig. 4.2, the model becomes trustworthy for $\tilde{\alpha} \approx 0.3$. For further discussion of this point, see Ref. [47].

References

1. G. Pöschl and E. Teller, *Z. Phys.* **83** (1933) 143. 64, 65
2. R. Rajaraman, *Solitons and Instantons.* North Holland, 1982. 65, 66, 67
3. R. F. Dashen, B. Hasslacher, and A. Neveu, *Phys. Rev.* **D10** (1974) 4114. 66
4. E. B. Bogomolny, *Sov. J. Nucl. Phys.* **24** (1976) 449. 76
5. M. K. Prasad and C. M. Sommerfield, *Phys. Rev. Lett.* **35** (1975) 760. 76
6. J. F. Schonfeld, *Nucl. Phys.* **B161** (1979) 125. 78
7. H. Nastase, M. A. Stephanov, P. van Nieuwenhuizen, and A. Rebhan, *Nucl. Phys.* **B542** (1999) 471. 78
8. K. Schoutens, *Nucl. Phys.* **B344** (1990) 665. 78
9. C. Ahn, D. Bernard, and A. LeClair, *Nucl. Phys.* **B346** (1990) 409. 78
10. C. Ahn, *Nucl. Phys.* **B354** (1991) 57. 78
11. G. V. Dunne, *Phys. Lett.* **B467** (1999) 238. 78
12. L.-H. Chan, *Phys. Rev.* **D55** (1997) 6223. 78
13. M. Bordag, A. S. Goldhaber, P. van Nieuwenhuizen, and D. Vassilevich, *Phys. Rev.* **D66** (2002) 125014. 78
14. A. S. Goldhaber, A. Litvintsev, and P. van Nieuwenhuizen, *Phys. Rev.* **D64** (2001) 045013. 78
15. D. V. Vassilevich, *Phys. Rev.* **D68** (2003) 045005. 78
16. A. Rebhan and P. van Nieuwenhuizen, *Nucl. Phys.* **B508** (1997) 449. 78, 81
17. A. D'Adda and P. Di Vecchia, *Phys. Lett.* **B73** (1978) 162. 78
18. A. D'Adda, R. Horsley, and P. Di Vecchia, *Phys. Lett.* **B76** (1978) 298. 78
19. R. Horsley, *Nucl. Phys.* **B151** (1979) 399. 78
20. S. Rouhani, *Nucl. Phys.* **B182** (1981) 462. 78
21. H. Yamagishi, *Phys. Lett.* **B147** (1984) 425. 78
22. A. Chatterjee and P. Majumdar, *Phys. Rev.* **D30** (1984) 844. 78
23. A. K. Chatterjee and P. Majumdar, *Phys. Lett.* **B159** (1985) 37. 78
24. A. Uchiyama, *Nucl. Phys.* **B244** (1984) 57. 78
25. A. Uchiyama, *Prog. Theor. Phys.* **75** (1986) 1214. 78
26. A. Uchiyama, *Nucl. Phys.* **B278** (1986) 121. 78
27. R. K. Kaul and R. Rajaraman, *Phys. Lett.* **B131** (1983) 357. 78
28. C. Imbimbo and S. Mukhi, *Nucl. Phys.* **B247** (1984) 471. 78

29. E. Witten and D. I. Olive, *Phys. Lett.* **B78** (1978) 97. 78
30. A. J. Niemi and G. W. Semenoff, *Phys. Rev.* **D32** (1985) 471. 81, 82
31. M. A. Shifman, A. I. Vainshtein, and M. B. Voloshin, *Phys. Rev.* **D59** (1999) 045016. 81
32. A. Losev, M. A. Shifman, and A. I. Vainshtein, *Phys. Lett.* **B522** (2001) 327. 82
33. B. Moussallam, *Phys. Rev.* **D40** (1989) 3430. 83
34. J. A. Bagger and S. G. Naculich, *Phys. Rev. Lett.* **67** (1991) 2252. 83
35. J. A. Bagger and S. G. Naculich, *Phys. Rev.* **D45** (1992) 1395. 83
36. R. J. Perry, *Nucl. Phys.* **A467** (1987) 717. 83
37. R. MacKenzie, F. Wilczek, and A. Zee, *Phys. Rev. Lett.* **53** (1984) 2203. 83
38. G. Ripka and S. Kahana, *Phys. Lett.* **B155** (1985) 327. 83
39. G. Ripka and S. Kahana, *Phys. Rev.* **D36** (1987) 1233. 83
40. R. Johnson and J. Schechter, *Phys. Rev.* **D36** (1987) 1484. 83
41. G. W. Anderson, L. J. Hall, and S. D. H. Hsu, *Phys. Lett.* **B249** (1990) 505. 83
42. S. Dimopoulos, B. W. Lynn, S. B. Selipsky, and N. Tetradis, *Phys. Lett.* **B253** (1991) 237. 83
43. S. G. Naculich, *Phys. Rev.* **D46** (1992) 5487. 83
44. E. D'Hoker and E. Farhi, *Nucl. Phys.* **B248** (1984) 77. 83, 86
45. E. D'Hoker and E. Farhi, *Nucl. Phys.* **B248** (1984) 59. 83, 86
46. S. R. Coleman, *Commun. Math. Phys.* **31** (1973) 259. 83
47. E. Farhi, N. Graham, R. L. Jaffe, and H. Weigel, *Nucl. Phys.* **B585** (2000) 443. 84, 88
48. J. Goldstone and F. Wilczek, *Phys. Rev. Lett.* **47** (1981) 986. 86

5 Spectral Analysis of Charges

Many field theory solitons have particularly interesting properties when they are coupled to fermions, because they act as strong background fields that can drastically alter the Dirac spectrum. Solitons that break invariance under charge conjugation ($\mathcal{C}$) and its combination with parity ($\mathcal{CP}$) can introduce asymmetries in the Dirac spectrum, which cause the soliton to carry fermion number, as we have seen in Chap. 4. In case of a non-topological soliton we may interpolate continuously between the trivial background and the soliton background and observe this fermion number as a level crossing in the Dirac spectrum. In this chapter we will derive results like Eq. (4.98) that enable us to precisely trace back these level crossings.

In addition, solitons with non-trivial topological boundary conditions can also carry fractional fermion number [1–3]. In the previous chapter we learned how Levinson's theorem pointed to the existence of an anomaly in the minimal supersymmetric model in one dimension. The anomaly was associated with a fractional charge, the Witten index of 1/2. We will show how conventional anomalies, and the associated fractional charges, can be derived with similar techniques. Our approach follows that of Ref. [4], which builds on previous work by Blanckenbecler and Boyanovsky [5, 6].

5.1 Basic Idea and Derivation

We consider a single Dirac fermion with mass m in n space dimensions and apply the scattering theory techniques we have developed to calculate the charge carried by a soliton background. We will assume that the background has rotational symmetry, so that the spectrum decomposes into a sum over eigenchannels α. In one dimension there are just two such channels, for even and odd parity, while in three dimensions the sum will run over parity and the rotational quantum numbers including the degeneracy within each channel. We begin by writing the fermion charge density as

$$j^0(x) = \frac{1}{2}\langle\Omega|[\Psi^\dagger(x), \Psi(x)]|\Omega\rangle, \tag{5.1}$$

where x is an $d = n + 1$-dimensional vector. Notice that the anticommuting fermion fields are ordered to preserve charge conjugation invariance: $[\bar{\Psi}, \Psi]$ is even under $\mathcal{C}$ while $[\bar{\Psi}, \gamma_5\Psi]$ and $[\bar{\Psi}, \gamma^\mu\Psi]$ are odd under $\mathcal{C}$.

Graham, N., et al.: *Spectral Analysis of Charges.* Lect. Notes Phys. **777**, 91–101 (2009)
DOI 10.1007/978-3-642-00139-0_5

The next step is a conventional Fock decomposition in terms of the eigenstates $\psi_\alpha(\boldsymbol{x},\omega)$ of the single-particle (stationary) Dirac equation as in Eq. (3.14). We find the expectation value of the charge density in the background of the soliton

$$\langle j^0(r)\rangle = -\frac{1}{\pi}\sum_\alpha\left(\int_{-\infty}^{\infty}\mathrm{sgn}(\omega)|\psi_\alpha(r,\omega)|^2 d\omega\right) - \frac{1}{2}\sum_{\alpha,j}\mathrm{sgn}(\omega)|\psi_{\alpha,j}(\omega)|^2, \quad (5.2)$$

where $\psi_\alpha(r,\omega)$ refers to the radial parts of the solutions to the Dirac equation that are normalized as in Eq. (3.15). As usual, the mode sum splits into a continuum piece from the scattering states and a sum over bound state contributions. The label α may refer to more general quantum numbers than just orbital angular momentum. For instance, in the bag model discussed in Sect. 5.4, it denotes *grand spin*, the vector sum of orbital angular momentum, spin, and isospin.

Our ultimate goal is to compute the charge as the radial integral of j^0, which involves the integral over the square of the radial wavefunction. For the bound state contribution this integral just gives $\pm\frac{1}{2}$ for each bound state. For the continuum contribution, we first have to subtract the undistorted wavefunctions squared, because we are only interested in the *change* of the charge due to the background. In Eq. (2.46) we have exactly related the spatial integral of that difference to the derivative of the phase shift.

Putting these results together we relate the charge to the phase shift via

$$\begin{aligned} Q &= -\sum_\alpha\left(\int_m^\infty\frac{d\omega}{2\pi}\frac{d\delta_\alpha(\omega)}{d\omega} + \sum_{\omega_\alpha^j>0}\frac{1}{2} - \int_{-m}^{-\infty}\frac{d\omega}{2\pi}\frac{d\delta_\alpha(\omega)}{d\omega} - \sum_{\omega_\alpha^j<0}\frac{1}{2}\right) \\ &= \frac{1}{2\pi}\sum_\alpha\left[\delta_\alpha(m) - \delta_\alpha(\infty) - \pi n_\alpha^> + \pi n_\alpha^< - \delta_\alpha(-m) + \delta_\alpha(-\infty)\right], \quad (5.3) \end{aligned}$$

where $n_\alpha^>$ and $n_\alpha^<$ give the number of bound states with positive and negative energy, respectively, in each channel. We will see that this result generalizes unchanged to cases with fractional charges, when the non-integer values appear through the phase shift at $\omega = \pm\infty$.

We will now rederive Eq. (5.3) from Levinson's theorem, which we studied in Sect. 2.4. This approach will provide additional physical motivation for Eq. (5.3) and will also enable us to further simplify it. Levinson's theorem gives the number of states N that have left the continuum in channel α by passing through the threshold at m as

$$\delta_\alpha(m) - \delta_\alpha(\infty) = N\pi. \quad (5.4)$$

These states typically appear as bound states (which give delta functions in the density of states), though it is possible that in cases where the spectrum is not charge conjugation invariant, they can reenter the continuum of states with opposite energy. We have derived Levinson's theorem as a sum rule for

the phase shift. (In some channels, cf. Sect. 2.4.3, an anomaly emerges so that the right-hand side of Eq. (5.4) is modified to $\left(N - \frac{1}{2}\right)\pi$.)

Computing the fermion number of a field configuration now becomes a matter of simple counting. We consider each channel separately. If a bound state leaves the positive continuum but appears as a positive-energy bound state, it has not changed the fermion number of the configuration. However, if it crosses $\omega = 0$ and becomes a negative-energy bound state, it is now filled in the vacuum and gives a fermion number of one. Thus we may read off the fermion number from the positive-energy spectrum

$$Q^{>} = \frac{1}{\pi} \sum_{\alpha} \left[\delta_\alpha(m) - \delta_\alpha(\infty) - \pi n_\alpha^{>}\right] . \tag{5.5}$$

Note that this result also recognizes the asymmetry that arises from a state that turned from a negative to a positive-energy bound state. Similarly the negative-energy spectrum yields

$$Q^{<} = \frac{1}{\pi} \sum_{\alpha} \left[\delta_\alpha(-\infty) - \delta_\alpha(-m) + \pi n_\alpha^{<}\right] . \tag{5.6}$$

Both calculations yield the same charge, as can be seen from Eq. (5.3) together with the fact that Levinson's theorem tracks all states that enter and leave the two continua, even in the presence of $\mathcal{CP}$ violation,

$$\delta_\alpha(m) - \delta_\alpha(\infty) - \pi n_\alpha^{>} + \delta_\alpha(-m) - \delta_\alpha(-\infty) - \pi n_\alpha^{<} = 0 , \tag{5.7}$$

so that

$$\begin{aligned} Q &= \frac{1}{\pi} \sum_{\alpha} \left(\delta_\alpha(m) - \delta_\alpha(\infty) - \pi n_\alpha^{>}\right) \\ &= \frac{1}{\pi} \sum_{\alpha} \left(\pi n_\alpha^{<} - \delta_\alpha(-m) + \delta_\alpha(-\infty)\right) . \end{aligned} \tag{5.8}$$

In the anomalous channels, we must subtract 1 from the left-hand side of Eq. (5.7) and $\frac{1}{2}$ from the subsequent expressions for Q because of the modification to Levinson's theorem.

We will next discuss a number of applications of Eq. (5.8).

5.2 Electrostatics and the Need for Regularization

The conserved charges we consider are not renormalized, i.e.,they do not receive any contributions from the counterterms of the theory.[1] Nonetheless, it is essential to include the effects of the regularization procedure used to

[1] This non-renormalization holds for all Noether currents of an unbroken, global, and linearly realized symmetry [7].

define the theory. The example of QED in 1+1 dimensions provides a clear illustration of this subtlety. Although the theory is finite, the regularization process is non-trivial.

The Lagrangian is

$$\mathcal{L} = -\frac{1}{4e^2} F_{\mu\nu} F^{\mu\nu} + \frac{1}{2} \left[\bar{\Psi}, (\gamma^\mu (i\partial_\mu - A_\mu) - m) \Psi \right], \tag{5.9}$$

where we again have used the commutator to ensure that the free theory is $\mathcal{C}$ and $\mathcal{CP}$ invariant. In ordinary perturbation theory, the vacuum polarization diagram computed in d spacetime dimensions is

$$\begin{aligned} \Pi_{\mu\nu}(p) = 2ie^2 N_d \int_0^1 d\xi \int \frac{d^d k}{(2\pi)^d} \\ \times \frac{2\xi(1-\xi)(g_{\mu\nu} p^2 - p_\mu p_\nu) + g_{\mu\nu} \left(m^2 - p^2 \xi(1-\xi) + k^2 (\frac{2}{d} - 1) \right)}{(k^2 + p^2 \xi(1-\xi) - m^2)^2}, \end{aligned} \tag{5.10}$$

where $2N_d$ is the dimension of the Dirac algebra, cf.Sect. 3.5. If we had not regulated the theory by analytically continuing the spacetime dimension, we would not have found the last term, because it vanishes if we set $d = 2$ from the outset. Performing the integral with $d \neq 2$ shows that this term exactly cancels the two preceding terms, leaving the transverse form of the vacuum polarization that is required by gauge invariance. Thus we must include in our definition of the field theory the additional information that the theory is regulated in a way that preserves gauge invariance at the quantum level.

The vacuum polarization diagram reflects the effect of the chiral anomaly. The anomaly is obtained from the leading correction to the vector current,[2] which is related to the polarization tensor by

$$j_\mu(x) = \int d^d y \Pi_{\mu\nu}(x-y) A^\nu(y), \tag{5.11}$$

where $\Pi_{\mu\nu}(x)$ denotes the Fourier transform of Eq. (5.10). Thus a completely transverse polarization tensor corresponds to a conserved vector current. Setting $d = 2$ from the outset gives an anomalous vector current and conserved axial current

$$\begin{aligned} \partial_\mu j^\mu &= \partial_\mu \bar{\Psi} \gamma^\mu \Psi = \frac{e N_d}{\pi} \partial_\mu A^\mu \\ \partial_\mu j_5^\mu &= \partial_\mu \bar{\Psi} \gamma^\mu \gamma_5 \Psi = 0, \end{aligned} \tag{5.12}$$

where we have used $j_5^\mu = -\epsilon^{\mu\nu} j_\nu$ for the axial vector current in $d = 2$. Including the contribution proportional to $\frac{2}{d} - 1$ in Eq. (5.10) transfers this anomaly to the axial vector current [8]

[2] More precisely, this statement refers to the vacuum expectation value of the current, $\langle \Omega | j_\mu(x) | \Omega \rangle$. For simplicity, we will omit the brackets $\langle \cdot \rangle$ in the following.

$$\partial_\mu j^\mu = \partial_\mu \bar{\Psi}\gamma^\mu \Psi = 0$$
$$\partial_\mu j_5^\mu = \partial_\mu \bar{\Psi}\gamma^\mu\gamma_5 \Psi = \frac{eN_d}{2\pi}\epsilon^{\mu\nu}F_{\mu\nu}\,. \tag{5.13}$$

If we choose a configuration with $A_1 = 0$ and adiabatically turn on a configuration $A_0(x)$ between $t = -\infty$ and $t = 0$, then integrating Eq. (5.12) yields

$$Q = \int j^0(x)dx = \frac{eN_d}{2\pi}\int A_0(x)dx, \tag{5.14}$$

when choosing not to regulate the finite polarization tensor, Eq. (5.10). By contrast, dimensional regularization gives $Q = 0$.

The phase shift approach shows exactly the same behavior. We consider the example of an electrostatic square well potential with depth φ and width $2L$. First we ignore subtleties of regularization and compute directly in $d = 2$. The phase shift in the negative parity channel $\delta_-(\omega)$ is determined by

$$\frac{m+\omega}{k}\tan(kL + \delta_-(\omega)) = \frac{m+\omega+e\varphi}{q}\tan qL, \tag{5.15}$$

with $k = \sqrt{\omega^2 - m^2}$ and $q = \sqrt{(\omega + e\varphi)^2 - m^2}$. Similarly, the phase shift in the positive parity channel $\delta_+(\omega)$ is determined by

$$\frac{k}{m+\omega}\tan(kL + \delta_+(\omega)) = \frac{q}{m+\omega+e\varphi}\tan qL\,. \tag{5.16}$$

As $\omega \to \pm\infty$, the total phase shift approaches $\pm 2e\varphi L$, giving a fractional contribution to the total fermion charge, in agreement with Eq. (5.14). Although such fractional charges are possible (and we will see examples of them in the next section), here this result indicates that the method of calculation has not preserved gauge invariance.

To preserve gauge invariance, we regularize the computation by calculating the phase shifts as analytic functions of the space dimension n. Since we are only concerned with the contribution from $\omega \to \pm\infty$, we can consider just the leading Born approximation. In arbitrary dimensions, the total phase shift is a sum over channels labeled by total spin $j = \frac{1}{2}, \frac{3}{2}, \ldots$ and by parity. Summing over parity, the leading Born approximation to the total phase shift in each channel j is given by

$$\delta^{(1)}_{n,j} = \omega e\pi \int_0^\infty A_0(r)\left(J_{\frac{n}{2}+j-\frac{3}{2}}(kr)^2 + J_{\frac{n}{2}+j-\frac{1}{2}}(kr)^2\right) r dr, \tag{5.17}$$

which has degeneracy $D(j)$ given by Eq. (3.74). Summing over j using Eqs. (3.72) and (3.54) yields the leading Born approximation to the total phase shift in n space dimensions

$$\delta^{(1)}_n(\omega) = \omega e\pi N_d \sum_{\ell=0}^\infty D(\ell)\int_0^\infty A_0(r)J_{\frac{n}{2}+\ell-1}(kr)^2 r dr$$

$$= \omega k^{n-2} \frac{N_d e\pi}{2^{n-2}\Gamma(\frac{n}{2})^2} \int_0^\infty A_0(r) r^{n-1} dr$$
$$= \omega k^{n-2} \frac{N_d L^n e\varphi\pi}{2^{n-2} n \Gamma(\frac{n}{2})^2} \tag{5.18}$$

which reduces to $\pm 2N_d e\varphi L$ if we send $n \to 1$ and then take the limit $\omega \to \pm\infty$. But the order of these limits is essential: If we first regulate the theory by holding the dimension fixed at $n < 1$, we then see that the contribution as $\omega \to \pm\infty$ vanishes. Only after we have taken the $\omega \to \pm\infty$ limits do we send $n \to 1$. This procedure, dictated by dimensional regularization, preserves gauge invariance and gives no fractional charge.

We note that other regularization methods commonly used in phase shift calculations, such as zeta-function regularization, would not preserve gauge invariance and would thus lead to the same spurious fractional result.

5.3 Chiral Bag Model in One Space Dimension

Chiral bag models provide simple illustrations where fractional fermion numbers do arise. We begin with a Dirac fermion in one dimension on the half-line $x \geq 0$, subject to the boundary condition

$$ie^{i\gamma_5\theta}\Psi = \gamma^1\Psi \tag{5.19}$$

at $x = 0$, with $-\frac{\pi}{2} \leq \theta \leq \frac{\pi}{2}$. For $x > 0$ we solve the free Dirac equation

$$\gamma^0(-i\gamma^1\partial_x + m)\Psi = \omega\Psi\,, \tag{5.20}$$

where the energy ω may be positive or negative. In the basis $\gamma^0 = \sigma_3$, $\gamma^1 = i\sigma_2$, and $\gamma_5 = \sigma_1$ the solutions are

$$\phi^\pm(x) = \begin{pmatrix} \pm k \\ \omega - m \end{pmatrix} e^{\pm ikx}. \tag{5.21}$$

The scattering solutions define the phase shifts by

$$\psi^\pm(x) = \phi^-(x) \pm e^{2i\delta^\pm(\omega)}\phi^+(x). \tag{5.22}$$

To extract the phase shifts from this expression, we apply the boundary condition, Eq. (5.19), to $\psi^\pm$ at $x = 0$, giving

$$\cot\delta^+(\omega) = -\frac{k}{\omega - m}\tan\beta \quad \text{and} \quad \tan\delta^-(\omega) = \frac{k}{\omega - m}\tan\beta, \tag{5.23}$$

where $\beta = \frac{\pi}{4} - \frac{\theta}{2}$ is taken to be positive. For $\beta > 0$ the phase shifts are smooth functions of the energy such that

$$\sum_{\alpha=\pm}\delta_\alpha(m)-\delta_\alpha(\infty)=-2\beta+\pi \quad \text{and} \quad \sum_{\alpha=\pm}\delta_\alpha(-m)-\delta_\alpha(-\infty)=2\beta\,. \tag{5.24}$$

To find the bound states, we look for solutions of the form

$$\phi(x)=\begin{pmatrix} i\kappa \\ \omega-m \end{pmatrix} e^{-\kappa x}, \tag{5.25}$$

with $\kappa=\sqrt{m^2-\omega^2}$. Imposing the boundary condition gives

$$m-\omega=\kappa\tan\beta\,, \tag{5.26}$$

which is solved by $\omega = m\sin\theta$. So there is exactly one bound state, which has positive (negative) energy for $\theta > 0$ ($\theta < 0$). Thus we have $\sum_\alpha n_\alpha^> = \frac{1}{2}\left[1+\mathrm{sign}(\theta)\right]$ and $\sum_\alpha n_\alpha^< = \frac{1}{2}\left[1-\mathrm{sign}(\theta)\right]$, which together with Eq. (5.24) can be substituted into Eqs. (5.5)–(5.8) to yield

$$Q=Q^>=Q^<=\frac{\theta}{\pi}-\frac{1}{2}\mathrm{sign}(\theta)\,. \tag{5.27}$$

For $\theta = 0$, γ_5 does not appear, and therefore the charge vanishes because there is no $\mathcal{CP}$ violation. Furthermore $Q(\theta=\pm\frac{\pi}{2})=0$, so this result can be periodically continued beyond the defining interval. As expected, a jump occurs at $\theta = 0$ when the bound states move from the positive to the negative spectrum and vice versa.

5.4 Chiral Bag Model in Three Space Dimensions

This simple model generalizes naturally to three dimensions. We consider an isodoublet of Dirac fermions subject to the boundary condition

$$ie^{i\theta\boldsymbol{\tau}\cdot\hat{\boldsymbol{x}}\gamma_5}\Psi=(\boldsymbol{\gamma}\cdot\hat{\boldsymbol{x}})\,\Psi \tag{5.28}$$

imposed on a sphere of radius R, where $\boldsymbol{\tau}$ are the isospin Pauli matrices. This condition is not invariant under space and isospin rotations individually, but it is invariant under combined space and isospin rotations, and under parity. Thus we can decompose the scattering problem into eigenchannels labeled by parity and total grand spin $G = 0,\ 1,\ 2, \ldots$ [9, 10], where grand spin $\boldsymbol{G}$ is the sum of orbital and spin angular momentum $\boldsymbol{j}=\boldsymbol{l}+\frac{1}{2}\boldsymbol{\sigma}$ and isospin $\frac{1}{2}\boldsymbol{\tau}$. These eigenstates are also important for the discussion in Chap. 6 and therefore we will explain their construction in detail here. The spherical harmonics, $Y_{\ell m}(\hat{\boldsymbol{x}})=\langle\hat{\boldsymbol{x}}|lm\rangle$, are the eigenfunctions of the orbital angular momentum $\boldsymbol{l}$. They couple with spin states $|s\rangle_S$ to form eigenstates of total spin $\boldsymbol{j}$

$$|j\ j_3\ \ell\rangle=\sum_{s=\pm\frac{1}{2}} C^{jj_3}_{\ell(m-s),\frac{1}{2}s}|l\ (m-s)\rangle|s\rangle_S\,, \tag{5.29}$$

where the $C^{jj3}_{\ell(m-s),\frac{1}{2}s}$ are Clebsch–Gordan coefficients. Similarly these states are combined with isospinors $|t\rangle_I$ to form grand spin states

$$|G\ M\ j\ \ell\rangle = \sum_{t=\pm\frac{1}{2}} C^{GM}_{j(j_3-t),\frac{1}{2}t}|j\ (j_3-t)\ \ell\rangle|t\rangle_I\,. \tag{5.30}$$

We define four-component grand spin spherical harmonic functions as the projection $\mathcal{Y}_{j\ell}(\hat{\boldsymbol{x}}) = \langle\hat{\boldsymbol{x}}|G\ M\ j\ \ell\rangle$, where on the left-hand side we suppress the conserved grand spin quantum numbers. The parity of $\mathcal{Y}_{j\ell}$ is $(-)^\ell$ and thus is determined by the orbital angular momentum, which may take values $\ell = G$ and $G \pm 1$. Next we have to combine the $\mathcal{Y}_{j\ell}(\hat{\boldsymbol{x}})$ with radial functions to form Dirac spinors. For the channels with parity $(-)^G$ we have two spinors that solve the Dirac equation away from the boundary[3]:

$$\begin{pmatrix} ig_1(r)\mathcal{Y}_{G+\frac{1}{2},G} \\ f_1(r)\mathcal{Y}_{G+\frac{1}{2},G+1} \end{pmatrix} \qquad \text{and} \qquad \begin{pmatrix} ig_2(r)\mathcal{Y}_{G-\frac{1}{2},G} \\ f_2(r)\mathcal{Y}_{G-\frac{1}{2},G-1} \end{pmatrix}. \tag{5.31}$$

For zero grand spin the second spinor is absent. In general these spinors have eight components. The Dirac spinors with parity $(-)^{G+1}$ have the four upper and four lower components exchanged.

We will now compute the S-matrix in the parity $(-)^G$ channels. While grand spin is conserved, the boundary condition in Eq. (5.28) mixes states with different ordinary spin j. We introduce the linear combinations that define the S-matrix:

$$\begin{aligned}\Psi_1 = \begin{pmatrix} iw^+h_G(kr)\mathcal{Y}_{G+\frac{1}{2},G} \\ w^-h_{G+1}(kr)\mathcal{Y}_{G+\frac{1}{2},G+1} \end{pmatrix} + S^{+,G}_{11}\begin{pmatrix} iw^+h^*_G(kr)\mathcal{Y}_{G+\frac{1}{2},G} \\ w^-h^*_{G+1}(kr)\mathcal{Y}_{G+\frac{1}{2},G+1} \end{pmatrix} \\ + S^{+,G}_{21}\begin{pmatrix} iw^+h^*_G(kr)\mathcal{Y}_{G-\frac{1}{2},G} \\ -w^-h^*_{G-1}(kr)\mathcal{Y}_{G-\frac{1}{2},G-1} \end{pmatrix},\end{aligned} \tag{5.32}$$

$$\begin{aligned}\Psi_2 = \begin{pmatrix} iw^+h_G(kr)\mathcal{Y}_{G-\frac{1}{2},G} \\ -w^-h_{G-1}(kr)\mathcal{Y}_{G-\frac{1}{2},G-1} \end{pmatrix} + S^{+,G}_{22}\begin{pmatrix} iw^+h^*_G(kr)\mathcal{Y}_{G-\frac{1}{2},G} \\ -w^-h^*_{G-1}(kr)\mathcal{Y}_{G-\frac{1}{2},G-1} \end{pmatrix} \\ + S^{+,G}_{12}\begin{pmatrix} iw^+h^*_G(kr)\mathcal{Y}_{G+\frac{1}{2},G} \\ w^-h^*_{G+1}(kr)\mathcal{Y}_{G+\frac{1}{2},G+1} \end{pmatrix},\end{aligned} \tag{5.33}$$

where $h_\ell(kr)$ refers to the spherical Hankel functions suitable to parameterize an incoming spherical wave. We have also introduced the kinematic factors $w^+ = \sqrt{1+\frac{m}{\omega}}$ and $w^- = \mathrm{sgn}(\omega)\sqrt{1-\frac{m}{\omega}}$, where $\omega = \pm\sqrt{k^2+m^2}$ and m are the energy and mass of the Dirac particle, respectively. In the case $G = 0$, the components with $j = G-\frac{1}{2}$ are absent and the S-matrix has only a single component $S^{+,0}_{11} = \exp(2i\delta^+_0)$.

Imposing the boundary condition, Eq. (5.28), on these wavefunctions gives the condition

[3] We adopt the standard representation for the γ-matrices in which γ_0 is diagonal.

$$\begin{pmatrix} \cos\theta & i\hat{\boldsymbol{x}}\cdot\boldsymbol{\tau}\sin\theta - i\hat{\boldsymbol{x}}\cdot\boldsymbol{\sigma} \\ i\hat{\boldsymbol{x}}\cdot\boldsymbol{\tau}\sin\theta + i\hat{\boldsymbol{x}}\cdot\boldsymbol{\sigma} & \cos\theta \end{pmatrix} \Psi_n \Big|_{r=R} = 0\,. \tag{5.34}$$

For each $n = 1, 2$ the projection onto grand spin spherical harmonics yields two equations, which allows us to extract all four components of the S-matrix. It is convenient to express the result in the form of a matrix equation:

$$\begin{pmatrix} X & Y \\ \bar{X} & \bar{Y} \end{pmatrix} \begin{pmatrix} S_{11}^{+,G} & S_{12}^{+,G} \\ S_{21}^{+,G} & S_{22}^{+,G} \end{pmatrix} = - \begin{pmatrix} X^* & Y^* \\ \bar{X}^* & \bar{Y}^* \end{pmatrix} \equiv -M(G)^*\,, \tag{5.35}$$

where the star denotes complex conjugation. For convenience we have not made explicit the grand spin dependence of the matrix elements, which can be computed from the Clebsch–Gordan coefficients in Eqs. (5.29) and (5.30) [10, 11]:

$$\begin{aligned} X &= h_G^*(kR)\cos\theta + \frac{k}{\omega+m}\left(1 + \frac{\sin\theta}{2G+1}\right) h_{G+1}^*(kR) \\ \bar{X} &= -h_G^*(kR)\cos\theta + \frac{k}{\omega+m}\left(1 + \frac{\sin\theta}{2G-1}\right) h_{G-1}^*(kR) \\ Y &= \frac{2\sqrt{G(G+1)}}{2G+1}\frac{k}{\omega+m} h_{G-1}^*(kR)\,\sin\theta \\ \bar{Y} &= \frac{2\sqrt{G(G+1)}}{2G+1}\frac{k}{\omega+m} h_{G+1}^*(kR)\,\sin\theta\,. \end{aligned} \tag{5.36}$$

The total phase shift in this grand spin channel is then given by

$$\delta_G^+ = -i\ln\left(\det S^{+,G}\right) = -i\ln\left(\frac{\det M(G)^*}{\det M(G)}\right)\,. \tag{5.37}$$

For the channels with parity $(-)^{G+1}$ the computation proceeds analogously and yields δ_G^-.

It is now straightforward to collect the resulting total phase shifts. In the $G = 0$ channel, the phase shifts in the two parity channels are

$$\delta_0^\pm(\omega) = -i\ln\left(ih_1(kR)\frac{k}{\pm\omega - m}\cos\theta + ih_0(kR)(1 \mp \sin\theta)\right)\,. \tag{5.38}$$

With this result, using Eq. (5.3) the contribution of the $G = 0$ channel to the fermion number can be read off to be $-\frac{\theta}{\pi}$. For $G > 0$ the total phase shift in each channel is given by

$$\begin{aligned} \delta_G^\pm(\omega) = -i\ln\Bigg(&\sin\theta\frac{h_G(kR)^2}{(\omega \mp m)R} + \frac{k}{\pm\omega - m} h_G(kR)\left(h_{G+1}(kR) - h_{G-1}(kR)\right) \\ &- \cos^2\theta\left[h_{G+1}(kR)h_{G-1}(kR)\left(\frac{k}{\pm\omega - m}\right)^2 - h_G(kR)^2\right]\Bigg)\,. \end{aligned} \tag{5.39}$$

Its contribution needs to be treated with care when summing over grand spin to obtain the total charge,

$$Q = \lim_{\substack{G_{\max}\to\infty \\ \Lambda\to\infty}} Q(\Lambda, G_{\max}) \qquad \text{with}$$

$$Q(\Lambda, G_{\max}) = \sum_{G=0}^{G_{\max}} (2G+1)\left[\delta_G^+(\Lambda) + \delta_G^-(\Lambda) - \delta_G^+(-\Lambda) - \delta_G^-(-\Lambda)\right], \quad (5.40)$$

where Λ is the momentum cutoff we use to regularize the theory. For large k, the dominant contribution stems from $G \approx kR$. We must follow a consistent regularization procedure in order to obtain the correct order of limits for both $G_{\max} \to \infty$ and $\Lambda \to \infty$. Our prescription is to first compute the total phase shift at $k = \Lambda$, summed over all partial waves, i.e.,with $G_{\max} \to \infty$. This sum then has a smooth limit as $\Lambda \to \infty$. If we had taken the limit in the opposite order by considering the $k \to \infty$ limit in each partial wave separately, we would incorrectly conclude that the contribution from $G > 0$ was identically zero.

To avoid mod(π) ambiguities in the numerical computation, it is convenient to first consider $\frac{dQ}{d\theta}$ by differentiating Eqs. (5.38) and (5.39) and then integrate to obtain Q as a function of θ. In Fig. 5.1 (taken from Ref. [4]), we give an example of the numerical evaluation of $dQ(\Lambda, G_{\max})/d\theta$ for particular values of θ and $G_{\max}$ as a function of the cutoff, which is parameterized in terms of the dimensionless variable $z = \Lambda R$. The contribution to $dQ/d\theta$ from the channels $G > G_{\max}$ is negligible for $z \ll G_{\max}$. For $z \approx G_{\max}/2$ the relation

$$\frac{dQ(\Lambda, G_{\max})}{d\theta} = -\frac{1}{\pi}(1 - \cos 2\theta) \quad (5.41)$$

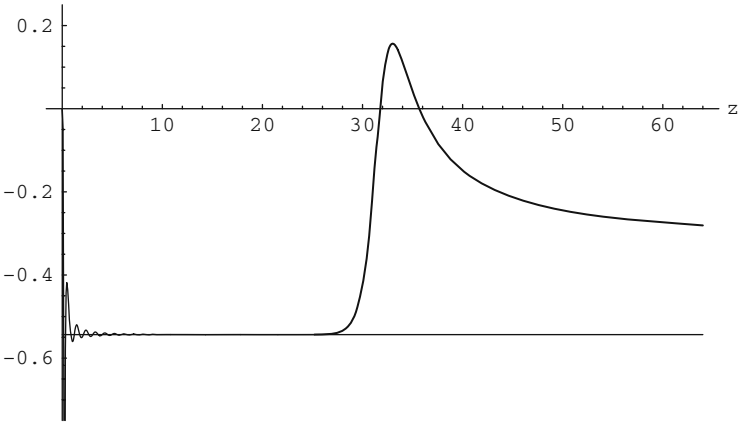

Fig. 5.1 Numerical computation of $\frac{d}{d\theta}G(\Lambda, G_{\max})$ evaluated at $\theta = \frac{3\pi}{8}$ and $m = 0$, summed up to $G_{\max} = 32$, and plotted as a function of $z = \Lambda R$. The horizontal line shows the right-hand side of Eq. (5.41) for this value of θ

is established numerically. For $z \gg G_{\max}$ only the contribution from the $G = 0$ channel, Eq. (5.38), is seen, which would lead to an incorrect result for the charge. Thus integrating the right-hand side of Eq. (5.41) with respect to θ yields our result for the charge of the bag boundary condition,

$$Q = -\frac{1}{\pi}(\theta - \sin\theta\cos\theta)\,. \tag{5.42}$$

This is the result Ref. [3] derived from a multiple reflection expansion for the Green's function of the bag model. Again we emphasize that an incorrect regularization which sends the cutoff to infinity before summing over channels would yield only the first term in (5.42).

References

1. J. Goldstone and F. Wilczek, *Phys. Rev. Lett.* **47** (1981) 986. 91
2. R. Jackiw and C. Rebbi, *Phys. Rev.* **D13** (1976) 3398. 91
3. J. Goldstone and R. L. Jaffe, *Phys. Rev. Lett.* **51** (1983) 1518. 91, 101
4. E. Farhi, N. Graham, R. L. Jaffe, and H. Weigel, *Nucl. Phys.* **B595** (2001) 536. 91, 100
5. R. Blankenbecler and D. Boyanovsky, *Phys. Rev.* **D31** (1985) 2089. 91
6. D. Boyanovsky and R. Blankenbecler, *Phys. Rev.* **D31** (1985) 3234. 91
7. J. C. Collins, *Renormalization. An Introduction to Renormalization, the Renormalization Group, and the Operator Product Expansion.* Cambridge University Press, UK, 1984. 93
8. M. E. Peskin and D. V. Schroeder, *An Introduction to Quantum Field Theory*, Ch. 19. Persus Books, 1995. 94
9. R. Alkofer, H. Reinhardt, and H. Weigel, *Phys. Rept.* **265** (1996) 139. 97
10. S. Kahana and G. Ripka, *Nucl. Phys.* **A429** (1984) 462. 97, 99
11. U. Zuckert, R. Alkofer, H. Reinhardt, and H. Weigel, *Nucl. Phys.* **A570** (1994) 445. 99

6 Hedgehog Configurations in $d = 3 + 1$

In this chapter we extend the approach of Chap. 4 to the case of three spatial dimensions. First we study the coupling of a Higgs doublet to chiral fermions, and then we generalize the background boson fields to an $SU_L(2)$ gauge theory. We will again use a systematic expansion in $\hbar$ and $1/N$ in which the dominant contribution arises from the fermion loop. Our goal is thus to compute the one-fermion loop contribution to the vacuum polarization energy.

6.1 Chiral Fermions

6.1.1 The Model

The model that we begin with consists of the Higgs sector of the standard model coupled to a fermion doublet in $3 + 1$ dimensions. Our goal is to explore the possibility that within this model there is a non-trivial Higgs field configuration with non-zero-fermion number whose energy is less than that of a state with the same quantum numbers built on top of the perturbative vacuum. The existence of such fermionic quantum solitons would provide an attractive resolution to the decoupling puzzle in the standard model and other chiral gauge theories. A fermion obtains its mass through Yukawa coupling to the scalar Higgs via the well-known Higgs mechanism. Explicit mass terms are forbidden by gauge invariance. So, as we increase the mass of a fermion we also increase its Yukawa coupling, which gives a corresponding enhancement to the interaction vertices. As a result, it may not decouple from the low-energy theory. Moreover, the heavy fermion cannot simply disappear from the spectrum, because then anomaly cancellation would be ruined. It is plausible, however, that the large Yukawa coupling gives rise to a quantum soliton in the low-energy theory, which carries the quantum numbers of the decoupled fermion and maintains anomaly cancellation according to the mechanism described by D'Hoker and Farhi [1].

As in the standard model, the fermions in our model acquire masses through their Yukawa coupling to the Higgs field. However, we make two essential simplifications of the full electroweak theory: we restrict all fermions to have equal mass, and we neglect the coupling to the (electroweak) gauge

Graham, N., et al.: *Hedgehog Configurations in* $d = 3 + 1$. Lect. Notes Phys. **777**, 103–142 (2009)
DOI 10.1007/978-3-642-00139-0_6

fields. The latter restriction will be lifted in the next section, where gauge field backgrounds will be introduced.

We write the Higgs doublet (φ_0, φ_+) in terms of a 2×2 matrix-valued field as

$$\Phi = \begin{pmatrix} \varphi_0 & -\varphi_+^* \\ \varphi_+ & \varphi_0^* \end{pmatrix} . \tag{6.1}$$

Then the Higgs Lagrangian is

$$\mathcal{L}_H = \frac{1}{4} \operatorname{tr} \left[\left(\partial_\mu \Phi^\dagger \right) \left(\partial^\mu \Phi \right) \right] - V(\Phi), \tag{6.2}$$

where

$$V(\Phi) = \frac{\lambda}{16} \left(\operatorname{tr} \left[\Phi^\dagger \Phi \right] - 2v^2 \right)^2 . \tag{6.3}$$

We take the vacuum expectation value to be

$$\langle \Phi \rangle = v \begin{pmatrix} 1 & 0 \\ 0 & 1 \end{pmatrix} \tag{6.4}$$

and note that the Higgs particle has mass $m_H = \sqrt{\lambda} v$ at tree level.

The chirally invariant coupling to the fermion doublet $q = (t, b)$ is given by

$$\mathcal{L}_{\mathrm{HF}} = g \bar{q}_L \Phi q_R + g \bar{q}_R \Phi^\dagger q_L, \tag{6.5}$$

which results in a tree-level mass $m = gv$ for both t and b. It is also convenient to rewrite Φ in terms of four real (dimensionless) fields s and $\boldsymbol{p}$ as

$$\Phi = v \left(s + i \boldsymbol{\tau} \cdot \boldsymbol{p} \right), \tag{6.6}$$

which gives the $d = 3 + 1$ generalization of the interaction in Eq. (4.23),

$$\mathcal{L}_{\mathrm{HF}} = m \bar{q} \left(s + i \gamma_5 \boldsymbol{\tau} \cdot \boldsymbol{p} \right) q . \tag{6.7}$$

Here and above $\boldsymbol{\tau}$ represents the isospin Pauli matrices. With these definitions, the classical energy is

$$E_{\mathrm{cl}}[\Phi] = \frac{v^2}{2} \int d^3 r \left(\partial_i s \partial_i s + \partial_i \boldsymbol{p} \cdot \partial_i \boldsymbol{p} + \frac{\lambda v^2}{4} (s^2 + \boldsymbol{p}^2 - 1)^2 \right) . \tag{6.8}$$

6.1.2 The Fermion Loop

In order to compute the fermion vacuum polarization contribution to the total energy we must first outline the renormalization process in the perturbative sector of the model. To leading order in $1/N$, quantum fluctuations—and thus possible divergences—come exclusively from the fermion, as we saw in the previous chapter [2]. The divergences can be canceled by counterterms of the form

$$\mathcal{L}_{\mathrm{ct}} = a \operatorname{tr} \left(\partial_\mu \Phi \partial^\mu \Phi^\dagger \right) - b \operatorname{tr} \left(\Phi \Phi^\dagger - v^2 \right) - c \operatorname{tr} \left(\Phi \Phi^\dagger - v^2 \right)^2 , \tag{6.9}$$

where a, b, and c are cutoff-dependent constants. The Yukawa coupling g and consequently the fermion mass m are not renormalized to this order.

In terms of the shifted Higgs field $h \equiv s - v$, our renormalization conditions are:

1. the vacuum expectation value of h vanishes, i.e., the VEV of the Higgs field is fixed;
2. the position m_H and the residue of the pole in the two-point function for h do not acquire quantum corrections, i.e., m_H is identified with the physical Higgs mass.

In order to fix the counterterms, it is therefore sufficient to expand the fermionic quantum correction to the action,

$$\mathcal{S}_{\text{eff}}[h] = -i \,\text{Tr}\, \ln \left\{ i\partial\!\!\!/ - g(v+h) \right\}, \tag{6.10}$$

up to quadratic order in h and combine the result with $\int d^4x \mathcal{L}_{\text{ct}}$. In dimensional regularization we obtain

$$\begin{aligned} a = &-\frac{g^2}{(4\pi)^2} \left\{ \frac{1}{\epsilon} - \gamma - \frac{2}{3} + \ln\left(\frac{4\pi\mu^2}{m^2}\right) \right. \\ &\left. -6 \int_0^1 dx x(1-x) \, \ln\left[1 - x(1-x)\mu_H^2\right] \right\} \end{aligned} \tag{6.11}$$

$$b = -\frac{g^2 m^2}{(4\pi)^2} \left\{ \frac{1}{\epsilon} - \gamma + 1 + \ln\left(\frac{4\pi\mu^2}{m^2}\right) \right\} \tag{6.12}$$

$$c = -\frac{g^4}{(4\pi)^2} \left\{ \frac{1}{\epsilon} - \gamma + \ln\left(\frac{4\pi\mu^2}{m^2}\right) - \frac{\mu_H^2}{4} - \frac{3}{2} \int_0^1 dx \, \ln\left[1 - x(1-x)\mu_H^2\right] \right\},$$

where $d \equiv 4 - 2\epsilon$ and μ is the scale required to keep the mass dimension of the loop integrals at the physical value 4. Here we have introduced the abbreviation $\mu_H = m_H/m$.

Having set up the model in the perturbative sector, we now turn to nontrivial field configurations. We restrict our attention to the spherical *ansatz* for the Higgs field, which is the famous hedgehog configuration [3]

$$\Phi(\boldsymbol{x}) = v \left[s(r) + i\boldsymbol{\tau} \cdot \hat{\boldsymbol{x}} \, p(r) \right], \tag{6.13}$$

with $r = \sqrt{\boldsymbol{x}^2}$. With the standard representation of the Dirac matrices, the corresponding Dirac operator becomes

$$h_D = \begin{pmatrix} ms(r) & -i\boldsymbol{\sigma} \cdot \boldsymbol{\nabla} + mi\boldsymbol{\tau} \cdot \hat{\boldsymbol{x}} \, p(r) \\ -i\boldsymbol{\sigma} \cdot \boldsymbol{\nabla} - mi\boldsymbol{\tau} \cdot \hat{\boldsymbol{x}} \, p(r) & -ms(r) \end{pmatrix}, \tag{6.14}$$

and the fermion field obeys the time-independent Dirac equation,

$$h_D \Psi = \omega \Psi \ . \tag{6.15}$$

Note that the energy eigenvalue ω can assume both positive and negative values. In general the spectrum of h_D also contains both discrete (bound) and continuum (scattering) states.

Now we can obtain the bound states ϵ_j as the solutions to Eq. (6.15) with $|\omega| < m$. We use Levinson's theorem to compute the number of bound states in each channel from the phase shifts. The phase shifts, in turn, are computed from the S-matrix, which is extracted from solutions to second-order differential equations obtained from the Dirac equation. Because we restrict our attention to backgrounds in the spherical *ansatz*, there are two conserved quantum numbers, grand spin and parity. The grand spin $\boldsymbol{G}$ is defined as the vector sum of isospin and total angular momentum (orbital plus spin) and can be interpreted as a generalized angular momentum. The parity Π is associated with space reflection in the usual way. The associated generalized spherical spinors have already been defined in Sect. 5.4.

We obtain separate second-order differential equations for the upper and lower components of the Dirac equation in the standard representation. After projecting onto a subspace with definite energy, grand spin, and parity, we are left with two coupled second-order differential equations for two radial functions, say $g_1(r)$ and $g_2(r)$, cf. Eq. (5.31). Together, the linearly independent solutions with incoming spherical wave boundary conditions in either of these channels define a two-channel scattering problem. In the following we will suppress the labels ω, G, and Π, which characterize this two-channel problem. The two linearly independent boundary conditions are labeled by $j \in \{1, 2\}$ and are implemented as follows:

In the free case, the radial functions corresponding to outgoing waves in each channel are Hankel functions, $g_1(r) = h_\ell^{(1)}(kr)$ and $g_2(r) = h_{\ell'}^{(1)}(kr)$. (Here ℓ and ℓ' are determined from grand spin G and parity Π: In the channel with parity $\Pi = +(-1)^G$, we have $\ell = \ell' = G$, while in the channel $\Pi = -(-1)^G$ we have $\ell = G + 1$ and $\ell' = G - 1$.) We define the two independent free spinor solutions in each channel by taking $\{g_1(r) = h_\ell^{(1)}(kr)\,,\, g_2(r) \equiv 0\}$ and $\{g_1(r) \equiv 0\,,\, g_2(r) = h_{\ell'}^{(1)}(kr)\}$. The Jost-like boundary conditions are defined as a modification of the free asymptotic solutions: For the boundary condition type $j \in \{1, 2\}$, we require that $g_i^{(j)}(r)$ corresponds to a (phase-shifted) outgoing wave if $i = j$, while it vanishes at large r for $i \neq j$. To simplify the notation, we arrange the two radial wavefunctions for the two boundary conditions in matrix form, $\mathscr{G}_{ij}(r) = g_i^{(j)}(r)$. The boundary conditions are then formulated as a multiplicative modification of the free matrix solution,

$$\mathscr{G}(r) = \begin{pmatrix} g_1^{(1)}(r) & g_1^{(2)}(r) \\ g_2^{(1)}(r) & g_2^{(2)}(r) \end{pmatrix} \equiv F(r)H(kr)\,, \tag{6.16}$$

where the free solution H is diagonal and can be expressed simply in terms of Hankel functions,

$$H(x) = \begin{pmatrix} h_\ell^{(1)}(x) & 0 \\ 0 & h_{\ell'}^{(1)}(x) \end{pmatrix}. \tag{6.17}$$

The elements of the 2×2 matrix $F(r)$ satisfy second-order differential equations obtained from the Dirac equation. In the standard representation of the Dirac matrices they are of the general form

$$F'' = -\frac{2}{r}F'\left(1 + rL'(kr)\right) + \frac{s'}{s \pm \omega/m}\left(F' + FL'(kr)\right) - VF + [K, F] \quad (6.18)$$

for the upper and lower components respectively, where

$$K = \frac{1}{r^2}\begin{pmatrix} \ell(\ell+1) & 0 \\ 0 & \ell'(\ell'+1) \end{pmatrix} \quad (6.19)$$

is the centrifugal barrier with ℓ and ℓ' as above. The 2×2 matrix V describes the coupling of the fermions to the Higgs background,

$$\begin{aligned} V_{11} &= -m^2\left[s^2 + p^2 - 1\right] + \frac{G}{r}\frac{s'}{s + \frac{\omega}{m}} - \frac{mp'}{2G+1} \\ &\quad -\frac{2}{r}\frac{(G+1)mp}{2G+1} + \frac{mp}{2G+1}\frac{s'}{s+\frac{\omega}{m}}, \\ V_{22} &= -m^2\left[s^2 + p^2 - 1\right] - \frac{G+1}{r}\frac{s'}{s + \frac{\omega}{m}} + \frac{mp'}{2G+1} \\ &\quad -\frac{2}{r}\frac{Gmp}{2G+1} - \frac{mp}{2G+1}\frac{s'}{s+\frac{\omega}{m}}, \\ V_{12} &= V_{21} = \frac{2\sqrt{G(G+1)}}{2G+1}\left[mp' + mp\left(\frac{1}{r} - \frac{s'}{s+\frac{\omega}{m}}\right)\right]. \end{aligned} \quad (6.20)$$

In Eqs. (6.18) and (6.20) the primes denote derivatives with respect to the radial coordinate r.

The matrix $L = \ln H$ is the only remnant of the Hankel functions,

$$L(x) = \begin{pmatrix} \ln h_\ell^{(1)}(x) & 0 \\ 0 & \ln h_{\ell'}^{(1)}(x) \end{pmatrix}. \quad (6.21)$$

Notice that only the derivative $L' = k\, dL(x)/dx|_{x=kr}$, whose matrix elements can be expressed as simple rational functions, appears in Eq. (6.18). As a result we avoid any instability in the numerical treatment that would be caused by the oscillating Hankel functions.

The 2×2 submatrix of the S-matrix for the $\Pi = (-1)^G$ channel is defined in Eqs. (5.32) and (5.33). The $\Pi = -(-1)^G$ case is defined in the analogous way. These submatrices are most conveniently constructed by superimposing solutions to Eq. (6.18). First we normalize F by imposing the boundary conditions $F(r \to \infty) = 1$ and $F'(r \to \infty) = 0$. Given these boundary conditions and the fact that the second-order differential equations for the g_i are real, the actual scattering wavefunction can be written as

$$\Psi_{\rm sc} = -F^*(r)H^*(kr) + F(r)H(kr)S, \quad (6.22)$$

where S is the 2×2 submatrix of the S-matrix that we seek. Requiring that the scattering solution be regular at the origin yields

$$S = \lim_{r \to 0} H^{-1}(kr)F^{-1}(r)F^*(r)H^*(kr)\,. \quad (6.23)$$

The quantity that enters the density of states is the total phase shift

$$\delta(k) = \frac{1}{2i} \text{ tr ln } S = \frac{1}{2i} \lim_{r\to 0} \text{ tr ln } \left(F^{-1}(r)F^*(r)\right), \tag{6.24}$$

from which the Hankel matrix H cancels because as $r \to 0$ the leading (singular) piece of $H(kr)$ is real, i.e., $\lim_{r\to 0} H^*(kr)H^{-1}(kr) = 1$. The unitarity of S guarantees that Eq. (6.24) yields a real phase shift.

Equation (6.24) only gives the phase shift modulo π. Of course, $\delta(k)$ should be a smooth function that vanishes as $k \to \infty$. An efficient way to avoid spurious jumps by π in the numerical calculation of $\delta(k)$ is to define

$$\delta(k, r) \equiv \frac{1}{2i} \text{ tr ln } \left[F^{-1}(r)F^*(r)\right]. \tag{6.25}$$

This is the multi-channel generalization of the variable phase method in Eq. (1.21). We then include

$$\frac{d\delta(k,r)}{dr} = \frac{1}{2i} \text{ tr } \left[\left(\frac{d}{dr}F^*(r)\right) F^{*-1}(r) - \left(\frac{d}{dr}F(r)\right) F^{-1}(r)\right] \tag{6.26}$$

in the numerical routine that integrates the differential equations for F, with the boundary condition $\lim_{r\to\infty} \delta(k, r) = 0$. Then $\delta(k) \equiv \lim_{r\to 0} \delta(k, r)$ is a smooth function of k that goes to zero as $k \to \infty$.

Finally, the general formalism for computing the vacuum polarization energy, Eq. (3.27), requires the Born series for $\delta(k)$. We introduce $F^{(n_s,n_p)}(r)$, where $n_s = 0, 1, \ldots$ and $n_p = 0, 1, \ldots$ label the order in the expansion around $s(r) = 1$ and $p(r) = 0$, respectively. Obviously, $F^{(0,0)}(r) = \mathbb{1}_2$. Then we find for the first two orders

$$\begin{aligned} \delta^{(1)}(k) &= \frac{1}{2i} \lim_{r\to 0} \text{ tr } \left[F^{(1)*}(r) - F^{(1)}(r)\right] \\ \delta^{(2)}(k) &= \frac{1}{2i} \lim_{r\to 0} \text{ tr} \left[F^{(2)*}(r) - F^{(2)}(r) - \frac{1}{2}[F^{(1)}(r)]^2 + \frac{1}{2}[F^{(1)*}(r)]^2\right], \end{aligned} \tag{6.27}$$

where $F^{(n)}(r) = \sum_{m=0}^{n} F^{(m,n-m)}(r)$. Note that these Born terms do not suffer from any π ambiguity. Subtracting these two terms from the full phase shift eliminates the *quadratic* divergence from the vacuum polarization energy. Eliminating the *logarithmic* divergence would be considerably more complicated because an expansion up to fourth order in $n_s + n_p$ would be necessary.[1] Instead we follow the method of [4] and subtract the Born approximation to a "fake" boson field with the same logarithmic divergences as the full fermion theory. We then compensate for this subtraction by including the corresponding diagram for this field, so that it implements the correct renormalization conditions for the full model. The resulting expression for the vacuum polarization energy, Eq. (3.27), then becomes

[1] When restricting to field configurations with $\Phi\Phi^\dagger = v^2$, two subtractions are sufficient [5, 6].

$$E_{\rm vac} = -\frac{1}{2}\sum_j (2G_j+1)|\epsilon_j| - \int_0^\infty \frac{dk}{2\pi}\,\sqrt{k^2+m^2}\,\frac{d}{dk}\,\bar\delta(k) \;+ E^{(2)}_{\rm ct} + E^{(4)}_{\rm log,ct}\,, \tag{6.28}$$

$$\begin{aligned}\bar\delta(k) = &\sum_{G,\sigma,\Pi}(2G+1)\left(\delta_{G,\sigma,\Pi}(k) - \delta^{(1)}_{G,\sigma,\Pi}(k) - \delta^{(2)}_{G,\sigma,\Pi}(k)\right) \\ &- m^4\left(\frac{1}{m}\arctan\frac{m}{k} + \frac{k}{k^2+m^2}\right) \\ &\qquad\times\int_0^\infty dr\,r^2\left[\big(s(r)^2+p(r)^2-1\big)^2 - 4(s(r)-1)^2\right],\end{aligned} \tag{6.29}$$

$$\begin{aligned}E^{(2)}_{\rm ct} = &\frac{m^2}{\pi^2}\int_0^\infty dq\,q^2\left[h^2(q)+p^2(q)\right]\Big\{q^2+m_H^2 \\ &\qquad - 6\int_0^1 dx\left[m^2+x(1-x)q^2\right]\ln\frac{m^2+x(1-x)q^2}{m^2-x(1-x)m_H^2}\Big\} \\ &- \frac{m^4}{\pi^2}\int_0^\infty dq\,q^2p^2(q)\Big\{\mu_H^2 + 2\int_0^1 dx\Big[3\ln\left(1-x(1-x)\mu_H^2\right) \\ &\qquad - 2\ln\left(1+x(1-x)\frac{q^2}{m^2}\right)\Big]\Big\},\end{aligned} \tag{6.30}$$

$$\begin{aligned}E^{(4)}_{\rm log,ct} = &\frac{m^4}{8\pi}\left(\mu_H^2 + 6\int_0^1 dx\,\ln\left[1-x(1-x)\mu_H^2\right]\right) \\ &\qquad\times\int_0^\infty dr\,r^2\left[\big(s(r)^2+p(r)^2-1\big)^2 - 4(s(r)-1)^2\right].\end{aligned} \tag{6.31}$$

The last term in $\bar\delta(k)$ implements the subtraction of the logarithmic divergence and is compensated by the terms in $E^{(4)}_{\rm log,ct}$ [4]. The label $\sigma = \pm 1$ denotes the sign of the energy eigenvalue, so that $\omega = \sigma\sqrt{k^2+m^2}$. We have also introduced the Fourier transforms

$$h(q) = \int_0^\infty dr\,r^2\,j_0(qr)\,[s(r)-1] \quad \text{and} \quad p(q) = \int_0^\infty dr\,r^2 j_1(qr)p(r)\,, \tag{6.32}$$

where $j_l(qr)$ are spherical Bessel functions.

To find the fermion number carried by the background field we apply the techniques developed in Chap. 5. In each channel, we compare the number of positive-energy bound states, $n^{(+)}_{G,\Pi}$, with the number of bound states that have left the positive-energy continuum, $\frac{1}{\pi}\delta_{G,+,\Pi}(0)$. If one level originating in the positive-energy continuum crosses zero, we will find that $n^{(+)}_{G,\Pi} = \frac{1}{\pi}\delta_{G,+,\Pi}(0) - 1$. Then that channel contributes $(2G+1)$ to the polarized vacuum charge. In total, the vacuum charge is given by

$$\begin{aligned}Q_{\rm vac} &= \sum_{G,\Pi}(2G+1)\left[\frac{1}{\pi}\delta_{G,+,\Pi}(0) - n^{(+)}_{G,\Pi}\right] \\ &= -\sum_{G,\Pi}(2G+1)\left[\frac{1}{\pi}\delta_{G,-,\Pi}(0) - n^{(-)}_{G,\Pi}\right]\,.\end{aligned} \tag{6.33}$$

The second equation reflects the equivalent counting procedure for negative-energy states. We are interested in configurations with fermion number 1. If $Q_{\rm vac} = 0$, the fermion number is obtained by explicitly occupying a level, which we will choose as the level with the largest binding to minimize the energy cost. If $Q_{\rm vac} = 1$, the polarized vacuum already provides the fermion number and none of the bound states needs to be occupied explicitly.

6.1.3 Numerical Analysis

Our formalism is set up to allow the consideration of an arbitrary background $\Phi(\boldsymbol{x})$ of the form (6.13). However, as in all variational methods, we limit ourselves to variation of a few parameters in an *ansatz* motivated by physical considerations. We will scale energies and lengths in terms of the fermion mass m and choose a four-parameter *ansatz*

$$\begin{aligned} s + i\boldsymbol{\tau}\cdot\boldsymbol{p} &= \rho(\xi)\exp\left[i(\boldsymbol{\tau}\cdot\hat{\boldsymbol{x}})\Theta(\xi)\right] \\ \rho(\xi) &= 1 + b_1\left[1 + b_2^2\frac{\xi}{w}\right]\exp\left(-b_2^2\frac{\xi}{w}\right) \\ \Theta(\xi) &= -\pi\frac{c-1}{c-3+2c^{\xi/w}}, \end{aligned} \tag{6.34}$$

where $\xi = mr$ and the variational parameters are w, b_1, b_2, and c. Note that $\Theta(0) = -\pi$, $\rho(0) = 1 + b_1$, and both $\rho - 1$ and Θ go to zero exponentially as $\xi \to \infty$, since we expect a Yukawa tail. As long as ρ does not vanish, this background has winding number one. The profile $\Theta(\xi)$ satisfies $\Theta(w) = -\pi/3$, irrespective of the variational parameters; we consider this the definition of the width w. Furthermore, we have ensured that $\frac{d}{d\xi}\rho(\xi)\big|_{\xi=0} = 0$, as required by the classical equations of motion.

In terms of $\rho(\xi)$ and $\Theta(\xi)$, the classical energy Eq. (6.8) is

$$\begin{aligned} E_{\rm cl} &= \frac{2m\pi}{g^2}\int_0^\infty d\xi\xi^2\left[\left(\frac{d\rho}{d\xi}\right)^2 + \left(\rho\frac{d\Theta}{d\xi}\right)^2 + \frac{2}{\xi^2}\sin^2\Theta + \frac{\mu_H^2}{4}\left(\rho^2-1\right)^2\right] \\ &\equiv \frac{m}{g^2}\,\mathscr{E}_{\rm cl}(w, b_1, b_2, c)\,. \end{aligned} \tag{6.35}$$

Then the total energy, $E_{\rm tot}$, of the configuration with fermion number 1 is

$$\frac{E_{\rm tot}}{m} = \frac{1}{g^2}\mathscr{E}_{\rm cl}(w, b_1, b_2, c) + (1 - Q_{\rm vac})\,\epsilon_1(w, b_1, b_2, c) + \mathscr{E}_{\rm vac}(w, b_1, b_2, c), \tag{6.36}$$

where $\mathscr{E}_{\rm vac} = E_{\rm vac}/m$, and $\epsilon_1 = \omega_1/m$ is the energy eigenvalue of the most strongly bound state. Note that in our scaling, for fixed μ_H the coupling g appears only in the coefficient of the classical term.

Configurations with $\Theta(0) = -\pi$ and $\Theta(\infty) = 0$ tend to strongly bind a state originating from the positive continuum in the $G^{\Pi} = 0^+$ channel. For w large enough, this bound state will cross zero, causing the polarized vacuum charge to be $Q_{\rm vac} = 1$. In that case the level is not explicitly occupied and the corresponding term drops out of Eq. (6.36).

(a) Sample Numerical Calculations

For a given set of variational parameters, we first compute the phase shifts and perform the subtractions according to Eq. (6.29), which allows us to carry out the momentum integral in Eq. (6.28). Using Levinson's theorem, we then find the number of bound states in a given channel from $\delta_{G,\sigma,\Pi}(k = 0)$ and use shooting methods to compute the bound state energies ϵ_j once we know how many states to look for. In terms of the scaled variables, the bound state and phase shift contributions in Eq. (6.28) depend on *ansatz* parameters, but not on model parameters. The dependence on model parameters is completely contained in $\mathscr{E}_{\rm cl}/g^2$, $\mathscr{E}^{(2)}_{\rm ct} = E^{(2)}_{\rm ct}/m$, and $\mathscr{E}^{(4)}_{\rm log,ct} = E^{(4)}_{\rm log,ct}/m$, which are simple integrals involving the background fields. Hence an efficient strategy is to choose a set of variational parameters and then consider the total energy as a function of the model parameters for that particular background configuration. In Fig. 6.1 we display a typical result for the total energy as a function of the Yukawa coupling g.

The existence of configurations with total energy $E_{\rm tot}/m < 1$ shows that there is a stable soliton whose energy is at most $E_{\rm tot}$. Apparently a sizeable Yukawa coupling g is needed to obtain a stable soliton. However, as we will discuss later, our model is not reliable for such large Yukawa couplings because the Landau pole appears at an energy scale comparable to $1/w$.

In Fig. 6.2 we display the total energy as a function of the depth parameters b_1 and b_2, for various values of the Yukawa coupling constant g and typical values of the remaining variational parameters w and c. We observe a shallow local minimum in the vicinity of $b_1 = -0.8$ for small and moderate values of g. However, at this minimum the total energy is larger than the

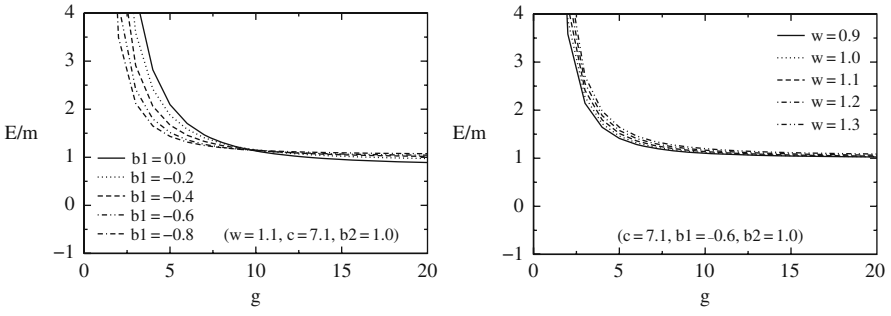

Fig. 6.1 The total energy as a function of the Yukawa coupling constant g with $m_H = 0.35v$

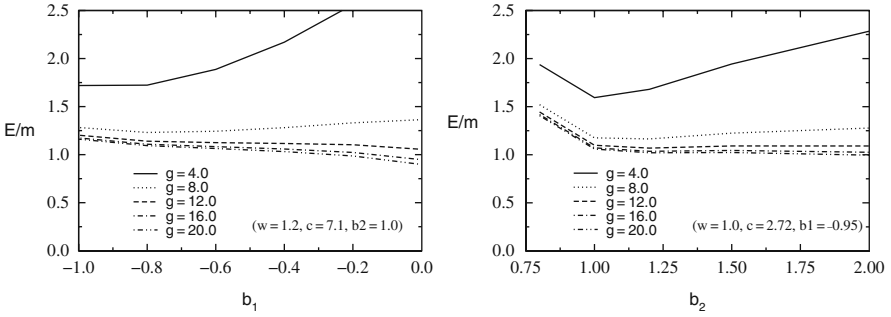

Fig. 6.2 Total energy as a function of the depth parameters b_1 and b_2 with $m_H = 0.35v$ and for various values of the Yukawa coupling constant g

mass m of the free fermion. For larger g, we obtain a total energy less than m for configurations with $b_1 \approx 0$. Configurations with $b_1 > 0$ are more strongly bound, but the one-fermion loop approximation fails for such configurations because the energy functional is not bounded from below. This caveat is exhaustively discussed in Appendix C of Refs. [4] and [7]. We have therefore restricted the space of variational parameters to configurations for which the vacuum is stable to one-loop order.

We observe a similar behavior for $E_{\rm tot}$ as a function of b_2. There exists a local minimum for small and moderate g that does not yield a bound soliton. For large g, a bound soliton seems possible if b_2 is big enough. In this case, the vacuum is stable at one-loop order for these values of the variational parameters. Note that when we find a marginally bound configuration, the vacuum polarization contribution to the energy $E_{\rm vac}$ tends to almost exactly compensate for the gain from binding a single level.

(b) Comparison with the Derivative Expansion

In order to check our computation of the vacuum polarization energy, in particular our simplified treatment of the logarithmic divergence, we have compared our results with the derivative expansion. The relevant formulae are provided in Appendix C of Ref. [4], see also Refs. [8, 9]. Denoting by $\mathscr{E}_{\rm grad}$ the energy computed to second order in the derivative expansion, we list the quantity

$$\Delta_1 \equiv \frac{\mathscr{E}_{\rm cl} + \mathscr{E}_{\rm vac} - \mathscr{E}_{\rm grad}}{\mathscr{E}_{\rm cl} + \mathscr{E}_{\rm vac} + \mathscr{E}_{\rm grad}} \tag{6.37}$$

as a function of the width parameter w in Table 6.1. The other variational parameters are kept at constant values $c = 2.72$, $b_1 = -0.4$, and $b_2 = 1.0$. Also, we consider various values for the Yukawa coupling constant g.

The quantity Δ_1 measures the relative deviation of our (exact) result from the second-order derivative expansion. From Table 6.1, we conclude

Table 6.1 Comparison of the classical and renormalized vacuum polarization energy with the derivative expansion, cf. Eq. (6.37)

w	1.0	2.0	2.5	3.0
$g = 5.0$	–0.127	–0.024	–0.008	0.003
$g = 10.0$	–0.240	–0.041	–0.013	0.005
$g = 15.0$	–0.287	–0.048	–0.015	0.007
$g = 20.0$	–0.308	–0.050	–0.015	0.006

that our calculation is in excellent agreement with the derivative expansion at large w, where the leading terms of the derivative expansion give reliable results. This agreement is an important check on our computational method and, in particular, tests our treatment of renormalization, since the derivative expansion is renormalized in the conventional way. On the other hand, it is clear from Table 6.1 that the second-order derivative expansion cannot be trusted for $w \approx 1.0$, i.e., for background configurations whose extension is close to the Compton wavelength of the fermion.

(c) The Landau Pole

From these results one might conclude that a soliton takes over the role of the lightest fermion once the Yukawa coupling constant g becomes large enough. The positive contribution to the total energy from $\mathscr{E}_{\rm cl}$ in Eq. (6.35), which disfavors the soliton, decreases quickly for large g. However, for large couplings the model itself becomes ill-defined. Since the model is not asymptotically free, it has a Landau singularity in the ultraviolet, signaling new dynamics at some cutoff scale. Thus the Landau pole sets a minimum distance scale below which the model is not consistent. Solitons that are large compared to this scale are relatively insensitive to the unknown dynamics at the cutoff scale, but solitons whose size is comparable to this scale cannot be trusted. In this section we will discuss the emergence of the Landau pole and estimate its effect on the vacuum polarization energy by comparing the present results with a calculation that removes this pole. Although this removal is somewhat ad hoc, it nevertheless provides some insight into the reliability of the computations in case of large g.

Denoting the Fourier transforms of $[s(r) - 1]$ and $\boldsymbol{p}(\boldsymbol{r})$ by $h(\boldsymbol{q})$ and $\boldsymbol{p}(\boldsymbol{q})$, respectively, the contribution of the two-point function to the total energy can be written as

$$E_2 = \frac{v^2}{2} \int \frac{d^3q}{(2\pi)^2} \left\{ G_h^{-1}(-\boldsymbol{q}^{\,2}) h(\boldsymbol{q}) h(-\boldsymbol{q}) + G_p^{-1}(-\boldsymbol{q}^{\,2}) \boldsymbol{p}(\boldsymbol{q}) \cdot \boldsymbol{p}(-\boldsymbol{q}) \right\}, \tag{6.38}$$

where

$$G_h^{-1}(q^2) = \frac{v^2}{2} \Bigg\{ \left(q^2 - m_H^2\right) \left(1 + \frac{g^2}{4\pi^2}\right) + \frac{g^2}{4\pi^2} 6 \int_0^1 dx \left[m^2 - x(1-x)q^2\right] \ln \frac{m^2 - x(1-x)q^2}{m^2 - x(1-x)m_H^2} \Bigg\}, \tag{6.39}$$

$$G_p^{-1}(q^2) = \frac{v^2}{2}\Bigg\{q^2\left(1+\frac{g^2}{4\pi^2}\right) + \frac{g^2}{4\pi^2}\Bigg[6\int_0^1 dx\left[m^2 - x(1-x)q^2\right]\ln\frac{m^2 - x(1-x)q^2}{m^2 - x(1-x)m_H^2} + 2m^2\int_0^1 dx\,\ln\frac{\left(1 - x(1-x)\frac{m_H^2}{m^2}\right)^3}{\left(1 - x(1-x)\frac{q^2}{m^2}\right)^2}\Bigg]\Bigg\}, \quad (6.40)$$

which includes classical, loop, and counterterm contributions. The form factor $G_p(q^2)$ has a pole (the Landau ghost pole) at space-like $q^2 = -m_G^2$ with residue Z_G. The pole location is easily obtained numerically from the condition $G_p^{-1}(q^2 = -m_G^2) = 0$. In the vicinity of $q^2 \approx -m_G^2$ we have the expansion

$$G_p^{-1}(q^2) = \frac{1}{Z_G}\left(q^2 + m_G^2\right) + \mathcal{O}\left(q^2 + m_G^2\right)^2, \quad (6.41)$$

with

$$\frac{1}{Z_G} = \frac{\partial}{\partial q^2} G_p^{-1}(q^2)\Big|_{q^2=-m_G^2} = \frac{v^2}{2}\Bigg\{1 - \frac{g^2}{4\pi^2}\Bigg[6\int_0^1 dx x(1-x)\ln\frac{m^2 + x(1-x)m_G^2}{m^2 - x(1-x)m_H^2} - 4\int_0^1 dx\frac{x(1-x)}{m^2 + x(1-x)m_G^2}\Bigg]\Bigg\}. \quad (6.42)$$

The existence of this pole yields an unphysical negative contribution to the total energy at large spatial momenta $\boldsymbol{q}$, or equivalently for narrow background field configurations. Based on the Källén–Lehmann representation for the two-point function, the authors of Ref. [10] suggested a procedure to eliminate the Landau pole while maintaining chiral symmetry. They replace Eq. (6.38) with

$$\bar{E}_2 = \frac{v^2}{2}\int\frac{d^3q}{(2\pi)^2}\Delta_p^{-1}(-\boldsymbol{q}^2)\left\{h(\boldsymbol{q})h(-\boldsymbol{q}) + \boldsymbol{p}(\boldsymbol{q})\cdot\boldsymbol{p}(-\boldsymbol{q})\right\}, \quad (6.43)$$

where $\Delta_p(q^2) = G_p(q^2) - Z_G/(q^2 + m_G^2)$ removes the Landau pole. We can easily adopt this procedure since we have already extracted the loop and counterterm contributions from the two-point function in Eq. (6.30). That is, we replace $E_{\rm cl} + E_{\rm ct}^{(2)}$, which enters Eq. (6.36), by $\bar{E}_2 + E_{\rm cl}^{(3,4)}$, with

$$\frac{1}{m}E_{\rm cl}^{(3,4)} = \frac{\pi m_H^2}{2m^2g^2}\int_0^\infty dx x^2\left\{\left[2(s-1) + (s-1)^2 + \boldsymbol{p}^2\right]^2 - 4(s-1)^2\right\}. \quad (6.44)$$

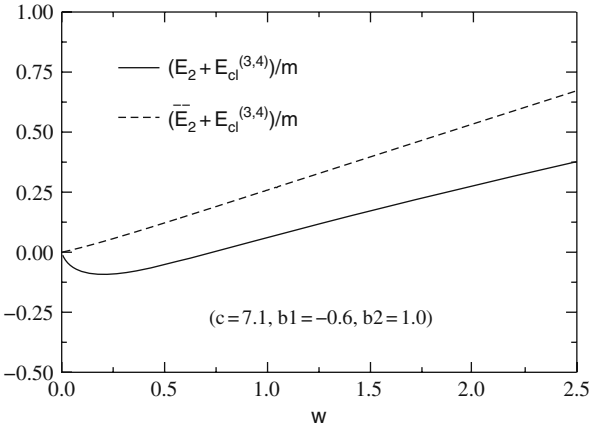

Fig. 6.3 The Landau pole subtraction, for $m_H = 0.35v$ and $g = 12$

In Fig. 6.3 we show the effect of this replacement as a function of the width parameter w for $g = 12$, which is in the region where a bound soliton can occur. For small w, we observe that the original computation, Eq. (6.38), gives a negative contribution. However, for small w there are only weakly bound states and the vacuum is almost undistorted. The relative contribution from the classical energy is also small since g is large. Hence the total energy is dominated by the renormalized Feynman diagram contribution $E^{(2)}_{\rm ct} + E^{(4)}_{\rm log,ct}$, which can be negative due to the Landau pole. Thus for small w and large g, the Landau pole dominates the binding of the soliton, and, even worse, the total energy could be negative, reflecting an unphysical vacuum instability [11]. Using the above prescription to eliminate this pole, the total energy turns out to be positive for all values of w, so the instability is removed. As can be seen from Fig. 6.3, for sensible w this prescription increases the total energy by about 0.25 m for the parameters chosen, which in turn unbinds the soliton. We conclude that the solitons found at large g are principally bound by unphysical effects associated with the Landau singularity, and not by reliable dynamical properties of the model.

(d) Scalar Backgrounds

We finish the numerical analysis with a calculation of the total energy when only a scalar background field $s(r)$ is present. Our goal is a brief comparison with the results of Ref. [7, 12], rather than a complete study. For $p \equiv 0$ the Dirac Hamiltonian is charge conjugation invariant. Hence the charge carried by the background field is zero and we must explicitly occupy the most strongly bound state. In Fig. 6.4 we show typical results of the numerical calculation for the total energy as a function of the coupling constant. A slightly bound soliton emerges even for modest values of the Yukawa

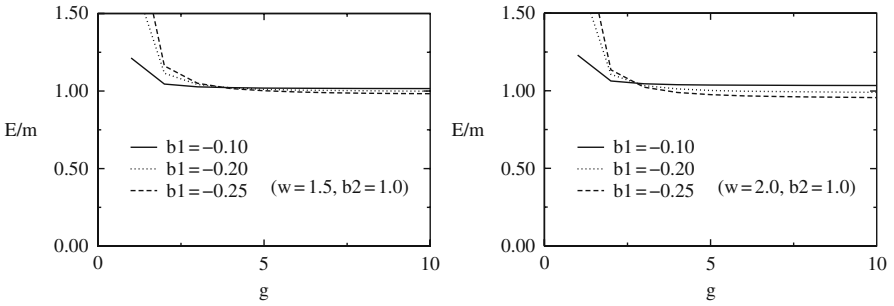

Fig. 6.4 The total energy with only the scalar background as a function of the Yukawa coupling constant g with $m_H = 0.35v$. Note that the variational parameter c is irrelevant without pseudoscalar fields

coupling. Its energy is up to 5% less than that of a fermion in the background of the translationally invariant scalar field. In this case, the Landau ghost singularity in G_p (cf. Eq. (6.40)) is irrelevant and we may trust the calculation even for small w. Furthermore, the second-order derivative expansion deviates from the full calculation by only a fraction of a percent even at moderate values of the width parameter, $w \approx 1.5$. Plotting the results from the derivative expansion would yield indistinguishable curves in Fig. 6.4. We thus confirm the findings of Ref. [7, 12], which used the derivative expansion to find a slightly bound soliton.

6.2 $SU_L(2)$ Gauge Theory

Next we extend our model to include $SU(2)$-valued gauge fields, $A_\mu = \boldsymbol{A}_\mu \cdot \frac{\boldsymbol{\tau}}{2}$. The classical Lagrangian now includes a gauge kinetic term

$$\mathcal{L}_G = -\frac{1}{2}\mathrm{tr}\left(F^{\mu\nu}F_{\mu\nu}\right), \tag{6.45}$$

which contains the field strength

$$F_{\mu\nu} = \partial_\mu A_\nu - \partial_\nu A_\mu - ig_2\left[A_\mu, A_\nu\right] \tag{6.46}$$

and thus defines the gauge coupling g_2. Furthermore, the Higgs field couples minimally to the gauge fields by extending the partial derivatives in Eqs. (6.2) and (6.10) to *covariant* ones,

$$D_\mu \Phi = \left(\partial_\mu - ig_2 A_\mu\right)\Phi, \tag{6.47}$$

while only the left-handed fermions couple to the gauge fields:

$$\mathcal{L}_F = \overline{\Psi}_L i\gamma^\mu D_\mu \Psi_L + \overline{\Psi}_R i\gamma^\mu \partial_\mu \Psi_R - g\left(\overline{\Psi}_L \Phi \Psi_R + \mathrm{h.c.}\right). \tag{6.48}$$

Ultraviolet divergences in our fermion loop calculation are compensated by counterterms

$$\mathcal{L}_H^{(\mathrm{ct})} = c_1 \mathrm{tr}\left(F^{\mu\nu}F_{\mu\nu}\right) + c_2 \mathrm{tr}\left(\left[D^\mu \Phi\right]^\dagger D_\mu \Phi\right) + c_3\left[\mathrm{tr}\left(\Phi^\dagger\Phi\right) - 2v^2\right] + c_4\left[\mathrm{tr}\left(\Phi^\dagger\Phi\right) - 2v^2\right]^2 , \tag{6.49}$$

which are formally identical to terms in the original Lagrangian. To fix the finite pieces in the coefficients c_i we impose the following renormalization conditions:

a. We choose the vacuum expectation value of $h(x)$ to vanish. Then the VEV $\langle\Phi\rangle = v\mathbb{1}$ stays fixed at its classical value and the perturbative fermion mass does not get renormalized, i.e., $m_f = m_f^{(0)} = vg$. This "no-tadpole" renormalization condition determines c_3.
b. We fix the pole of the Higgs propagator to be at the tree-level mass, $m_h = m_h^{(0)} = v\sqrt{\lambda}$, with residue one. The Higgs self-interaction strength λ is defined in Eq. (6.3). These conditions yield c_2 and c_4.
c. There are various choices to fix the remaining undetermined counterterm coefficient c_1. We choose to set the residue of the pole of the gauge field propagator to 1 in unitary gauge, implying the proper normalization of physical one-particle gauge field states. Then the position of this pole, i.e., the mass m_w of the gauge field, is a prediction,

$$m_w^2 = \left(m_w^{(0)}\right)^2\left[1 + \frac{g^2}{8\pi^2}\left\{\frac{2}{3} - \frac{m_w^2}{m_f^2}\left(\frac{1}{6} - \int_0^1 dx x^2(1-x)^2\frac{m_w^2}{\Delta(x,m_w^2)}\right) + 6\int_0^1 dx x(1-x)\ln\frac{\Delta(x,m_h^2)}{m_f^2} - \int_0^1 dx \ln\frac{\Delta(x,m_w^2)}{m_f^2}\right\}\right], \tag{6.50}$$

with $\Delta(x,q^2) \equiv m_f^2 - x(1-x)q^2$, where $m_w^{(0)} = gv/\sqrt{2}$ is the tree-level perturbative mass of the gauge fields.

Before evaluating vacuum polarization energies we discuss classical gauge field configurations inspired by the topological structure of the model, which will provide useful starting points in our variational search for quantum solitons.

6.2.1 Classical Sphalerons

There are several configurations of gauge and Higgs fields that solve the classical equations of motion. We sketch a general prescription that uses topologically non-trivial maps into the gauge group to find known solutions in the Euclidean theory and motivate the existence of new ones. The basic idea is due to Manton [13] with generalizations by Klinkhamer [14].

A finite Euclidean-action configuration is pure gauge at spacetime infinity:

$$A_\mu^{(\infty)} = \frac{i}{g} U \partial_\mu U^\dagger \qquad \text{together with} \qquad \Phi^{(\infty)} = vU\,. \tag{6.51}$$

Here U maps the spacetime boundary to $SU(2)$.

The third and fourth homotopy groups of $SU(2)$ are non-trivial:

$$\Pi_3(SU(2)) = \mathbb{Z}\,, \qquad \Pi_4(SU(2)) = \mathbb{Z}_2\,. \tag{6.52}$$

The maps from $\mathbb{S}_3$ into $SU(2)$ fall into classes labeled by an integer, and any map in a given class cannot be deformed continuously into a map from a distinct class. Similarly, each map from $\mathbb{S}_4$ into $SU(2)$ belongs either to the trivial class (which contains the trivial map) or the non-trivial class.

We take topologically non-trivial maps into $SU(2)$ and identify a subspace of the domain with the spacetime boundary. The remaining coordinates in the domain are interpolation parameters that define a sequence of configurations. The sequence becomes a loop when we restrict the configurations on the boundary of the interpolation space to be trivial, i.e.,$A_\mu = 0, \Phi = v\mathbb{1}$. The non-trivial topology prevents the loop from shrinking to a point. The top of the tightest non-contractible loop is expected to be an unstable solution, which is generically referred to as a *sphaleron*.

For example, we consider a winding number one map from $\mathbb{S}_3$ (parameterized by the angles β_1, β_2, α) to $SU(2)$:

$$\begin{aligned} U^{(1)}(\beta_1, \beta_2, \alpha) = e^{i\beta_1\tau_3} \left[\cos(\beta_1)\mathbb{1} + i\sin(\beta_1)\cos(\beta_2)\tau_3 + \right. \\ \left. i\sin(\beta_1)\sin(\beta_2)\{\cos(\alpha)\tau_1 + \sin(\alpha)\tau_2\}\right], \end{aligned} \tag{6.53}$$

where $\beta_i \in (0, \pi)$ and $\alpha \in (0, 2\pi)$. When we identify an $\mathbb{S}_2$ subspace of the domain with the space boundary, we get a sequence of maps from the space boundary to $SU(2)$:

$$U_{\beta_1}(\theta, \phi) = U^{(1)}(\beta_1, \theta, \phi)\,, \tag{6.54}$$

where θ, ϕ parameterize the spatial boundary and the remaining coordinate, β_1, is the interpolation parameter. U_{β_1} defines a sequence of asymptotic configurations (using Eq. (6.51)), which can be smoothly continued into the bulk of space for each β_1. The configurations at the end points of the sequence ($\beta_1 = 0, \pi$) are trivial because U_{β_1} is the identity at the end points. Since $U^{(1)}$ has non-zero winding number, the loop we have constructed is non-contractible. Therefore, we can extend the asymptotic configuration at $\beta_1 = \pi/2$ to the *weak sphaleron* [13, 15], the unstable, static solution at the top of the tightest loop. The sphaleron is the lowest barrier between topologically inequivalent vacua, and its energy determines the rate of fermion number violating processes at temperatures comparable to the electroweak phase transition scale.

As another example, we can identify the whole domain of the map in Eq. (6.53) with the boundary $\mathbb{S}_3 \equiv \partial\mathbb{R}^3$ of spacetime so that there are no remaining interpolation parameters. Then we have a topologically stable solution—the *weak instanton* [16]. It describes fermion number violation via tunneling. Alternatively, we may consider static configurations with one trivial dimension (say z) and identify an $\mathbb{S}_1$ subspace of the $\mathbb{S}_3$ domain with the boundary $\partial\mathbb{R}^2 \equiv \mathbb{S}_1$ of the $x-y$ plane. In this way, we get a two-parameter non-contractible loop of configurations, the top of which is the *W-string* [17, 18]. We discuss such configurations in detail in Chap. 8.

Using the above procedure for a winding number n map from $\mathbb{S}_3$ to $SU(2)$ indicates the existence of *multi-instantons*, *multi-sphalerons* [19], and *winding number n W-strings*. Finally, if we use a non-trivial map from $\mathbb{S}_4$ to $SU(2)$ to construct non-contractible loops, there is evidence for a number of novel solutions: (i) I^*, a topologically trivial Euclidean solution with one unstable direction [20]; (ii) S^*, a static solution with two unstable directions [21]; and (iii) W^*, a static solution with one trivial dimension and three unstable directions.

Note that these topological arguments do not guarantee the existence of the solutions described above, because the configuration space is a non-compact manifold and the non-contractible loops may run off to infinity. Nor is it clear that two different loops give two distinct solutions. Nevertheless, the topology points to possible solutions in the vast configuration space. Once we know where to apply the variational approach, we can verify whether a solution exists.

6.2.2 Energetically Stabilized Solitons

We advance the search of Sect. 6.1.3a for solitons stabilized by quantum dynamics (the analog of the one-dimensional solitons we found in Sect. 4.4) by extending to the $SU_L(2)$ model. Then the potential for strong binding emerges from the sphaleron-type configurations having the tendency to tightly bind fermions. We generalize to configurations that have fermion number N_f and compute the effective energy

$$E_{\text{eff}}^{(N_f)}[C] = E_{\text{cl}}[C] + E_{\text{vac}}^{\text{ren}}[C] + E_{\text{occ}}^{(N_f)}[C] \tag{6.55}$$

carried by a configuration $C = \{A, \Phi\}$. An energetically stabilized soliton exists when $E_{\text{eff}}^{(N_f)}[C] < m_f N_f$, where m_f is the mass of the perturbative fermion. The classical energy, E_{cl}, is straightforwardly computed from the action, cf. Eq. (6.61). The computation of the renormalized vacuum polarization energy, $E_{\text{vac}}^{\text{ren}}$, follows that of Sect. 6.1.2 but is more laborious since more fields are involved. For the gauge fields an additional complication arises because the anomalous fermion number violation must be accounted for when identifying the induced vacuum fermion number, N_f^{vac}. These issues are discussed thoroughly in Ref. [22]. The resulting N_f^{vac} is crucial for the

precise definition of $E_{\rm occ}^{(N_f)}$, the energy contribution from occupying fermion-bound states. Only $N_f - N_f^{\rm vac}$ levels must be filled to accommodate total fermion number N_f. To minimize $E^{(N_f)}[C]$ we fill the levels with the lowest energy eigenvalues of the single-particle Dirac Hamiltonian, extracted from Eq. (6.48).

6.2.3 The Search for the Soliton

In this section we describe our search for the soliton with the Higgs and gauge field background. Our goal is to find the configuration $C_{\rm min}$ that minimizes the effective energy, Eq. (6.55), for fixed fermion number. We first review the spherical ansatz for the gauge and Higgs fields and then outline the restrictions imposed on the variational ansätze used to search for a soliton. Finally, we explore the energy surface for two physically motivated sets of ansätze: the "twisted Higgs" and "paths over the sphaleron." Throughout this section the perturbative fermion mass is set to one so that energies and lengths are measured in units of m_f and $1/m_f$, respectively.

(a) The Spherical Ansatz

We consider static gauge and Higgs fields in the spherical ansatz. This enables us to expand the fermion S-matrix in terms of partial waves labeled by the grand spin G as explained in Sect. 6.1.2. Under these restrictions (and in the Weyl gauge $A_0 = 0$, which for smooth fields can always be obtained by a non-singular gauge transformation), the fields are expressed in terms of five real radial functions:

$$\begin{aligned} A_i(\boldsymbol{x}) &= -A^i(\boldsymbol{x}) = \frac{1}{2g}\left[a_1(r)\tau_j\hat{x}_j\hat{x}_i + \frac{\alpha(r)}{r}(\tau_i - \tau_j\hat{x}_j\hat{x}_i) + \frac{\gamma(r)}{r}\epsilon_{ijk}\hat{x}_j\tau_k\right] , \\ \Phi(\boldsymbol{x}) &= v\left[s(r) + ip(r)\tau_j\hat{x}_j\right] , \end{aligned} \tag{6.56}$$

where $\hat{\boldsymbol{x}}$ is the unit three vector in the radial direction. Let us consider the transformation properties of the ansatz under a $U(1)$ subgroup of the full $SU(2)$ gauge symmetry of the form

$$g(\boldsymbol{x}) = \mathrm{e}^{if(r)\boldsymbol{\tau}\cdot\hat{\boldsymbol{x}}/2} . \tag{6.57}$$

Then a_1 behaves as a one-dimensional vector field, $s + ip$ as a complex scalar with charge $1/2$, and $\alpha + i(\gamma - 1)$ as a complex scalar with charge 1. It is thus convenient to introduce the moduli ρ, Σ and phases θ, η for the charged scalars:

$$-i\rho e^{i\theta} \equiv \alpha + i(\gamma - 1) \quad \text{and} \quad \Sigma e^{i\eta} \equiv s + ip . \tag{6.58}$$

For the gauge transformation $g(\boldsymbol{x})$ in Eq. (6.57) to be non-singular, we require $f(0) = -2n\pi$, where n is an integer, which we denote as a superscript: $f(r) \equiv$

$f^{(n)}(r)$. If $f^{(n)}(r)$ is restricted to be 0 as $r \to \infty$ (which is equivalent to $g(r \to \infty) = \mathbb{1}$) then n is the winding of the map $g(\boldsymbol{x}) : \mathbb{S}^3 \to SU(2)$. So the topology of the zero-classical-energy configurations can also be realized within the spherical ansatz. A prototype of winding number n zero-classical-energy configuration of Eq. (6.51) is

$$\begin{aligned} &\rho(r) = 1\,, \quad \Sigma(r) = 1\,, \\ &\theta(r) = f^{(n)}(r)\,, \quad \eta(r) = \frac{f^{(n)}(r)}{2}\,, \quad a_1(r) = f^{(n)\prime}(r)\,. \end{aligned} \tag{6.59}$$

Regularity of $A_i(\boldsymbol{x})$ and $\Phi(\boldsymbol{x})$ at $\boldsymbol{x} = 0$ requires that

$$\begin{aligned} &\rho(0) = 1\,, && \rho'(0) = 0\,, \\ &\theta(0) = -2n_\theta\pi\,, && a_1(0) = \theta'(0)\,, \text{ and} \\ &\Sigma(0) = 0 \qquad \text{or} && \eta(0) = -n_\eta\pi\,. \end{aligned} \tag{6.60}$$

Here n_θ, n_η are integers and primes denote derivatives with respect to the radial coordinate. For this spherical ansatz the classical energy associated with the bosonic Lagrangian, Eqs. (6.2) with (6.47) and (6.45), reads

$$\begin{aligned} E_{\rm cl} = 4\pi \int_0^\infty dr \Bigg\{ &\frac{1}{g_2^2}\left[\rho'^2 + \rho^2(\theta' - a_1)^2 + \frac{(\rho^2-1)^2}{2r^2}\right] \\ &+\frac{1}{f^2}\Bigg[r^2\Sigma'^2 + r^2\Sigma^2(\eta' - \frac{1}{2}a_1)^2 + \frac{r^2}{4}m_h^2(\Sigma^2-1)^2 \\ &+\frac{1}{2}\Sigma^2\left((\rho-1)^2 + 4\rho^2\sin^2\frac{\theta-2\eta}{2}\right)\Bigg]\Bigg\}\,. \end{aligned} \tag{6.61}$$

Since we want the Higgs and gauge fields to have finite classical energy, we require a field configuration of the form Eq. (6.59) as $r \to \infty$. The restriction that $f^{(n)}(\infty) = 0$ uniquely specifies the boundary conditions on the fields at infinity. At $\boldsymbol{x} = 0$, the boundary conditions on ρ specified in Eq. (6.60) make the energy density finite without any additional constraints.

(b) Restrictions on the Variational Ansätze

We may consider any static, spherically symmetric configuration, C, in the Higgs gauge sector specified by the five real functions $a_1(r)$, $\rho(r)$, $\theta(r)$, $\Sigma(r)$, and $\eta(r)$. In principle, we could numerically minimize the fermionic energy, $E^{(1)}_{\rm eff}[C]$, in terms of the five functions and determine if a soliton exists. Since an exhaustive search is impractical we vary a few parameters in ansätze motivated by physical considerations. In addition to the boundary conditions we have discussed, we restrict the Higgs fields to lie within the chiral circle, $\Sigma(r) < 1$, because, as we have already mentioned, otherwise the effective potential is unbounded from below. As explained in Sect. 6.1.3, the

effective theory has a Landau pole in the ultraviolet, reflecting new dynamics at some cutoff energy scale or equivalently at a minimum distance scale. Configurations that are large compared to this distance scale are relatively insensitive to the new dynamics at the cutoff, but smaller configurations are sensitive. For small widths and large couplings, the Landau pole becomes significant and leads to unphysical negative effective energies via $E_{\rm vac}^{\rm ren}$ in Eq. (6.55) [11]. We have to be wary of this limitation when we estimate the reliability of our results.

(c) Twisted Higgs

Even without gauge fields, twisted Higgs configurations with $n = 1$ tend to strongly bind a fermion level, cf. Sect. 6.1.3. The existence of this tightly bound level makes such twisted Higgs configurations attractive candidates for the variational search also in the presence of gauge fields.

It is handy to consider one such twisted Higgs configuration with a width characterized by a variational parameter w,

$$\eta = -\pi e^{-r/w} \tag{6.62}$$

and add various perturbations to it. For instance, we consider a four-parameter ansatz (in the gauge $\theta = 0$) with parameters $p_0, \ldots, p_3$:

$$\begin{aligned} \eta &= -\pi e^{-r/w} + p_0 \frac{r/w}{1+(r/w)^2} e^{-r/w}\,, & \Sigma &= 1 + p_1 \frac{1}{1+(r/w)} e^{-r/w}\,, \\ a_1 &= p_2 \frac{r/w}{1+(r/w)^2} e^{-r/w}\,, & \rho &= 1 + p_3 \frac{(r/w)^2}{1+(r/w)^3} e^{-r/w}\,, \end{aligned} \tag{6.63}$$

where $-1 < p_1 < 0$ (to keep the Higgs field within the chiral circle and its magnitude positive) and $p_3 > -5.23$ (to keep ρ positive). For a prescribed set of theory parameters (m_w, m_h, and f) we determine the gauge coupling $g = \sqrt{2} m_w^{(0)}/v$ from the renormalization constraint Eq. (6.50). Then we vary the ansatz parameters $(w, p_0, \ldots, p_3)$ to lower the fermionic energy $E_{\rm eff}^{(1)}$. The search in Ref. [22] found that the gain in binding energy is insufficient to compensate for the increase in the effective energy from the vacuum polarization, so that $E_{\rm eff}^{(1)}$ was always found to be strictly greater than m_f. The same result was obtained in Sect. 6.1 without gauge fields, and the extra gauge degrees of freedom do not seem to help in the twisted Higgs ansatz.

As an example we consider a linear interpolation ($0 \le \xi \le 1$) from the trivial zero-classical-energy configuration to the twisted Higgs configuration in Eq. (6.62) with gauge fields set to zero,

$$\Sigma e^{i\eta} = 1 - \xi + \xi \exp\left(-i\pi e^{-r/w}\right)\,. \tag{6.64}$$

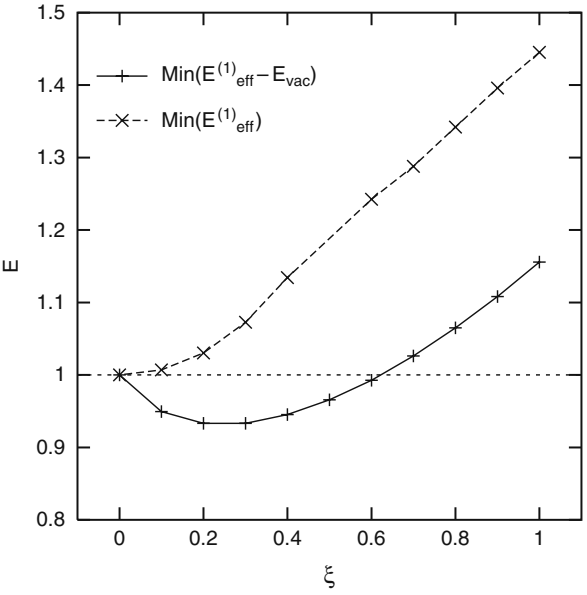

Fig. 6.5 Minimum fermionic effective energies (in units of m_f), with and without $E_{\rm vac}$ contributions, along the interpolation in Eq. (6.64). The model parameters are $f = 10$ and $m_h = v/\sqrt{2}$. Figure adopted from Ref. [22]

Figure 6.5 shows $E^{(1)}_{\rm eff}$ and $E^{(1)}_{\rm eff} - E_{\rm vac}$ as functions of ξ, optimizing the width w at a given value of ξ to minimize the energy. If $E_{\rm vac}$ is omitted, for $0 < p < 0.6$, we have configurations that have fermionic energies lower than the mass of the perturbative fermion. These configurations indicate the existence of a local minimum on the $E^{(1)}_{\rm eff} - E_{\rm vac}$ surface which would be a soliton. The $E_{\rm vac}$ contribution, however, raises the energies of the configurations to above m_f, and the would-be solitons are destabilized.

(d) Paths Over the Sphaleron

The gauge fields introduce another mechanism for strongly binding a fermion level because there is a zero mode in the background of the sphaleron [23, 24]. Let $\mathcal{C}^{(n)}$ be the class of configurations that asymptotically approach a pure gauge configuration with winding number n, cf.Eq. (6.51), so that the sphaleron is on the border between $\mathcal{C}^{(n)}$ and $\mathcal{C}^{(n+1)}$. The zero mode arises along an interpolation of the background fields from a configuration in $\mathcal{C}^{(n)}$ to a configuration in $\mathcal{C}^{(n+1)}$, because a fermion level leaves the positive continuum, crosses zero from above, and finally enters the negative continuum. The lowering of the occupation energy, $E^{(1)}_{\rm occ}$, as zero is approached from above is balanced against the increase of $E_{\rm cl} + E_{\rm vac}$, so it is crucial to determine whether the former can dominate the latter. Such interpolating configurations are also useful to find quantum corrections to the sphaleron barriers between

topologically inequivalent vacua. In addition, new barriers in the one-fermion energy surface may emerge when the perturbative fermion becomes heavier than the quantum-corrected sphaleron. These last two phenomena affect the stability of the heavy fermion and in some models may be significant for baryogenesis.

Exhaustive numerical studies were performed in Ref. [22]. The theory parameters ($g \sim 10$ and $g_2 \sim 7$) considered represent large deviations from those of the standard model in order to exaggerate the effects of heavy perturbative fermions. Still, these choices ensure that the results do not become meaningless because of the Landau pole.

In a first numerical study taken from Ref. [22], we consider a linear interpolation between winding number zero and one zero-classical-energy configurations,

$$\Phi = v(1-\xi)\mathbb{1} + \xi v U^{(1)} \quad \text{and} \quad A_j = \xi \frac{i}{g_2} U^{(1)} \partial_j U^{(1)\dagger}, \tag{6.65}$$

with $\xi = 0, \ldots, 1$. In the spherical ansatz, $U^{(1)}(\boldsymbol{x}) = g(\boldsymbol{x})$ is specified by a single function, as in Eq. (6.57), e.g.,

$$f^{(1)}(r) = -2\pi \mathrm{e}^{-r/w}, \tag{6.66}$$

where w characterizes the width of the configuration. This interpolation also varies the Chern–Simons number

$$N_{\mathrm{CS}} = -\frac{g_2^2}{8\pi^2} \epsilon_{ijk} \int d^3x \, \mathrm{tr} \left(A_i \partial_j A_k - \frac{2}{3} i g A_i A_j A_k \right), \tag{6.67}$$

so that the vacuum polarization energy can be viewed as a function thereof. Along the interpolation[2] $0 \leq N_{\mathrm{CS}} \leq 1/2$, the width is varied to minimize $E^{(1)}_{\mathrm{eff}}$, giving an upper bound on the minimum $E^{(1)}_{\mathrm{eff}}$ as a function of N_{CS}. For $N_{\mathrm{CS}} = 1/2$, it is an upper bound on the quantum-corrected sphaleron energy as well, because $E^{(1)}_{\mathrm{eff}} = E_{\mathrm{eff}}$ in the presence of a fermion zero mode (the occupation energy is then 0).

In a second study, instanton-like configurations have been explored, where the Euclidean time $\xi = x_4 \in \mathbb{R}$ acts as the interpolation parameter. They mediate between two topologically inequivalent zero-classical-energy configurations:

$$\begin{aligned} A_\mu &= h(r,\xi) \frac{i}{g_2} U_{\mathrm{inst}}(\boldsymbol{x},\xi) \partial_\mu U^\dagger_{\mathrm{inst}}(\boldsymbol{x},\xi), \\ \Phi &= v \sqrt{h(r,\xi)}\, U_{\mathrm{inst}}(\boldsymbol{x},\xi), \end{aligned} \tag{6.68}$$

where

[2] By charge conjugation this interpolation also covers the regime $1/2 \leq N_{\mathrm{CS}} \leq 1$.

$$U_{\rm inst}(\boldsymbol{x},\xi) = \frac{\xi + i\boldsymbol{\tau}\cdot\boldsymbol{x}}{\sqrt{r^2+\xi^2}}\,. \tag{6.69}$$

Here h is a function of the Euclidean spacetime radius ($\sqrt{r^2+\xi^2}$) and goes from 0 to 1 as this radius goes from 0 to ∞. A Gaußian parameterization

$$h(r,\xi) = 1 - e^{-(r^2+\xi^2)/w^2} \tag{6.70}$$

was chosen to have a well-defined scattering problem. This choice deviates from 't Hooft's electroweak instanton [25] since minimization of the classical energy is not demanded. Indeed, the configurations that minimize $E^{(1)}_{\rm eff}$ turn out to be rather different from those that minimize $E_{\rm cl}$. Since the technical computation of the Dirac spectrum requires the Weyl gauge $A_0 = 0$, a gauge transformation of the form of Eq. (6.57) with

$$f(r,\xi) = \int_{-\infty}^{\xi} d\xi' \frac{2r}{r^2+(\xi')^2} h(r,\xi') - 2\pi \tag{6.71}$$

must be applied to this parameterization.

Figure 6.6 shows the minimum effective energies in both the zero-fermion sector ($E^{(0)}_{\rm eff}$) and the one-fermion sector ($E^{(1)}_{\rm eff}$) as obtained from the parameterizations, Eqs. (6.65) and (6.66). To highlight the contribution of the fermion vacuum polarization energy, $E_{\rm vac}$, the effect of its omission is also displayed.

At $N_{\rm CS} = 0$, both $E^{(0)}_{\rm eff}$ and $E_{\rm cl}$ are minimized at the trivial zero-classical-energy configuration, Eq. (6.59) with $f^{(0)}(r) = 0$. At $N_{\rm CS} = 1/2$, $E^{(0)}_{\rm eff}$ is minimized at the quantum-corrected sphaleron while $E_{\rm cl}$ is minimized at

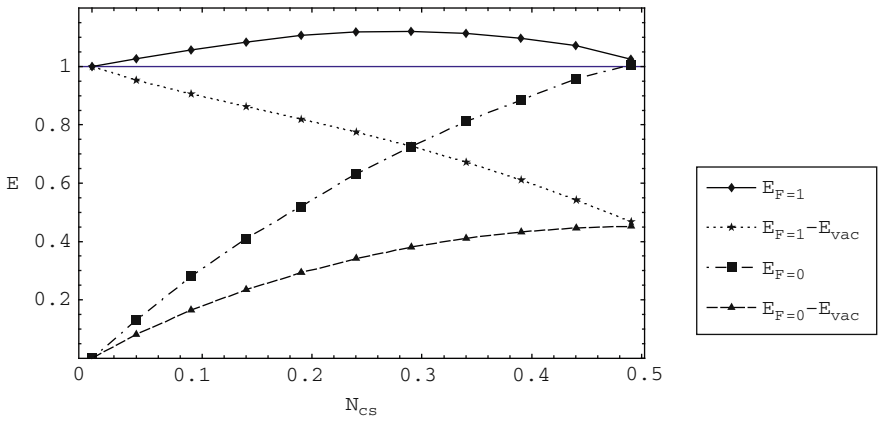

Fig. 6.6 Minimum effective energies (in units of m_f) along the linear path in Eqs. (6.65) and (6.66), in both the zero-fermion and one-fermion sectors (with and without the $E_{\rm vac}$ contributions)

the classical sphaleron. Within the variational ansatz, the parameters that minimize $E_{\rm eff}^{(0)}$ at $N_{\rm CS} = 1/2$ are different from those that minimize $E_{\rm cl}$. As a result, the fermion vacuum polarization energy correction to the sphaleron turns out to be rather large. While the classical sphaleron has an energy of $0.45 m_f$,[3] the quantum-corrected sphaleron has an energy of $1.02 m_f$.

Since the classical sphaleron has an energy much smaller than the perturbative fermion mass, one would expect that the perturbative fermion would have an unsuppressed decay mode over the sphaleron, as first pointed out by Rubakov [26]. The $E_{\rm eff}^{(1)} - E_{\rm vac}$ curve indeed displays this decay path. The fermion vacuum polarization energy modifies this picture in two crucial ways. First, the fermion quantum corrections to the sphaleron raise its energy to be roughly degenerate with the fermion, so the threshold mass is significantly increased. Second, the plot of $E_{\rm eff}^{(1)}$ shows that there is an energy barrier between the fundamental fermion and the quantum-corrected sphaleron. So, even when the fermion becomes heavier than the sphaleron, there might exist a range of masses for which the decay continues to be exponentially suppressed (since it can only proceed via tunneling).

Figure 6.7 shows the minimized effective energy in the one-fermion sector as a function of $N_{\rm CS}$ for the interpolations we have discussed and two different values of the gauge coupling g_2.

The two seemingly different interpolating configurations studied above produce very similar minimum $E_{\rm eff}^{(1)}$ curves. Furthermore, extensions of the variational ansätze did not reduce the energies by any significant amount [22]. Hence the plotted curves may be close to the true minimum $E_{\rm eff}^{(1)}$ curve. This

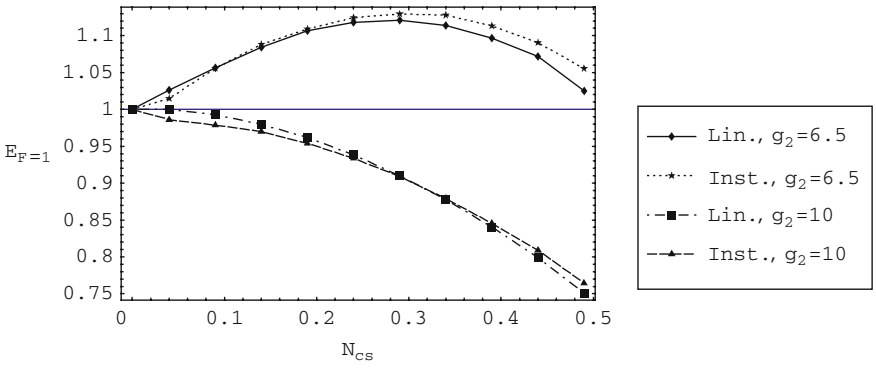

Fig. 6.7 Minimum $E_{\rm eff}^{(1)}$ (in units of m_f) for paths from a zero-classical-energy configuration to the sphaleron. Curves denoted "Lin." refer to the linear path in Eqs. (6.65) and (6.66) while those labeled "Inst." are associated with the instanton path, Eqs. (6.68), (6.69), and (6.70)

[3] The small deviation from the (exact) numerical estimate of $0.42 m_f$ [15] for the same theory parameters arises from the restricted variational space.

is the justification for considering only the linear interpolation in Fig. 6.6 and taking the evidence for the emergence of a new barrier and the significant energy change of the sphaleron seriously.

As the gauge coupling increases, the energy of the quantum-corrected sphaleron is decreased and the barrier between the fundamental fermion and the sphaleron does not persist indefinitely. As shown in Ref. [22], for $g_2 = 10$, when m_f is approximately 1.3 times the quantum-corrected sphaleron, there is no barrier and the decay mode is unsuppressed.

Just as in the case of the twisted Higgs variational ansatz, no configuration was found for which the associated fermion energy was lower than the sum of the perturbative fermion and the quantum-corrected sphaleron. Thus, no evidence could be found for the existence of fermionic solitons in the low-energy spectrum of the standard model.

6.2.4 Beyond the Spherical Ansatz

In hindsight it is not too surprising that no quantum soliton appears within the spherical ansatz. As mentioned in Sect. 6.2.2, the existence of such solitons would maintain anomaly cancellation when fermions are decoupled. Without the hypercharge gauge field, the only anomaly is Witten's global anomaly [27] due to topologically non-trivial maps $\mathbb{S}_4 \mapsto SU(2)$. However, in the spherical ansatz, the theory reduces to a $U(1)$ theory in which $\Pi_3(SU(2))$ persists as $\Pi_1(U(1))$ but there is no remnant of $\Pi_4(SU(2))$. So the quantum soliton that could resolve the decoupling puzzle probably lies outside this ansatz.

One route beyond the spherical ansatz is the use of non-trivial $\Pi_4(SU(2))$ mappings to construct non-contractible loops and corresponding classical sphalerons, cf. Sect. 6.2.1. Because the sphaleron backgrounds have exact fermion zero modes, neighboring configurations along these paths will have tightly bound fermion levels. Moreover, since the non-trivial topology that gives rise to Witten's anomaly is built into the construction of such configurations, they are promising candidates for objects that maintain anomaly cancellation in the decoupled theory. As shown in Ref. [28], electroweak string solutions are closely related to non-perturbative anomalies and thus represent particularly attractive possibilities for this approach. In this scenario, a classically unstable electroweak string could be stabilized quantum mechanically by carrying fermion number. We will investigate these configurations more thoroughly in Chap. 8.

References

1. E. D'Hoker and E. Farhi, *Phys. Lett.* **B134** (1984) 86. 103
2. E. Farhi, N. Graham, R. L. Jaffe, and H. Weigel, *Phys. Lett.* **B475** (2000) 335. 104
3. W. Pauli, *Meson Theory of Nuclear Forces.* Interscience Publishes, Inc., New York, 1946. 105

4. E. Farhi, N. Graham, R. L. Jaffe, and H. Weigel, *Nucl. Phys.* **B630** (2002) 241. 108, 109, 112
5. J. Baacke, *Z. Phys.* **C53** (1992) 402. 108
6. J. Baacke and A. Surig, *Z. Phys.* **C73** (1997) 369. 108
7. J. A. Bagger and S. G. Naculich, *Phys. Rev.* **D45** (1992) 1395. 112, 115, 116
8. I. J. R. Aitchison and C. M. Fraser, *Phys. Lett.* **B146** (1984) 63. 112
9. I. J. R. Aitchison and C. M. Fraser, *Phys. Rev.* **D31** (1985) 2605. 112
10. J. Hartmann, F. Beck, and W. Bentz, *Phys. Rev.* **C50** (1994) 30883. 114
11. G. Ripka and S. Kahana, *Phys. Rev.* **D36** (1987) 1233. 115, 122
12. J. A. Bagger and S. G. Naculich, *Phys. Rev. Lett.* **67** (1991) 2252. 115, 116
13. N. S. Manton, *Phys. Rev.* **D28** (1983) 2019. 117, 118
14. F. R. Klinkhamer and C. Rupp, *J. Math. Phys.* **44** (2003) 3619. 117
15. F. R. Klinkhamer and N. S. Manton, *Phys. Rev.* **D30** (1984) 2212. 118, 126
16. A. A. Belavin, A. M. Polyakov, A. S. Shvarts, and Y. S. Tyupkin, *Phys. Lett.* **B59** (1975) 85. 119
17. T. Vachaspati, *Phys. Rev Lett.* **68** (1992) 1977. [Erratum-ibid. 69, 216 (1992)]. 119
18. F. R. Klinkhamer and P. Olesen, *Nucl. Phys.* **B422** (1994) 227. 119
19. B. Kleihaus and J. Kunz, *Phys. Lett.* **B329** (1994) 61. 119
20. F. R. Klinkhamer and J. Weller, *Nucl. Phys.* **B481** (1996) 403. 119
21. F. R. Klinkhamer, *Phys. Lett.* **B246** (1990) 131. 119
22. E. Farhi, N. Graham, R. L. Jaffe, V. Khemani, and H. Weigel, *Nucl. Phys.* **B665** (2003) 623. 119, 122, 123, 124, 126, 127
23. J. Boguta and J. Kunz, *Phys. Lett.* **B154** (1985) 407. 123
24. A. Ringwald, *Phys. Lett.* **B213** (1988) 61. 123
25. G. 't Hooft, *Phys. Rev.* **D14** (1976) 3432. 125
26. V. A. Rubakov, *Nucl. Phys.* **B256** (1985) 509. 126
27. E. Witten, *Phys. Lett.* **B117** (1982) 324. 127
28. F. R. Klinkhamer and C. Rupp, *Nucl. Phys.* **B495** (1997) 172. 127

7 Boundary Conditions and Casimir Forces

As an important application of the spectral method we study the *Casimir effect*. The Casimir effect and the corresponding force were originally discovered in 1947 by Casimir and Polder in their study of the relativistic van der Waals force between neutral atoms [1]. In the same year, Casimir showed that the tiny force between grounded conducting plates could be understood as a modification of the vacuum fluctuations of the electromagnetic field due to conducting boundary conditions on the plates [2]. There has been renewed interest in the Casimir force from applied physics because of its importance at nanometer scales and, in particular, in micro-mechanical devices. For a comprehensive overview, see Ref. [3].

Modeling conductors with boundary conditions is a mathematical idealization that does not always capture the underlying physics. This idealization emerges as the strong coupling limit of the physical interactions between the quantum field and material bodies. It is only appropriate in a situation where the important interactions between the material and the vacuum fluctuations are well approximated by the strong coupling limit. For the electromagnetic Casimir interaction between rigid bodies those modes are the photons with wavelengths comparable to the distance between the bodies [4]. Then the boundary condition approach predicts [2]

$$F = -\frac{\hbar c \pi^2}{240(2a)^4} \tag{7.1}$$

for the Casimir force per unit area between two parallel conducting plates that are separated by $2a$. This prediction has by now been verified experimentally with precision of about 1% [5–7]. Though the photon–material interaction is governed by QED, its coupling constant, the elementary charge e, does not appear in Eq. (7.1) because this equation represents the limit $e \to \infty$. If e were zero, the force would be zero as well. Since no real material can constrain modes of the quantum field with wavelengths much smaller than the typical length scale of the inter-atomic interactions there is thus a natural cutoff above which the interactions become negligible. A good example is the plasma frequency in a realistic metal [8, 9].

There is another obstacle. Since the idealized boundary conditions constrain the fluctuation modes of any wavelength, they affect the high-energy

Graham, N., et al.: *Boundary Conditions and Casimir Forces*. Lect. Notes Phys. **777**, 129–142 (2009)
DOI 10.1007/978-3-642-00139-0_7

modes from quantum loops. As we argued in Chaps. 2 and 3, the latter must be regularized and renormalized. As a result, in the boundary condition approach the handling of divergences may significantly affect the result. Using ad hoc surface counterterms [10] or special computational methods [11, 12] to discard infinities may suppress a physical cutoff dependence, not a mere calculation artifact; it can even lead to inconsistent and contradictory results, as we will discuss in Sect. 7.2.

We will see that the interaction of the high-energy modes with the boundary induces additional divergences that cannot be fully removed by the standard counterterms of quantum field theory [13]. This result can be most elegantly deduced by formulating the Casimir problem so that the fluctuating quantum field interacts with a smooth background field, which in a certain singular limit induces the boundary conditions [14, 15]. This procedure corresponds to the strong coupling limit mentioned above. Before taking this limit, only physically unobservable divergences occur, which are absorbed in the model parameters in a controlled manner through renormalization. When the singular limit is approached, any remaining divergence indicates that the physical answer will depend on the details of the material interactions.

In this chapter, we will employ the spectral method to discuss the simplest case, viz. a scalar background field that implements Dirichlet boundary conditions for a neutral spinless boson field in the singular boundary condition limit. We will study both the renormalized total energy and the energy density in various space dimensions. In the boundary condition limit the Casimir energy density is finite, but it diverges as the boundary is approached. This divergence is so severe that its spatial integral, i.e.,the total energy, ceases to exist. Fortunately, that is not the end of the story, because in most cases we are not interested in the total energy. Rather we would like to know the change in energy when we move objects relative to each other, which determines the forces that objects exert on each other. These forces stay finite as long as we do not modify the shape of the objects. Both the force between rigid bodies and the energy density away from the boundary surfaces fall into this class, which explains why Eq. (7.1) is a trustworthy result. By contrast, observables such as the *Casimir stress* on a single surface, which is the response to an infinitesimal change of the surface geometry, cannot be described in an idealized manner by boundary conditions. They will depend in detail on the physics of the surface material and its interaction with the quantum field.

These findings agree with the work of Candelas and Deutsch [16]. They point out that the vacuum polarization energy density diverges as one approaches a boundary, and further conclude that the divergences are not the ones that can be canceled by standard counterterms. The famous special cases where the divergences happen to cancel—the conformal scalar field near a

planar boundary [17] and the electromagnetic field near a sphere [18]—are indeed exceptional. These cancellations fail and the Casimir energy diverges when the same calculation is repeated with a tiny shape imperfection in the boundary. This result clearly casts doubts on the traditional way of performing these calculations. Similar subtleties were addressed in the context of dispersive media in Ref. [19].

The results derived in this chapter refer to the simple case of Dirichlet boundary conditions for a spinless boson field, but it is expected that they generalize to more realistic situations. The electromagnetic interaction with conducting boundary conditions are, of course, physically more interesting, since they are directly related to experiment and nano-technology applications. Spectral techniques for the calculation of electromagnetic Casimir forces have been developed recently [20, 21].

7.1 Dirichlet Conditions from Quantum Field Theory

We consider a renormalizable interaction of the fluctuation field ϕ with a static scalar background field $\sigma(\boldsymbol{x})$,

$$\mathscr{L} = \frac{1}{2}\partial_\mu\phi\,\partial^\mu\phi - \frac{m^2}{2}\phi^2 - \frac{\lambda}{2}\phi^2\,\sigma(\boldsymbol{x}) + \mathscr{L}_{\rm ct}[\sigma]\,. \tag{7.2}$$

Dirichlet boundary conditions are implemented by a twofold limiting scenario: (i) the sharp limit in which the spatial extension Δ of $\sigma(\boldsymbol{x})$ approaches zero and (ii) the strong limit in which the coupling λ tends to infinity. The sharp limit, $\Delta \to 0$, indicates that $\sigma(\boldsymbol{x})$ becomes a surface δ-function with support on the given surface $\mathscr{S}$. This surface characterizes the body for which we want to compute the Casimir energy. However, this sharp limit is not sufficient to enforce the Dirichlet boundary condition on $\mathscr{S}$ for all quantum modes ϕ until we combine it with the strong limit, $\lambda \to \infty$. Both parameters Δ and λ represent physical cutoffs that characterize the (idealized) material with which the fluctuating field interacts. We may consider Δ as the physical thickness of the surface, while λ plays a role similar to the plasma frequency: Modes with frequency much larger than the scale set by λ are not constrained at the boundary $\mathscr{S}$.

A typical Casimir calculation thus involves a strongly peaked background and a large coupling strength. These conditions make it impossible to use the gradient expansion or perturbation theory as calculational tools without summing all orders [22, 23]. Since the spectral method does exactly that, cf.Sect. 3.5, the Casimir problem is indeed an ideal application thereof.

The basic question is whether the Casimir force exists in the boundary condition limit ($\Delta \to 0$ *and* $\lambda \to \infty$) without specifying any other feature

of $\sigma(\boldsymbol{x})$. In particular, the action for σ need not be specified except for the counterterms $\mathscr{L}_{\rm ct}$ induced by the interactions with ϕ. The renormalization conditions are independent of the particular choice of background field $\sigma(\boldsymbol{x})$ so that results for different geometries can be directly compared. For the simple model Eq. (7.2), the only counterterms required are $\mathscr{L}_{\rm ct} = c_1\sigma(\boldsymbol{x})$ for one or two spatial dimensions and $\mathscr{L}_{\rm ct} = c_1\sigma(\boldsymbol{x}) + c_2\sigma(\boldsymbol{x})^2$ for three. These two terms renormalize the tadpole and vacuum polarization graphs, respectively.

7.2 Rigid Bodies: Dirichlet Points and Parallel Plates

As a first illustrative example we consider the force between isolated Dirichlet points in one spatial dimension. As we have already discussed, the scattering problem in one space dimension differs from the general case described in Chap. 2. We write the Green's function at coincident points for imaginary momentum as

$$G(x,x,it) = \frac{g(it,x)h_+(it,x)}{tg(it,0) - g'(it,0)} + \frac{h_-(it,x)g(it,x)}{g(it,0)}. \tag{7.3}$$

This expression differs from Eq. (2.17) because (i) the boundary condition for $h_+(it,x)$ is such that the derivative of the wavefunction in Eq. (2.15) vanishes at $x = 0$, rather than the wavefunction itself, and (ii) the two channels have identical differential equations, hence $g(it,x)$ is the same for both. The corresponding Jost functions are obtained from this single function and its spatial derivative at $x = 0$,

$$F_+(it) = g(it,0) - \frac{1}{t}g'(it,0) \qquad \text{and} \qquad F_-(it) = g(it,0)\,. \tag{7.4}$$

The sharp limit is benign in one space dimension and we can directly start from the background configurations

$$\sigma_1(x) = \delta(x)\,, \qquad \sigma_2(x) = \delta(x-a) + \delta(x+a) \tag{7.5}$$

for a single Dirichlet point at $x = 0$, or two Dirichlet points separated by the distance $2a$, respectively. For the background σ_2 we find the radial functions [24]

$$\begin{aligned} g(it,x) &= \begin{cases} 1 \\ 1 + \frac{\lambda}{2t}\left[1 - e^{2t(x-a)}\right], \end{cases} \\ h_+(it,x) &= \frac{1}{2}\begin{cases} 1 + e^{-2tx} + \frac{\lambda}{2t}\left[1 + e^{-2ta} - e^{-2tx} - e^{-2t(x-a)}\right], \\ 1 + e^{-2tx} \end{cases} \\ h_-(it,x) &= \frac{1}{2t}\begin{cases} 1 - e^{-2tx} + \frac{\lambda}{2t}\left[1 - e^{-2ta} + e^{-2tx} - e^{-2t(x-a)}\right] \\ 1 - e^{-2tx} \end{cases}, \end{aligned} \tag{7.6}$$

where the upper and lower cases correspond to $x > a$ and $0 \le x < a$, respectively. The region $x < 0$ is obtained by reflection. These functions are found without difficulty by noting that for $|x| \neq a$ the Jost solution $f(it,x) = g(it,x)\,\mathrm{e}^{-tx}$ and the physical scattering solutions $\phi_\pm(it,x) = h_\pm(it,x)\,\mathrm{e}^{tx}$ solve free Schrödinger equations for complex momenta and that the δ-functions in the potential merely induce cusps at $x = \pm a$. The radial functions for the background σ_1 are easily obtained from Eq. (7.6) by setting $a = 0$ and replacing $\lambda \to \lambda/2$. Then only the symmetric channel is affected, because the antisymmetric wavefunction vanishes at the location of the δ-function.

The energy density is obtained from a momentum integral involving the resulting local spectral density[1]

$$[\rho(it,x)]_0 = \frac{\lambda}{\lambda^2 - (2t+\lambda)^2 e^{4ta}} \begin{cases} \left[2t - \lambda + (2t+\lambda)e^{4ta}\right] e^{2t(a-|x|)} \\ 2\left[(2t+\lambda)e^{2ta}\cosh(2tx) - \lambda\right] , \end{cases} \tag{7.7}$$

as in Eqs. (3.19) and (3.22). Since it vanishes exponentially at large t, it will yield a finite energy density for $|x| \neq a$. According to Eq. (3.26), we find the total energy by integrating the logarithm of the Jost functions. To this end we substitute the expressions for $g(it,0)$ into Eq. (7.4) and obtain

$$E_2(a,\lambda) = \int_m^\infty \frac{dt}{2\pi} \frac{1}{\sqrt{t^2 - m^2}} \left\{ t \ln\left[1 + \frac{\lambda}{t} + \frac{\lambda^2}{4t^2}\left(1 - e^{-4ta}\right)\right] - \lambda \right\} . \tag{7.8}$$

The last term in curly brackets is the $N = 1$ Born subtraction. Carrying out a similar calculation for a single δ-function background σ_1 yields

$$E_1(\lambda) = \int_m^\infty \frac{dt}{2\pi} \frac{t \ln\left[1 + \frac{\lambda}{2t}\right] - \frac{\lambda}{2}}{\sqrt{t^2 - m^2}} . \tag{7.9}$$

From the above equations we immediately verify that E_1 and E_2 obey the consistency conditions $\lim_{a\to\infty} E_2(a,\lambda) = 2E_1(\lambda)$ and $\lim_{a\to 0} E_2(a,\lambda) = E_1(2\lambda)$.

In the limit of large λ the total energy associated with a single δ-function approaches minus infinity as $-\lambda \ln \lambda$ [24], which cannot be canceled by any available counterterm. Thus the energy is infinite in this limit. We must conclude that the Dirichlet–Casimir energy is not well defined in the context of renormalizable quantum field theory. However, we can compute the force between two δ-functions for finite λ and subsequently take the $\lambda \to \infty$ limit,

$$F(a) = -\lim_{\lambda\to\infty} \frac{\partial E_2(a,\lambda)}{\partial(2a)} = -\int_m^\infty \frac{dt}{\pi} \frac{t^2}{\sqrt{t^2 - m^2}\,(e^{4ta} - 1)} , \tag{7.10}$$

[1] A factor $1/2$ is included here because we now define the energy density with respect to $x \in [-\infty, \infty]$ rather than $x \in [0, \infty]$ as in Eqs. (3.22) and (3.23).

which is equal to the result found using boundary conditions [3, 11]. The massless limit does not exist for the vacuum polarization energy in Eq. (7.9), even for finite λ. This is to be expected since massless scalar field theories are infrared divergent in $1+1$ dimensions [25]. However, it exists for the force, yielding the well-known result

$$\lim_{m\to 0} F(a) = -\frac{\pi}{96a^2}\,. \tag{7.11}$$

These limits support our earlier statement that Casimir forces between rigid bodies can be reliably computed in the boundary condition framework.

Let us compare these results with those from the boundary condition calculation. As already noted, away from the boundary the energy density is finite even without Born subtraction or renormalization. This comes as no surprise: Since the counterterms are local monomials in the background field $\sigma(\boldsymbol{x})$, they are generally concentrated directly on the Dirichlet surfaces and no renormalization is necessary for the density away from the surfaces. Furthermore, the strong coupling limit $\lambda \to \infty$ can also be performed, giving the same result as if we had assumed the Dirichlet boundary conditions from the start. For instance, we find from Eq. (7.7) [24], cf.Eq. (3.22)

$$\epsilon_2(x,a) = -\frac{1}{2\pi}\begin{cases} m^2\, K_0(2m(|x|-a)) & |x|>a \\ 2\displaystyle\int_m^\infty \frac{dt}{\sqrt{t^2-m^2}}\,\frac{t^2-m^2+m^2e^{2ta}\cosh(2tx)}{e^{4at}-1} & |x|<a\,. \end{cases} \tag{7.12}$$

The analogous result for a single Dirichlet point, $\epsilon_1(x) = \frac{m^2}{2\pi}K_0(2m|x|)$, is obtained from $a \to 0$. This agrees with the exact energy density obtained from Eq. (7.7) as long as $|x| \neq a$. At these points the exact density diverges even for finite λ. In a boundary condition calculation, however, we would integrate Eq. (7.12) to obtain the total energy [3, 11]

$$\tilde{E}_2(a) = -\frac{m}{2} - 2a\int_m^\infty \frac{dt}{\pi}\,\frac{\sqrt{t^2-m^2}}{e^{4at}-1}\,, \tag{7.13}$$

where the tilde indicates the omission of divergent contributions from the Dirichlet points. This omission does not cause a problem in calculating the attractive *force* between the two Dirichlet points,

$$\tilde{F}(a) \equiv -\frac{d\,\tilde{E}_2(a)}{d(2a)} = -\int_m^\infty \frac{dt}{\pi}\,\frac{t^2}{\sqrt{t^2-m^2}\;(e^{4at}-1)}\,, \tag{7.14}$$

which reduces to the standard results

$$\tilde{E}_2(a) = -\frac{\pi}{48a} \qquad \text{and} \qquad \tilde{F}(a) = -\frac{\pi}{96a^2} \tag{7.15}$$

in the massless limit. The corresponding limit for the single Dirichlet point yields $\tilde{E}_1 = 0$. While $F(a) = \tilde{F}(a)$, the energies $\tilde{E}_i$ differ from those computed

previously in the field theory framework. In particular, they do not satisfy the consistency conditions discussed after Eq. (7.9).

These inconsistencies of the boundary condition approach may seem to be a mere nuisance. This is not so: As we will see below, there are cases in which the same inconsistencies lead to false conclusions about physically measurable quantities! The field theory approach is not afflicted by such problems: For any finite coupling λ, we can compute the energy density for all positions x, including the points on the boundaries. Even after including the contributions from the counterterms, the energy density on Dirichlet boundaries may not be finite in the boundary condition limit. It is, in general, not even integrable, and this singularity is precisely the reason for the failure of the boundary condition approach. The contribution to the energy density of the Dirichlet boundaries cannot be excluded without introducing internal inconsistencies.[2]

It should finally be noted that the Jost functions for the Dirichlet points, Eq. (7.4), can also be used to compute the energy per unit area, $\mathscr{E}$, for two Dirichlet plates in three space dimensions. This is a typical application of the interface formula derived in Sect. 3.7. Here we require the energy per unit area for one non-trivial and two trivial dimensions. When evaluating the integral Eq. (3.89) for $\mathscr{E} = \mathscr{E}_{2,1}$ in the complex momentum plane, we pick up a contribution from the cut in $\sqrt{k^2 + m^2}^3$. Formally we find

$$\mathscr{E} = \frac{1}{4\pi^2} \int_m^\infty dt\, t\sqrt{t^2 - m^2} \sum_{\ell=\pm} [\nu_\ell(t)]_2 + \left[\mathscr{E}^{(2)}_{\mathrm{FD}} + \mathscr{E}_{\mathrm{ct}}\right] . \tag{7.16}$$

The sharp limit corresponds to $\nu_\pm(t) = \ln F_\pm(it) = \ln\left[1 + \lambda(1 \pm e^{-2at})/2t\right]$. In that limit Eq. (7.16) diverges even for finite couplings λ. However, the divergence is independent of the distance $2a$ between the plates. Thus the physically measurable *pressure* on the plates, $\mathscr{P}(a) = -d\mathscr{E}/d(2a)$, is finite in the sharp limit. The subsequent strong coupling limit $\lambda \to \infty$ indeed yields a finite pressure

$$\mathscr{P}(a) = -\frac{C(2ma)}{(2a)^4} \qquad \text{with} \qquad C(x) \equiv \frac{1}{2\pi^2} \int_x^\infty d\tau\, \frac{\tau^2\sqrt{\tau^2 - x^2}}{e^{2\tau} - 1} . \tag{7.17}$$

In the massless case, $m \to 0$, the standard result is recovered [3, 11, 12],

$$\mathscr{P}(a) = -\frac{\pi^2}{480\,(2a)^4}, \tag{7.18}$$

which also follows from the boundary condition calculation.

[2] Ad hoc counterterms introduced to cancel the extra divergences in the Dirichlet limit pose a different problem: The comparison of various background configurations is only reliable if the same counterterms and renormalization conditions are used for all σ. In particular, the Casimir energy will then diverge for any smooth background, since the extra ad hoc counterterms are not balanced by any infinite diagrams.

A brief side comment on this result is in order. The quartic behavior $\mathscr{P}(a) \sim a^{-4}$ for a massless quantum field is in fact generic for three space dimensions: For $m \to 0$ and all other coupling constants going to infinity in the Dirichlet limit, the final answer can only depend on a (and $\hbar = c = 1$). Simple dimensional analysis implies $\mathscr{P}(a) \sim a^{-4}$, as confirmed by Casimir's initial calculation in the electromagnetic case. Even though the prefactors in typical Casimir formulae are minuscule (in physical units) and the measured forces are in the range of $10^{-9}N$ and below, the a^{-4} behavior would eventually dominate all long-ranged (electrostatic) forces—up to distances of $a \sim 10^{-10}$m, where the atomic nature of the materials is resolved and the macroscopic picture of potential scattering is invalid. This simple dimensional analysis reveals why Casimir forces are of particular importance to devices at the nanometer scale.

7.3 The Casimir Stress on a Dirichlet Ring

For the Dirichlet points, the inconsistencies of the traditional boundary condition approach had no immediate consequences on observable quantities such as the force. For physically measurable observables that directly probe the energy density on the boundaries, however, the traditional approach leads to incorrect conclusions. A typical example is the Casimir stress on an isolated Dirichlet surface $\mathscr{S}$. It is defined as the response of the quantum field to an infinitesimal change in the geometry of $\mathscr{S}$. While the force between rigid bodies requires moving the surfaces $\mathscr{S}$ relative to each other but keeping the shape of $\mathscr{S}$ fixed, the stress compares situations in which the geometry of $\mathscr{S}$ has actually changed. The strong interactions on $\mathscr{S}$ will thus cause the stress to diverge. Of course, this divergence is not physical; it simply means that the stress will depend on the material cutoffs defining the real interactions. As a result no idealized Casimir formula can be derived for self-stresses.

This line of reasoning casts doubts on the well-known calculation of the Casimir stress on a grounded sphere [18]. While it may be true that the infinities of the energy density cancel between the inside and the outside in a principle value prescription, this cancellation must be considered accidental: Even the slightest imperfection of the sphere's geometry will cause the cancellation to fail and the stress will become cutoff dependent. Thus the boundary condition approach with the principal value prescription must be regarded as a mathematical oddity rather than a real physical description. By contrast, the field theory approach predicts a cutoff-dependent stress for all shape geometries, with no special role attributed to the perfectly round sphere.

To corroborate these statements, we consider the simple example of the Casimir stress on a Dirichlet ring in two spatial dimensions.[3] In the sharp limit the total energy is divergent when the number of spatial dimensions is larger than one, so we generalize to a Gaußian background profile of width Δ, concentrated on a ring of radius a,

$$\sigma(r) = A \exp\left(-\frac{(r-a)^2}{2\Delta^2}\right) . \tag{7.19}$$

The normalization A is chosen such that $\sigma(r) \to \delta(r-a)$ as $\Delta \to 0$. As in the case of one spatial dimension, the energy density can be studied in this sharp limit as long as $r \neq a$. The local spectral density $\rho(it, r)$, cf.Eq. (3.17), vanishes exponentially for large t, so that both the t-integral and the sum over channels in Eq. (3.22) are uniformly convergent. The subsequent strong limit $\lambda \to \infty$ can be taken under the sum and the integral, giving the same energy density $\tilde{\epsilon}(r, a)$ as the traditional calculation, where the boundary condition $\phi(a) = 0$ is assumed from the start. Again, no renormalization is necessary for the density away from the boundaries, since the counterterms are local in the background $\sigma(r)$.

The boundary condition approach adopts $\tilde{\epsilon}(r, a)$ as the full answer and omits the contributions from the ring at $r = a$. To see whether this is legitimate, we proceed along the lines of Sect. 2.2 and solve numerically for the relevant scattering functions $g_\ell(k, r)$ and $h_\ell(k, r)$ entering the Green's function for $\Delta > 0$. The only subtlety is in the s-wave channel, where a subleading logarithmic piece in the free Jost solution requires a somewhat modified boundary condition on $h_0(k, r)$, as described in Ref. [24]. Since $\sigma(r) \neq 0$ for any r, the first Born approximation must now be subtracted to ensure the convergence of the t-integral in Eq. (3.22), for all radii. The corresponding first-order diagram is local, and in the no-tadpole scheme this counterterm cancels the first-order diagram completely. This $N = 1$ Born subtraction in Eq. (3.22) suffices to give a finite energy and energy density for any fixed $\lambda < \infty$ and $\Delta > 0$.

Figure 7.1 displays the dependence of the energy density on the width Δ of the Gaußian background field for various values of r. The limit $\Delta \to 0$ is non-uniform. In particular, the energy density approaches a finite limit at any fixed r as $\Delta \to 0$, but the limiting function itself diverges as $r \to a$. Sufficiently far away from the location of the ring, say around $|r - a| \geq 3\Delta$, the energy density quickly approaches the limiting form corresponding to the result for the δ-function background. As $r \to a$, the convergence to the sharp limit gets worse, and no such limiting value exists at $r = a$. In fact, the divergence at $r = a$ is non-integrable, so that the total Casimir energy does not exist for any sharp background. Since the strong limit $\lambda \to \infty$ worsens this divergence, no idealized Casimir energy, as would be found using a boundary condition calculation, exists for a Dirichlet ring.

[3] This restriction is mainly to simplify the renormalization.

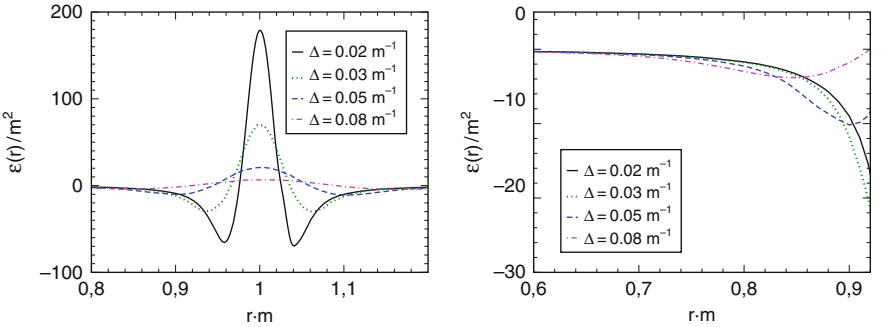

Fig. 7.1 The energy density in units of m^2 for the Gaußian ring located at $a = 1.0/\mathrm{m}$ with coupling strength $\lambda = 3.0$ m for various values of the width Δ. The left panel shows the energy density for all radii. The right panel focuses on the region where the densities can be seen to converge toward the sharp limit

This fact can also be clearly seen from Fig. 7.2, where we display the contributions, E_ℓ, from the orbital angular momentum channel ℓ to the total Casimir energy $E = \sum_\ell E_\ell$. For any finite width Δ, the E_ℓ decrease steeply enough as a function of ℓ to yield a convergent sum. However, this asymptotic regime commences at a value that increases as Δ decreases. This reflects the non-uniform behavior that for any fixed width, there always is a channel ℓ_0 large enough such that the energies E_ℓ decay as $1/\ell^2$ for $\ell \geq \ell_0$. On the other hand, for every fixed channel ℓ, we always find a width Δ small enough such that we are far from the asymptotic region. Eventually, as $\Delta \to 0$, the asymptotic region is never reached and the total energy diverges.

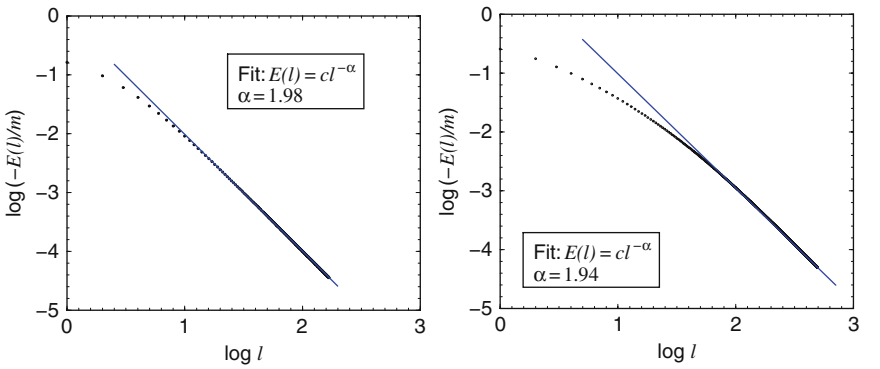

Fig. 7.2 Contributions E_ℓ to the total quantum energy of a Gaußian ring from various angular momentum channels. The left panel corresponds to the parameters $a = 1.0/\mathrm{m}$, $\Delta = 0.1/\mathrm{m}$, and $\lambda = 3\,\mathrm{m}$. The decay with ℓ is consistent with the asymptotic form $E_\ell \sim 1/\ell^2$ for all $\ell \geq 5$. In the right panel, the width is decreased to $\Delta = 0.008/\mathrm{m}$; for the asymptotic decay to be valid, we require $\ell \geq 50$

7.4 Oversubtraction and Diagrammatic Analysis

The divergence of the boundary condition limit can be studied in precise detail by the oversubtraction technique, cf.Sect. 2.4. Only a small number of low-order renormalized Feynman diagrams diverge as $\Delta \to 0$ [13]. We extract these diagrams by subtracting more Born approximations than required by renormalization. We must compensate for this oversubtraction by adding back the equivalent Feynman diagrams. That is, in Eq. (3.26) we choose N larger than required by the superficial divergence. For the Dirichlet ring in two spatial dimensions only the tadpole graph is ultraviolet divergent and $N = 1$ is the minimal number of Born subtractions. If we take $N = 2$ instead, the sharp limit $\Delta \to 0$ can be taken for the phase shift part of the calculation. The non-existence of the sharp limit must therefore be attributed solely to the $N = 2$ Feynman diagram. This reasoning generalizes: For any number of dimensions, we can take the sharp limit $\Delta \to 0$ for the phase shift part, if enough Born subtractions are applied. The non-existence of the Casimir energy as $\Delta \to 0$ must therefore be rooted in low-order Feynman diagrams.[4]

For the Dirichlet ring, the relevant $N = 2$ diagram

$$E_{\mathrm{FD}}^{(2)} \overset{\Delta\to 0}{\to} -\frac{\lambda^2 a^2}{8} \lim_{\Lambda\to\infty} \int_0^\Lambda dp\, J_0^2(ap) \arctan\frac{p}{2m} \tag{7.20}$$

diverges logarithmically. The divergence originates in the high momentum components of the Fourier transformation of $\sigma(r) \to \delta(r - a)$, i.e.,in the external rather than the loop momentum. If we included a local counterterm to cancel this divergence, this counterterm would produce infinities for any smooth background, such as the Gaußian ring with $\Delta > 0$. Therefore, the extra divergence must instead be regulated by having finite values for the material parameters Δ and λ that characterize the interaction. Because the contribution Eq. (7.20) varies with the radius a of the circle, it gives an infinite contribution to the stress dE/da. Thus, unlike the force between rigid bodies, the Casimir stress on isolated surfaces receives a contribution with a cutoff dependence that cannot be consistently removed.

We will next use the oversubtraction technique to analyze the case of three spatial dimensions more thoroughly [15]. As expected from dimensional analysis, the first *two* diagrams are ultraviolet divergent for $\Delta > 0$. Since the second-order diagram is not local, it cannot be canceled completely by the counterterm $\mathscr{L}_{\mathrm{ct}} = c_2\, \sigma(\boldsymbol{x})^2$. A conventional renormalization condition is to require that the vacuum polarization vanishes at an arbitrary renormalization scale μ. The result is

[4] The subsequent strong coupling limit, however, involves all orders in λ. For instance, the $(\lambda \ln \lambda)$ divergence of the Casimir energy for Dirichlet points cannot be attributed to any finite set of Feynman diagrams.

$$E^{(2)}[\sigma] = \frac{\lambda^2}{64\pi^2} \int \frac{d^3p}{(2\pi)^3}\, \tilde{\sigma}(\boldsymbol{p})\tilde{\sigma}(-\boldsymbol{p}) \int_0^1 dx\, \ln \frac{m^2 + x(1-x)\boldsymbol{p}^2}{m^2 + x(1-x)\mu^2}\,, \qquad (7.21)$$

where $\tilde{\sigma}(\boldsymbol{p})$ denotes the Fourier transform of the background profile. Other renormalization conditions differ only by a finite renormalization, which can be absorbed in the definition of μ. We first consider plate-type geometries:

- a single plate of thickness Δ:

$$\sigma_|(z) = \Delta^{-1}\,[\Theta(z + \Delta/2) - \Theta(z - \Delta/2)];$$

- two plates of thickness Δ, separated by a distance $2a$:

$$\sigma_\parallel(z) = \Delta^{-1}\,[\Theta(|z| - a + \Delta/2) - \Theta(|z| - a - \Delta/2)]$$

as representatives for rigid bodies and postpone the sphere geometry to the next section. The normalization is such that $\int_{-\infty}^{\infty} dz\sigma(z)$ counts the numbers of plates. Then the coupling constant λ has unit mass dimension. Alternative normalizations are, of course, possible and they may have an impact on the mass dimension and scaling of various parameters. We will return to this issue in Sect. 7.5.

Upon Fourier transforming these profiles and substituting them into Eq. (7.21), the sharp limit $\Delta \to 0$ can be studied in detail. The calculation [15] is lengthy and we will focus on the central result, which can be neatly presented in the simplified case of massless quantum fluctuations. We find the renormalized second-order diagram to be

$$E^{(2)}[\sigma_|, \sigma_\parallel] = -\frac{\lambda^2}{32\pi^2}\, \frac{\mathscr{A}}{\Delta}\, [\ln(\mu\Delta) + \gamma - 1] + \cdots, \qquad (7.22)$$

where γ is Euler's constant and the ellipsis refers to contributions that remain finite in the sharp limit. The proportionality to the area $\mathscr{A}$ of the Dirichlet surface indicates that the divergence indeed stems from the infinite energy density on the surfaces. As long as we are only interested in those forces that do not require this area to be changed—or more generally, the material bodies to be deformed—we need not be troubled by the cutoff dependence in the energy.

7.5 The Dirichlet Sphere

Similarly to the above analysis we consider a spherical shell of thickness Δ and radius R,

$$\sigma_\circ(r) = \Delta^{-1}\,\left[\Theta(r - R) - \Theta(r - R - \Delta)\right]\,. \qquad (7.23)$$

We have normalized this background $\int dr\, \sigma_\circ(r) = 1$ so that the dimensionality of the coupling constant, λ, is the same as for the plate configuration. We then find the second-order contribution

$$E^{(2)}[\sigma_\circ] = -\frac{\lambda^2 R^2}{8\pi^2}\left(\frac{1}{\Delta}\left[\ln(\mu\Delta)+\gamma-1\right]-\frac{\ln(\mu\Delta)}{R}\right)+\cdots . \tag{7.24}$$

If the surface size or geometry has to be varied, as is the case for the stress $\mathscr{P} = -\partial E[\sigma_\circ]/\partial R$, the sharp limit gives a divergent (or cutoff-dependent) result. Since $\mathscr{A}(\sigma_\circ) = 4\pi R^2$, Eqs. (7.24) and (7.22) are formally identical up to the subleading divergence proportional to $\ln(\Delta)$. This suggests a surface-type divergence for the sphere as well. However, this identification only holds for the particular normalization of the background potential. If instead we chose to normalize to the entire spatial volume, $\int d^3x\, \widetilde{\sigma}_\circ(\boldsymbol{x}) = 1$, i.e.,

$$\widetilde{\sigma}_\circ(r) = 3/(4\pi((R+\Delta)^3 - R^3))\,\left[\Theta(r-R)-\Theta(r-R-\Delta)\right], \tag{7.25}$$

the prefactor of the energy in Eq. (7.22) changes:

$$E^{(2)}[\widetilde{\sigma}_\circ] = -\frac{\widetilde{\lambda}^2}{128\pi^3 R^2}\left(\frac{1}{\Delta}\left[\ln(\mu\Delta)+\gamma-1\right]-\frac{\ln(\mu\Delta)}{R}\right)+\cdots . \tag{7.26}$$

We have introduced a modified coupling constant $\widetilde{\lambda}$ because the dimensionality of the background has changed as $\sigma_\circ \to \widetilde{\sigma}_\circ$. However, this modification does not involve the geometrical quantities R or Δ, since renormalization determines $\widetilde{\lambda}$ independently from the background. Obviously, the new second-order energy, Eq. (7.26), also gives an infinite contribution to the stress. The reader might be tempted to eliminate the R-dependence from the divergences altogether by searching a suitable normalization of $\sigma_o(r)$ and redefining $R \to R + \Delta/2$. Such a transformation is indeed possible, but it does not solve the problem: As shown in Fig. 7.3 for the case of massive

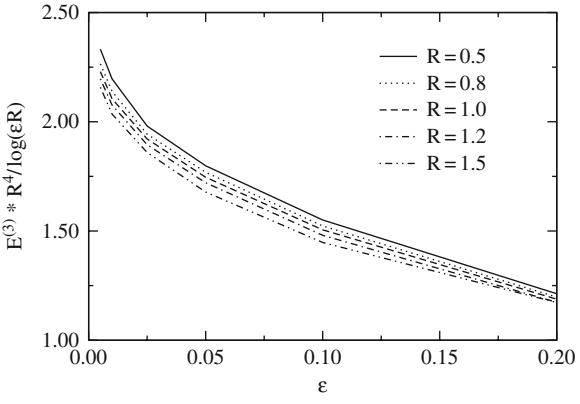

Fig. 7.3 The contribution of the third-order Feynman diagram to the energy of a spherical Dirichlet shell of radius R and thickness Δ, plotted as a function of $\epsilon = \Delta/R$. All dimensionful quantities are measured in units of the mass m of the fluctuating field. For the energy on the ordinate, a scale was chosen which highlights the R-dependence as well as the logarithmic divergence with Δ

quantum fluctuations, the third-order diagram in the sphere geometry (computed with the normalization of Eq. (7.23)) diverges as well in the sharp limit $\Delta \to 0$. The explicit formulae are somewhat involved in this case [15], but the numerical evidence from Fig. 7.3 and integral estimates for the complete formula indicate that $E^{(3)}[\sigma_\circ] \to \text{const} \cdot \ln \Delta + \cdots$. Since the third-order diagram has three insertions of $\tilde{\sigma}_\circ$, no normalization for $\sigma_\circ(r)$ can be found that eliminates the R-dependence from the infinite pieces in both the second- and third-order diagram simultaneously. The stress on a Dirichlet sphere in three spatial dimensions is thus infinite (or material cutoff dependent) in the sharp limit. The subsequent strong coupling limit $\lambda \to \infty$ will only worsen the divergence.

References

1. H. B. G. Casmir and D. Polder, *Phys. Rev.* **73** (1948) 360. 129
2. H. B. G. Casimir, *Indag. Math.* **10** (1948) 261. 129
3. M. Bordag, U. Mohideen, and V. M. Mostepanenko, *Phys. Rept.* **353** (2001) 1. 129, 134, 135
4. R. L. Jaffe, *Phys. Rev.* **D72** (2005) 021301. 129
5. S. K. Lamoreaux, *Phys. Rev. Lett.* **78** (1997) 5. 129
6. U. Mohideen and A. Roy, *Phys. Rev. Lett.* **81** (1998) 4549. 129
7. G. Bressi, G. Carugno, R. Onofrio, and G. Ruoso, *Phys. Rev. Lett.* **88** (2002) 041804. 129
8. G. Barton, *J. Phys.* **A38** (2005) 2997. 129
9. G. Barton, *J. Phys.* **A38** (2005) 3021. 129
10. K. Symanzik, *Nucl. Phys.* **B190** (1981) 1. 130
11. V. M. Mostepanenko and N. N. Trunov, *The Casimir Effect and its Applications*. Clarendon Press, Oxford, UK, 1997. 130, 134, 135
12. K. A. Milton, *The Casimir Effect: Physical Manifestations of Zero-Point Energy*. World Scientific, River Edge, USA, 2001. 130, 135
13. J. Baacke and G. Krüsemann, *Z. Phys.* **C30** (1986) 413. 130, 139
14. N. Graham et al., *Phys. Lett.* **B572** (2003) 196. 130
15. N. Graham et al., *Nucl. Phys.* **B677** (2004) 379. 130, 139, 140, 142
16. D. Deutsch and P. Candelas, *Phys. Rev.* **D20** (1979) 3063. 130
17. L. S. Brown and G. J. Maclay, *Phys. Rev.* **184** (1969) 1272. 131
18. T. H. Boyer, *Phys. Rev.* **174** (1968) 1764. 131, 136
19. G. Barton, *J. Phys.* **A34** (2001) 4083. 131
20. T. Emig, N. Graham, R. L. Jaffe, and M. Kardar, *Phys. Rev. Lett.* **99** (2007) 170403. 131
21. T. Emig, N. Graham, R. L. Jaffe, and M. Kardar, *Phys. Rev.* **D77** (2008) 025005. 131
22. G. V. Dunne, *Phys. Lett.* **B467** (1999) 238. 131
23. L.-H. Chan, *Phys. Rev.* **D55** (1997) 6223. 131
24. N. Graham et al., *Nucl. Phys.* **B645** (2002) 49. 132, 134, 137
25. S. R. Coleman, *Commun. Math. Phys.* **31** (1973) 259. 134

8 String-Type Configurations

An important class of non-trivial field configurations in gauge field theories are extended tubes of magnetic flux, also called *vortices*. In the first section of this chapter we will be concerned with the coupling of electromagnetic flux tubes to fluctuating fermions. We then extend this analysis to non-abelian gauge fields to study electroweak strings in the standard model of particle physics.

We will consider models in both $d = 2 + 1$ and $d = 3 + 1$ dimensions. In $d = 2 + 1$ the strings appear as ordinary soliton solutions to the classical equations of motion, with localized energy density in the xy-plane. The same configurations in $d = 3 + 1$ extend homogeneously along the z-direction, i.e., the region where the energy density is concentrated takes the form of a tube. Such field configurations are commonly called *cosmic strings* to distinguish them from the fundamental objects in string theory. We will use the term *strings* or *vortices*, even for objects that are ordinary solitons in $d = 2 + 1$.

8.1 Flux Tubes in Quantum Electrodynamics

We consider continuum quantum electrodynamics, an abelian gauge theory that allows for vortices carrying arbitrary magnetic flux. In such a theory the phase of the fermion wavefunction cannot be unique. A beautiful manifestation of this phase ambiguity is the Aharonov–Bohm effect [1], with important consequences for fermion scattering in general [2]. Parity anomalies [3], condensate formation [4], and exotic quantum numbers [5–7] are also closely tied to the non-perturbative vortex topology.

A reliable description of such phenomena is only possible with an accurate understanding of the quantum effects induced by the vortex background. To one-loop order, these are just the small-amplitude electron fluctuations. Proper renormalization is essential in this scenario in order to ensure that the masses, couplings, and states correspond to experimental (or conventional) values. We will apply our spectral methods to this problem, with a particular focus on the subtleties introduced by the non-trivial topology of the vortex and the reliability of the derivative expansion. We will use the interface formalism of Sect. 3.7.1 to extend from vortices in $d = 2 + 1$ dimensions to

Graham, N., et al.: *String-Type Configurations*. Lect. Notes Phys. **777**, 143–169 (2009)
DOI 10.1007/978-3-642-00139-0_8

strings in $d = 3 + 1$ dimensions, and show that these cases yield consistent and comparable results. Our calculation [8] builds on previous work including that of Refs. [9–11].

8.1.1 The Vortex Configuration

We consider a gauge field, A_μ, and a four-component[1] Dirac fermion ψ,

$$\mathscr{L} = -\frac{1}{4} F_{\mu\nu} F^{\mu\nu} + \bar{\psi} \left(i\partial\!\!\!/ + eA\!\!\!/ - m \right) \psi + \mathscr{L}_{\rm ct} \,. \tag{8.1}$$

As usual, m and e are the mass and charge of the fermion, respectively, and $F_{\mu\nu} \equiv \partial_\mu A_\nu - \partial_\nu A_\mu$. Vortices are localized, cylindrically symmetric magnetic fields (pointing in the z-direction in $d = 3 + 1$), with a net flux Φ through the xy-plane. In radiation gauge the corresponding background field reads

$$A_0 = 0 \,, \qquad \boldsymbol{A} = \frac{\Phi}{2\pi r} \, f(r) \, \boldsymbol{e}_\varphi \,, \tag{8.2}$$

where $r = \sqrt{x^2 + y^2}$ measures the planar distance from the center of the vortex and φ is the corresponding azimuthal angle. In $d = 2 + 1$ dimensions Eq. (8.2) generates a pseudoscalar magnetic field of the form

$$B(r) = \frac{\Phi}{2\pi r} \, \frac{df(r)}{dr} , \tag{8.3}$$

while $d = 3{+}1$ has the same field pointing in the z-direction,[2] $\boldsymbol{B}(r) = B(r) \, \boldsymbol{e}_z$. The profile function $f(r)$ goes to unity at large distances, and regularity at $r = 0$ requires that $f(r) = \mathcal{O}(r^2)$ near the origin. It is convenient to measure the flux in units of $2\pi/e$ and define the dimensionless quantity,

$$\mathscr{F} = \frac{e}{2\pi} \, \Phi \,. \tag{8.4}$$

For the numerical investigations we adopt a Gaußian profile of width w,

$$f(r) = 1 - e^{-r^2/w^2} \qquad \text{whence} \qquad B(r) = B(0) \, e^{-r^2/w^2} \,, \tag{8.5}$$

so that $\Phi = \pi w^2 \, B(0)$ or $\mathscr{F} = e w^2 \, B(0)/2$.

8.1.2 The Quantum Energy of the Vortex

In $d = 3{+}1$, the vortex is an interface with a trivial dimension along the vortex core. Thus the relevant quantities are the quantum energy in $d = 2 + 1$ and

[1] The $d = 2 + 1$ case describes a parity-invariant electromagnetism with two degenerate Weyl spinors of equal mass m and charge e.

[2] Notice that Φ, e, A_μ, and thus the magnetic field $B(r)$ have different mass dimensions in $d = 2 + 1$ and $d = 3 + 1$.

the quantum energy per unit length in $d = 3 + 1$. We will use the expression *quantum energy* in both cases and denote it by E. Since photons do not carry charge, their quantum fluctuations start contributing to E at two-loop order. Hence the one-loop quantum energy is the sum of a classical part and the contribution from the fermion vacuum polarization, $E = E_{\rm cl} + E_{\rm vac}$. For both $d = 2 + 1$ and $d = 3 + 1$, the classical part is given by

$$E_{\rm cl} = \frac{1}{2} \int d^2\boldsymbol{x}\, B^2(\boldsymbol{x})\,. \tag{8.6}$$

According to our master formula, Eq. (3.27), the vacuum polarization energy is written as the sum of two separately finite terms $E_{\rm vac} = E_\delta + E_{\rm FD}^{\rm ren}$, with $E_{\rm FD}^{\rm ren} = E_{\rm FD} + E_{\rm ct}$.

Due to the axial symmetry of the vortex, the fermion scattering matrix decomposes into partial waves labeled by the z-component of the total angular momentum, M. For each partial wave there are two energy eigenvalues $\pm\sqrt{k^2 + m^2}$ with two spin states for each given momentum k. So we have a total of four degenerate states for a given angular momentum. We obtain the phase shift contribution

$$E_\delta = 2 \sum_j \left(|\omega_j| - m\right) + \frac{2}{\pi} \int_0^\infty dk \frac{k}{\sqrt{k^2 + m^2}} \sum_M \left[\delta_M(k)\right]_2\,, \tag{8.7}$$

$$\begin{aligned} E_\delta = &-\frac{1}{2\pi} \sum_j \left(\omega_j^2 \ln \frac{\omega_j^2}{m^2} + m^2 - \omega_j^2 \right) \\ &-\frac{1}{\pi^2} \int_0^\infty dk\, k\, \ln \frac{k^2 + m^2}{m^2} \sum_M \left[\delta_M(k)\right]_2\,, \end{aligned}$$

for $d = 2 + 1$ and $d = 3 + 1$, respectively. Here ω_j (δ_M) refers to one representative of the bound state energies (phase shifts) from the four degenerate contributions. While we have oversubtracted the integrand for $d = 2 + 1$, finiteness of the integral requires the two indicated subtractions for $d = 3+1$.

We add back in the subtracted Born terms as Feynman diagrams. For the vortex configuration, Eq. (8.2), the required second-order piece is

$$\begin{aligned} E_{\rm FD} = &\frac{8\pi \mathscr{F}^2}{(4\pi)^{d/2}} \int_0^\infty dp \left[\int_0^\infty dr\, \frac{df(r)}{dr} J_0(pr) \right]^2 \\ &\times \int_0^1 dx\, \frac{x(1-x)\, p\, \Gamma(2 - d/2)}{[m^2 + p^2 x(1-x)]^{2-d/2}}\,, \end{aligned} \tag{8.8}$$

which is to be supplemented by the counterterm contribution

$$E_{\rm ct} = \frac{c}{2} \int d^2\boldsymbol{x}\, B^2(\boldsymbol{x})\,. \tag{8.9}$$

To fix the (potentially infinite) coefficient c, it is customary to impose the on-shell renormalization condition that the residue of the pole of the photon

propagator at $p^2 = m^2$ be unity. This condition ensures that the photon creation and annihilation operators in the Fock decomposition generate physical one-photon states. In turn it also maintains the physical electron charge. In dimensional regularization we then find

$$c_{d=3} = -\frac{e^2}{6\pi m}\,, \qquad c_{d=4-\epsilon} = -\frac{e^2}{12\pi^2}\left(\frac{2}{\epsilon} - \gamma + \ln\frac{4\pi}{m^2}\right). \tag{8.10}$$

The coefficient is *finite* in $d = 2 + 1$, reflecting that regularization is not mandatory in this case.

8.1.3 Subtleties of Configurations with Net Flux and Embedding

The non-zero magnetic flux of the vortex causes subtle complications for the fermion scattering problem. The gauge potentials only fall as $1/r$ for large radii, no matter how localized the magnetic field is. As a consequence, the phase shifts are discontinuous in the limit $k \to 0$. Although this issue does not cause problems for the momentum integral in Eq. (8.7), we can no longer determine the number of bound states from Levinson's theorem.

To understand the origin of the discontinuity, we briefly sketch the calculation of the phase shifts. Using the standard representation for the Dirac matrices, the Dirac equation in the vortex background decomposes into 2×2 blocks,

$$H\Psi = \begin{pmatrix} m & H_2 \\ H_2 & -m \end{pmatrix} \Psi = \omega\,\Psi\,. \tag{8.11}$$

Since the wavefunction has a simple dependence on the z-coordinate along the string, $\Psi \sim e^{ipz}$, the off-diagonal 2×2 block in the Hamiltonian takes the form

$$H_2 = \begin{pmatrix} p & L^\dagger \\ L & -p \end{pmatrix} \quad \text{with} \quad L = -ie^{i\varphi}\left[\partial_r + eA_\varphi(r) + \frac{i}{r}\partial_\varphi\right]. \tag{8.12}$$

Here r and φ are polar coordinates in the xy-plane. We square Eq. (8.11) and introduce two spinors η and ξ via $\Psi = (\eta, \xi)$. This disentangles the scattering channels,

$$H_2^2\eta = (\omega^2 - m^2)\eta = (k^2 + p^2)\eta \quad \text{with} \quad H_2^2 = \begin{pmatrix} p^2 + L^\dagger L & 0 \\ 0 & LL^\dagger + p^2 \end{pmatrix}, \tag{8.13}$$

and similarly for ξ. The operators $LL^\dagger$ and $L^\dagger L$ are straightforwardly diagonalized by separation in r and φ. The latter introduces the angular momentum quantum number $\ell \in \mathbb{Z}$ while the radial part of the equation of motion reads

$$e^{-i\ell\varphi}\,L^\dagger L\left[g_\ell^{(1)}(r)\mathrm{e}^{i\ell\varphi}\right] = \left\{-\partial_r^2 - \frac{1}{r}\partial_r + \frac{(\ell - h(r))^2}{r^2} - \frac{h'(r)}{r}\right\} g_\ell^{(1)}(r)$$

$$
\begin{aligned}
&= k^2\, g_\ell^{(1)}(r) \\
e^{-i(\ell+1)\varphi} L L^\dagger \left[g_\ell^{(2)}(r)\, \mathrm{e}^{i(\ell+1)\varphi} \right] &= \left\{ -\partial_r^2 - \frac{1}{r}\partial_r + \frac{(\ell+1-h(r))^2}{r^2} + \frac{h'(r)}{r} \right\} g_\ell^{(2)}(r) \\
&= k^2\, g_\ell^{(2)}(r)\,, \qquad (8.14)
\end{aligned}
$$

where $h(r) \equiv erA_\varphi(r) = \mathscr{F} f(r)$ in terms of the profile function Eq. (8.2). These equations represent standard scattering problems in two spatial dimensions with the potentials

$$
\begin{aligned}
V_1^{(\ell)}(r) &= \frac{h(r)^2}{r^2} - 2\ell\frac{h(r)}{r^2} + \frac{h'(r)}{r} \\
V_2^{(\ell)}(r) &= \frac{h(r)^2}{r^2} - 2(\ell+1)\frac{h(r)}{r^2} - \frac{h'(r)}{r}\,. \qquad (8.15)
\end{aligned}
$$

Each of the two radial functions $g_\ell^{(s)}$ can be used to construct Dirac spinors of total angular momentum $M = \ell \pm \frac{1}{2}$, corresponding to spin up or down, respectively. We can then apply standard techniques for analyzing these second-order differential equations to compute the phase shifts that enter Eq. (8.7).

It is straightforward to understand the problem at $k = 0$. For large radii $h(r) \to \mathscr{F}$, so the asymptotic form of the scattering problem (8.14) does *not* describe a free particle. Instead, the differential equation is solved by a free Bessel function with the angular momentum shifted by the flux: $\ell \to \ell - \mathscr{F}$. This is the wavefunction of an ideal or *thin* vortex along the z-axis. From the asymptotics of the Bessel functions, it is easy to extract the phase shifts of the thin vortex *exactly* [12].

We could define the Jost function and phase shift relative to the thin vortex, and simply add the known phase shift of the latter. This procedure breaks down, however, at $k = 0$, when the asymptotic form of the thin vortex solution is never reached. As a consequence, the phase shift at $k = 0$ is ill-defined. Fortunately the k-integral in the phase shift formula (8.7) still exists.[3] The problems at $k = 0$ are associated with threshold bound states and prevent us from applying Levinson's theorem [8]. Hence Eq. (8.7) can still be used provided that the bound states are carefully searched for.

The subtleties at $k = 0$ originate solely from the long-ranged nature of the potentials, Eq. (8.15). Instead of modifying the spectral method, it is more appropriate to modify the problem such that regular scattering potentials arise which fall fast enough at infinity. This can be done by the *embedding* procedure to be introduced next.

Bianchi's identity tells us that flux lines in $d = 3+1$ must either be closed or end in magnetic (Dirac) monopoles. Hence a single flux tube extending to infinity is not physical. The same conclusion can be reached in $d = 2 + 1$,

[3] See also Refs. [13–15] for a discussion of the relation between the discontinuity of the phase shifts and the anomaly in $d = 2 + 1$.

since in that case Bianchi's identity states that magnetic flux is conserved and cannot be created by a smooth deformation of the vacuum. To embed the vortex line in a physically sensible configuration, we must include a region of *return flux* such that the initial vortex closes at (compactified) infinity. Once the flux tube is embedded in a configuration with zero net flux, the potentials for the scattering problem fall fast enough at spatial infinity and the subtleties mentioned above do not emerge.

This solution comes, however, at a price: We must now ensure that the quantum energy of the return flux can be disentangled from the energy of the vortex flux tube. We have to make sure that it is well separated from the vortex core and integrates to a negligible contribution. We will numerically establish that this is indeed the case once (i) the separation between the vortex and the return flux region is much larger than the vortex extension and (ii) the return flux is diffuse. Then the quantum energy of the vortex is not affected by the embedding and there is no need to disentangle the vortex core region explicitly.

Technically, the embedding can be achieved by a modification of the profile function $f(r)$ from Eq. (8.2). We must add a piece $f_R(r)$ that ensures $f(r) + f_R(r) \to 0$ at large radii $r \geq R \gg 1/m$, while leaving the vortex core $r < w$ and a large intermediate region $w < r < R$ unchanged. For the Gaußian flux tube, Eq. (8.5), a suitable family of return profiles is

$$f_R(r) = -\frac{\arctan[\Xi(r^2/R^2 - 1)] + \arctan(\Xi)}{\frac{\pi}{2} + \arctan(\Xi)}\,, \tag{8.16}$$

where we will fix $\Xi = 16$ and vary the parameter R. A straightforward calculation demonstrates explicitly that the classical energy is unaffected by the embedding at large R: $\lim_{R\to\infty} E_{\rm cl}[f + f_R] = E_{\rm cl}[f]$. Figure 8.1 shows that this is also the case for the renormalized Feynman diagram contribution to the quantum energy, cf. Eqs. (8.8) and (8.9).

8.1.4 Numerical Results for the Quantum Energy

In this section we present the central results of numerical studies and compare our results with approximate methods such as the derivative expansion [4, 16, 17]. It approximates the fermion determinant for slowly varying background fields and becomes exact when the background field becomes spatially constant. In the present parameterization, Eq. (8.5), this implies that the width w of the flux tubes tends to infinity while the magnetic field at the origin, $B(0)$, is held fixed.

In $d = 2 + 1$, the first two orders of the (unrenormalized) expansion are

$$E_{\rm DE} = \int d^2x \left(\frac{|eB|}{4\pi}\right)^{\frac{3}{2}} \int_0^\infty \frac{ds}{\sqrt{s^3}} \exp\left(-\frac{sm^2}{|eB|}\right) \left(\coth(s) - \frac{1}{s}\right)$$

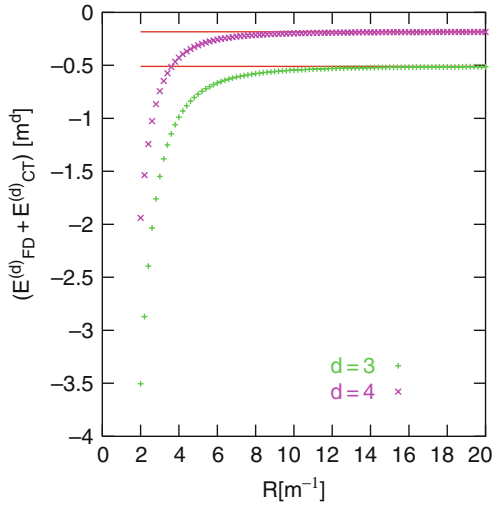

Fig. 8.1 Renormalized $d = 2{+}1$ and $d = 3{+}1$ Feynman diagram energies, Eq. (8.8), in appropriate units of m as functions of the return flux radius for $w = 1/\mathrm{m}$ and $\mathscr{F} = 4.8$. The *solid lines* correspond to the energies without the return flux

$$+\frac{1}{4}\int d^2x\,\frac{|e\boldsymbol{\partial}B|^2}{|4\pi eB|^{\frac{3}{2}}}\int_0^\infty \frac{ds}{\sqrt{s}}\exp\left(-\frac{sm^2}{|eB|}\right)\frac{d^3(s\coth s)}{ds^3}+\cdots. \quad (8.17)$$

If we take $B(x)$ as the Gaußian flux tube (8.5) and take $B(0)$ *independent* of the width w, a simple scaling argument reveals that the first term is of order $\mathcal{O}(w^2)$, the second one of order $\mathcal{O}(w^0)$, and all omitted terms contain more derivatives so that they vanish as $w \to \infty$. This hierarchy would not be present if, as in Ref. [10], the flux $\mathscr{F}$ were held fixed.

To compare our results to the derivative expansion, we must use the same (on-shell) renormalization prescription in both calculations. For $d = 2 + 1$, this requires a finite counterterm even though no ultraviolet divergence is encountered,

$$E_{\mathrm{ct}} = \frac{e^2\,B(0)^2w^2}{24m}\,. \quad (8.18)$$

This term is of order $\mathcal{O}(w^2)$ and thus affects the leading term in the expansion. In $d = 3 + 1$, the same approximation for the renormalized one-loop energy (per unit length) reads [16, 17]

$$\begin{aligned}E_{\mathrm{DE}} = &\int d^2x\frac{|eB|^2}{8\pi^2}\int_0^\infty\frac{ds}{s^{-2}}\exp\left(-\frac{sm^2}{|eB|}\right)\left(\coth(s)-\frac{1}{s}-\frac{s}{3}\right)\\ &-\int d^2x\frac{|e\boldsymbol{\partial}B|^2}{|32\pi^2eB|}\int_0^\infty ds\exp\left(-\frac{sm^2}{|eB|}\right)\\ &\times\left(1-4\coth^2 s+3\coth^4 s+\frac{3\coth s}{s}(1-\coth^2 s)\right)+\cdots. \quad (8.19)\end{aligned}$$

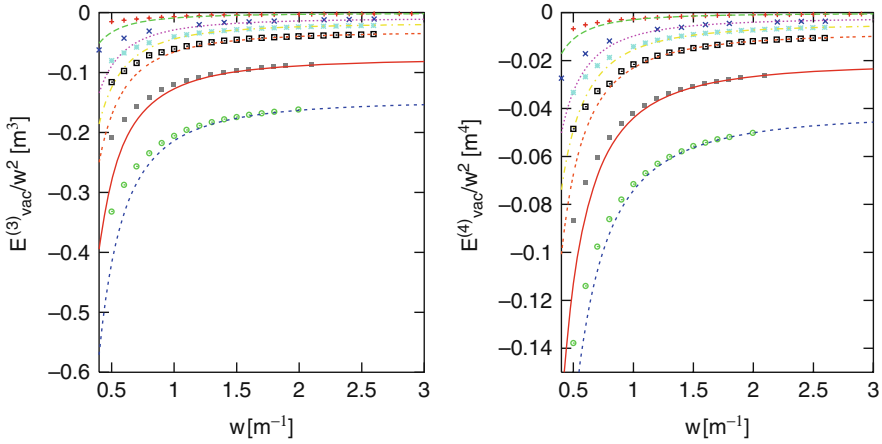

Fig. 8.2 Renormalized one-loop energies for fixed values of the magnetic field at the origin, plotted as functions of the width of the flux tube. The left panel corresponds to $d = 2 + 1$ while the right panel shows $d = 3 + 1$. The lines correspond to the prediction of the derivative expansion as explained in the main text. From top to bottom, $eB(0)/m^2 = 1.1, 2, 2.5, 3, 4, 5$

Again, when $B(0)$ is held fixed for a Gaußian profile, this expansion is strictly organized in inverse powers of the width w.

In Fig. 8.2 we compare the exact result from Eqs. (8.7)–(8.10) to the derivative approximation for different values of the fixed magnetic field $eB(0)$. The first important observation is that the vacuum polarization energies are *negative* in all cases, i.e.,the binding to the fermions tends to decrease the vortex energy. The effect is, however, much too small to produce a negative total energy—as we should expect since otherwise it would indicate an instability of the vacuum against spontaneous formation of vortices. Second, there is excellent agreement with the derivative expansion for all widths $w \geq 1/m$ and also no qualitative difference between the $d = 2 + 1$ and $d = 3 + 1$ cases. For the latter the finite renormalization in $d = 2 + 1$ is essential, since the counterterm contributes at leading order.

If, alternatively, the flux $\mathscr{F}$ rather than $B(0)$ is held fixed as w is varied, the perturbation expansion applies as $w \to \infty$. It thus suffices to consider the renormalized two-point functions,

$$E^{(2)}_{\mathrm{FD}} = \frac{\mathscr{F}^2}{30\, m^3 w^4} \times \begin{cases} 1 + \mathcal{O}(w^{-6}) & d = 2 + 1 \\ \frac{1}{\pi} + \mathcal{O}(w^{-6}) & d = 3 + 1\,. \end{cases} \tag{8.20}$$

There is an important observation for the $d = 2+1$ case where the two-point function is finite without renormalization: Without the finite renormalization, Eq. (8.10), $E^{(2)}_{\mathrm{FD}}$ would start at $\mathcal{O}(w^{-2})$ suggesting a severe difference from the $d = 3+1$ case. We see that identical renormalization conditions are mandatory

for a sensible comparison. Then the two cases appear to be very similar. Finally, the result for the two-point function and similar scaling arguments for all higher orders show that the one-loop energy of a vortex vanishes with increasing width w. This explains why the return flux does not contribute to the quantum energy in the embedding scenario.

8.1.5 Quantum Energy Density

The quantum energy *density* gives more detailed information on how the vacuum polarization energy is distributed between the vortex core and the return flux in the embedding scenario. We will observe that the respective contributions are cleanly identified and disentangled.

In Sect. 3.2.1 we have defined the radial quantum energy density to be the vacuum expectation value of the quantum energy–momentum tensor: $\epsilon(r) = 2\pi r \langle T_{00}(\boldsymbol{x})\rangle$. Figure 8.3 shows the radial quantum energy density of a Gaußian flux tube, Eq. (8.2), supplemented by a return flux as described above. The behavior is exactly as expected: There is a clear separation between the vortex core and the return flux region; furthermore, the density of the return flux becomes suppressed as the flux moves out ($R \to \infty$). Finally, the energy density in the vortex core region is completely unaffected by the embedding, once the return flux is separated by more than roughly five times the core width.

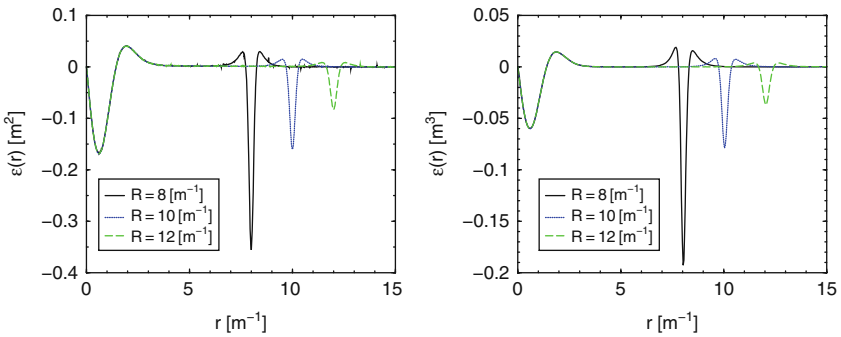

Fig. 8.3 One-loop energy densities of configurations with zero net flux, plotted as functions of the separation $R = 8, 10, 12/m$ between the vortex core and the return flux. The parameters are $eB(0) = 4m^2$ and $w = 1.5/m$. The left and right panels show $d = 2 + 1$ and $d = 3 + 1$, respectively

Figure 8.4 shows that the Feynman diagram parts dominate in both the vortex core and return flux regions. For small core widths, the phase shift piece is completely negligible, while it gives about a 30% contribution to the

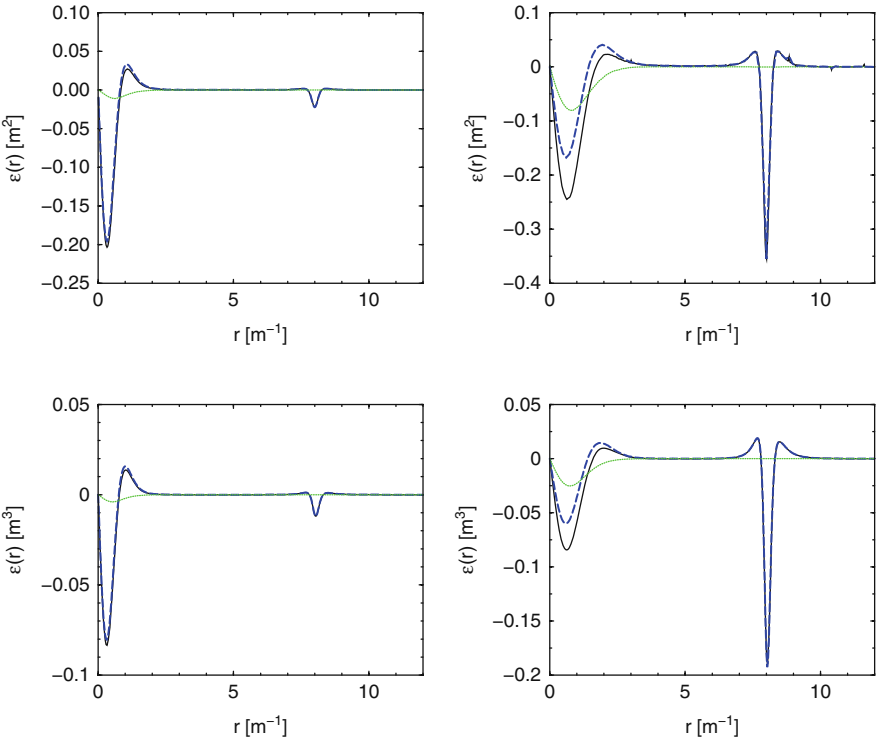

Fig. 8.4 Feynman diagram (*dashed*) and phase shift (*dotted*) contributions to the energy density for configurations with zero net flux. The sum (full) of the two contributions is the one-loop energy density. Two cases are considered, $w = 0.75/m$ (*left panel*) and $w = 1.5/m$ (*right panel*), both with $eB(0) = 4m^2$ and $R = 8/m$, for $d = 2 + 1$ (*top*) and $d = 3 + 1$ (*bottom*)

vortex density at larger widths. In the return flux region, the phase shift contribution is essentially zero. A closer look at the numerical results reveals that this result stems from a cancellation after summing over many (several hundred) angular momentum channels.

As seen in Fig. 8.4 the magnitude of the energy density increases with w in the return flux region when R and $B(0)$ are fixed. However, it has contributions of either sign and essentially integrates to zero. This result confirms our earlier statement that the return flux can be neglected.

We can obtain an expression for the derivative expansion approximation to the energy density by simply omitting the space integral in Eqs. (8.17) and (8.19), but it may differ from $\epsilon(r)$ by a total derivative. Fitting an *ansatz* for this (unknown) total derivative term allows for a fairly good agreement of the exact density and its derivative approximation in the vortex core region [8].

8.2 Flux Tubes and Strings in the Electroweak Standard Model

Since its introduction in the early 1970s, the electroweak standard model has had impressive success in the perturbative description of particle properties and processes involving the weak force. There were early attempts to explore the non-perturbative sector of the model [18], too, but the issue was not actively pursued until the mid-1980s [19, 20], when it became clear that electroweak solitons could have a profound impact on cosmological questions.

The classical equations of motions in electroweak theory admit extended string-like solitons called *Z-strings* or *electroweak strings* [18, 21, 22]. They are not topological, hence any stabilization must result from dynamical processes, which are difficult to compute. A perturbative evaluation of the fermion determinant at weak couplings suggests that the fermion fluctuations tend to destabilize the string [23]. But this need not be the final answer. Binding fermions to the string core might gain enough energy to stabilize the string at a fixed fermion number. Of course, the consistent description of such a mechanism must include the polarization of the entire Dirac spectrum by the string background.

Stable electroweak strings could have significant cosmological consequences [24–26]: A network of strings could contribute to the dark energy that is required to explain the observed cosmic acceleration [27, 28], although the understanding of the underlying dynamics is still incomplete [29–31]. Like any magnetic flux tube, the electroweak string must either be closed or end in monopole–antimonopole pairs, which would provide a primordial magnetic field [18]. Finally, at the electroweak phase transition a cluster of stable strings provides a scenario for baryogenesis, since the core of the string has copious baryon number violation due to the vanishing Higgs condensate. As pointed out in Ref. [32], the string clusters provide out-of-equilibrium regions without the need for a first-order phase transition, in contrast to the traditional bubble-nucleation approach.

There is also theoretical interest in the quantum properties of electroweak strings. Decoupling arguments [33, 34] suggest that for an $SU(2)$ fermion doublet with large Yukawa coupling (and thus large mass) soliton configurations enter the low-energy spectrum to cancel the Witten anomaly and maintain consistency of the theory. Connections between electroweak strings and non-perturbative anomalies were also demonstrated in Refs. [35, 36].

Central to these questions is an unambiguous and exact evaluation of the fermion determinant in the string background. Previous attempts in this direction have been hampered by problems with the separation of finite and divergent pieces in the quantum energy and the ensuing renormalization [37]. The spectral approach is, of course, ideally suited to handle such complications. Because of the complexity of the standard model calculation we consider a simplified model [38] in which:

1. the spacetime dimension is reduced to $d = 2 + 1$ (analogous to a translationally invariant configuration in $d = 3 + 1$ dimensions). The smaller number of dimensions simply reduces the number of Feynman diagrams to be computed;
2. the Weinberg angle θ_W is set to zero, i.e., the $U(1)$ factor in the gauge group decouples. This avoids long-ranged photon fields associated with the Aharonov–Bohm phases and the need for embedding;
3. as justified in the large-N limit, quantum corrections are taken from the fermion sector only;
4. we consider only a single heavy fermion doublet, with the CKM matrix set to the identity;
5. the masses within the fermion doublet are taken equal to enable a partial wave expansion of the quantum fluctuations.

8.2.1 The Bosonic Sector

In the bosonic (Higgs-gauge) sector the action functional reads

$$S_{HG}[\phi, W] = \int d^3x \left[-\frac{1}{2}\mathrm{tr}\,(F^{\mu\nu}F_{\mu\nu}) + (D^\mu\phi)^\dagger\, D_\mu\phi - \lambda\left(\phi^\dagger\phi - v^2\right)^2 \right], \tag{8.21}$$

where $F_{\mu\nu} = \partial_\mu W_\nu - \partial_\nu W_\mu + ig[W_\mu, W_\nu]$ is the field strength tensor associated with the $SU(2)$ gauge field

$$W_\mu = W_\mu^a\, T^a\,. \tag{8.22}$$

The $SU(2)$ generators are defined in terms of Pauli matrices: $T^a = \tau^a/2$. We also define $Z_\mu = W_\mu^3$ and $W_\mu^\pm = \frac{1}{\sqrt{2}}\left(W_\mu^1 \pm iW_\mu^2\right)$. The complex scalar Higgs field lives in the fundamental representation of $SU(2)$,

$$\phi = \begin{pmatrix} \phi_+ \\ \phi_0 \end{pmatrix}, \tag{8.23}$$

and couples *minimally* to the gauge fields via the covariant derivative

$$D_\mu\phi = (\partial_\mu + igW_\mu)\phi = \left[\partial_\mu - igQ_Z Z_\mu - ig\left(W_\mu^+ T^- + W_\mu^- T^+\right)\right]\phi\,. \tag{8.24}$$

By construction, the action, Eq. (8.21), is invariant under $SU(2)$ gauge rotations $V = \exp(i\theta^a(x)T^a)$,

$$\phi \to V\phi \qquad \text{and} \qquad ig\,W_\mu \to V\,(\partial_\mu + ig\,W_\mu)\,V^\dagger\,. \tag{8.25}$$

For positive values of the self-coupling $\lambda > 0$, the Higgs doublet acquires a vacuum expectation value (VEV), conventionally chosen as

$$\langle\phi_0\rangle = v\,, \qquad \langle\phi_+\rangle = 0\,. \tag{8.26}$$

As a consequence, the isospin symmetry breaks completely and there are three would-be Goldstone modes from the ϕ-fluctuations, which become longitudinal modes of the gauge field as it acquires the tree-level mass $M_\mathrm{W} = gv/\sqrt{2}$. The remaining Higgs excitations have tree-level mass $M_\mathrm{H} = 2v\sqrt{\lambda}$.

8.2.2 The String Solutions

We introduce radial and angular coordinates ρ and φ in the xy-plane. As $\rho \to \infty$ the field configuration must be a pure gauge,

$$\phi^{(\infty)} = V \begin{pmatrix} 0 \\ v \end{pmatrix} \qquad \text{and} \qquad g W_\mu^{(\infty)} = i\, V \partial_\mu V^{-1}\,, \tag{8.27}$$

where the $SU(2)$ rotation $V = V(\varphi)$ maps the circle S_1 at infinity onto the gauge group G. In the electromagnetic case $G = U(1)$, this map is characterized by an integral winding number, $\Pi_1(U(1)) = \mathbb{Z}$, meaning that the resulting *Nielsen–Olesen vortex* [39] is topologically stable. For the weak gauge group $G = SU(2)$, Nielsen–Olesen type of solutions can be embedded by considering maps from the spatial boundary S_1 to any $U(1)$ subgroup of $G = SU(2)$. Since $\Pi_1(SU(2)) = 0$, the embedded string configuration is not *topologically stable* against deformations in the full $SU(2)$ group.

We choose the $U(1)$ subgroup associated with the W_μ^3 gauge fields. In our model this choice is arbitrary, but it corresponds to the *Z-string* in the full electroweak model. The boundary conditions at $\rho \to \infty$ are specified by the map

$$V(\varphi) = e^{-2in\varphi\,\tau_3}\,, \tag{8.28}$$

where n must be an integer to maintain a single-valued Higgs fields. Next we insert $V(\varphi)$ in Eq. (8.27) and furnish the fields with profile functions to model the vortex core:

$$\phi_0 = v f_H(\rho)\, \mathrm{e}^{in\varphi} \qquad \text{and} \qquad \boldsymbol{W}^3 = \frac{2n}{g\rho}\, f_G(\rho)\, \boldsymbol{e}_\varphi\,, \tag{8.29}$$

with all other fields zero. The profile functions f_H and f_G must vanish near the origin to avoid singularities and approach unity at infinity to comply with Eq. (8.27). Minimizing the classical energy of the vortex leads to ordinary differential equations for f_H and f_G, which can be integrated numerically [39].

The vortex carries quantized magnetic flux $\mathscr{F}$, which we compute from the pseudoscalar magnetic field $B = \partial_1 W_2^3 - \partial_2 W_1^3$,

$$\mathscr{F} \;=\; \int d^2x\, B \;=\; \frac{4\pi n}{g}\,, \tag{8.30}$$

in $d = 2 + 1$. This flux would flow along the vortex tube in $d = 3 + 1$. The classical energy density creates a pressure that tends to spread out the flux, while the Higgs condensate is suppressed in the region of non-vanishing B, which tends to compress the flux. Balancing these two competing effects stabilizes the vortex at an equilibrium thickness.

8.2.3 The Sphaleron Square

Since any string solution can be continuously deformed into the vacuum along a path for which the energy is always finite, such a path is a good starting point for the string ansatz to be used in our variational studies.

We construct two-parameter loops of configurations with the Z-string at the top of the tightest loop [36, 40]: Let the angles $\xi_1, \xi_2 \in [0, \pi]$ and $\alpha \in [0, 2\pi]$ parameterize a three-dimensional sphere S_3 that is embedded in $\mathbb{R}^4$,

$$\hat{n}(\xi_1, \xi_2, \alpha) = \begin{pmatrix} \sin\xi_1 \sin\xi_2 \cos\alpha \\ \cos\xi_1 \\ \sin\xi_1 \cos\xi_2 \\ \sin\xi_1 \sin\xi_2 \sin\alpha \end{pmatrix} . \tag{8.31}$$

This unit vector defines a map $S_3 \mapsto SU(2)$ with unit winding number: $\mathscr{U}(\xi_1, \xi_2, \alpha) = \hat{n}_0 \mathbb{1} - i\hat{\boldsymbol{n}} \cdot \boldsymbol{\tau}$. From $\mathscr{U}$, we can construct a map with winding number n as the nth power of $\mathscr{U}$ or by scaling the azimuthal angle: $\mathscr{U} \to \mathscr{U}(\xi_1, \xi_2, n\alpha)$ [41]. If the S_1 subspace spanned by α is identified with the circle at $\rho \to \infty$, a two-parameter family of maps characterizing possible string boundary conditions (8.27) emerges,

$$V_{\xi_1\xi_2}(\varphi) = \mathscr{U}(\xi_1, \xi_2, \varphi) . \tag{8.32}$$

As before, $V_{\xi_1\xi_2}$ induces string configurations by furnishing the asymptotic form, Eq. (8.27), with appropriate profile functions,

$$\begin{aligned} \phi &= v f_H(\rho) \begin{pmatrix} -i\cos\xi_1 - \sin\xi_1 \cos\xi_2 \\ \sin\xi_1 \sin\xi_2 \, \mathrm{e}^{in\varphi} \end{pmatrix} \\ \boldsymbol{W}^3 &= \frac{2n}{g\rho} \boldsymbol{e}_\varphi f_G(\rho) \, \sin^2\xi_1 \, \sin^2\xi_2 , \\ \boldsymbol{W}^- &= \frac{\sqrt{2}n}{g\rho} \boldsymbol{e}_\varphi \, \mathrm{e}^{-in\varphi} \, f_G(\rho) \, \sin\xi_1 \, \sin\xi_2 \, (i\cos\xi_1 + \sin\xi_1 \, \cos\xi_2) . \end{aligned} \tag{8.33}$$

The choice $\xi_1 = \xi_2 = \pi/2$ yields the Nielsen–Olesen Z-string. From there we can go to any point on the boundary of the square, say $\xi_1 = 0$, and then deform $f_H(\rho)$ smoothly to unity everywhere to reach a vacuum configuration. The classical energy *density* on the sphaleron square is straightforwardly computed from the integrand in Eq. (8.21),

$$\begin{aligned} \mathscr{E}_{\mathrm{cl}} = &\left[\frac{2}{g^2} \left(\frac{f_G'}{\rho} \right)^2 + \frac{v^2}{\rho^2} f_H^2 \left(1 - f_G \right)^2 \right] n^2 \, \sin^2\xi_1 \, \sin^2\xi_2 \\ &+ v^2 \left(f_H' \right)^2 + \lambda v^4 \left(1 - f_H^2 \right)^2 . \end{aligned} \tag{8.34}$$

The classical energy of these configurations is maximal at the Z-string; we use the term "sphaleron" here to indicate that this situation is analogous to the standard sphaleron of $SU(2)$ Higgs-gauge theory [20].

As a last minor extension of the vortex ansatz, we introduce an additional radial function for the charged Higgs field:

$$\phi = \begin{pmatrix} f_H(\rho)(-i\cos\xi_1 - \sin\xi_1\cos\xi_2) + f_P(\rho) \\ f_H(\rho)\,\sin\xi_1 \sin\xi_2\, \mathrm{e}^{in\varphi} \end{pmatrix} \tag{8.35}$$

and $\boldsymbol{W}^{(i)}$ given in Eq. (8.33). The new profile function $f_P(\rho)$ is non-zero at the origin and vanishes as $\rho \to \infty$. The classical energy density, Eq. (8.34), is supplemented by

$$\Delta\mathscr{E}_{\mathrm{cl}} = v^2 \left[f_P'^2 + \frac{n^2}{\rho^2} f_P^2 f_G^2 \,\sin^2\xi_1 \right] + v^4 f_P^2 \left[f_P^2 + 2f_H^2 - 2 \right] . \tag{8.36}$$

The magnitude of the Higgs field takes the simple form $|\phi|^2 = f_H^2 + f_P^2$ along the line $\xi_2 = \pi/2$, onto which will restrict our variational search.

We will refer to the two-parameter family of configurations of Eqs. (8.33) and (8.35), as the *sphaleron square*.

8.2.4 The Fermion Action

In $d = 2+1$ the action for the degenerate isospin doublet Ψ is[4]

$$S_F[\Psi, \Phi, W_\mu] = \int d^3x \left[\bar\Psi i\gamma^\mu D_\mu P_L \Psi + \bar\Psi i\gamma^\mu \partial_\mu P_R \Psi - f\bar\Psi \left(\Phi P_R + \Phi^\dagger P_L \right) \Psi \right] , \tag{8.37}$$

where

$$P_{L,R} = \frac{1 \mp \gamma^5}{2} \qquad \text{and} \qquad \Phi = \begin{pmatrix} \phi_0^* & \phi_+ \\ -\phi_+^* & \phi_0 \end{pmatrix} . \tag{8.38}$$

As in the full electroweak theory, only left-handed fermions couple to the gauge fields via the covariant derivative D_μ in Eq. (8.24). The Higgs field VEV v induces the degenerate fermion mass $m_f = fv$.

In $d = 2+1$ the use of the standard electroweak parameters is problematic because the (dimensionful) gauge coupling constant g can no longer be expressed by the Fermi constant $G_F \approx 10^{-5} m_{\mathrm{proton}}^{-2}$ via $G_F/\sqrt{2} = g^2/M_{\mathrm{W}}^2 = 2/v^2$. To see which value of v should be chosen, consider the classical energy (or energy per unit length) in Eq. (8.34). In any number of dimension this quantity takes the form v^2 times a dimensionless function involving only ratios of masses. Thus the mass dimension stems from the prefactor v^2 only, and it is this factor which must be modified from its known $d = 3+1$ value to $d = 2+1$ by multiplication with an appropriate length scale. Since all dimensionful quantities are related to the mass m_f of the heavy fermion, we expect that the appropriate length scale is the Compton wavelength of the heavy fermion, $2\pi/m_f$. This is almost correct; the treatment of the QED flux tube in the previous section (cf. Eq. (8.20)) indicates that the proper scaling factor is in fact *half* the Compton wavelength. Thus we take

[4] As before, we use four-component Dirac spinors. Together with the two isospin degrees of freedom, the quark spinors Ψ thus have eight complex components.

$$v_{d=2+1}^2 = \frac{\pi}{m_f} v_{d=3+1}^2 = \frac{\pi}{2\sqrt{2} G_F m_f} \,. \tag{8.39}$$

The remaining parameters, i.e., the masses that determine the coupling constants f, g, and λ, are fixed by electroweak phenomenology,

$$\begin{aligned} m_f = f v_{d=3+1} = 170\,\mathrm{GeV}\,, \quad \frac{g v_{d=3+1}}{\sqrt{2}} = 80\,\mathrm{GeV}\,, \\ \text{and} \qquad 2 v_{d=3+1} \sqrt{\lambda} = 115\,\mathrm{GeV}\,. \end{aligned} \tag{8.40}$$

Here the heavy fermion doublet is identified with the top/bottom pair and m_f corresponds to the experimental top quark mass. In the numerical studies below, parameter sets with a very heavy fermion will also be investigated to study possible decoupling scenarios.

8.2.5 Fermions on Strings

It is conceivable that quantum interactions with leptons and quarks stabilize the classically unstable string. The Higgs condensate is suppressed in the vortex core so that the fermions become light (or even massless, for $\xi_1 = \pi/2$) on the string and energy can be gained by populating these bound states. If the energy gain is large enough, the string eventually becomes a stable multi-fermion object.

Let us assume that N_f fermions are trapped along the string by occupying N_f of the bound states induced by the string background. These bound states are characterized by energy eigenvalues[5] $0 \le \omega_i < m_f$. The explicit occupation of N_f-bound states then contributes

$$E_{\mathrm{occ}}^{(N_f)} = \sum_{i=1}^{N_f} \omega_i \tag{8.41}$$

to the total energy. The minimal total energy is found when the N_f most tightly bound states are occupied. In total, the energy of this configuration is

$$E_{\mathrm{eff}}^{(N_f)} = E_{\mathrm{cl}} + E_{\mathrm{occ}}^{(N_f)} + E_{\mathrm{vac}}\,. \tag{8.42}$$

For consistency of the $\hbar$-expansion we must also include the vacuum polarization energy, E_{vac}. This effective energy is to be compared with the mass of N_f perturbative fermions, so that stabilization occurs when

$$E_{\mathrm{eff}}^{(N_f)} < m_f N_f\,. \tag{8.43}$$

Within the variational search for a configuration that satisfies Eq. (8.43), certain situations are favorable:

[5] The vortex ansatz Eq. (8.35) leads to CP-invariant interactions for the fermions. Hence it suffices to consider non-negative-energy eigenvalues.

1. The perturbative fermion should be as heavy as possible. Thus we concentrate on the top quark contribution to $E_{\rm eff}^{(N_f)}$.
2. A large internal (color) degeneracy N_C enhances the quantum piece of the total energy. With such a degeneracy, the fermion number is $(N_f\, N_C)$ and the stability criterion reads

$$E_{\rm cl} + N_C \left[E_{\rm occ}^{(N_f)} + E_{\rm vac} \right] < m_f\, (N_f\, N_C) \tag{8.44}$$

with all energies on the left computed at $N_C = 1$.

8.2.6 The Vacuum Polarization Energy

As usual, the most difficult part of the calculation is the properly renormalized $E_{\rm vac}$. The main difficulty in previous attempts [37] was the extraction of divergences and the (perturbative) renormalization of a non-perturbative background. Obviously, the spectral approach is perfectly suited to address this problem. We compute $E_{\rm vac}$ as the sum of two separately finite pieces: an integral over Born-subtracted phase shifts and a set of renormalized Feynman diagrams, cf.Eq. (3.27). We discuss the latter first.

(a) Feynman Diagrams and Counterterms

We do not give explicit formulae for the renormalized Feynman diagram contribution but merely outline the computation. We obtain the one-fermion loop Feynman diagrams by expanding

$$-\,T \sum_{n=0}^{\infty} E_{\rm FD}^{(n)} = -i \ln \det \left[i\gamma^\mu \partial_\mu - m_f \mathbb{1} - U(W, \Phi) \right] , \tag{8.45}$$

in powers of the background potential $U(W, \Phi)$ with the vortex configuration, Eqs. (8.33) and (8.35), substituted for W and Φ. By gauge invariance, the Feynman diagrams with external lines representing gauge fields are finite in $d = 2 + 1$. In order to make contact with the $d = 3 + 1$ problem, however, we include all counterterms from Eq. (6.49). In the case at hand, only the coefficient c_3 diverges when the ultraviolet regulator is removed. We impose renormalization conditions similar to those in Sect. 6.2:

a. choose the *no-tadpole* condition to fix c_3. This ensures that neither the *VEV* $\langle \phi \rangle = v\,(0\,,\ 1)^T$ nor the perturbative fermion mass m_f receive radiative corrections;
b. fix the pole of the Higgs propagator to be at its tree-level mass, $M_{\rm H}$, with residue one. These conditions yield c_2 and c_4;
c. set the *residue* of the pole of the gauge field propagator to one in unitary gauge. This fixes c_1 and predicts the position of that pole, i.e., the mass of the gauge field, $M_{\rm W}$.

Having fixed these coefficients, the counterterm energy, $E_{\rm ct}$, is straightforwardly computed by substituting the vortex configuration. Denoting by $E_{\rm FD}^{(2H)}$ the Feynman diagrams that have one or two external Higgs but no gauge boson lines, the finiteness of c_1, c_2, and c_4 suggests that

$$E_{\rm FD}[W,\Phi] = E_{\rm FD}^{(2H)}[W,\Phi] + E_{\rm ct}[W,\Phi] \tag{8.46}$$

is the finite quantity that resembles the last two terms in Eq. (3.27). Unfortunately, this is not true. Since individual Feynman diagrams are not gauge invariant, the twist in the vortex Higgs field at spatial infinity yields infrared divergences in both the diagrams and the spectral calculation. However, for $d = 2 + 1$, only the c_3 counterterm involves an ultraviolet divergence and therefore any configuration with identical $\Phi^\dagger\Phi$ can be considered in the subtraction process. In particular, we may consider the *fake* configuration $\widetilde{W}$ and $\widetilde{\Phi}$ that is defined on the boundary of the sphaleron square: $\xi_1 = 0$ and $\xi_2 = \pi/2$. That is, the last two terms in Eq. (3.27) are replaced by

$$\widetilde{E}_{\rm FD}[W,\Phi] = E_{\rm FD}^{(2H)}[\widetilde{W},\widetilde{\Phi}] + E_{\rm ct}[W,\Phi]\,. \tag{8.47}$$

Explicit (but lengthy) expressions for $\widetilde{E}_{\rm FD}[W,\Phi]$ can be found in Ref. [38].

(b) Phase Shift Piece

The Born subtractions in the phase shift calculation must also be performed with $\widetilde{W}$ and $\widetilde{\Phi}$. We call $\delta_\ell(k)$ the total phase shift, which is $\frac{1}{2i}$ times the logarithm of the trace of the scattering matrix, in the channel with generalized angular momentum ℓ. This conserved quantum number emerges because for the degenerate fermion doublet the fermion scattering matrix is block-diagonal with respect to the operator

$$K = L_3 + S_3 - nT_3\gamma_5\,. \tag{8.48}$$

In the next step we compute the first two terms in the Born expansion for the phase shift for the background fields $\widetilde{W}$ and $\widetilde{\Phi}$. We denote these phase shifts by $\widetilde{\delta}_\ell^{(n)}(k)$, where the superscript $n = 1, 2$ refers to the order of the Born series. We get

$$[\delta(k)]_2 = \sum_\ell \left[\delta_\ell - \widetilde{\delta}_\ell^{(1)}(k) - \widetilde{\delta}_\ell^{(2)}(k)\right]\,, \tag{8.49}$$

which subtracts all ultraviolet divergences in $d = 2 + 1$. We compute the vacuum polarization energy from

$$E_{\rm vac} = -\tfrac{1}{2}\sum_{j=\text{b.s.}}(|\omega_j| - m_f) - \tfrac{1}{2}\int_0^\infty \frac{dk}{\pi}\,(\sqrt{k^2+m_f^2} - m_f)\frac{d}{dk}\,[\delta(k)]_2 + \widetilde{E}_{\rm FD}[W,\Phi]\,, \tag{8.50}$$

where ω_j are the bound state energies.

The final ingredients for the computation are the phase shifts in the vortex background. This calculation is similar to the QED case studied in the last chapter, but technically more challenging since it is a multi-channel scattering problem, like the hedgehog configurations discussed in Chap. 6.

The starting point is the Dirac equation in $2+1$ dimensions[6]

$$h_D \Psi_{\omega,N_\ell}(\rho,\varphi) = \omega \Psi_{\omega,N_\ell}(\rho,\varphi)\,, \tag{8.51}$$

where the single-particle Dirac operator is read off from Eq. (8.37),

$$h_D = -i\alpha^i \partial_i + \gamma^0 f\left(P_R \Phi + P_L \Phi^\dagger\right) - g\,\alpha^i \left[Z_i\, Q_Z + P_L (W_i^+ T^- + W_i^- T^+) \right]. \tag{8.52}$$

For the vortex backgrounds with winding number n the generator K, Eq. (8.48), commutes with the Hamiltonian h_D, so that its eigenvalues $N_\ell = \ell + \frac{1}{2} + \frac{n}{2}$ label the scattering channels. Furthermore α_3 anticommutes with h_D. Hence, any eigenstate Ψ of the Hamiltonian has a partner $\alpha_3 \Psi$ with the opposite sign of the energy so that the spectrum of h_D is symmetric about zero.

We turn the Dirac equation into a coupled set of ordinary differential equations for eight radial functions $y_1, \ldots, y_8$ by the parameterization

$$\Psi_{\omega,N_\ell}(\rho,\varphi) = \begin{pmatrix} y_5\, e^{i\ell\varphi}\,|\tfrac{1}{2}\rangle + y_7\, e^{i(\ell+n)\varphi}\,|-\tfrac{1}{2}\rangle \\ iy_6\, e^{i(\ell+1)\varphi}\,|\tfrac{1}{2}\rangle + iy_8\, e^{i(\ell+n+1)\varphi}\,|-\tfrac{1}{2}\rangle \\ y_1\, e^{i(\ell+n)\varphi}\,|\tfrac{1}{2}\rangle + y_3\, e^{i\ell\varphi}\,|-\tfrac{1}{2}\rangle \\ iy_2\, e^{i(\ell+n+1)\varphi}\,|\tfrac{1}{2}\rangle + iy_4\, e^{i(\ell+1)\varphi}\,|-\tfrac{1}{2}\rangle \end{pmatrix}. \tag{8.53}$$

Here the kets are eigenstates of T^3. Shooting for square integrable solutions that are regular at $\rho = 0$ yields the bound state energies ω_j. To treat the scattering problem, we eliminate the left-handed fields Ψ_L, which are the upper components $(y_5, \ldots, y_8)$ in the chiral representation. Then we are left with four complex second-order equations for the radial functions $y_1, \ldots, y_4$. For a given N_ℓ (or ℓ) we write formally (omitting the angular momentum label ℓ)

$$\sum_{j=1}^{4} \left\{ \mathscr{D}(\rho) + \mathscr{N}(\rho)\,\frac{d}{d\rho} + \mathscr{M}(\rho) \right\}_{ij} y_j(\rho) = 0\,. \tag{8.54}$$

The operator $\mathscr{D}$ is associated with a generalized centrifugal barrier,

$$\mathscr{D}(\rho) = \mathbb{1}\left(\frac{d^2}{d\rho^2} + \frac{1}{\rho}\frac{d}{d\rho} + k^2\right) - \frac{1}{\rho^2}\,\mathrm{diag}\left[(\ell+n)^2\,, (\ell+n+1)^2\,, \ell^2\,, (\ell+1)^2\right], \tag{8.55}$$

[6] For z-independent configurations in $d = 3+1$ the same equation and thus the interface formalism (Sect. 3.7) hold since we adopt four-component Dirac spinors.

where $k^2 = \omega^2 - m_f^2$. The matrices $\mathscr{N}(\rho)$ and $\mathscr{M}(\rho)$ contain the vortex background. Their explicit form is lengthy and we refrain from presenting them explicitly. At large radii $\rho \to \infty$, both $\mathscr{M}$ and $\mathscr{N}$ vanish and the four equations decouple. Notice that the free case $\mathscr{M} = \mathscr{N} = 0$ describes a non-trivial vacuum of winding number n rather than the trivial vacuum with all fields vanishing.[7] In turn, no long-range background fields emerge in the scattering problem and no embeddings or return fluxes as in the QED case are required.

In each angular momentum channel, there are four independent vector solutions $\boldsymbol{y}(\rho)$, which we combine in the *rows* of a matrix $\mathscr{Y}$, cf. Sect. 6.1.2. In analogy to Eq. (6.16), we factorize the solutions at vanishing background with outgoing spherical wave boundary conditions, $\mathscr{Y}(\rho, k) = \mathscr{F}(k, \rho) \cdot \mathscr{H}(k\rho)$, with

$$\mathscr{H}(x) = \mathrm{diag}\left[h^{(1)}_{|\ell+n|}(x)\,,\, h^{(1)}_{|\ell+n+1|}(x)\,,\, h^{(1)}_{|\ell|}(x)\,,\, h^{(1)}_{|\ell+1|}(x)\right]\,. \tag{8.56}$$

The differential equation for the *Jost matrix* $\mathscr{F}(k, \rho)$ becomes

$$\mathscr{F}'' + \frac{1}{\rho}\mathscr{F}' + 2\mathscr{F}'\mathscr{L}' + \frac{1}{\rho^2}[\mathscr{F}, \mathscr{C}] + \mathscr{N}(\mathscr{F}' + \mathscr{F}\mathscr{L}') + \mathscr{M}\mathscr{F} = 0\,, \tag{8.57}$$

where $\mathscr{L}(k\rho) \equiv \ln \mathscr{H}(k\rho)$ and primes denote derivatives with respect to the radial coordinate. The boundary conditions at $\rho \to \infty$ are obviously $\mathscr{F}(k, \rho) \to \mathbb{1}$ and $\mathscr{F}'(k, \rho) \to 0$.

The matrices $\mathscr{M}$ and $\mathscr{N}$ have complex elements. Thus the conjugated matrix $\mathscr{Y}^*$ does not solve the equations of motion. Instead, incoming waves are described by a separate set $\overline{\mathscr{Y}}$, which must be computed from Eq. (8.54) with the replacement $\mathscr{H} \to \overline{\mathscr{H}} = \mathscr{H}^*$. The scattering analysis now proceeds as in Sect. 6.1.2 with $\mathscr{Y}^*$ replaced by $\overline{\mathscr{Y}}$. The S-matrix parameterizes the full scattering solution as $\mathscr{Y}_{\mathrm{sc}}(\rho) = -\overline{\mathscr{Y}}(\rho) + \mathscr{Y}(\rho) \cdot \mathscr{S}(k)$ and the requirement that $\mathscr{Y}_{\mathrm{sc}}(\rho)$ is regular at the origin determines $\mathscr{S}$, from which the sum of the eigenphase shifts, $\delta(k)$, is extracted. The final result is $\delta(k) = \delta(k, 0)$ where [38]

$$\delta(k, \rho) \equiv \frac{1}{2i}\mathrm{tr}\ln\left[\mathscr{F}^{-1}(k, \rho) \cdot \overline{\mathscr{F}}(k, \rho)\right]\,. \tag{8.58}$$

Again, ambiguities of multiples of 2π in the numerical computation are avoided by integrating

$$\frac{\partial\delta(k, \rho)}{\partial\rho} = -\frac{1}{2i}\,\mathrm{Tr}\,\left[\mathscr{F}' \cdot \mathscr{F}^{-1} - \overline{\mathscr{F}}' \cdot \overline{\mathscr{F}}^{-1}\right] \quad \text{with} \quad \lim_{\rho\to\infty}\delta(k, \rho) = 0\,, \tag{8.59}$$

from $\rho = \infty$ to 0, along with the system for $\mathscr{F}$ and $\overline{\mathscr{F}}$.

Alternatively, the complex 4×4 problem can be elevated to a real 8×8 one from which a scattering matrix is extracted as in Sect. 6.1.2. Then the

[7] As in the case of the sphaleron, we have infinitely many gauge-equivalent ground states separated by a finite barrier.

number of degrees of freedom is doubled and one can verify numerically [38] that the resulting sum over eigenphase shifts is $2\delta(k,\rho)$.

8.2.7 Numerical Results

The central goal is to find a vortex configuration which is energetically favored over the trivial vacuum *of the same fermion number*, so that Eq. (8.44) is satisfied. The scan of even a restricted configuration space is numerically expensive and cannot be exhaustive. Here we restrict ourselves to the ansatz of Sect. 8.2.3 and introduce variational parameters by deforming the Z-string configuration:

$$f_H(\rho) = 1 - e^{-\rho/w_H}\,, \quad f_G(\rho) = 1 - e^{-(\rho/w_G)^2}, \quad \text{and} \quad f_P(\rho) = a_P e^{-\rho/w_P}\,. \tag{8.60}$$

Such deformations also ensure that the profile functions obey the proper boundary conditions and that the classical energy is always finite. Altogether, the *ansatz* contains five variational parameters, w_H, w_G, w_P, and a_P from the profiles and ξ_1 from the sphaleron square.[8] Of course, it is still possible that there exist stable configurations outside the space spanned by this *ansatz*.

In all numerical studies we adopt unit winding number, $n = 1$. If not explicitly stated, we measure dimensionful quantities in units of the fermion mass, m_f, or its inverse.

(a) Classical Energy

The scale is set by the classical energy of the string background on the sphaleron square $E_{\rm cl} = 2\pi \int_0^\infty d\rho\, \rho\, \mathscr{E}_{\rm cl}(\rho)$, with $\mathscr{E}_{\rm cl}$ given in Eqs. (8.34) and (8.36). For the empirically motivated parameter set, Eq. (8.40), the classical energy depends strongly on the angle ξ_1 [38], favoring small values of ξ_1 and narrow Higgs fields, i.e.,$w_H \ll 1$, since $E_{\rm cl}$ increases roughly quadratically with w_H at small ξ_1. The dependence on other parameters, in particular the charged Higgs component, is rather small; for $a_P \geq 0.5$ the energy rises linearly with the amplitude of the charged Higgs. The largest possible admixture of gauge fields, $\xi_1 = \pi/2$, corresponds to the pure Z-string. Then a minimum emerges at a moderate width $w_H \sim 3$, but the overall value of the minimum is much larger than in the cases of smaller ξ_1.

For artificially large fermion masses, $m_f = 1.5\,\text{GeV}$, the Higgs field *VEV* is reduced because of the scaling in Eq. (8.40), and the classical energy becomes insensitive to the shape of the Higgs field. Instead, the dependence on the width of the gauge field is now enhanced, except at very small ξ_1, where the gauge field is suppressed and $E_{\rm cl} \simeq 0.4$ is nearly constant. At $\xi_1 = 0.5$, the classical energy varies strongly, from 25 to 2, as the gauge field width w_G is increased from 1.5 to 5.5. Close to the Z-string ($\xi_1 \lesssim \pi/2$), this effect is even more dramatic: $E_{\rm cl}$ drops from around $E_{\rm cl} = 50$ at $w_G \sim 1.5$ to $E_{\rm cl} \sim 2$

[8] We recall that ξ_2 is fixed to $\pi/2$, cf.Eqs. (8.33) and (8.35).

at $w_G = 12$. Thus the classical energy favors a suppression of the gauge field contribution, either by having the gauge admixture ξ_1 small or by diffusing the gauge field to very large widths w_G. The central question is whether the gain in energy due to the emergence of a fermion zero mode at $\xi_1 = \pi/2$ compensates for the increase in the classical energy. Since $E_{\rm cl} \sim 20$ for the Z-string, and every zero mode gives an energy gain of one, a large number of fermions (around 20 or so) is required to break even, unless the vacuum polarization produces large additional bindings.

(b) Bound States

For the original Z-string, i.e., $\xi_1 = \pi/2$ and $\phi_+ = 0$, an exact zero mode exists and much emphasis was put in the early literature on possible stabilizing effects from this mode. However, the perturbative analysis of Naculich [23] indicated that the zero mode does not stabilize the Z-string against a ϕ_+ condensation, once the fermion determinant is (approximately) included. However, the most important result from studying the whole bound state spectrum is that there exist *very many* bound states. This happens both in individual channels and spreads over a large range of angular momenta. In turn, the properties of individual strongly bound states (or zero modes) can be less important than previously thought.

Though the gauge field creates stronger binding of the lowest lying state, the pure Higgs configuration can (partially) compensate for this by occupying many of the less-strongly bound states; after all, a large fermion number is required anyhow. Since the near-zero mode in the gauge vortex is *not* accompanied by further tightly bound states, the increase of binding of the lowest lying mode has only a small stabilizing effect.

The total number of bound states is plotted in Fig. 8.5 as a function of the Higgs width w_H. Bound states mainly emerge from a "hole" in the Higgs condensate, since a region with $|\Phi| < |\langle\Phi\rangle|$ produces an attractive potential for the fermions. Thus, it is expected that the number of bound states increases roughly quadratically with the width w_H. By contrast, the mixing angle ξ_1 has only little effect, both on the total number of bound states and also on the number of tightly bound states. The bound state contribution to the quantum energy (first term in Eq. (8.50)),

$$E_{\rm B} = \frac{1}{2} \sum_j \left(m_f - |\omega_j| \right) \tag{8.61}$$

is shown in Fig. 8.6 as function of w_H and ξ_1. Again, E_B increases roughly quadratically with w_H, while the dependence on the other variational parameters is weaker. In the right panel, the dependence of $E_{\rm B}$ on ξ_1 is investigated. Even though E_B is large for some of the configurations near the Z-string ($\xi_1 = \frac{\pi}{2}$), the maximal values are still found for small ξ_1. Since in addition the classical energy grows dramatically with ξ_1, it is unlikely to find stable objects in the region of large ξ_1.

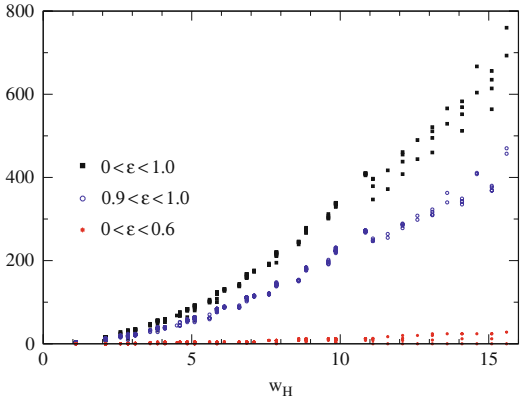

Fig. 8.5 The number of bound states as a function of the width w_H of the Higgs field at $\xi_1 = 0.1 \times \pi/2$ in specified energy ranges. The towers in each entry come from variations of parameters (other than ξ_1 and w_H) that are not displayed

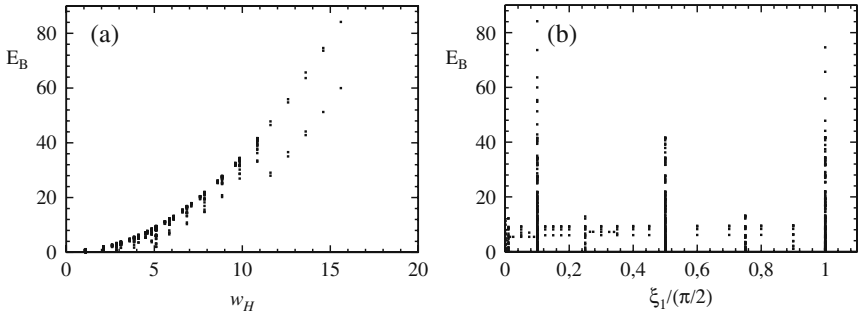

Fig. 8.6 The bound state contribution, E_B, to the vacuum polarization energy as a function of the variational parameters (**a**) w_H and (**b**) ξ_1. The towers in each entry show the effect of variations in the other parameters. The ξ_1-parameter space has not been covered uniformly

The shooting algorithm might miss states when they come in degenerate pairs. Such a degeneracy occurs for $\xi_1 = 0$, for which the CP symmetry is elevated to individual C and P symmetries. The point $\xi_1 \equiv 0$ was therefore avoided in the numerical studies of Ref. [38]. Similarly, very near-threshold states may be missed. Since their number is given by Levinson's theorem, the resulting error can be estimated. Configurations were rejected for which this error exceeded a prescribed limit.

(c) Vacuum Polarization Energy

Results for the fermion determinant, $E_{\rm vac}$ in Eq. (8.50), have been accumulated for about 1000 sets of variational parameters [38]. Figure 8.7 shows a selection thereof characterized by $m_f = 170\,\mathrm{GeV}$. Generically, the fermion determinant gives a positive contribution to the quantum energy. Nevertheless there are some configurations for which $E_{\rm vac}$ is negative; most notably for moderate extensions of both the Higgs and the gauge fields: $w_H \sim w_G \sim 3$. A charged Higgs condensate with $a_p \neq 0$ and $w_P \sim 3$ also has a beneficial effect, while the dependence on the angle ξ_1 is marginal.

The maximal energy gain from $E_{\rm vac}$ is only of the order $(-m_f)$. The lowest value among the 1000 data points is $E_{\rm vac} = -0.33 m_f$ at a very small value for ξ_1, i.e.,for an almost pure Higgs configuration. In total, the vacuum polarization energy is insufficient to stabilize the string. This result is confirmed by the derivative expansion of the fermion determinant [23], which agrees well with the exact calculation [38].

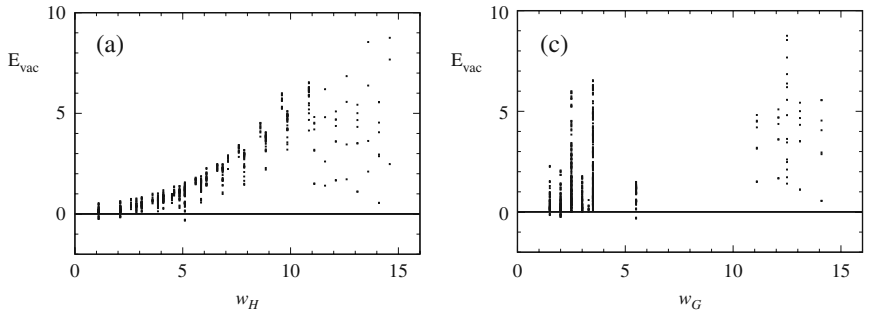

Fig. 8.7 The vacuum polarization energy, $E_{\rm vac}$, as a function of the width w_H and w_G of the Higgs and gauge field, respectively. The towers in each entry show results from variations of the remaining parameters

(d) Populating Bound States

Populating the N_f lowest lying states also defines an extended object of extremal energy. According to Eq. (8.44), the binding energy of this object is

$$\begin{aligned} B(N_f) &= E_{\rm cl} + N_C \left[E_{\rm occ}^{(N_f)} + E_{\rm vac} \right] - N_C N_f m_f \\ &= E_{\rm cl} + N_C \sum_{j=1}^{N_f} (\omega_j - m_f) + N_C\, E_{\rm vac}\,. \end{aligned} \tag{8.62}$$

Obviously $B(N_f) < 0$ suggests the existence of an energetically stable object with fermion number $N_f\, N_C$. If there are fewer than N_f bound levels for the configuration under consideration, we have to occupy scattering states at

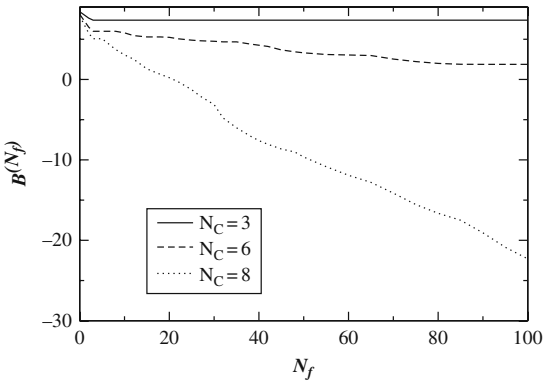

Fig. 8.8 The extremal (negative) binding energy, $B(N_f)$, as a function of the number N_f of populated bound state levels

threshold, which do not contribute to the binding energy. Figure 8.8 shows the maximal binding observed within the variational approach for a prescribed number N_f. Bound objects exist for sufficiently large N_C; e.g., $N_C \geq 8$ yields a bound object with $N_f > 20$.

Figure 8.9 shows the binding energy Eq. (8.62) for fixed values of N_C and N_f, as a function of the width w_H. Again, bound objects with $B(N_f) < 0$ exist for sufficiently large N_C. This binding mechanism requires us to populate up to $N_f \sim 50$ levels.

The additional charged Higgs condensate with amplitude a_P in Eq. (8.35) is novel in the context of strings in the standard model. Since the fermion zero mode on the Z-string exists only for $a_P = 0$ and furthermore $a_P > 0$ increases the effective fermion mass, minimizing E_B favors $a_P \to 0$. On the other hand the fermion determinant decreases with increasing a_P and may even become negative at large a_P. Hence for a moderate number N_f of occupied bound states, this may balance the smaller bound state contribution. But in this case N_f is too small to overcome the classical energy. In the parameter regime where we detect stable strings, N_f is so large that $a_P \to 0$ is favorable.

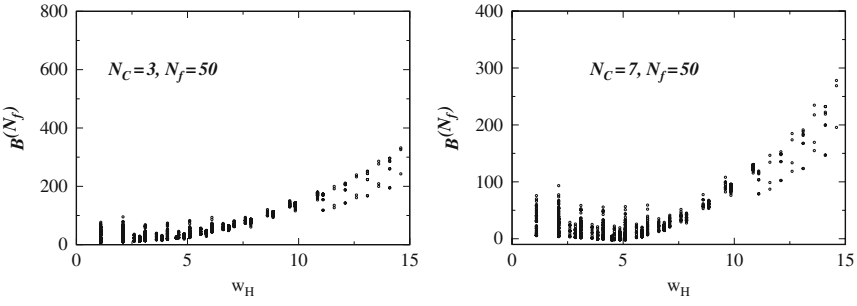

Fig. 8.9 The binding energy as a function of the width w_H for two values of the degeneracy N_C

(e) Large Fermion Mass

Finally, we consider the case of a very heavy fermion, for which decoupling arguments [33, 34] suggest the existence of a stable soliton. A large fermion mass arises from a drastically increased Yukawa coupling f, which tends to enhance the stabilizing effect of the fermion fluctuations. At the same time, it decreases the $d = 2+1$ *VEV* of the Higgs according to Eq. (8.39), thereby reducing the classical energy.

Figure 8.10 shows the resulting binding energy for the choice $m_f = 1.5\,\mathrm{TeV}$. As expected, there is a stable object for the physical value of $N_C = 3$ and a large number of populated fermion levels. We also check if a fermion number zero object ($N_f = 0$) acquires binding, meaning that the vacuum would be *unstable* against the formation of weak strings. The left panel of Fig. 8.10 shows that for $N_C = 3$ and $m_f = 1.5$ TeV, there is only negligible binding for $N_f = 0$. For the physical value $m_f = 170\,\mathrm{GeV}$, we do not see any significant binding unless the number of colors is increased to $N_C \sim 100$.

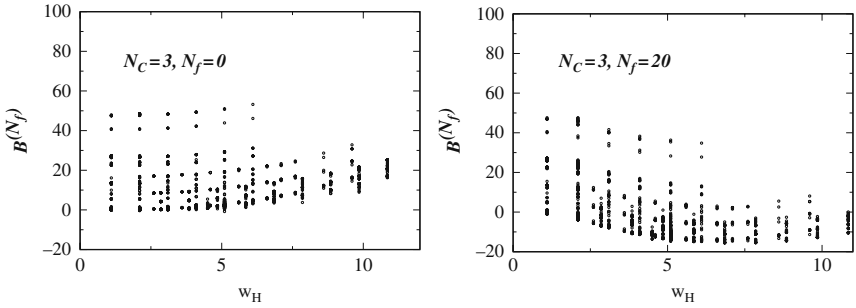

Fig. 8.10 The binding energy as a function of the Higgs field width, w_H, for a large fermion mass, $m_f = 1.5\,\mathrm{TeV}$, and two values of the number of populated levels

References

1. Y. Aharonov and D. Bohm, *Phys. Rev.* **115** (1959) 485. 143
2. M. G. Alford and F. Wilczek, *Phys. Rev. Lett.* **62** (1989) 1071. 143
3. A. N. Redlich, *Phys. Rev.* **D29** (1984) 2366. 143
4. D. Cangemi, E. D'Hoker, and G. V. Dunne, *Phys. Rev.* **D51** (1995) 2513. 143, 148
5. R. Blankenbecler and D. Boyanovsky, *Phys. Rev.* **D34** (1986) 612. 143
6. J. E. Kiskis, *Phys. Rev.* **D15** (1977) 2329. 143
7. A. J. Niemi and G. W. Semenoff, *Phys. Rept.* **135** (1986) 99. 143
8. N. Graham, V. Khemani, M. Quandt, O. Schröder, and H. Weigel, *Nucl. Phys.* **B707** (2005) 233. 144, 147, 152
9. M. Bordag and K. Kirsten, *Phys. Rev.* **D60** (1999) 105019. 144
10. K. Langfeld, L. Moyaerts, and H. Gies, *Nucl. Phys.* **B646** (2002) 158. 144, 149
11. P. Pasipoularides, *Phys. Rev.* **D67** (2003) 107301. 144

12. S. N. M. Ruijsenaars, *Ann. Phys.* **146** (1983) 1. 147
13. D. Boyanovsky and R. Blankenbecler, *Phys. Rev.* **D31** (1985) 3234. 147
14. A. P. Polychronakos, *Nucl. Phys.* **B281** (1987) 241. 147
15. A. P. Polychronakos, *Nucl. Phys.* **B278** (1986) 207. 147
16. V. P. Gusynin and I. A. Shovkovy, *J. Math. Phys.* **40** (1999) 5406. 148, 149
17. H. W. Lee, P. Y. Pac, and H. K. Shin, *Phys. Rev.* **D40** (1989) 4202. 148, 149
18. Y. Nambu, *Nucl. Phys.* **B130** (1977) 505. 153
19. N. S. Manton, *Phys. Rev.* **D28** (1983) 2019. 153
20. F. R. Klinkhamer and N. S. Manton, *Phys. Rev.* **D30** (1984) 2212. 153, 156
21. A. Achucarro and T. Vachaspati, *Phys. Rept.* **327** (2000) 347. 153
22. T. Vachaspati, *Phys. Rev. Lett.* **68** (1992) 1977. [Erratum-ibid. 69, 216 (1992)]. 153
23. S. G. Naculich, *Phys. Rev. Lett.* **75** (1995) 998. 153, 164, 166
24. T. W. B. Kibble, *J. Phys.* **A9** (1976) 1387. 153
25. M. B. Hindmarsh and T. W. B. Kibble, *Rept. Prog. Phys.* **58** (1995) 477. 153
26. A. Vilenkin, *Phys. Rept.* **121** (1985) 263. 153
27. Supernova Cosmology Project Collaboration, S. Perlmutter et al., *Astrophys. J.* **517** (1999) 565. 153
28. Supernova Search Team Collaboration, A. G. Riess et al., *Astron. J.* **116** (1998) 1009. 153
29. D. Spergel and U.-L. Pen, *Astrophys. J.* **491** (1997) L67. 153
30. P. McGraw, *Phys. Rev.* **D57** (1998) 3317. 153
31. M. Bucher and D. N. Spergel, *Phys. Rev.* **D60** (1999) 043505. 153
32. R. H. Brandenberger and A.-C. Davis, *Phys. Lett.* **B308** (1993) 79. 153
33. E. D'Hoker and E. Farhi, *Nucl. Phys.* **B248** (1984) 77. 153, 168
34. E. D'Hoker and E. Farhi, *Nucl. Phys.* **B248** (1984) 59. 153, 168
35. F. R. Klinkhamer and C. Rupp, *J. Math. Phys.* **44** (2003) 3619. 153
36. F. R. Klinkhamer and P. Olesen, *Nucl. Phys.* **B422** (1994) 227. 153, 156
37. M. Groves and W. B. Perkins, *Nucl. Phys.* **B573** (2000) 449. 153, 159
38. N. Graham, M. Quandt, O. Schröder, and H. Weigel, *Nucl. Phys.* **B758** (2006) 112. 153, 160, 162, 163, 165, 166
39. H. B. Nielsen and P. Olesen, *Nucl. Phys.* **B61** (1973) 45. 155
40. V. Khemani, hep-th/0404234. Ph. D. thesis. 156
41. H. Weigel, B. Schwesinger, and G. Holzwarth, *Phys. Lett.* **B168** (1986) 321. 156

9 Quantum Corrections to Q-Balls

So far we have focused on static field configurations. In this chapter we show how our methods can be extended to systems with simple time dependence.

9.1 The Q-Ball

A complex scalar theory in three dimensions with a cubic coupling can support classically stable, time-dependent, non-topological solutions to the equations of motion that carry a global charge Q, called Q-balls [1]. Supersymmetric extensions of the standard model generically contain such objects [2]. They become particularly interesting in cosmological applications at small values of Q, because then it is easier for them to form in the early universe [3]. In this regime, quantum corrections to the soliton's energy become increasingly important in determining its stability. In this chapter, we extend our methods to Q-balls. We show how to express the calculation in terms of an effective time-independent problem. In this formalism, the full one-loop quantum correction can be computed efficiently. We also derive a very simple estimate for this result. This calculation enables us to compare the energy of the Q-ball in the quantum theory to the energy of free particles carrying the same charge Q and determine if the Q-ball remains stable in the quantum theory.

Our starting point is the classical analysis of Q-balls carried out in Refs. [1, 3]. We will take the same simple model,

$$\mathscr{L} = \frac{1}{2}(\partial_\mu \varphi)^*(\partial^\mu \varphi) - U(\varphi), \tag{9.1}$$

where φ is a complex field, and choose the potential

$$U(\varphi) = \frac{1}{2}M^2|\varphi|^2 - A|\varphi|^3 + \lambda|\varphi|^4\,, \tag{9.2}$$

so that $\varphi = 0$ is a minimum of the potential and the global $U(1)$ symmetry is unbroken. A particular configuration $\varphi(\boldsymbol{x}, t)$ has charge

$$Q = \frac{1}{2i}\int d^3x\,(\varphi^*\partial_t\varphi - \varphi\partial_t\varphi^*)\ . \tag{9.3}$$

Graham, N., et al.: *Quantum Corrections to Q-Balls.* Lect. Notes Phys. **777**, 171–177 (2009)
DOI 10.1007/978-3-642-00139-0_9

With these conventions, an asymptotic state with momentum $\boldsymbol{k}$ has unit charge.

To restrict to configurations of fixed charge Q, we introduce a Lagrange multiplier χ, so that the energy functional becomes

$$E_\chi[\varphi] = \int d^3x \frac{1}{2}|\partial_t\varphi - i\chi\varphi|^2 + \int d^3x \left(\frac{1}{2}|\nabla\varphi|^2 + U_\chi(\varphi)\right) + \chi Q\,, \qquad (9.4)$$

where

$$U_\chi(\varphi) = U(\varphi) - \frac{1}{2}\chi^2|\varphi|^2\,. \qquad (9.5)$$

Then minimizing the energy over χ fixes the configuration to have charge Q, and the classical Q-ball solution is obtained by minimizing the energy with respect to independent variations of $\varphi(\boldsymbol{x}, t)$ and χ. The form of the kinetic energy ensures that the Q-ball solution has the simple time dependence

$$\varphi(\boldsymbol{x}, t) = e^{i\chi t}\phi(\boldsymbol{x}), \qquad (9.6)$$

and we must simply minimize

$$E_\chi[\phi] = \int d^3x \left(\frac{1}{2}|\nabla\phi|^2 + U_\chi(\phi)\right) + \chi Q \qquad (9.7)$$

by varying χ and $\phi(x)$. As shown in Ref. [1], if the quantity $U(\phi)/\phi^2$ is minimized at $\phi_0 > 0$, then for $\chi_0 = \sqrt{2U(\phi_0)/\phi_0^2}$, the effective potential $U_{\chi_0}(\phi)$ will have degenerate minima. For $\chi > \chi_0$, we can find a spherically symmetric solution to the equations of motion,

$$\frac{d^2}{dr^2}\phi_0(r) + \frac{2}{r}\frac{d}{dr}\phi_0(r) = U'_\chi(\phi_0(r))\,, \qquad (9.8)$$

where a prime labels the derivative with respect to the argument. This solution is the "bounce" for tunneling in three Euclidean dimensions [4]. Here the boundary conditions are

$$\lim_{r\to\infty}\phi_0(r) = 0 \quad \text{and} \quad \left.\frac{d}{dr}\phi_0(r)\right|_{r=0} = 0\,. \qquad (9.9)$$

We can find the solution using the shooting method detailed in Ref. [4] and minimize the resulting energy over χ to ensure that φ carries charge Q. For large enough Q, the optimal value of χ approaches χ_0, allowing Ref. [1] to use the thin-wall approximation in order to demonstrate the existence of a global minimum, which is the Q-ball solution. For small Q, the optimal value of χ approaches M, and Ref. [3] uses the thick-wall approximation to show that there exists a global minimum in this case as well. Thus classically bound solitons exist all the way down to $Q = 1$. For all Q, we have $\chi_0 < \chi < M$. We can thus consider the classical binding energy as a function of Q by comparing

the energy of the Q-ball to QM, the energy of a collection of free particles carrying charge Q, since it is a conserved quantity.

Although Q-balls are classically stable even as $Q \to 1$, the binding energy per charge is going to zero in this limit. This case is of particular interest for cosmological applications, since Q-balls of large charge, while favored energetically, are disfavored as the temperature increases by their low entropy. To answer the question of whether Q-balls have a significant chance of being formed in the early universe, we must therefore verify that the classical conclusions are not invalidated by quantum corrections.

9.2 Quantum Corrections

To compute the leading quantum correction to the Q-ball energy, we write the quantum field φ as the classical solution plus a quantum correction,

$$\varphi(\boldsymbol{x}, t) = e^{i\chi t}\phi_0(r) + \eta(\boldsymbol{x}, t). \tag{9.10}$$

We expand the field equations in the small fluctuations $\eta(\boldsymbol{x}, t)$. The $\mathscr{O}(\hbar)$ information is contained in the leading (harmonic) order, which reads

$$\left[(\partial_t + i\chi)^2 - \nabla^2 + U''(\phi_0(x))\right]\eta(\boldsymbol{x}, t) = 0\,. \tag{9.11}$$

Parameterizing $\eta(x, t) = e^{i\chi t}e^{-i\omega t}\psi(x)$ gives the mode an energy $\omega - \chi$, where the time-independent wavefunction $\psi(x)$ solves

$$\left[-\nabla^2 + U''(\phi_0(x))\right]\psi(\boldsymbol{x}) = \omega^2\psi(\boldsymbol{x})\,, \tag{9.12}$$

which is an ordinary Schrödinger equation. The unrenormalized (bare) vacuum polarization energy is given formally by the sum over zero-point energies of these oscillations

$$E_{\text{vac}}^{\text{bare}}[\phi_0] \sim \frac{1}{2}\sum_j |\omega_j - \chi|\,. \tag{9.13}$$

Since the spectrum of Eq. (9.12) is symmetric in $\omega \to -\omega$, we can sum over both signs of the energy and obtain the formal expression

$$E_{\text{vac}}^{\text{bare}}[\phi_0] \sim \frac{1}{2}\sum_{\omega_j \geq 0}\left(|\omega_j + \chi| + |\omega_j - \chi|\right) = \sum_{\omega_j \geq 0}\max\left(|\chi|, |\omega_j|\right)\,. \tag{9.14}$$

We will use the spectral method to extract the quantum correction to the energy in terms of the continuum scattering data for the reduced problem of Eq. (9.12). Since the potential is spherically symmetric, we can decompose the spectrum into partial waves ℓ. We have wavefunctions

$$\psi(\boldsymbol{x}) = \sum_{l,m}\frac{Y_{\ell m}(\hat{\boldsymbol{x}})}{r}\psi_\ell(r) \tag{9.15}$$

for $m = -\ell, -\ell+1, \ldots, \ell-1, \ell$, where the radial wavefunction $\psi_\ell(r)$ satisfies

$$\left(-\frac{d^2}{dr^2} + \frac{\ell(\ell+1)}{r^2} + U''(\phi_0(r))\right)\psi_\ell(r) = \omega^2\psi_\ell(r) \tag{9.16}$$

with scattering boundary conditions.

In each partial wave, we will find a continuum starting at $\omega = M$ and possibly bound states with $0 \le \omega_j \le M$. It is instructive to consider the properties of Eq. (9.12) that reveal its origin from a field theory soliton. The full oscillation spectrum should have a zero mode in the $\ell = 1$ channel, corresponding to the translation invariance of the Q-ball solution. The threefold degeneracy of this state corresponds to the three directions of translation. From Eq. (9.13), we see that in the reduced problem, the zero mode appears as a bound state with energy $\omega = \chi$. Since this state appears in the $\ell = 1$ channel, there must exist an even more tightly bound state in the $\ell = 0$ channel. In the case of an ordinary static solution, this state would correspond to an instability of the full soliton. (This result is simply another form of Derrick's theorem [5], which prohibits the existence of scalar solitons in more than one space dimension.) But from Eq. (9.14), we see that the destabilizing effect of this mode is neutralized by the time dependence of the classical solution. Thus the $\ell = 0$ bound state makes the same contribution to the vacuum polarization energy as the zero modes do. All other modes have energies greater than χ.

Having rewritten the vacuum polarization energy in terms of the eigenmodes of the reduced scattering problem in Eqs. (9.12) and (9.16), we are prepared to apply the spectral methods we have developed earlier. As before, we obtain the renormalized vacuum polarization energy as Feynman diagram contribution together with a sum over partial waves ℓ in which each term consists of a sum over positive-energy bound states $\omega_{j,\ell}$ and an integral over continuum states. We thus obtain the renormalized vacuum polarization energy

$$E_{\rm vac}[\phi_0] = \sum_{\ell=0}^{\infty}(2\ell+1)\left[\int_0^\infty \frac{dk}{\pi}\omega\frac{d}{dk}\left(\delta_\ell(k) - \delta_\ell^{(1)}(k) - \delta_\ell^{(2)}(k)\right) + \sum_j \max(\chi, \omega_{j,\ell})\right] + E_{\rm FD}^{\rm ren}[\phi_0]\,, \tag{9.17}$$

where $k = \sqrt{\omega^2 - M^2}$, $\delta_\ell(k)$ is the scattering phase shift in partial wave ℓ, and $\delta_\ell^{(1)}(k)$ and $\delta_\ell^{(2)}(k)$ are its first and second Born approximations, respectively. Finally $E_{\rm FD}^{\rm ren} = \sum_{i=1}^{2} E_{\rm FD}^{(i)} + E_{\rm CT}$ is the contribution to the energy from the two-point function, computed in ordinary Feynman perturbation theory, cf.Eq. (3.27). This piece includes the counterterms, which we fix using physical renormalization conditions: We demand that the tadpole graph

vanish,[1] and that the mass of the free φ particle, i.e.,the pole of the φ-propagator, is unchanged. We also perform wavefunction renormalization so that the residue of this pole is unchanged as well.

The contribution to the energy from the two-point function is computed using conventional techniques, giving

$$E^{\rm ren}_{\rm FD}[\phi_0] = \int_0^\infty \frac{4q^2 dq}{(4\pi)^4} \left[\left(2\frac{\sqrt{q^2+4M^2}}{q} \operatorname{arctanh} \frac{q}{\sqrt{q^2+4M^2}} - \frac{5\pi}{3\sqrt{3}} + 1 \right) |\tilde{\sigma}(q)|^2 - 4q^2 \left(\frac{2\pi}{3\sqrt{3}} - 1 \right) |\tilde{\phi}(q)|^2 \right], \quad (9.18)$$

where $\tilde{\sigma}(q)$ and $\tilde{\phi}(q)$ are the $\ell = 0$ Fourier transforms of $U''(\phi_0(r)) - M^2$ and $\phi(r)$, respectively.

Examining this calculation in detail yields an accurate estimate for the quantum correction to the energy that is easy to compute. Using the analysis of bound states above, we can separate Eq. (9.17) into

$$E_{\rm vac}[\phi_0] = \sum_{\ell=0}^\infty (2\ell+1) \left[\int_0^\infty \frac{dk}{\pi} \omega \frac{d}{dk} \left(\delta_\ell(k) - \delta_\ell^{(1)}(k) - \delta_\ell^{(2)}(k) \right) + \sum_j \omega_{j,\ell} \right] + \chi - \omega_0 + E^{\rm ren}_{\rm FD}[\phi_0], \quad (9.19)$$

where ω_0 is energy of the most tightly bound state, which appears in the $\ell = 0$ channel. (It is the only state with energy less than χ.) To set up the approximation it is instructive to define the reduced vacuum polarization energy as the quantum energy without the most tightly bound state,

$$\begin{aligned} E^{\rm red}_{\rm vac}[\phi_0] &= E_{\rm vac}[\phi_0] - (\chi - \omega_0) \\ &= \sum_{\ell=0}^\infty (2\ell+1) \left[\int_0^\infty \frac{dk}{\pi} (\omega - M) \frac{d}{dk} \left(\delta_\ell(k) - \delta_\ell^{(1)}(k) - \delta_\ell^{(2)}(k) \right) + \sum_j (\omega_{j,\ell} - M) \right] + E^{\rm ren}_{\rm FD}[\phi_0], \end{aligned} \quad (9.20)$$

where we have used Levinson's theorem in the second equation. We claim that the contribution from Eq. (9.20) is small: Since χ does not appear explicitly, Eq. (9.20) is simply the vacuum polarization energy of a time-independent soliton giving rise to the reduced small oscillations of Eq. (9.12). (Of course, such a soliton would not solve the field theory equations of motion, but we could imagine holding it in place with an external source). The potential $U''(\phi_0(x))$ is shallow and slowly varying, especially in the limit of small Q, which corresponds to χ approaching M. It causes only a slight deformation of

[1] As in the scalar theories discussed in previous chapters, the tadpole graph is local. Thus the first-order Feynman diagram is fully canceled.

the small oscillations spectrum—in particular, there is only one state bound more tightly than χ. For a generic potential of this kind, the contributions from the bound states and continuum will be opposite in sign, since any rearrangement of the continuum spectrum partially compensates for the effect of the states that become bound.

Alternatively, we can also estimate Eq. (9.20) in the derivative expansion. To lowest order, we have simply the effective potential contribution [4]

$$E_{\rm vac}^{\rm red,DE}[\phi_0] = \int_0^\infty \frac{r^2 dr}{8\pi} M^4 \left((1+z(r))^2 \log(1+z(r)) - z(r) - \frac{3}{2} z(r)^2 \right), \tag{9.21}$$

where we have introduced the radial function

$$z(r) = \frac{U''(\phi_0(r)) - M^2}{M^2}\,. \tag{9.22}$$

Using either this technique or explicit computations, we find that the reduced vacuum polarization energy is indeed very small compared to the classical binding energy of the Q-ball (typically 5% or less for small Q). Thus we lose very little accuracy by dropping this term, which results in a very simple estimate for the vacuum polarization energy:

$$E_{\rm vac}[\phi_0] \approx E_{\rm vac}^{\rm est}[\phi_0] = \chi - \omega_0\,. \tag{9.23}$$

9.3 Applications

To see whether the Q-ball is stable, we must compare its energy to the energy of a state with the same charge built on the trivial vacuum

$$\mathcal{B}[\phi_0] = E[\phi_0] - QM\,. \tag{9.24}$$

Figure 9.1 shows the result of different calculations of E, each as a function of Q, for two choices of the coupling constants. In both cases, the parameters are chosen so that $\varphi = 0$ remains the global minimum of $U(\varphi)$. We work in units of M, which sets the scale of the problem. In the classical approximation,

$$\mathcal{B}_{\rm class}[\phi_0] = E_\chi[\phi_0] - QM, \tag{9.25}$$

we see the result of [3]: The Q-ball is stable for all Q, though the binding energy per charge is going to zero as $Q \to 0$. In the full one-loop calculation,

$$\mathcal{B}_{\rm full}[\phi_0] = E_\chi[\phi_0] + E_{\rm vac}[\phi_0] - QM, \tag{9.26}$$

we see that the quantum corrections overwhelm the weak classical binding up to $Q_{\rm min} \approx 7$. Above this value, the Q-ball remains stable. The spherically symmetric Q-ball is unbound below $Q_{\rm min}$, though we cannot exclude stable

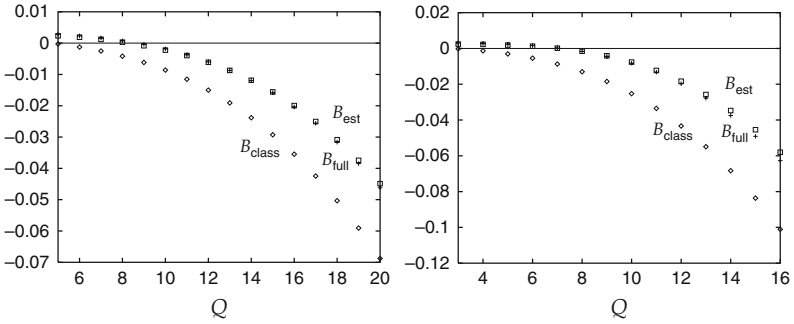

Fig. 9.1 Q-ball binding as a function of Q, in units of M. Parameters are $A = 0.325M$ and $\lambda = 0.055$ (*left panel*), and $A = 0.425M$ and $\lambda = 0.095$ (*right panel*). Shown are three calculations of the difference $\mathcal{B}$ between the energy of a Q-ball and the energy of a state with charge Q built on the trivial vacuum: the classical approximation $\mathcal{B}_{\rm class}[\phi_0]$, the full one-loop calculation $\mathcal{B}_{\rm full}[\phi_0]$, and the estimated one-loop result $\mathcal{B}_{\rm est}[\phi_0]$

configurations outside the spherically symmetric *ansatz*, Eq. (9.6). Finally, we see that using Eq. (9.23) to approximate to the one-loop result gives an expression

$$\mathcal{B}_{\rm est}[\phi_0] = E_\chi[\phi_0] + E^{\rm est}_{\rm vac}[\phi_0] - QM \tag{9.27}$$

that is very close to the full one-loop result. It is also interesting to note that this approximation is particularly good near the value of Q at which the Q-ball becomes bound in the full one-loop calculation.

References

1. S. R. Coleman, *Nucl. Phys.* **B262** (1985) 263. 171, 172
2. A. Kusenko, *Phys. Lett.* **B405** (1997) 108. 171
3. A. Kusenko, *Phys. Lett.* **B404** (1997) 285. 171, 172, 176
4. S. Coleman, *Aspects of Symmetry.* Cambridge University Press, 1985. 172, 176
5. D. H. Derrick, *J. Math. Phys.* **5** (1965) 1252. 174

Index